Single Molecule Electronics

By

KEISHA MICHAEL MPHYS.

H. H. Wills Physics Laboratory
UNIVERSITY OF BRISTOL

A dissertation submitted to the University of Bristol in accordance with the requirements of the degree of DOCTOR OF PHILOSOPHY in the Faculty of Science.

MAY 2020

Word count:≈40500

Abstract

Single molecule electronics represents a rapidly growing area of interest within the electronics community. As the size of electronics continue to miniaturise, the use of metal-molecule-metal junctions has the potential to provide a useful step in this process via the bottom-up approach. The majority of previous work in the molecular electronics field has focused on junctions using gold as the contact metal. However, alternative contact materials such as the ferromagnetic 3d transition metals provide an exciting opportunity to probe new effects including spin-dependent transport.

Here, a mechanically controllable break junction technique has been developed and used to measure the conductance of single molecules using both gold and ferromagnetic (nickel and cobalt) electrodes. A scanning tunnelling microscope break junction technique was also employed to provide a comparison between measurements using both methods.

To date, work on single-molecule junctions incorporating 3d transition metals has been limited due to the tendency of these metals to oxidize under ambient conditions. It has been observed within, that it can be possible to measure the conductance of single molecule junctions without using techniques such as electrochemical control to protect the metal contacts from oxidation. A number of metal-molecule-metal junctions have been studied to determine their most probable value of conductance. Several further techniques such as 2D histograms, I-V curves, 2D correlation histograms and conditional histograms have been used to expand on this analysis.

Magnetoresistance measurements using the mechanically controllable break junction method were explored for Co | pentanedithiol | Co junctions by comparing the conductance obtained with and without the presence of a magnetic field. A magnetoresistance of 567% was measured. Anisotropic magnetoresistance experiments were performed on the same junction and an anisotropic magnetoresistance of 77% was measured. Magnetoresistance measurements were also performed using the scanning tunnelling microscope break junction method on Ni | 1,4-benzenedithiol | Ni junctions. However, no magnetoresistance effect was observed.

Dedication and acknowledgements

Firstly, I would like to thank Professor Walther Schwarzacher for his support over the last 3.5 years. I have particularly enjoyed his unwavering enthusiasm, lunches at his house and his seemingly endless supply of biscuits.

Secondly, I offer thanks to Dr Richard Brooke, who taught me pretty much everything I know. I don't think I would have progressed half as far with this project if I hadn't had someone so helpful to get me started. I also really appreciate his ongoing assistance even when he wasn't being paid to help me any more!

Additional thanks are extended to Patrick Alexander and Adrian Crimp in the Physics workshop who constructed the MCBJ. They went above and beyond fitting me in to make small changes and I am very grateful for that. Furthermore I would like to thank Dr Andrew Murray who spent a lot of time teaching me to use clean room equipment and giving me advice on how to improve my fabrication.

I am extremely appreciative of the great amount of help I have received from Yang, who reminded me how to use the STM and helped me to take my first measurements after I had taken a long break from the method and selflessly shared his solutions with me throughout our shared time in the group.

I would also like to thank Fred for all the help he has offered with my coding. Although he didn't seem to think it was much (and he most likely cancelled out the time his help saved me by distracting me with crosswords, Rubik's cubes, kendamas and other pointless activites) it made a really huge difference to me. On a similar note, I would like to thank Nathan for his willingness to listen to me rant about electrochemistry and magnetism, and occasionally chipping in with a nugget of wisdom that helped my understanding fall into place.

I would like to thank the EPSRC for providing the means for this work by funding my PhD.

On a personal level, my parents have supported me both emotionally and financially throughout my studies. It is their willingness to back me in whatever I choose to do that has gotten me to this point and I greatly appreciate the encouragement they have provided without ever asking too many physics related questions! Moreover, I am pleased that my siblings have always been there to provide ample distraction from anything research related.

Finally, I am so thankful to Strachan. I can't come up with good enough words to describe my appreciation for your steadfast support. Sorry!

AUTHOR'S DECLARATION

I declare that the work in this dissertation was carried out in accordance with the requirements of the University's Regulations and Code of Practice for Research Degree Programmes and that it has not been submitted for any other academic award. Except where indicated by specific reference in the text, the work is the candidate's own work. Work done in collaboration with, or with the assistance of, others, is indicated as such. Any views expressed in the dissertation are those of the author.

SIGNED: ..... DATE: .....

TABLE OF CONTENTS

List of Tables

List of Figures

CHAPTER 1

INTRODUCTION

Moore's Law is the observation made in 1965 that the number of transistors in a dense integrated circuit doubles approximately every two years [117]. This is a prediction which still holds true today. Moore's Law has been enabled by the ability to miniaturise electronic components such as the MOSFET. As a result of the success of this scaling, we are approaching the physical limits of silicon based electronics. Silicon power electronic components may prove insufficient if we want to continue to miniaturise electronics while maintaining adequate power density and keep up with the demands of an industry that requires increasingly compact and efficient devices. A number of solutions have been suggested in order to overcome this issue. The use of molecules as electronic components is an idea initiated by Aviram and Ratner in 1974 when they described a current rectifier using a single organic molecule [6]. Since then, the concept of single molecule electronics has provided a promising approach to miniaturising electronic devices through the bottom up strategy. Molecular junctions have a range of optical, magnetic, thermoelectric, electromechanical and molecular recognition properties [127]. In addition to these properties, molecules are highly versatile as electronic components due to the variety of molecular structures that can be produced via synthetic chemistry. For example, one may choose to tune the electronic properties of the molecule by adding specific chemical groups to the structure. This is a particularly exciting prospect for single molecule electronics as it could result in devices not possible using conventional materials [11, 20, 133, 139, 153, 173, 185].

More recently, investigations have progressed from predominately gold electrodes contacting the molecules to a range of different metals. Ferromagnetic contacts are proving particularly interesting due to the potential for harnessing spintronic effects in single molecule devices [26, 68, 166].

1.1 Molecular Conductance

1.1.1 Conductance Quantization

Macroscopic electrical conductivity can be defined by Equation 1.1

$$\sigma_{xx} = \rho_{xx}^{-1} = \frac{Il}{VA}, \tag{1.1}$$

where ρ is the longitudinal resistivity, I is the current flowing through the sample, V is the applied voltage, A is the cross sectional area and l is the length of the sample. However, as the scale of the conductor is reduced, we lose the ability to define the conductance accurately by the dimensions of the sample, A and l. Conductance is often defined by Equation 1.2

$$G = R^{-1} = \frac{I}{V}, \tag{1.2}$$

where G is the electrical conductance and R is the resistance. At the mesoscopic scale, the mean free path of an electron becomes much longer than the length scale of the conductor. This means the transport becomes ballistic rather than diffusive and the electrons propagate coherently rather than taking a random path through the material due to scattering as they would in macroscale electrical conduction. The resistance in ballistic conductors arises from the interface resistance between the conductor and contact pads in a system. In addition, it depends on the number of transverse modes in this system, M, which each contribute some transmission, T, to the total conductance. This is described by the Landauer formula, shown in Equation 1.3.

$$G = \frac{2e^2}{h} MT, \tag{1.3}$$

where h is Planck's constant, e is the electron charge, T is the transmission coefficient and

$$\frac{2e^2}{h} = G_0 \approx 7.75 \times 10^{-5} S, \tag{1.4}$$

is known as the conductance quantum. The conductance quantum can be derived in the following way:

A 1D wire, such as that in Figure 1.1, that connects two chemical potential reservoirs with potentials μ_1 and μ_2 adiabatically has a density of states described by

$$\frac{dn}{d} = \frac{2}{hv}, \tag{1.5}$$

where v is the electron velocity. The voltage will be

$$V = -\frac{(\mu_1 - \mu_2)}{e}, \tag{1.6}$$

Assuming that the number of transverse modes in the system, M, is constant over the energy range $\mu_1 > E > \mu_2$, the 1D current travelling across the wire is given by the current [38]

$$I = \frac{2e^2}{h} M \frac{(\mu_1 - \mu_2)}{e} \tag{1.7}$$

FIGURE 1.1. A 1D wire, connecting two reservoirs of potential μ_1 and μ_2 adiabatically, as described in Section 1.2 to determine the conductance in a mesoscopic system.

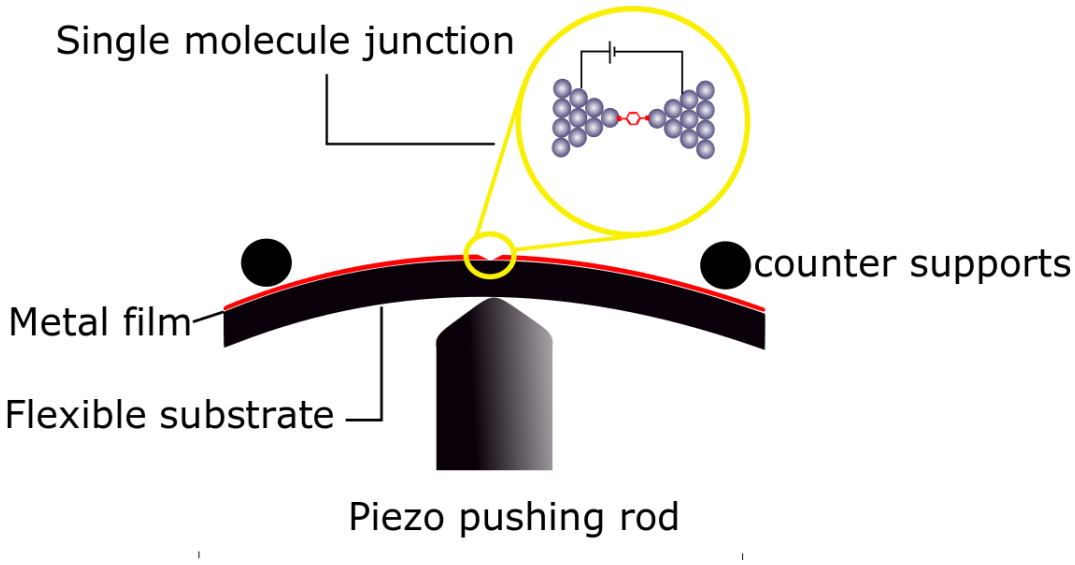

FIGURE 1.2. A schematic diagram of a mechanically controllable break junction showing the three point bending system consisting of two counter supports and the piezo pushing rod. The yellow circle shows a zoomed in schematic of a potential molecular junction that may form between the electrodes.

Finally, using Equation 1.2, we can determine Equation 1.4. By looking at Equation 1.3, it is clear that one may expect to see the conductivity of mesoscopic conductors changing in discrete steps depending on the number of transverse conducting modes that are present.

1.2 Measurement Techniques

The most common techniques used to fabricate and study metal-molecule-metal junctions (MMMJs) are scanning probe based techniques and the mechanically controllable break junction (MCBJ) method [154, 163]. The concept of an MCBJ was put forward by Moreland in 1985 [118].

His experiment consisted of an Nb-Sn filament mounted on a flexible glass beam that could be broken to form an electron tunnelling junction between the fractured elements. This idea led to the use of the MCBJ technique to study quantum size effects on conduction in metallic constrictions in 1993. In this work quantization, of conductance in a Pt sample was observed [123]. The first MCBJ molecular conductance measurements followed in 1997, performed by Reed using benzene-1,4-dithiol molecules which were self-assembled onto two facing Au electrodes. This showed charge transport through the molecules [140]. The substrates used to measure molecular conductance here consisted of a notched Au wire, glued to a bendable substrate. The wire became fractured, forming two electrodes, when a piezo actuator was used to bend the substrate.

At this time, STM (Scanning Tunnelling Microscopy) had already been used to measure atomic and molecular systems but the technique as it is used today was pioneered by Xu and Tao in 2003 [22, 44, 188]. They measured the conductance of single molecules, including hexanedithiol, octanedithiol, decanedithiol, and 4,4'- bipyridine, contacted by two Au electrodes. Conductance histograms were formed from thousands of measurements and used to locate the most probable conductance of the molecule in question.

Molecules can be applied to the substrates by a number of different methods. More recent advances to these methods have included using clean room fabricated, lithographically patterned samples rather than notched wire [84]. There are also examples of more rigorous statistical analysis [81] and correlation analysis [105] which provide a wider view of what happens when junctions are formed and the statistical relationship between different conduction configurations of the same molecule .

1.2.1 MCBJ

A schematic of MCBJ is shown in Figure 1.2. It consists of a piezo actuator which is used to bend a flexible substrate which could be made, for example, from phosphor bronze. The most basic version of the samples used for MCBJ are similar to those used by Reed and coworkers, as described in section 1.2, and consist of a notched wire fixed to a bendable substrate. The electrodes formed when the notched wire becomes fractured can be brought closer together and further apart by moving the piezo down or up respectively. The vertical movement of the piezo, δy, is related to the horizontal movement of the electrodes, δx, by the following equation:

$$r = \frac{\delta x}{\delta y} = \frac{6ut}{l^2}, \tag{1.8}$$

where u is the distance between the points at which the wire is fixed to the substrate, l is the distance between the counter supports and t is the thickness of the bendable substrate as shown in Figure 1.3.

More recently, nanofabrication has permitted major advances in the samples used for MCBJ. Figure 1.4 shows the process involved in constructing a thin-film MCBJ sample. The electrode pattern can be applied to the sample using an electron beam writer which leaves a mask

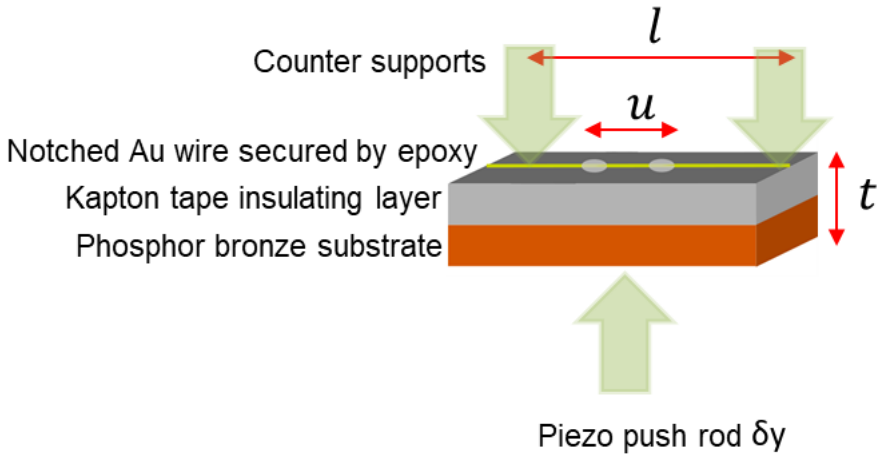

FIGURE 1.3. A schematic diagram of the notched wire samples used for mechanically controllable break junction. Labelled distances are used in Equation 1.8, to calculate the ratio between piezo push rod (vertical) movement, and electrode separation (horizontal).

over which the metal can be deposited by evaporation or sputtering. This results in electrodes remaining in the desired pattern. They are then etched in an isotropic plasma which leaves the narrowest parts of the metal pattern suspended, forming the bridge which will be broken during the MCBJ process. A benefit of these thin-film samples is an improved reduction ratio, r (detailed in Equation 1.8) when compared with notched wire samples. Typically, notched wire samples have an r value of 10^{-3} to 10^{-2} whereas for the thin-film samples, r is likely to be 10^{-6} to 10^{-4} [35]. It also results in more reproducible samples as there is a high level of precision when using these techniques to form electrodes. Notching a wire is less reproducible and can lead to unpredictable breaking mechanisms during the MCBJ process and hence unpredictable electrode shapes.

1.2.2 Scanning Probe Techniques

STM-BJ measurements are taken by crashing an electrochemically etched STM tip into a prepared substrate using a piezoelectric scanner. The tip is then withdrawn and a thin chain of atoms is formed which may result in single atomic contacts. When this contact breaks, if a suitable molecule is available it may link to the now free atomic contacts allowing its conductance to be measured. This process is described by Figure 1.5 There are also techniques known as soft touch techniques (including the I(s) and I(t) method) which involve the use of STM, but no direct contact is made between the STM tip and substrate [125]. During I(t) measurements, the tip is held at a fixed distance above the substrate which is smaller than the smallest dimension of the molecule. The current is monitored and jumps can be observed due to the spontaneous formation

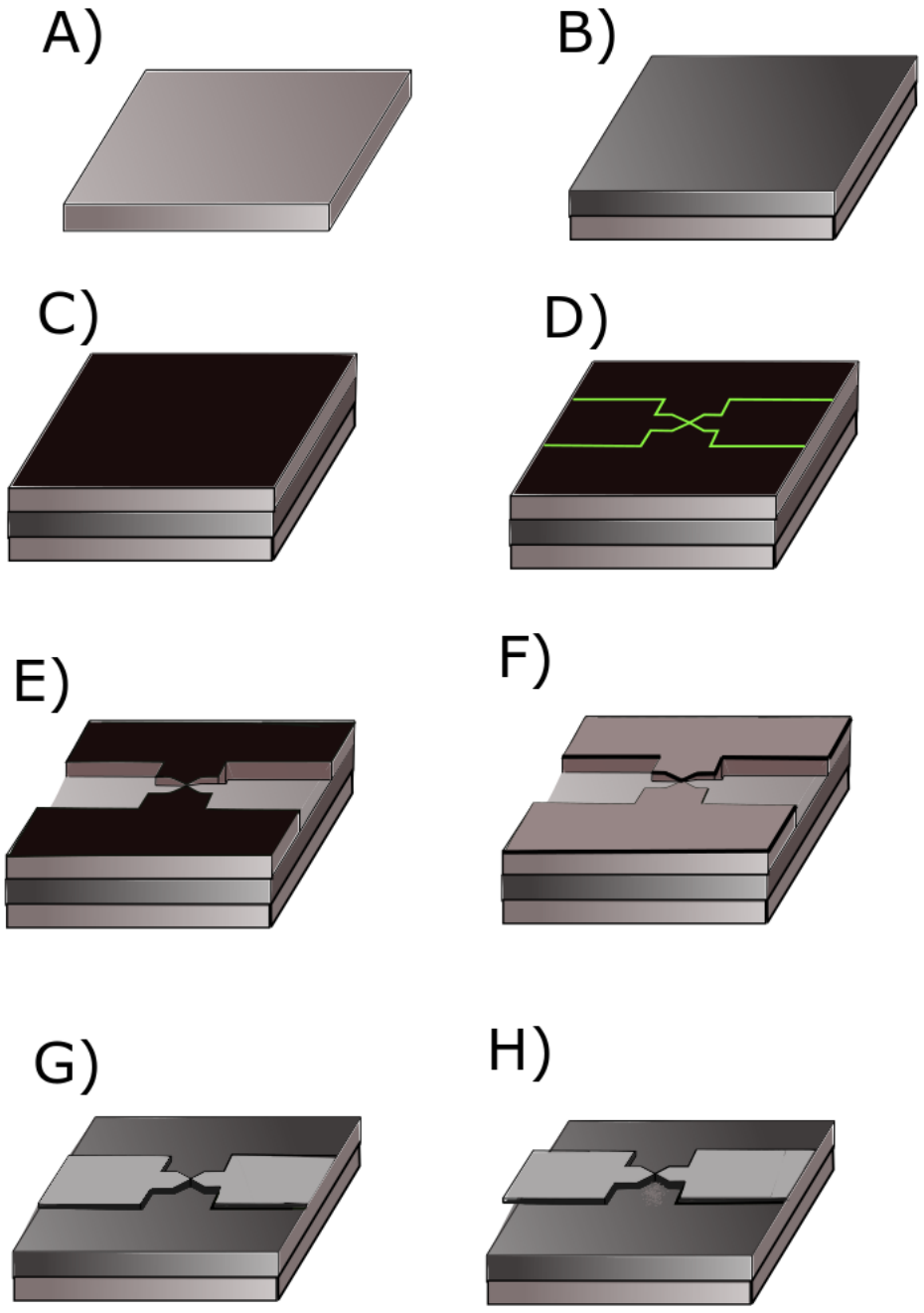

FIGURE 1.4. A schematic diagram of the process of fabrication of lithographically patterned MCBJ samples, modified from [35]. A) The flexible substrate, B) Polyimide is spin coated, C) Photoresist or resin is spin coated and baked, D) Sample is patterned using an electron beam, E) Sample is developed in solvent, exposed parts of the resin are selectively removed, F) Metal is deposited, G) Mask is lifted off H) The thickness of the polyimide is reduced, forming a free-standing electrode bridge.

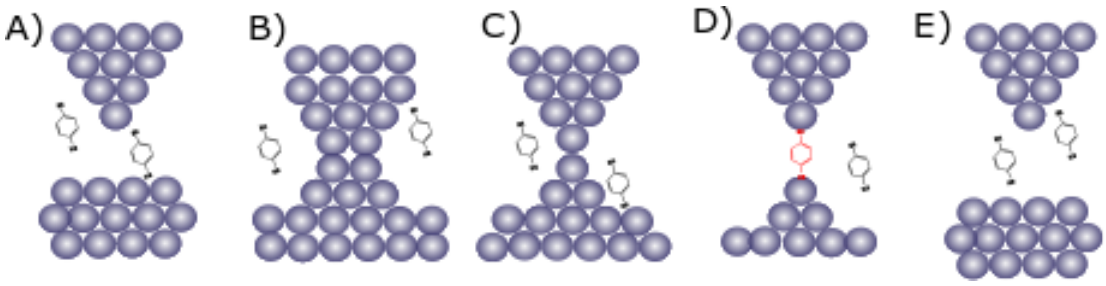

FIGURE 1.5. A schematic diagram showing the procedure of STM-BJ measurements. (A) The tip and substrate are in a solution containing molecules. (B) The tip is crashed into the substrate. (C) The tip is withdrawn. (D) A gap is formed between the tip and the substrate which is filled by a molecule forming a molecular junction. (E) The junction is broken and the process is repeated.

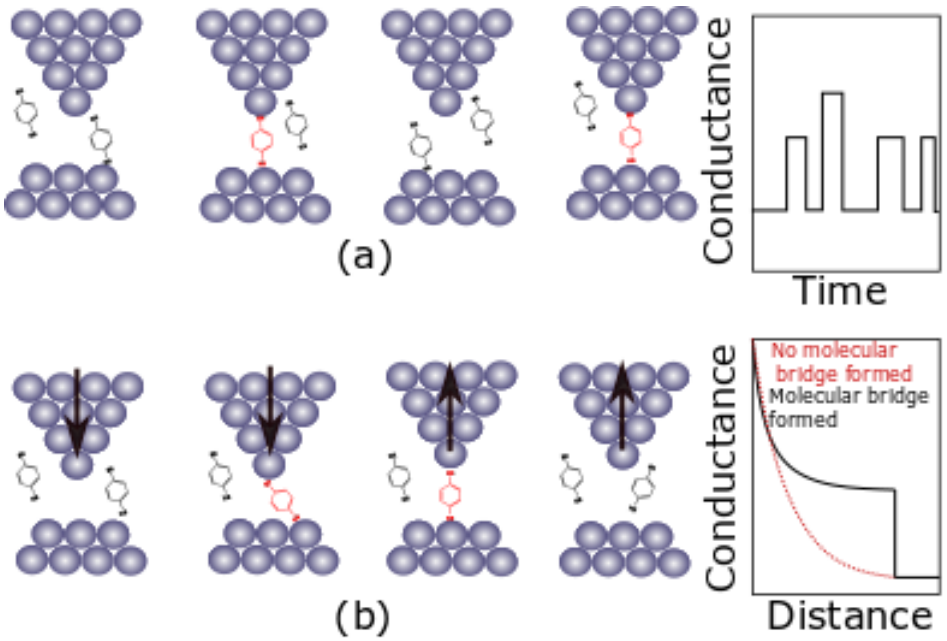

FIGURE 1.6. A schematic diagram showing the procedure and schematic examples of resultant conductance traces of soft touch STM-BJ measurements including (a) the I(t) technique (b) the I(s) technique where the red line shows schematic decay without a molecular bridge and the black line shows schematic decay when a molecular bridge is formed.

and breaking of molecular bridges between the tip and substrate. The I(s) procedure involves reducing the tip-substrate distances, to less than the length of the molecules. A fixed bias is applied and the current is measured as the tip is withdrawn from the surface. This process is explained further in Figure 1.6.

1.2.3 Electromigration

A problem in molecular electronics that needs to be overcome is the difficulty in creating nanoscale electrodes to contact the molecules. Electromigration is the transport of material caused by the gradual movement of ions in a conductor by the direct force (due to the electric field) or the force caused by momentum transfer between conducting electrons and diffusing metal atoms. When an electric field is applied to a metallic nanowire, the atoms of the metal migrate, resulting in the breakage of the nanowire. Although the effect is generally considered to be a negative one throughout electronics, causing huge numbers of failures due to the decreasing size of the metallic interconnects without reducing the current by the same factor, it can provide a valuable role in molecular electronics [35]. This process can be harnessed to form an electrode gap comparable to the size of a single molecule [97, 155]. As an electrical current is continuously ramped up, the resistivity is monitored and the process is stopped at the desired resistance. A large disadvantage of this method is that it is not easy, and sometimes impossible to fine tune the gap created. For example, it is not possible to close the wire again after it has been opened and it can be difficult to control the final stages of the electromigration process as the character of the transport changes from ohmic to wave-like [35]. These issues can be overcome by combining the method with MCBJ. A wire can be thinned out, creating a narrow constriction of approximately 10 nm which can then be bent and broken using an MCBJ.

1.2.4 Electrochemistry

Another way to overcome the difficulty in forming nanoscale electrodes is through use of electrochemistry [193]. A diagram explaining how this can be done is shown in Figure 1.7. Starting with metal electrodes that have a small gap (order of 1 μ m) between them, other metals can be deposited and dissolved onto or from one or both of the electrodes using a potentiostat. The current can be monitored so the deposition can be stopped when the electrodes are at an appropriate distance apart. Samples constructed in this way can then be used in conjunction with MCBJ to measure the conductance of single molecules. Typically gold is used as the electrode material as it is has weak chemical reactivity and silver is used for the formation of atomic contacts as it can be easily dissolved in acids and has well studied transport properties [160, 186]. This technique is particularly versatile as techniques have been developed for electrodeposition of a large number of metals. It is also simple and highly stable because there are no suspended parts. There are some disadvantages, such as the requirement to work in a liquid environment. It can, however, be combined with MCBJ to allow variation of the electrode separation in a dry environment.

1.2.5 Advantages/Disadvantages

There are many advantages and disadvantages to the use of both STM techniques and MCBJ techniques. The MCBJ benefits from high mechanical stability due to the short parts with high

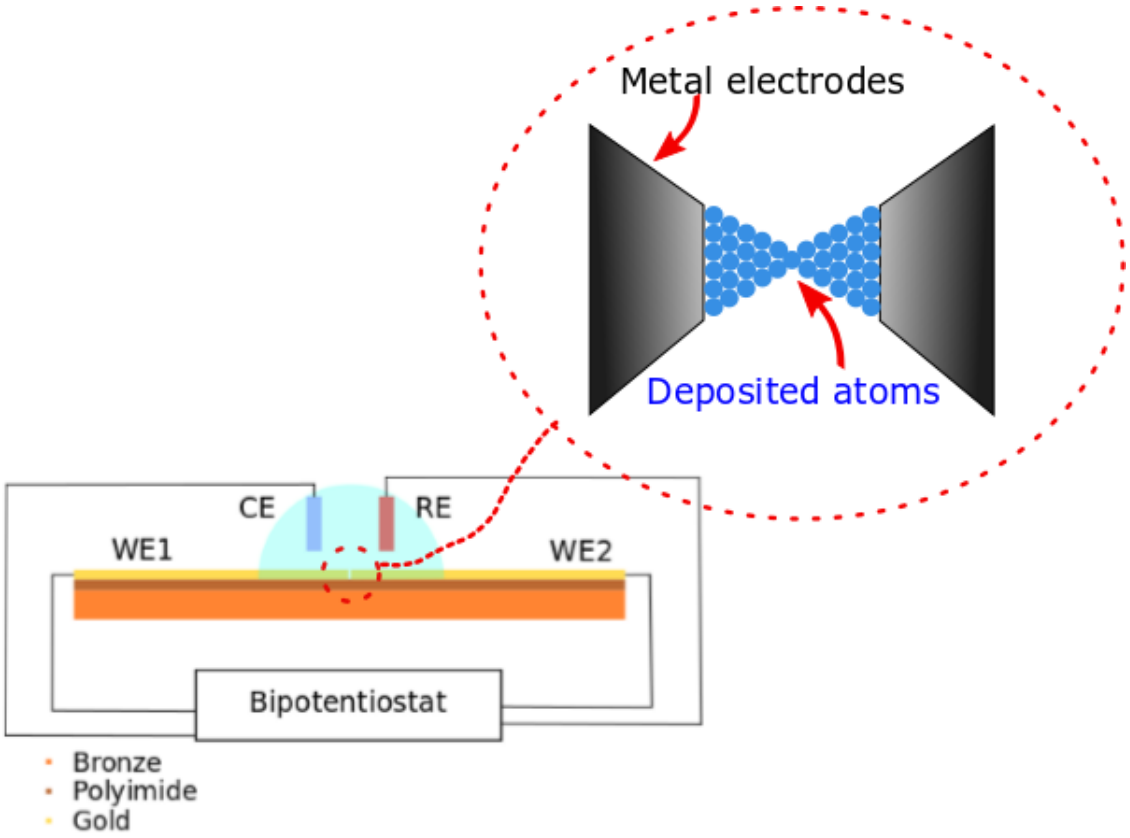

FIGURE 1.7. A schematic diagram explaining how electrodeposition can be used to create nanoscale electrode gaps using a droplet of solution (pale blue) across the electrodes. Where WE1 and WE2 are both working electrodes, CE is the counter electrode and RE is the reference electrode. A zoomed in version providing more detail of what happens between the electrodes is shown in the red ring.

resonant frequency. This enables measurements to be taken over longer time periods, something which has been demonstrated by Dulic and coworkers, who observed impressive stability of their MCBJ in the presence of the molecules [46]. This included metal-molecule-metal junctions maintained for 24 hours [46]. Another thing that contributes to the ability to take measurements over long periods of time is the electrode size gap controllability. Equation 1.8 shows that vertical movement of the piezo actuator translates to reduced horizontal motion of the electrodes. In fact, the ratio of these displacements can be as low as 10^{-6}, which allows for sub-Ångstrom control of the electrode separation [177]. This means that the influence of disturbances to the piezo actuator such as vibrations, thermal expansion or voltage instability on the electrode separation can be greatly reduced [184].

An MCBJ can be integrated more easily than an STM into other systems such as Raman spectroscopy which provides a useful tool to help identify molecules in the electrode gap [75, 184].

For example, Kaneko and coworkers used a hybrid technique (simultaneous surface enhanced Raman scattering and current-voltage measurements) to achieve single site-selection at a single molecule junction [75]. This is important as adsorption sites of molecules play an important part in the electric and photonic properties of the stability of the metal-molecule interface.

In MCBJ measurements, the influence of contaminants is low as the electrodes are formed during the experiments by breaking a notched wire, rather than prepared beforehand.

The STM has the ability to take measurements at a higher rate so it is possible to collect large quantities of data in much less time. It can be operated at breaking speeds of up to 100 nms^{-1} in comparison with the MCBJ which is generally broken at no more than 1 nms^{-1} [100, 161].

When using notched wire MCBJ samples, the wires are often notched using a scalpel. With this method it is difficult to be consistent in the notching process which leads to an unpredictable breaking process resulting in unpredictable electrode geometry. There is evidence to suggest that the interface geometry of a molecular junction can impact the measured conductance and so it is generally important to keep the geometry consistent [10]. It is not possible to analyse surface topography of the sample using MCBJ, which in some cases may make it less desirable that STM techniques. Soft touch techniques can be preferable in some circumstances as they tend to result in less damage to the tips or substrate when compared with break junction techniques. However, they often require data selection due to low junction formation probability.

1.2.6 Clean Room Techniques

1.2.6.1 Photolithography

Photolithography is a cost effective process used to pattern substrates covered in a layer of a photosensitive chemical by exposing areas of it to light. This photosensitive organic material is called photoresist. There are two types of photoresist; for positive photoresist, the regions that have been exposed to light are removed during development, for negative photoresist the opposite is true. Photolithography is a process that provides high precision patterning, and can create patterns on the tens of nanometer scale. The minimum feature size that can be fabricated is defined by the following equation:

$$CD = k_1 . \frac{\lambda}{NA}, \tag{1.9}$$

where CD is the minimum feature size or critical dimension, k_1 is a coefficient encorporating process-related factors and is generally equal to 0.4, λ is the wavelength of the light used and NA is the numerical aperture of the lens as seen from the substrate. This equation shows that reducing the wavelength of the light used will result in smaller minimum feature sizes. A schematic showing the processes involved in photolithography is shown in Figure 1.8.

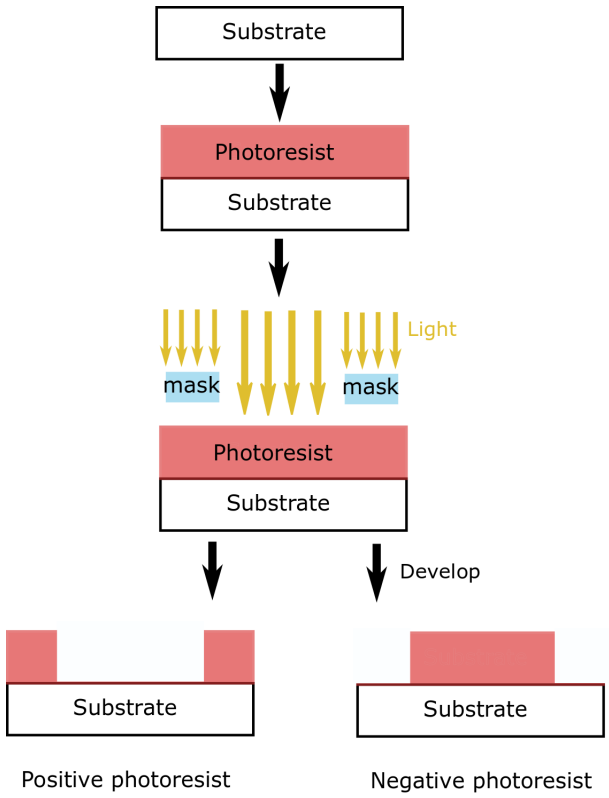

FIGURE 1.8. A schematic diagram showing the process involved in using photoresist for photolithography. First, the photoresist is spin coated onto the substrate and baked, then a mask is used to expose only certain areas of the substrate to light. Finally, a developer is used to reveal the desired pattern. If the photoresist used was negative, the regions exposed to light remain after development. If positive photoresist was used the areas that have been exposed to light are removed during development.

1.2.6.2 Thermal Evaporation

Thermal evaporation is used to deposit thin films onto substrates. A hot metal source will evaporate and the metal will then condense on the substrate. Since this process takes place in a vacuum, it allows the evaporated particles to travel to the substrate without interacting with background gas, which could result in a reaction and contaminate the thin film.

1.2.6.3 Reactive Ion Etching

Reactive ion etching (RIE) is a type of anisotropic, dry etching that uses chemically reactive plasma to remove material deposited on substrates. A standard RIE system, consists of two electrodes (labelled 1 and 4 in Figure 1.9). These create an electric field (labelled 3 in Figure 1.9) for the acceleration of ions (labelled 2 in Figure 1.9) towards the surface of the samples (labelled 5 in Figure 1.9). The ions in the system are formed when a strong radio frequency electromagnetic

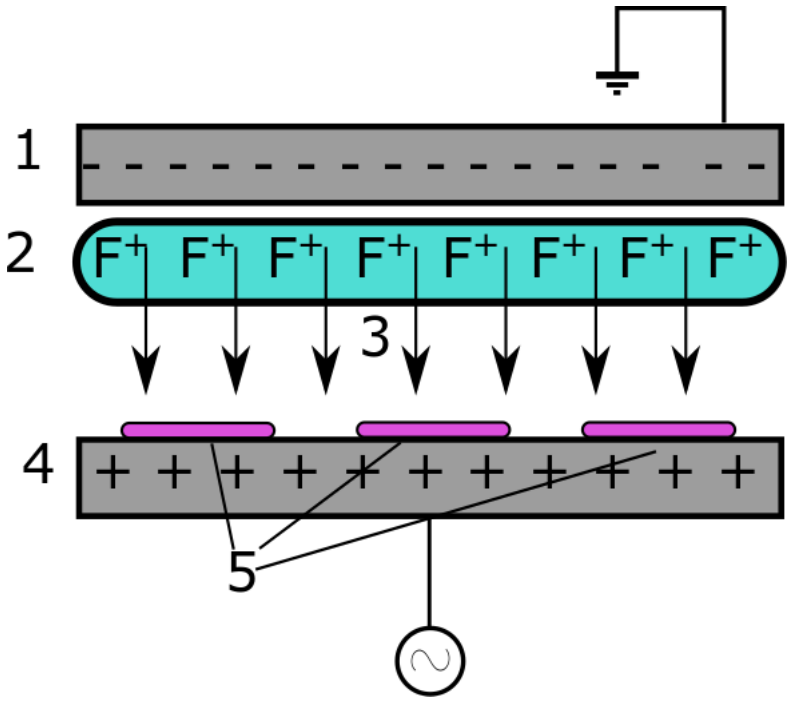

FIGURE 1.9. A schematic demonstrating the process involved in reactive-ion etching. 1 and 4 represent two electrodes that create an electric field (labelled 3) which is used to accelerate ions (labelled 2, F^+ represents the fluorine ions frequently present in the source gas for plasma.) towards the surface of the substrate being etched (labelled 5).

field is applied. It typically has a frequency of several megahertz, applied at a few hundred watts. This causes the gas molecules to become ionised by stripping their electrons which creates plasma. When the ions collide with the substrate surface, they physically sputter away.

1.3 Anchoring Groups and Contacts

Selecting appropriate molecules and contacts is crucial for successful molecular conductance measurements. For example, molecules in which a benzene ring or other conjugated moiety forms the backbone of the molecule are generally expected to show larger conductance values when compared to resistive alkane based molecules. This is because they tend to have smaller HOMO (highest occupied molecular orbital)-LUMO (lowest unoccupied molecular orbital) gaps which in turn produces a larger conductance as the Fermi level of the contacts will be more closely aligned with the energy of one of the conducting molecular orbitals resulting in a smaller barrier height for electron tunnelling.

Perhaps more important than the molecular backbone is the choice of anchoring group. The choice of anchoring groups on the end of a molecule can impact the junction stability, formation

probability, conductance, and current-voltage profiles including current rectification [126]. It is critical to have a "good" anchoring group if one wishes to obtain reliable binding of the molecule to the electrodes in order to achieve reproducible structures and electron transport from one device to another. A popular anchoring group in early molecular conductance measurements was the thiol (SH) group [59, 140, 188]. This is most likely due to its well established ability to form self assembled monolayers (SAMs) [128, 168].

More recently, the interest in combinations of anchoring groups and electrode materials, particularly using asymmetry has increased. Although some of the founding studies in molecular electronics were designed to show rectification using asymmetric molecular monolayers, the most well studied molecular junction systems remain symmetrical systems with similar anchoring groups at each end of the junction linked by gold contacts [114]. Asymmetric configurations provide an exciting opportunity in molecular electronics. They provide the possibility of new ways of generating electrical functionality, such as rectification, switching, molecular transistor behaviour and charge storage [62]. There have been studies where one gold contact is used in combination with a second contact made of graphite or graphene [29], or semiconductors including gallium arsenide and silicon [5, 173]. Examples of other studies carried out to investigate asymmetry in single molecule junctions include that by Martin *et al.* who demonstrated that the conductance of a series of molecules with asymmetric anchoring groups (SH-$(CH_2)_n$-COOH) will be lower than that of comparable symmetric molecules [108]. Both Wang *et al.* and Diez-Perez *et al.* have studied current rectification arising from asymmetric anchoring groups [43, 181]. Wang *et al.* investigated 1,4-disubstituted benzene molecular junctions and Diez-Perez *et al.* achieved single molecule current rectification by controlling the orientation of an asymmetric diblock dipyrimidinyldiphenyl molecule between two gold electrodes which responded as a single molecule diode. Also in this area, there have been interesting investigations into asymmetric hybrid Au-molecule-graphene junctions, using dithiol, diamine and dicarboxylic acid groups [99, 197, 198]. It was observed that asymmetric molecular junctions with a graphene bottom electrode contact results in a lower current attenuation factor than similar gold-molecule-gold junctions. Recently, the effect of asymmetric anchoring groups and electrodes was investigated by Yang *et al.* who measured the electronic transport in Au-S-$(CH_2)_n$-COOH-graphene molecular junctions. These results showed an unexpected trend, exhibiting a high conductance and smaller attenuation factor for the Au-S-$(CH_2)_n$-COOH-graphene configuration when compared with the equivalent symmetrical junction using the HOOC-$(CH_2)_n$-COOH series [62].

1.3.1 Anchoring Groups

1.3.1.1 Thiol

Alkanedithiols are possibly the most popular type of molecule used in conductance measurements. Alkane chains are generally considered to be poorly conducting as they have a large HOMO-LUMO gap, generally 7-9 eV, which essentially forms an insulating barrier between the electrodes

[85]. The charge transport across this barrier is predicted to occur via tunnelling along the methylene (-CH_2) backbone and can be described by the Simmons[1] tunnelling model. This prediction has been verified experimentally a number of times, where it has been observed that the molecular conductance decreases exponentially as a function of the number of methylene units present in the alkane chain [30, 93, 172, 188]. By varying the number of methylene groups, it is possible to study the molecular length dependence without significantly altering the HOMO-LUMO gap. This makes it easier to study isolated molecule-electrode contact effects [30]. This, combined with the simplicity in modelling the system and the strong affinity of sulphur to gold[2] explains why alkanedithiols are so frequently studied.

Another well studied thiol-ended molecule is 1,4-benzenedithiol (BDT). It is a conjugated molecule with one aromatic ring and a good candidate for molecular electronics due to the delocalized electrons in the molecule. There are a huge variety of conflicting theoretical predictions and experimental findings for the values of conductance of the Au | BDT | Au junction measured by different groups [60, 84, 90, 167, 185]. These predictions and findings show that the conductance may vary by over three orders of magnitude [90]. This is likely to be because the conductance is highly sensitive to microscopic details of the molecule-electrode contact, so that a change in junction geometry can result in a large variation in conductance [185]. If the variations of the geometry, and hence the conductance, of the MMMJ can be controlled, this would provide an exciting step towards single molecule devices [76, 84]. It has also been shown that the stretching of the junction as the conductance is measured can result in variations in conductance [21]. This is due to changes in the metal-molecule bond length and configuration. The variations in conductance measured can generate up to three different conductance groups for thiols, often referred to as top, hollow and bridge [159]. These positions are described in Figure 1.10. The top position is thought to result in the lowest conductance and orginates from a single bond between the sulphur and gold atoms on each head group. It is most likely to occur on flat surfaces. The bridge position results in a higher conductance than the top position. It is predicted that it originates from adsorption of one head group at a step edge, which increases the wavefunction overlap of the molecule and the electrode is is coupled with. Finally, the hollow position is when both head groups adsorb at a step edge. This increases the coupling even further [58].

1.3.1.2 Nitrogen

Amine terminated alkanes will form a stable monolayer on gold nanocrystals. The nature of this binding is best described by a weak covalent bond [92, 135]. It has been demonstrated that

[1] Used when V<ψ_b where V is the applied bias ψ_b is the height of the potential barrier between the electrodes. When V«ψ_b, the model is simplified to a linear form resulting in approximately ohmic conductance[95, 174] According to the Simmons model, the potential barrier shape is dependent upon the geometric structures of a junction. Hence, a single molecule junction can have a number of conductance values [69]

[2] Au–S bonds are very strong when compared with Au–Au bonds. Lifetime measurements of single molecule measurements have suggested that the breakage of a single-molecule junction with an Au–S bond breaks the Au–Au bond close to the Au–S rather than the Au–S bond itself. [158]

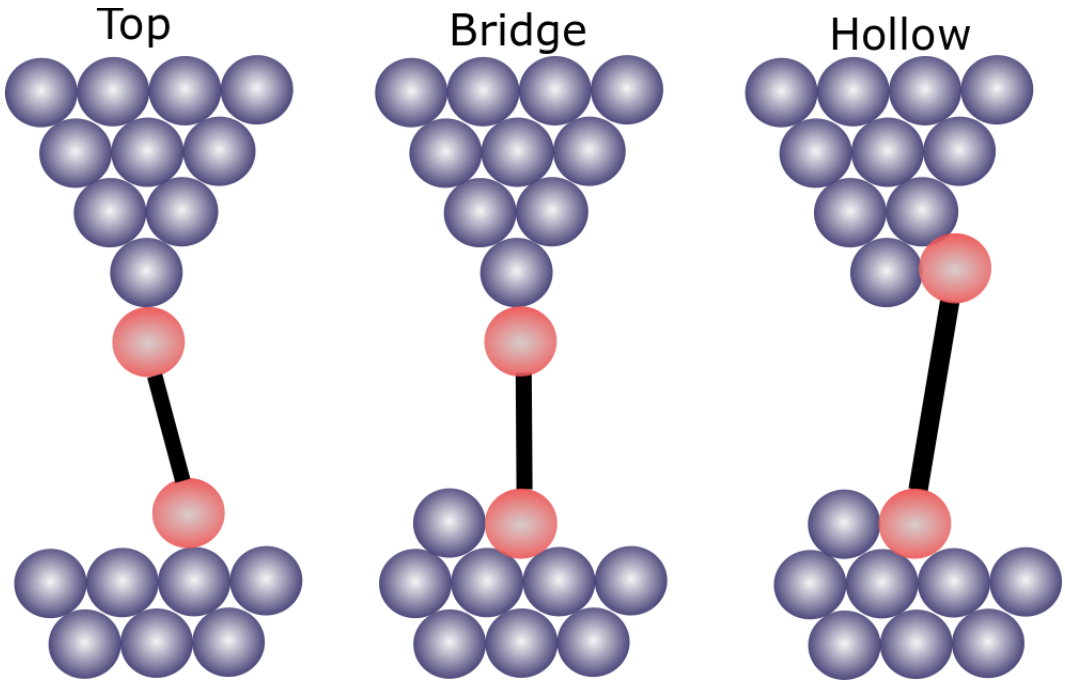

FIGURE 1.10. A schematic diagram showing some of the commonly proposed sulphur-gold bonding sites, known as top, hollow and bridge, as described in Section 1.3.1.1. The sulphur atoms are shown here in red, linked simply by a black line which represents the rest of the molecule.

amine anchored molecules can provide results with reproducible and well defined conductance values [67, 139, 172]. Venkataraman *et al.* used this well defined conductance to suggest that the only binding mechanism between the amine anchor and gold electrodes was due to the lone pair on the nitrogen atom bonding to coordinatively unsaturated gold atoms [172]. This was then tested by adding steric bulk around the nitrogen atom which diminished the molecular bond formation [172]. Another molecule anchored by nitrogen is 4,4'-bipyridine (4,4'-BP). 4,4'-BP has two lone electron pairs at each nitrogen atom. It was first studied by Xu *et al.* in their pioneering STM-BJ work [188]. They observed peaks in the conductance histogram at 0.01 G_0, 0.02 G_0 and 0.03 G_0. When explaining these findings, they suggested that each peak corresponded to measurements taken with one, two or three 4,4'-bipyridine molecules present in the junction. Quek *et al.* measured the high and low conductance values of 4,4'-BP to be 6×10^{-4} G_0 and 1.6×10^{-4} G_0, they also demonstrated that it is possible to reversibly switch between the high and low conductance states of the Au | 4,4'-BP | Au junction by repeatedly elongating and compressing the junction [138]. The low conductance state is measured when the the nitrogen-gold bond is perpendicular to the π-system. This is a weaker molecule-substrate coupling than the high conductance state, which is achieved in more compressed junctions when the molecule is tilted. This results in stronger electronic coupling between the molecule and gold contact, this is shown

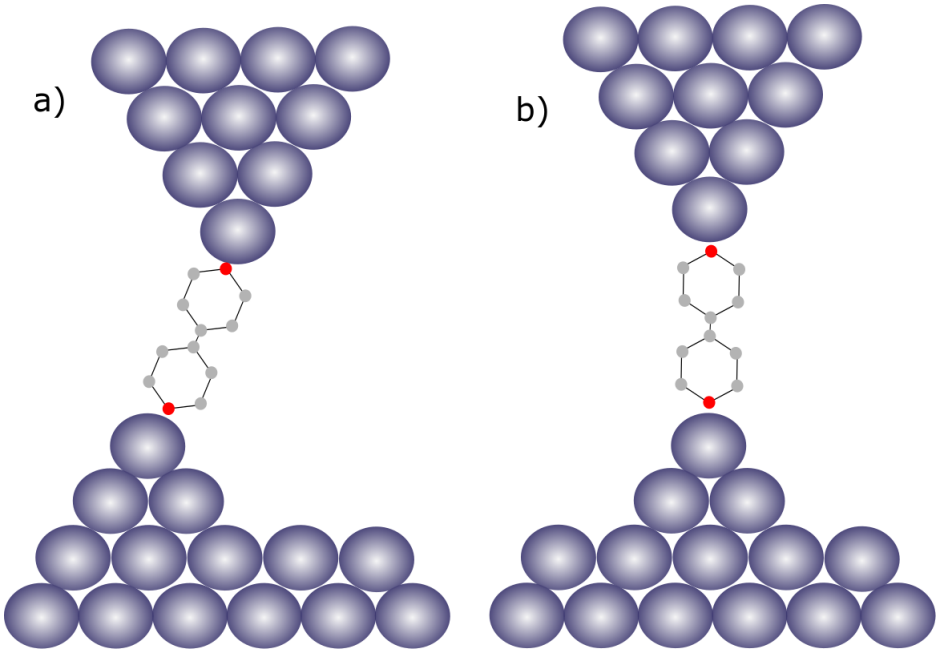

FIGURE 1.11. Schematic showing the potential junction geometry configurations of 4,4'-BP. a) The molecule is tilted between the electrodes, resulting in higher conductance. b) The molecule is linear between the electrodes, resulting in low conductance.

in Figure 1.11. [126, 138]. As the conductance values they obtained have been determined during a number of different experiments and theory works, it has been accepted that these are the most probable values for Au | 4,4'-BP | Au single molecule junctions [4, 16, 55, 74, 83]. Interestingly, in contrast to the Au | 4,4'-BP | Au junction, the Ni | 4,4'-BP | Ni junction does not show two distinct conductance states. It is has been suggested through DFT-based calculations that the conductance of a 4,4'-BP molecule contacting a nickel electrode is insensitive to the contact binding angle [19].

1.3.1.3 Other Interesting Work

In 2018, Kiguchi and co workers studied the formation of a chain-like water single molecule junction with Pd electrodes [48]. They investigated the interaction between the water molecule and Pd electrodes at cryogenic temperatures using the MCBJ technique. They found that the electronic transport through a single water molecule takes place via ballistic regime and that the molecular conductance of water was around 1 G_0. They confirmed these measurements using vibrational spectroscopy where the water-Pd vibrational mode of 70 meV was measured [48].

Pure carbon molecules such as fullerenes are promising candidates for molecular electronics. For example, C_{60} has a completely delocalized π system which makes it a good choice for electronic applications [69].

There have been a number of studies measuring the electrical conductivity of DNA molecules [36, 56, 149]. These provide applications of single molecule junctions outside of electronics.

One of these applications is a single-molecule quantum sequencer that reads DNA base and peptide amino acid sequences at the single-molecule level. Another application is as a sensor that enables detection of attomole RNA. Theoretical calculations have shown that the single-molecule conductance of DNA-RNA is dependent on its structure, and changes depending on base sequences [96, 158].

1.3.2 Contact Metals

The most commonly studied electrode material in molecular electronics is gold. This is because it offers high stability, an oxide free surface under ambient conditions, good electrical conductivity and compatibility with a large range of chemical anchoring groups [126]. The use of indium tin oxide, palladium and platinum have also been demonstrated in some experiments [29, 48, 85, 168]. Pd and Pt are group 10 elements with stronger d-orbital characteristics, and a larger local density of states near the Fermi level. Hence, the preferable binding configuration and the strength of molecules on Pd and Pt were expected to be different from those on Au, a group 11 element exhibiting relatively strong s-orbital contributions [148]. It was observed in the work of Chen *et al.* that for thiol-Pt bonds, the conductance was almost twice as large as thiol-Au bonds. They also measured the conductance of the isothiocyanate-Pt bond to be up to 3.5 times greater than the isothiocyanate-Au conductance and 1.5 times greater than the isothiocyanate-Pd conductance [29]. This demonstrates the significance of the choice of metal when measuring the conductance and the importance of the molecule-metal bond. This idea has been explored further by Venkataraman and coworkers who showed that SAM measurements of dithiol-terminated molecular junctions exhibit significantly lower conductance than solution measurements of the same molecule [68]. They suggested that this is due to the linking mechanism of the molecule, claiming that the gold-sulphur bond of the SAMs does not have a chemisorbed character. In contrast, the gold-sulphur bond formed during measurements with the molecule in solution is likely to have a chemisorbed character, which resulted in differences in the conductance measured.

Electrodes can be selected to result in specific effects within a device. For example, Batra *et al.* used a symmetric, conjugated molecular backbone with a single methylsulfide group linking one end to a gold electrode and a covalent gold-carbon bond at the other end to provide current rectification through a single molecule [11]. Indium tin oxide is electrically conductive and optically transparent, which has led to many applications in organic light emitting diodes and photovoltaic devices [25].

It is possible to take measurements using ferromagnetic electrodes if one is investigating spintronic properties of a metal-molecule-metal junction. The surfaces of these metals oxidise quickly in ambient conditions, however it is possible to use electrochemistry to keep the surface oxide free and hence take measurements with the bare substrate surface [19].

Conduction mechanism	**Characteristic behaviour**	**Temperature dependence**	**Voltage dependence**
Direct tunnelling	$J \sim V exp\left(-\frac{2d}{h}\sqrt{2m\phi B}\right)$	none	$J \sim V$
Fowler-Nordheim tunnelling	$J \sim V^2 exp\left(-\frac{4d\sqrt{2m}\phi_B^{3/2}}{3qhV}\right)$	none	$ln(\frac{J}{V^2}) \sim \frac{1}{V}$
Thermionic emission	$J \sim T^2 exp\left(-\frac{\phi_B - q\sqrt{qV/4\pi\epsilon d}}{k_B T}\right)$	$ln(\frac{J}{T^2}) \sim \frac{1}{T}$	$ln(J) \sim V^{1/2}$
Hopping conduction	$J \sim V exp\left(-\frac{\phi_B}{k_B T}\right)$	$ln(\frac{J}{V}) \sim \frac{1}{T}$	$J \sim V$

Table 1.1: Possible conduction mechanisms, where J is the current density, V is the bias voltage, ϕ_B is the barrier height, d is the barrier length and T is the temperature.[91]

1.3.3 Molecular Electronics

The energy state of a typical single molecule when it is connected between two metal electrodes is shown in Figure 1.12. The electrodes have a continuum of electronic states which are filled up to the Fermi level, E_F, which is located between the HOMO and the LUMO. In contrast, the electronic properties of an isolated molecule can be described in terms of discrete energy levels separated by energy gaps. When considering electronic transport through an MMMJ, it is often sufficient to consider only the HOMO or the LUMO as the HOMO-LUMO gap can reach several eV or more and generally molecules are either HOMO or LUMO conductors depending on which of the conducting energy levels aligns closest with E_F [158]. When a molecule interacts with the electrodes, the discrete molecular energy levels become broadened due to hybridisation of the molecular orbitals with the delocalised wave functions of the metal electrodes. The greater the overlap between the molecular orbitals and the contacts, the greater the density of states available and hence, the greater the energy spread [38]. It is the degree of broadening of the molecular orbitals that distinguishes between weak and strong coupling. Fractional charge transfer between the metal and molecule results in the formation of an electric dipole, which can lead to a shift of the molecular orbitals relative to the metal Fermi level. Although here I have assumed that a single-molecule junction only experiences resonant tunnelling, in reality, multiple conducting mechanisms such as hopping and coulomb blockade can coexist, making it difficult to fully explain experimental results [78, 110].

1.3.4 Identifying the transport mechanism in single-molecule junctions

Some of the potential conduction mechanisms and their characteristic temperature and voltage dependencies of the current are shown in Table 1.1. One of the best ways to determine which transport mechanism is taking place is by assessing the I-V characteristic of a metal-molecule-metal junction. The temperature dependence of the I-V characteristics is also an important

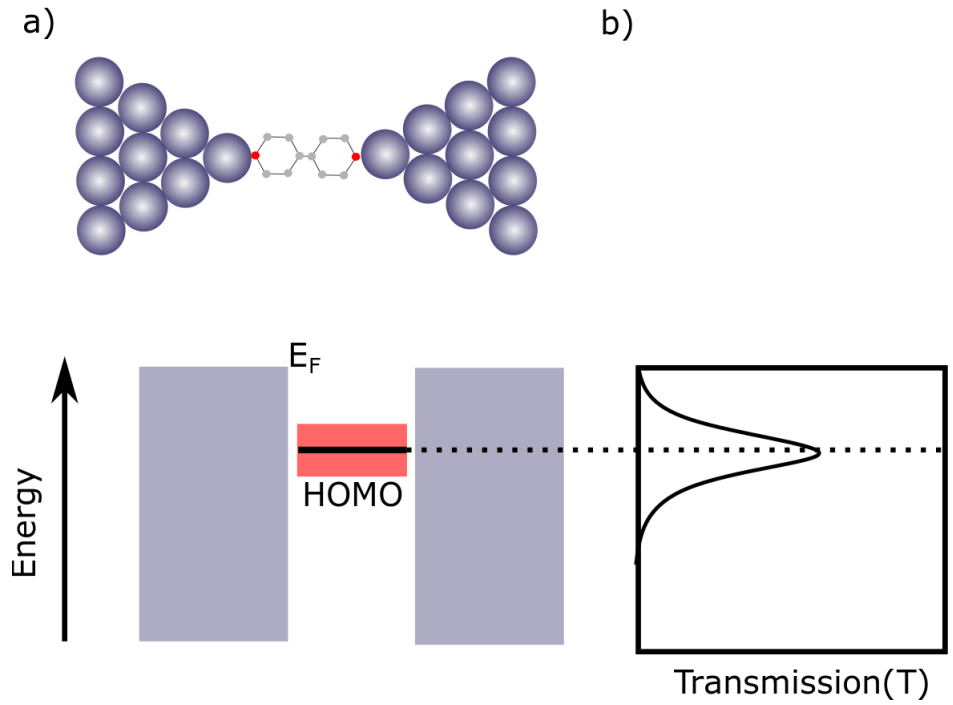

FIGURE 1.12. Schematic showing the a) energy diagram and b) energy transmission at zero applied bias diagram of a molecular junction adapted from [158].

tool.

1.4 Spintronics

Spintronics is the study of electron spin and its transport in a material. Spin dependent effects such as magnetoresistance are commonly studied, and have led to developments in devices such as faster data processing speeds and lower power consumption [137].

Ferromagnetism describes how materials including iron, cobalt and nickel form permanent magnets. Magnetic moments of individual atoms within a ferromagnetic material are caused by the incomplete filling of 3d or 4f electron shells. For the transition metals, which exhibit magnetism due to unfilled 3d electron shells, the magnetism is itinerant. For the rare earth metals, which exhibit magnetism due to unfilled 4f orbitals, the magnetism is localised. When the temperature is below the Curie temperature, these individual magnetic moments are aligned by the so-called exchange interaction. This results in spontaneous splitting of the electronic bands which leads to a net spin imbalance, causing a spontaneous magnetic moment. In contrast, paramagnetism is a form of magnetism where some materials including aluminium, oxygen and titanium exhibit temporary magnetism when they are exposed to an externally applied magnetic field. The presence of unpaired electrons in the material is responsible for paramagnetism. The external magnetic field causes unpaired electrons which have a magnetic dipole moment to align

parallel to the field, resulting in a net attraction. Al and Ti exhibit Pauli paramagnetism which occurs in metals and is described by the tendency of free electrons in metals (which form a Fermi gas as they are weakly interacting and delocalised in space) to align with external magnetic fields. In contrast, regular paramagnetism occurs when there are unpaired electrons in an orbital structure according to Hund's rules. Pauli paramagnetism is generally weaker than regular paramagnetism as stronger forms of paramagnetism tend to require localized electrons.

In contrast to electronic transport in Au contacts (which, as mentioned previously, have a conductance of almost exactly 1 G_0 due to a single conduction channel from the Au half-filled 6s band, which has almost 100% transmission), transport in transition metals, including ferromagnetic atomic contacts is more complex. This is due to the additional influence of conduction channels from the d-orbitals. The conductance of ferromagnetic electrodes has been investigated experimentally by a number of groups [33, 42, 70, 79, 88, 101, 119]. Several conflicting results have been reported. For instance, groups report seeing peaks in their conductance histograms at half-integer multiples of G_0 [34, 129, 130]. This was initially interpreted as half-integer conductance quantization, suggesting the existence of a fully spin polarised current [35]. However, it is now thought that those peaks could be a result of the adsorption of hydrogen molecules on the electrodes [79, 88].

In contrast, some groups have observed featureless histograms at room temperature or with a single peak above 1 G_0 at low temperatures [170]. These differences were explained by the fact that room temperature experiments in ambient conditions are more susceptible to contamination by foreign atoms or molecules, a concept which is supported by the evidence of the impact hydrogen molecules can have on the measured conductance [79].

Theoretical studies have suggested that one would not expect to observe any kind of quantization in ferromagnetic materials due to the fundamental role of the d bands in their electronic transport. [37, 57]. This idea is supported by Figure 1.13. For all three ferromagnets shown, the Fermi level for the minority spins lies inside the d bands, suggesting a significant role of the d orbitals in transport. The Fermi level is close to the edge of the d band for the majority spins. Theoretical studies have also been able to predict the conductance of Fe, Co and Ni contacts. Figure 1.14 shows the total transmission for majority and minority spins as a function of energy (here we have assumed that spin up denotes majority spins and spin down denotes minority spins), and the individual transmission coefficients for those geometries [57]. This allows us to compare electronic transport between different ferromagnetic contacts. It can be seen in the Figure that for Fe, there are 3 majority spin channels, yielding $G_\uparrow = 1.24e^2/h$. In addition to this there are 3 minority spin channels contributing $G_\downarrow = 0.7e^2/h$, resulting in a total conductance of $0.97G_0$ and a polarization (the degree to which spin is aligned in a particular direction) $P = +28\%$. For the Co contact, the total conductance is approximately 1.6 G_0, formed from 3 majority spin channels and 6 minority spin channels, $G_\uparrow = 0.9e^2/h$ and $G_\downarrow = 2.23e^2/h$. The polarization is $P = -42\%$. Finally, the Ni contact has a total conductance of $1.8G_0$, with a single majority channel contributing

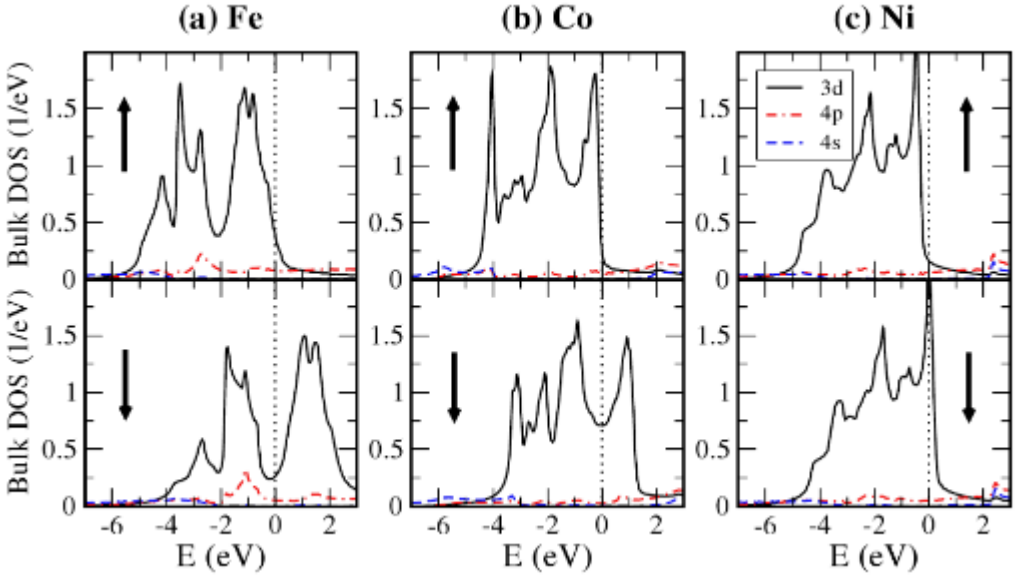

FIGURE 1.13. Spin resolved bulk density of states of iron, cobalt and nickel, shown with respect to individual contributions of 3d, 4s and 4p orbitals. Dashed vertical line here represents the Fermi level This diagram is reprinted from [57] Copyright 2008 by the American Physical Society.

$G_\uparrow = 0.86e^2/h$ and 4 minority channels contributing $G_\downarrow = 2.66e^2/h$. The polarization is $P = -51\%$ [57]. What we can conclude from the analysis of Häfner *et al.* is that both spin bands play a significant role in the electronic transport in ferromagnetic single-atom contacts. In addition, the d bands contribute significantly to the conductance of minority spins and result in several conductance channels. For iron electrodes, the contribution from the majority spins is dominated by d and s orbitals. In contrast, for cobalt and nickel, s orbitals have the most significant role in transport.

In 1936, Nevill Mott hypothesized that since d-states are responsible for ferromagnetic or paramagnetic behaviour in transition metals, there should be a direct link between the electrical conductivity of these metals and their magnetic properties [122]. In support of this hypothesis, Mott observed that the resistivity of nickel increases suddenly when the temperature increases past the Curie temperature. Explaining this result, Mott stated that below the Curie temperature, the unoccupied d-states acquire a spin direction antiparallel to the local magnetisation. Hence, only electrons with a spin antiparallel to the local magnetisation could be excited into a d-state. This reduces the number of electrons excited into traps. However, close to the Curie temperature, unoccupied d-states of each spin direction increase the chance of such a state becoming occupied by a conduction electron, thus explaining the observed increase in resistivity close to the Curie

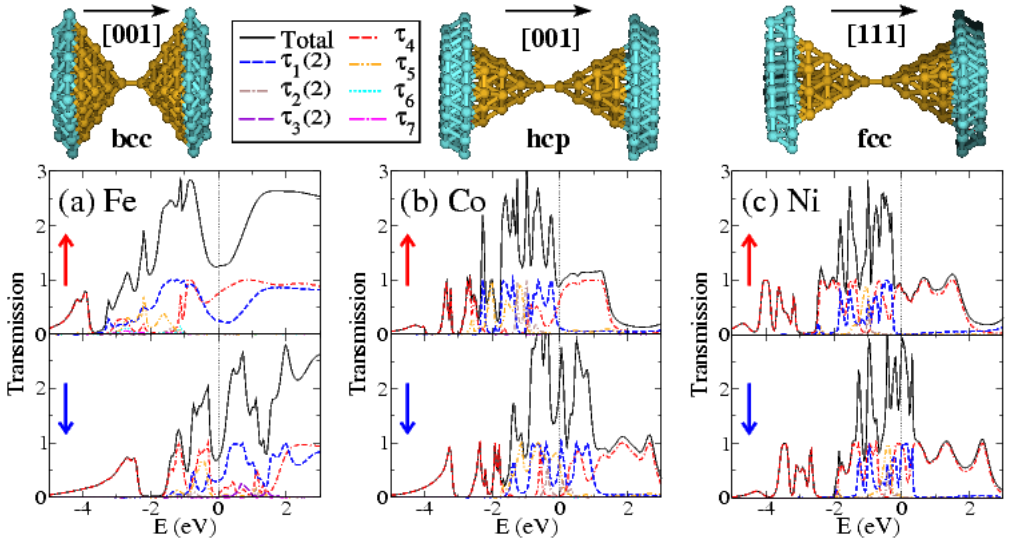

FIGURE 1.14. Transmission as a function of energy for the three single-atom contacts of (a) Fe, (b) Co, and (c) Ni, which are shown in the upper panels. We present the total transmission (black solid line) for both majority spins and minority spins as well as the transmission of individual conduction channels that give the most important contribution at the Fermi energy, which is indicated by a vertical dotted line. The blue, brown and violet dash-dotted lines of τ_1, τ_2, and τ_3 refer to twofold degenerate conduction channels. The legends in the upper graphs indicate in which direction the contacts are grown. These contacts contain in the central region 59 atoms for Fe, 45 for Co, and 39 for Ni. The blue atoms represent a part of the atoms of the leads (semi-infinite surfaces) that are coupled to the central atoms in the model.This diagram and caption are reprinted from [57] Copyright 2008 by the American Physical Society.

temperature, and the observed decrease upon application of a magnetic field [122]. The main source of resistance in transition metals is the scattering of the conducting 4s electrons into less mobile 3d states which act as trap states. This explanation is enhanced by the diagrams shown in Figure 1.15. For ferromagnets, there is less chance of a conduction electron from an s-state, scattering into a d-state because fewer d-states are available. This leads to the concept of minority and majority spin channels which is where, during conduction spins in either state experience higher and lower resistances respectively. The shift in band structure causes a net spin imbalance due to the presence of minority and majority spin states. Due to the asymmetrical spin transport properties a ferromagnet can be used as a source of spin polarised carriers.

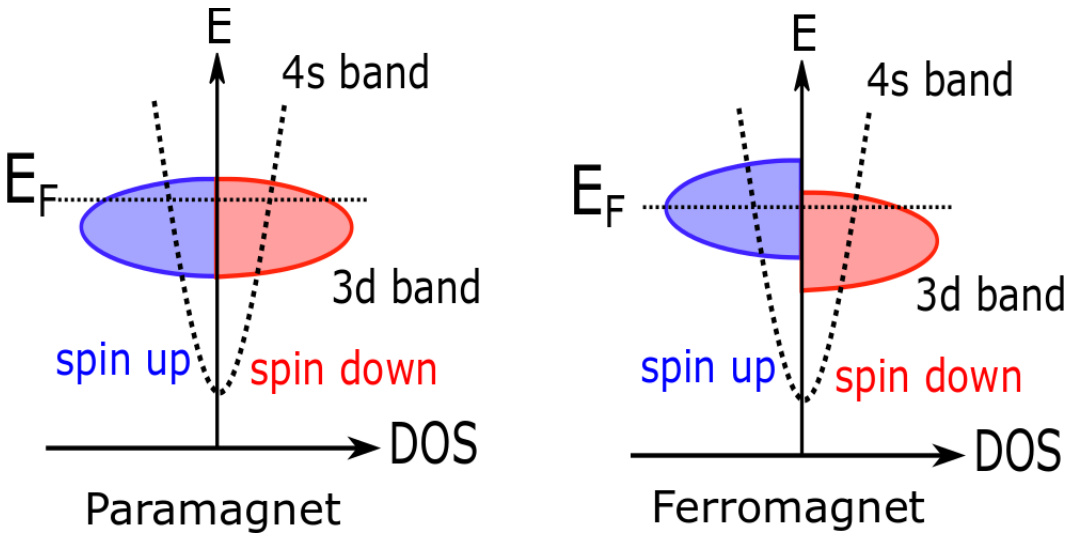

FIGURE 1.15. Schematic showing the density of states of a ferromagnet and a paramagnet for transition metals in the first row of the periodic table with partially filled d-states.

1.4.1 Magnetoresistance

Magnetoresistance is defined as the change in electrical resistance of a material upon the application of a magnetic field. It can be described mathematically by the following equation

$$MR = \frac{R_H - R_0}{R_H} \times 100\%, \tag{1.10}$$

where R_H is the resistance in the presence of a magnetic field and R_0 is the resistance with no field applied. The following sections detail some of the types of magnetoresistance.

1.4.1.1 Giant Magnetoresistance

In 2007, the Nobel prize for physics was jointly awarded to Albert Fert and Peter Grünberg for the discovery of Giant Magnetoresistance (GMR). GMR is a quantum mechanical effect that can be observed in multilayers composed of alternating ferromagnetic and non-magnetic conductive layers. In the cases of Fert and Grünberg, they independently observed a large magnetoresistance in layered iron/chromium/iron structures [8, 13]. For Grünberg, the magnetoresistance was observed to be in the region of 1.5% at room temperature, increasing further to around 10% when measured at around 5K. A larger magnetoresistance was measured at 5K by Fert [8, 13]. The effect is dependent on whether the magnetisation of the ferromagnetic layers are in parallel or antiparallel alignment, this can be controlled by applying a magnetic field. The result is minimised resistance for parallel alignment and maximised resistance for antiparallel alignment. This effect is explained by Mott's two-current model as shown in Figure 1.16. This model is based on the fact that the resistivity is due to electron scattering [72]. In magnetic materials,

this is dependent on spin orientation. When the magnetic layers have antiparallel alignment, the spin-up electrons can travel easily through the first magnetic layer. However, the second magnetic layer has opposite magnetisation and so they experience strong scattering. Similarly, the spin-down electrons experience enhanced scattering in the first magnetised layer but travel easily through the second. When the magnetic layers have parallel alignment, one of the spin channels experiences enhanced scattering in both layers and in the other, spin polarised electrons can travel easily through both layers. This results in a minimised resistance overall. The effect on resistance is shown by a schematic of the change in resistance as a function of the applied magnetic field in Figure 1.17. The GMR effect is exploited for spin valves; these are devices whose electrical resistance can be altered depending on the alignment of the magnetization of the two or more conducting magnetic materials that are separated by a non-magnetic material to form the spin valve. The main applications of the GMR effect is in magnetic field sensors which may include hard disk drives (though the use of tunnelling magnetoresistance in Fe/MgO layers is now standard for this practise) and magnetic RAM.

1.4.1.2 Tunnelling Magnetoresistance

Tunnelling magnetoresistance (TMR) is an effect, similar to GMR that can occur in magnetic tunnel junctions (MTJ). A magnetic tunnel junction consists of two ferromagnetic layers separated by a thin (typically a few nanometres) insulating layer. The thinness of the insulating layer allows electrons to tunnel quantum mechanically from one ferromagnetic layer to the other. A TMR of approximately 14% was first observed by Michel Jullière in Fe/Ge/Co junctions at 4.2K in 1975 [73]. Jullière explained the TMR effect with the spin polarisations of the ferromagnetic electrodes, where the spin polarisation can be calculated from the density of states at the Fermi energy which is shown in the equation below.

$$P = \left. \frac{DOS_{spinup} - DOS_{spindown}}{DOS_{spinup} + DOS_{spindown}} \right|_{E=E_F}, \tag{1.11}$$

In this case, the spin-up electrons are oriented parallel to the external magnetic field and the spin down electrons are oriented antiparallel to the external magnetic field. The TMR ratio is then given by the spin polarisations of the two ferromagnets, P_1 and P_2 using the following equation:

$$TMR = \frac{2P_1P_2}{1 - P_1P_2} \tag{1.12}$$

In 1991, the effect was observed again by Miyazaki, who initially found a TMR of 2.7% in room temperature experiments, though this increased to 18% when using iron/aluminium oxide/iron MTJs [116]. More recently the TMR effect has been used for tuneable wireless communication [89].

TMR arises because of a change in the probability that an electron will tunnel across the insulating barrier. This can be explained using Mott's two-current model and the diagram

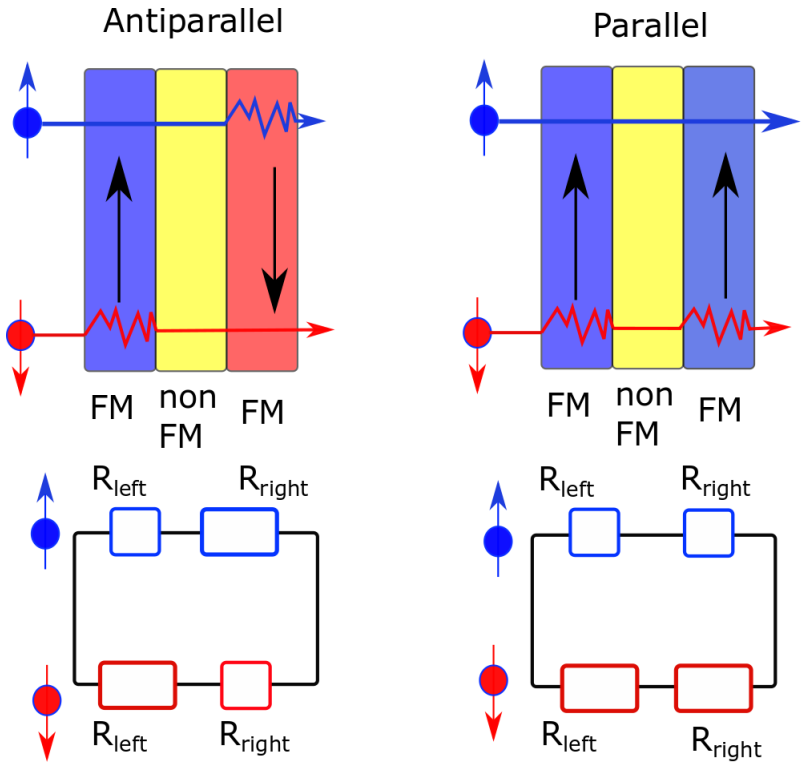

FIGURE 1.16. Schematic diagram explaining the giant magnetoresistance effect, showing the difference in scattering of electrons of different spin in the layers of the magnetic | non-magnetic | magnetic structure when the layers have antiparallel or parallel magnetisation. Black arrows represent magnetisation direction, red and blue arrows represent the direction of spin. Circuit diagrams portray a representation of the different resistance spin up or spin down electrons may experience when passing through different layers of the structure.

shown in Figure 1.18. When the ferromagnetic layers of an MTJ are magnetised in antiparallel alignment, the spin up electrons have a large density of states at the fermi level in the left electrode and a low density of states in the right electrode. In contrast, the spin down electrons have a low density of states at the fermi level in the left electrode and high in the right. If a bias is applied to the MTJ and the current flows from left to right in the system, spin up electrons dominate the current due to their high density of states and spin down electrons contribute very little to the current. If the ferromagnetic layers in the MTJ are magnetised with parallel alignment, the majority spin carriers (spin up) will tunnel into the majority states, indicated in blue Figure 1.18. The minority spin carriers (spin down), will tunnel into the minority states, indicated in red in Figure 1.18. This results in an increase in probability that the electrons will tunnel and hence a lower resistance.

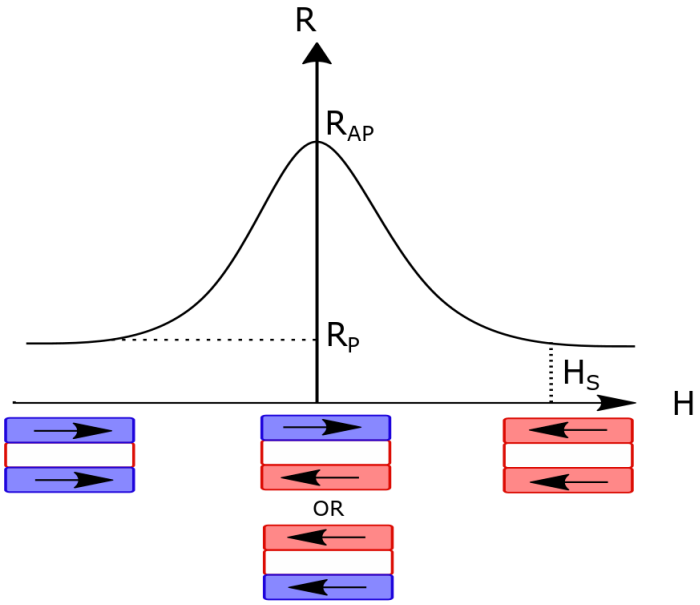

FIGURE 1.17. Schematic diagram showing how resistance varies with magnetic field strength and orientation during GMR. R_{AP} is the resistance when the magnetic alignment of the ferromagnetic layers is antiparallel, R_P is the resistance when the magnetic alignment of the ferromagnetic layers is parallel

1.4.1.3 Anisotropic Magnetoresistance

Anisotropic magnetoresistance (AMR) was first observed around 1856 by William Thomson, who observed variation in the resistance of iron and nickel samples with the direction in which a magnetic field was applied [162]. He saw that when a magnetic field was applied to Ni and Fe samples in parallel with the current flow, the resistance increased. The resistance was noted to decrease in these samples when the magnetic field was applied perpendicular to it, whilst measurements with brass samples showed no change in resistance. This effect is a result of how the magnetisation direction of a sample relative to the current flow will impact the amount of scattering conduction electrons experience. The scattering arises from spin-orbit interaction. When the magnetisation direction is parallel to the current flow, the resistance is maximised, and minimised when the magnetisation direction is perpendicular to the current [182]. Quantitatively, the AMR ratio can be described by

$$AMR = \frac{R_{\parallel} - R_{\perp}}{R_{\perp}}, \tag{1.13}$$

The resistance can be described as a function of the angle between the magnetisation and the current flow which follows a $cos^2\theta$ relationship [182].

Although AMR is usually a small effect in the bulk which only changes the resistance of the metal by a few percent, anisotropic magnetoresistance with magnitudes up to 50% have been

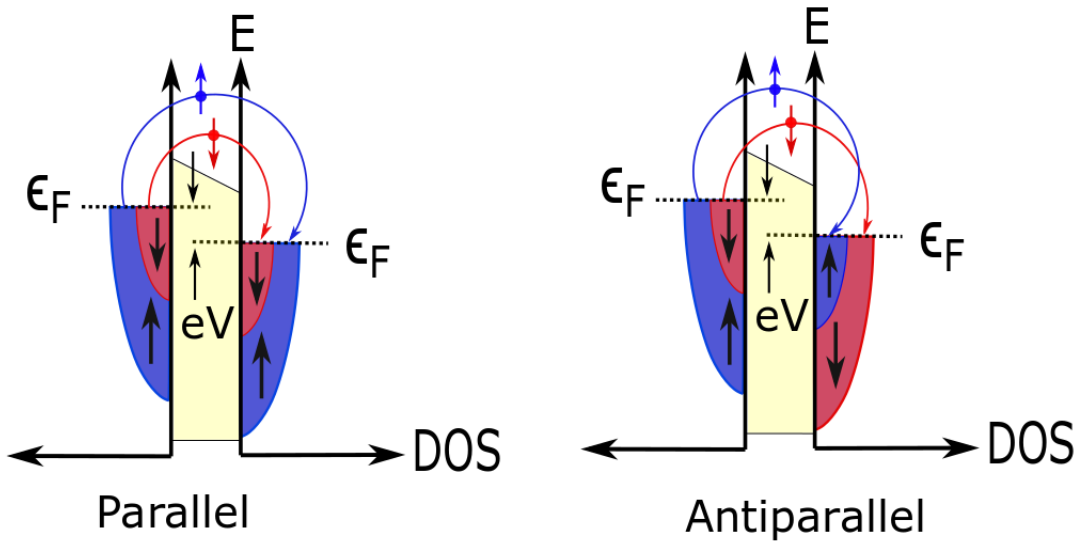

FIGURE 1.18. Schematic diagram explaining TMR, explaining the difference in probability for electrons of different spin to tunnel between the ferromagnetic layers through an insulating barrier. Arrows are used to represent spin direction.

observed in some ferromagnetic uranium compounds and more recently it has been possible to demonstrate the giant AMR reaching 160% at low-T in a simple resistor plate of spin-orbit coupled AFM Sr_2IrO_4 single crystal [182] [179].

1.4.1.4 Tunnelling Anisotropic Magnetoresistance

Tunnelling anisotropic magnetoresistance (TAMR) occurs when tunnelling takes place into a material with large spin-orbit coupling and magnetic anisotropy [53]. Magnetic anisotropy is a description of the magnetic properties of a magnet and their dependence on the direction in which the magnetic field is applied. TAMR results from the strong coupling between the holes and the system of the material. This translates the magnetic anisotropy into an anisotropy in the transport density of states. In this process, only one ferromagnetic electrode is required [24]. This effect was first observed by Gould and coworkers, who observed a spin-valve like behaviour of 3% amplitude in a Au/AlO_x/(Ga,Mn)As tunnel structure [54]. Since this first observation there

have been a number of investigations concerning TAMR [23, 24, 32, 180].

1.4.2 Molecular Spintronics

Metal-molecule-metal junctions formed of two ferromagnetic electrodes sandwiching an organic molecule are good candidates for novel spintronic devices, and are becoming increasingly interesting to a large number of researchers [144]. They have large spin relaxation times, which means they are capable of transferring spins over large distances without losing information [136, 144]. There are two types of junction which may exhibit spintronic properties. The first is the use of magnetic molecules [14]. The second is by contacting a non-magnetic molecule using ferromagnetic metal electrodes [26, 68, 166]. They are also highly versatile due to the variety of molecular structures that can be produced using chemical synthesis. For example, one may choose to tune the electronic properties of the molecule by adding specific chemical groups to the structure. Conduction in organic molecules takes place via the HOMO and LUMO levels and is highly localized. The HOMO or LUMO level can be adjusted using organic chemistry in order that the necessary conduction band is well matched to the Fermi level of the electrode, resulting in maximised spin injection into the organic molecule. This combined with the possibility of cheap, flexible devices which can be compatible with plastic technology and new applications including disposable and wearable electronics have led to a increased amount of recent interest in this still emerging field [143].

1.4.2.1 Alq3

One of the most commonly studied organic molecules in spintronics is the chemical compound Tris(8-hydroxyquinolinato)aluminium which has the formula ($Al(C_9H_6NO)_3$), and is widely abbreviated to Alq_3. The structure of this molecule is shown in Figure 1.19. It is a π-conjugated organic semiconductor that is known to have a strong electron-phonon coupling and a large spin relaxation length when compared with metals [187]. Conduction in Alq3 takes place by electron hopping through the π states which are delocalized throughout the entire molecule and are concentrated in the carbon chains away from the Al atom producing a low spin-orbit and hyperfine interaction [136]. The first organic spintronic sandwiched device was designed in 2002 by Dediu *et al.* [39]. This device (LSMO[3]/T_6/LSMO) had a lateral structure, where T_6 is sexithienyl, a prototypical organic semiconductor. They measured a magnetoresistance of around 30% at room temperature. The first demonstration of an organic spin-valve with a vertical structure based around Alq3 was by Xiong *et al.* [187]. It was a LSMO/Alq_3/Co device that exhibited a magnetoresistance of approximately 40% at 11K but no magnetoresistance was observed at temperatures above 150K. This was an interesting result because their magnetoresistance was negative, with the lower resistance measured in the antiparallel state. This encouraged researchers to focus

[3]Lanthanum strontium manganite is an oxide ceramic material with the general formula $La_{1-x}Sr_xMnO_3$, where x describes the doping level.

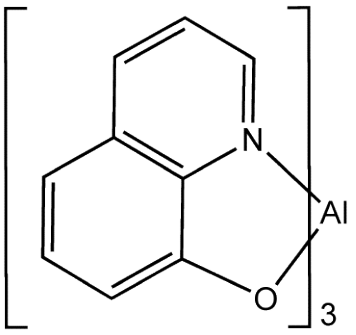

FIGURE 1.19. The structure of an Alq_3 molecule.

on achieving room temperature magnetoresistance using a variety of magnetic electrodes such as LSMO, Co, FeCo and NiFe and organic semiconductors such as Alq_3, P3HT and rubrene [40, 104, 121, 150, 178]. To date, the largest magnetoresistance of approximately 300% at 10K has been reached in Alq_3-based organic spin valves using LSMO and Co electrodes [9]. However, recently it has been shown that a $(La_{2/3}Pr_{1/3})_{5/8}Ca_{3/8}MnO_3$ thin film with pronounced electronic phase separation can be used in Alq_3-based organic spin valves resulting in a magnetoresistance up to 440% at T=10K [192]. In this case, the MR can still be seen up to 120K but reduces as temperature increases.

1.5 Single Molecule Devices

Many properties of molecules have been investigated which may make them advantageous when compared with silicon technology. An example of one of these properties is switching. The ability to vary a signal between a low current and a high current state is an important part of electronics. As silicon based technology reduces in size and approaches the sub-5 nm range, leakage currents make it increasingly difficult to maintain large high-to-low current ratios [147]. Molecular junctions exhibit switching behaviour due to a number of stimuli, including optical and gating of the molecular orbitals using electrochemistry or electrostatic means [98, 152, 157, 171]. Electric field induced conductance switching has also been explored [147]. The possibility of controlling this switching behaviour may bring us closer to single-molecule electronic devices.

Incorporating single-molecule junctions into electronic devices is a great challenge in molecular electronics. Devices generally require functional robustness, meaning the function of the component must be maintained as it is integrated into the final assembly [86]. This idea was investigated by Koepf and coworkers who assessed the properties of molecular diodes based on N-phenylbenzamide backbones [86]. They demonstrated that the choice of anchoring group can enhance the rectification ratio of a molecular backbone with intrinsic rectification. In addition, they show that changing the anchoring groups will not have an impact on the nature of the dominant transport channel, but it does affect the coupling with the HOMO of the N-phenylbenzamide

backbone which was responsible for rectification in this case.

1.6 Proposed Experiments

The use of electrodes constructed from metals such as nickel, cobalt and iron has provided a challenge to researchers due to the speed at which they oxidise under ambient conditions. This work utilises a different approach to measurements using cobalt, where a self assembled monolayer of thiol-ended molecules is formed on the surface of the substrate, which may provide a protective barrier against oxidation. This method also helps to target another issue faced in the field of how to incorporate single molecule junctions into devices. Previous measurements have relied on the use of electrochemistry to remove surface oxide from substrate surfaces. However, this results in a large and bulky experimental set up which reduces the likelihood of the molecular junction being successfully integrated into an electronic device. Similarly, molecular conductance measurements are often carried out in UHV at low temperatures which is not practical for future applications in electronic devices. The work within was all carried out under ambient conditions at room temperature. This provides a much more useful approach, which will be more applicable to electronic devices in every day life.

So far, relatively little investigation into magnetoresistance in metal-molecule-metal junctions has taken place. Magnetoresistance is important in the field of spintronics as it can be utilised to manipulate spin currents. In technology, it has data storage applications and is used in magnetic sensors and hard disk read heads. There are some obstacles that make magnetoresistance difficult to measure, such as magnetostriction which has previously resulted in misleading data [65]. Within this thesis attempts have been made to measure magnetoresistance in metal-molecule-metal junctions in order to increase the information available in the area.

The purpose of this work is to study electronic and spintronic transport through single organic molecules using primarily gold and cobalt electrodes. Also included will be initial investigations into single molecule magnetoresistance effects. The structure of this thesis is outlined below.

Firstly, the details of the home built MCBJ used to carry out measurements will be described, including a description of its design and construction and proof of concept experiments. The proof of concept experiments were carried out using Au-Au electrodes, as there is a large amount of literature available on this topic for comparison. This will also encompass the different types of samples used with the MCBJ. The details of clean room work carried out in attempt to create lithographically patterned MCBJ samples will be detailed, along with notched wire samples and spherical tip samples. Chapter 3 will contain details of molecular conductance measurements carried out with Au electrodes.

In Chapter 4, single molecule experiments using ferromagnetic electrodes (Ni and Co) will be discussed. These were carried out both with MCBJ and STM-BJ techniques under electrochemical control and under ambient conditions.

Finally, single molecule conductance measurements were carried out in the presence of a magnetic field. Chapter 5 contains the results of these measurements and discussions of possible magnetoresistance effects.

CHAPTER 2

DESIGNING AND CONSTRUCTING AN MCBJ

A mechanically controllable break junction was designed in order to carry out measurements with the potential to be more stable than those carried out using STM.

2.1 Design, Construction and Software

Mechanically controllable break junctions are described in Section 1.2.1 and a schematic diagram of the MCBJ is shown in Figure 2.1. The key components of an MCBJ are a three-point bending stage to hold the sample and a piezo actuator with a push rod attached. In this case, the main requirements were that the casing should be sturdy to hold the sample securely as it is bent and that it should be made from non-magnetic material. In addition, it should fit in the centre of a quadrupole magnet, shown in Figure 2.2. The main body of the MCBJ was fabricated from stainless steel and measures approximately 100 mm by 100 mm by 120 mm. A photograph of the MCBJ can be seen in Figure 2.3. This shows a sample held in place in the MCBJ. A beam which can only move up and down is visible below the sample, attached to the top of the push rod. This enabled a uniform force to be applied over the sample width, and prevented damage to the push rod.

2.1.1 Piezos and Drivers

The piezo actuator used in this set up was the Physik Instrumente N-216 NEXLINE® Linear Actuator[1]. A photograph of it is shown in Figure 2.4. It has sub-nanometer precision over a travel range of 20 mm, a driving force of 600 N and a holding force of 800 N. The piezo possesses three

[1] https://www.physikinstrumente.co.uk/en/products/linear-actuators/piezowalk-actuators-with-high-force-and-stability/n-216-nexline-linear-actuator-1000765/

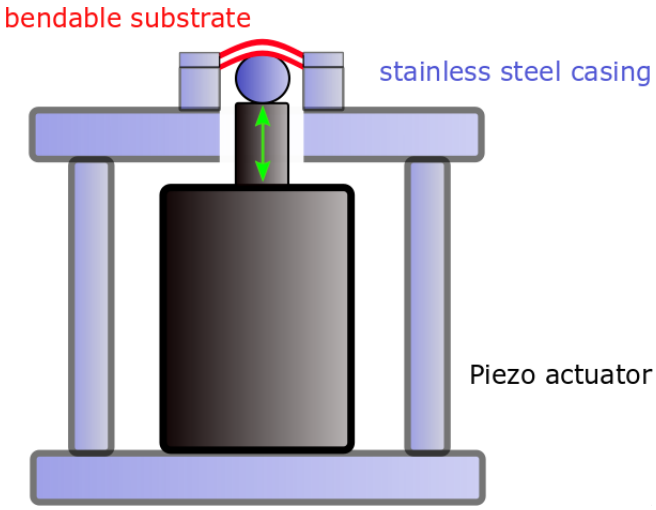

FIGURE 2.1. Schematic diagram showing the structure of the MCBJ constructed for use in this work. Visible is the bendable substrate, stainless steel casing and piezo actuator.

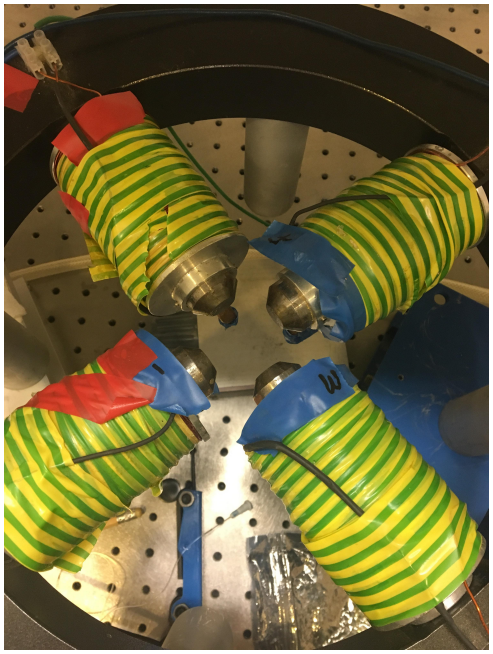

FIGURE 2.2. Photograph of the quadrupole magnet that the MCBJ was designed to sit in the centre of.

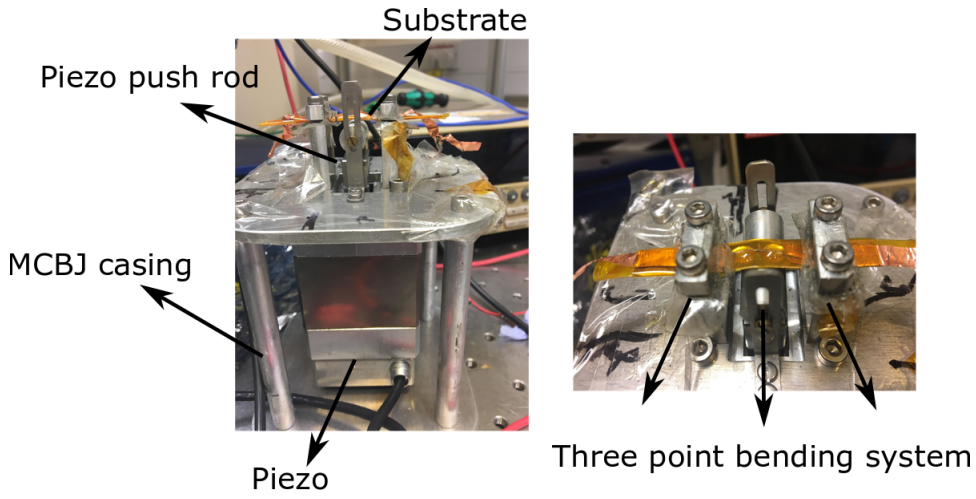

FIGURE 2.3. Photographs showing MCBJ with key features labelled.

modes of operation. Firstly, the full step mode, which offers the highest velocity and highest dynamic forces. Secondly, the nanostepping mode which provides low vibration and has good uniformity of motion. These two modes can cover a range of 20 mm. Here, the nanostepping mode was used in the initial breaking process of the samples. Finally, the piezo has an analog mode which offers millisecond response time and picometre resolution over a 6 μm range. The analog mode was used throughout conductance measurements. Although this actuator delivers relatively slow velocities when compared with others, fast moving speeds are not necessary for the work carried out here. The piezo actuator is also suitable for applications in strong magnetic fields, which is necessary for this work. It is driven by the PI E-755 Digital NEXLINE® controller.

2.1.2 Data Acquisition and Software

Software was required to control the motion of the piezo and collection of current data. Initially, the notched wire needed to be broken, and then the newly formed electrodes needed to be repeatedly brought into contact and separated whilst the current was monitored. For the electrical measurements, the sample was connected to a Keithley 2400 source meter, from which a voltage (generally 100mV) was applied to the sample and the corresponding current was measured by the Keithley.

The software used to control the piezo and process the electrical measurements was written in LabVIEW and the processes involved in this are depicted in the flowcharts in Figures 2.5 and 2.6. The sample was fixed in the MCBJ and the push rod was moved up to break the sample, the current was monitored through the Keithley via LabView, taking up to 80 readings per second. When the sample was broken, the push rod retracted, bringing the newly formed electrodes back together until the measured current reached 12 G_0. Previous work has shown that if this value is too low, there will be insufficient fusion of the break junction contacts between measurements. If

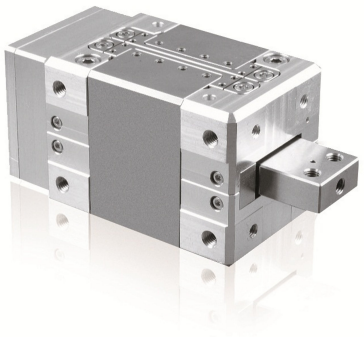

FIGURE 2.4. Photograph of N-216 NEXLINE® Linear Actuator.

it is too high, the probability of forming a molecular contact can also be reduced [107]. The push rod is then raised again, drawing the electrodes further apart until the constantly monitored current reaches the noise level (the current level which corresponds to full separation of the electrodes) and the process repeats itself. The current measurements are plotted in real time so one can observe the traces as they are measured and the data were saved as individual traces in individual files.

2.1.2.1 Analysis

The analysis software used to assess MCBJ data was written in Python. The traces were cropped at the noise level so that the histograms do not show the noise of the equipment. Two conductance histograms were then plotted: a histogram with a logarithmic scale and one on a linear scale. In these histograms, the y-axis has been normalised so that the area under the graph is equal to 1. The individual traces used to form the histogram were also plotted in one window which allows the user to scroll between each trace. At this stage, traces that were extremely noisy or did not decay sufficiently were manually removed. Aside from this, manual data selection for plateaus in the current data was not generally carried out. However the plateau finding software described in Section 3.1.2 was compatible with the MCBJ data and could be used for data selection.

2.2 Electromagnet

MCBJ experiments using ferromagnetic electrodes were performed in the presence of an applied magnetic field. This provided control of the magnetisation of the contacts. A quadrupole electromagnet designed and constructed at the University of Exeter was used for the experiments, a photograph of which is shown in Figure 2.2. It is beneficial to use electromagnets rather than permanent magnets as they allow variation of the magnetic field strength and the magnet can be switched on and off during experiments. The quadrupole magnet also offers greater versatility

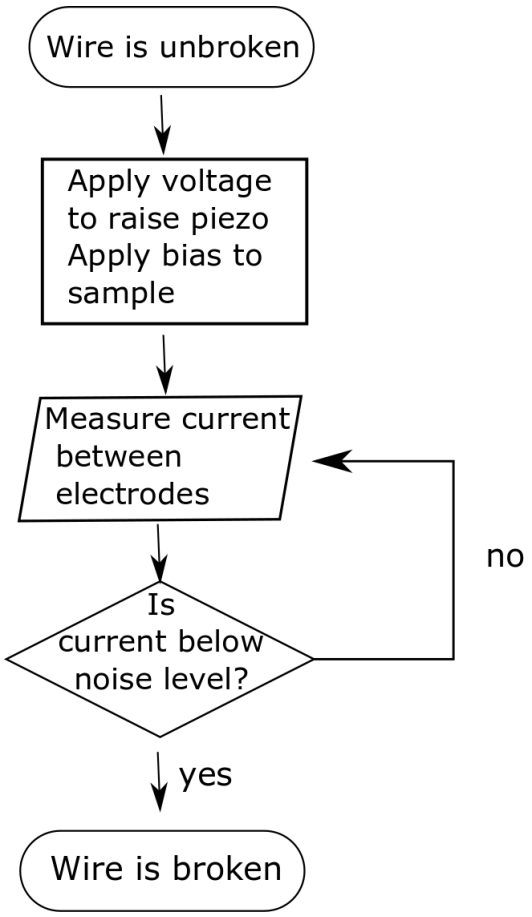

FIGURE 2.5. Flowchart describing how the software (written in LabView) is used to initially break the wire forming two electrodes.

as it has the ability to provide magnetic fields in various directions by varying the ratios of the currents applied to the orthogonal pairs of poles. An inbuilt water cooling system prevented the temperature of the MCBJ sample increasing significantly whilst the magnet was running.

2.2.1 Calibration

The coils of the electromagnet are driven by a Kepco BOP36-12D bipolar power supply, which provided a constant current. The magnet was calibrated at the University of Exeter; the calibration graph is shown in Figure 2.7. The calibration curve is linear within error between currents -3 A and +3 A which provides a magnetic field between -1 kOe and +1 kOe. After this the relationship between current and magnetisation becomes nonlinear and begins to saturate. The electromagnet provides a maximum magnetic field of around 2 kOe. In addition, the magnet had a remnant field of only 17 Oe when the magnet was switched off from +2 kOe.

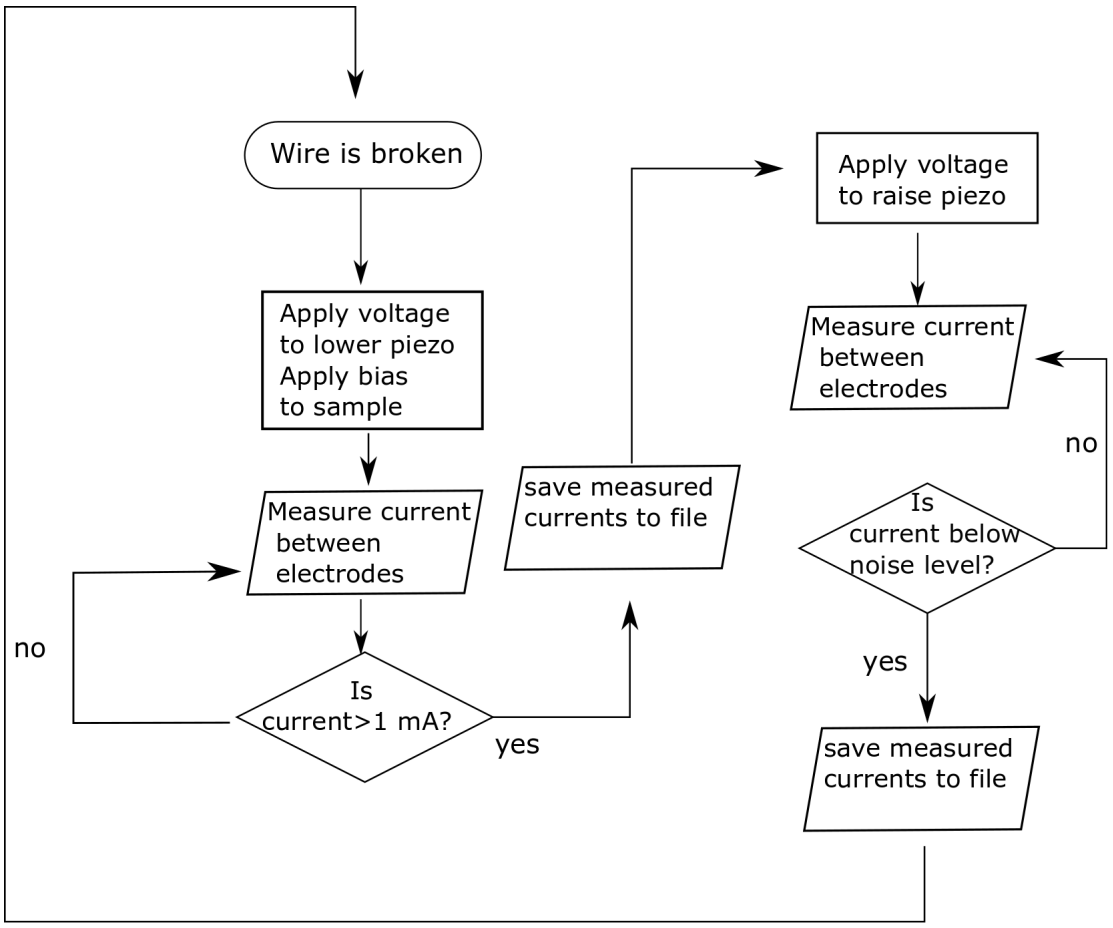

FIGURE 2.6. Flowchart describing how software (written in LabView) is used to take measurements, including measuring molecular conductance, after the initial break is used to form two electrodes.

2.3 Sample Design

2.3.1 Notched Wire

Samples for the MCBJ were initially based on the traditional notched wire samples [6]. They were constructed from phosphor bronze foil cut to 6 mm x 50 mm. Kapton ® tape was used to insulate the phosphor bronze substrate. An example of one of these samples is shown in Figure 2.8. Proof of concept experiments were carried out using gold electrodes. As previously mentioned, gold electrodes have been well studied and it is easy to establish whether a simple gold-gold conductance experiment is successful. Therefore, a gold wire was fixed using epoxy to the surface of the substrate, notched, and broken completely in the MCBJ. The notching process was carried out by hand using an optical microscope and a scalpel. It is easy to notch gold wire by hand as it is soft, but could be beneficial when using other metals such as cobalt to use a process such as electrochemical etching. Optical microscope images showing a sample without a notch, a

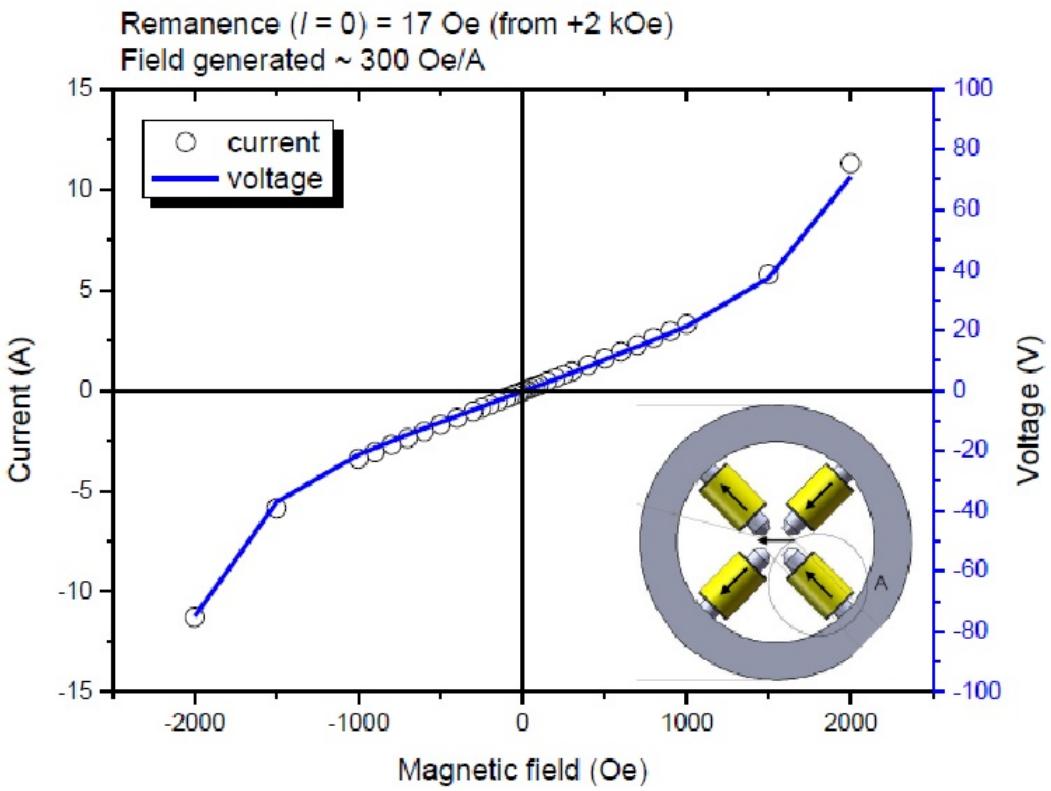

FIGURE 2.7. Calibration curve of the quadrupole electromagnet used for MCBJ experiments. The electromagnet provides a maximum magnetic field of around 2 kOe. Inset shows diagram of the electromagnet.

notched sample and a broken sample are shown in Figure 2.9. These gold samples were used to demonstrate the quantization of conductance in gold-gold junctions. This acted as a proof of concept experiment and the results are shown in Figure 2.10. Although it was possible to obtain results that proved the MCBJ and samples were working in the way expected, it was concluded that the notched wire samples may not be the best way to proceed. It is impossible to predict or reproduce the geometry of an electrode formed by notching and it is not possible to produce precise nanoscale electrodes.

2.4 Testing Notched Wire Samples

The MCBJ was tested using Au | Au junctions without the presence of junction-forming organic molecules. Conductance vs piezo movement traces were obtained by measuring the current as

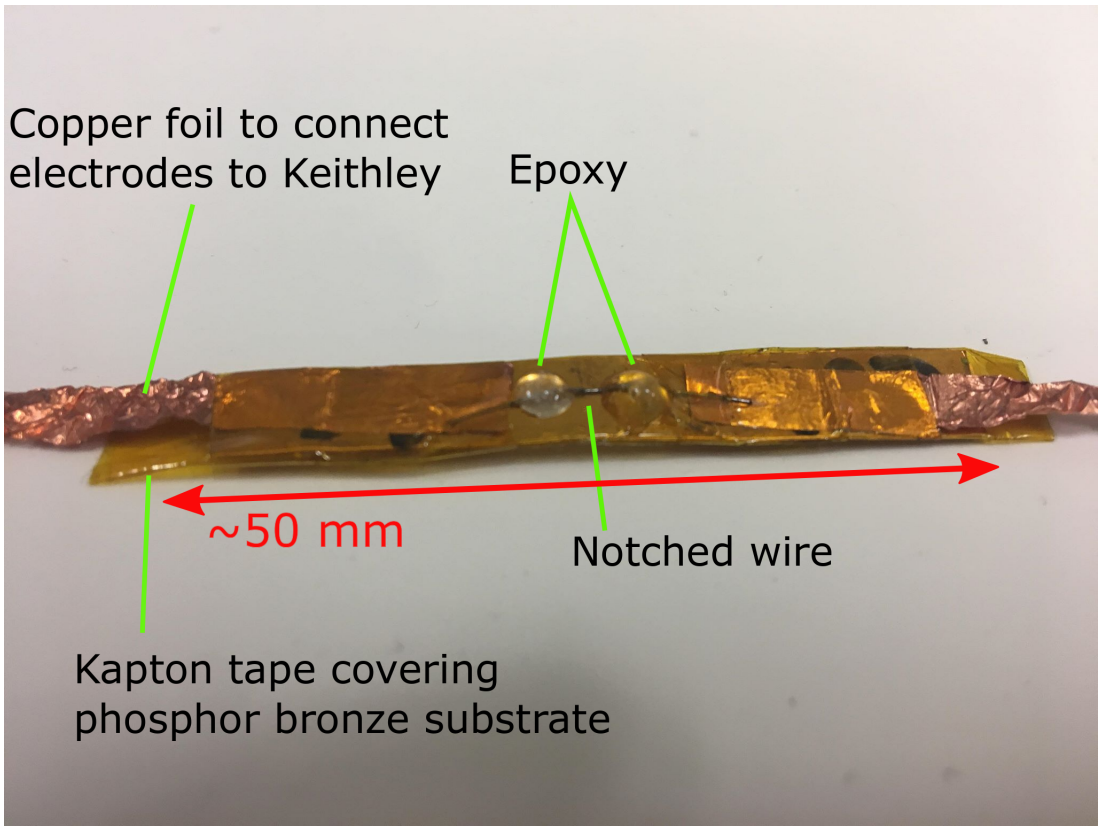

FIGURE 2.8. Photograph of a typical MCBJ notched wire sample, with the scale marked.

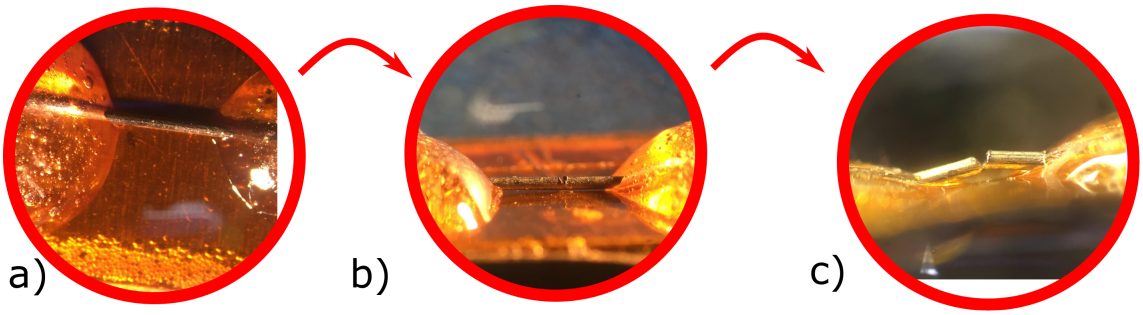

FIGURE 2.9. Optical microscope images of notched wire samples. **(a)** Wire before notching **(b)**Wire after it has been notched using a scalpel. **(c)** Sample after MCBJ has been used to break the wire at the point of the notch.

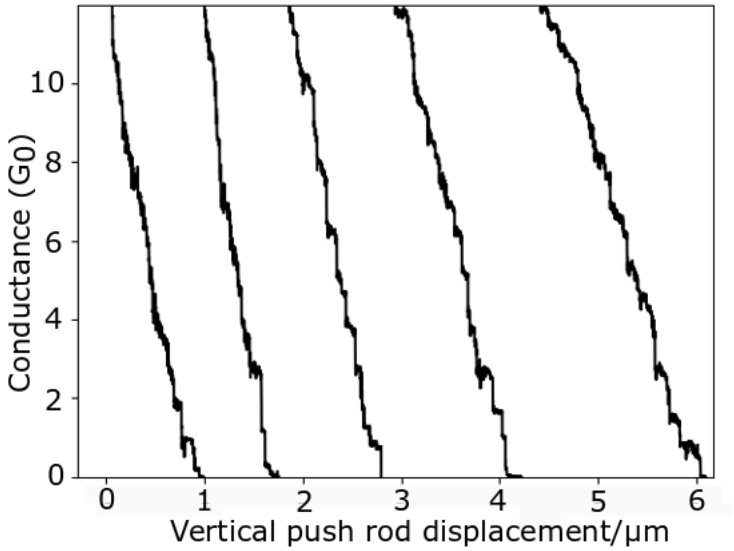

FIGURE 2.10. Examples of Au | Au conductance traces taken whilst testing the function of the MCBJ. These are shifted horizontally for clarity. Steps in the traces indicating quantization of conductance are visible.

a function of electrode separation with a 100 mV bias voltage applied between the electrodes. Examples of typical traces collected from these measurements can be seen in Figure 2.10. During each trace, as the electrodes are separated, the conductance decreases in discrete steps, each of which is separated by a plateau. Plateaus tend to appear around integer multiples of G_0, in particular at 1 G_0, 2 G_0 and 3 G_0, resulting in clear peaks in conductance histograms such as those in Figure 2.11.

2.4.1 Snap Back Analysis

As the electrodes are separated, when the final atomic plateau (at approximately $1G_0$) is broken, there is a sudden decrease in the conductance. This sudden decrease occurs when the apex atoms rearrange themselves to minimise surface energy and is known as "snap-back". "Snap-back" is followed by a period of quantum tunnelling over the small gap between the newly formed electrodes. The period of quantum tunnelling is represented by exponential decay of the current, seen as a straight line on the log graph in Figure 2.12. There are some inconsistencies in the Au | Au MCBJ data as not all of the traces appear to exhibit this "snap-back" feature. However, this inconsistency was also observed by Van der Zandt and co workers in 2008 [107]. They observed that the conductance drop after $1G_0$ is much less pronounced for MCBJ measurements when compared with those taken during STM. In addition, during MCBJ measurements, counts were measured across the entire range of conductances below $1G_0$. They suggest that this may

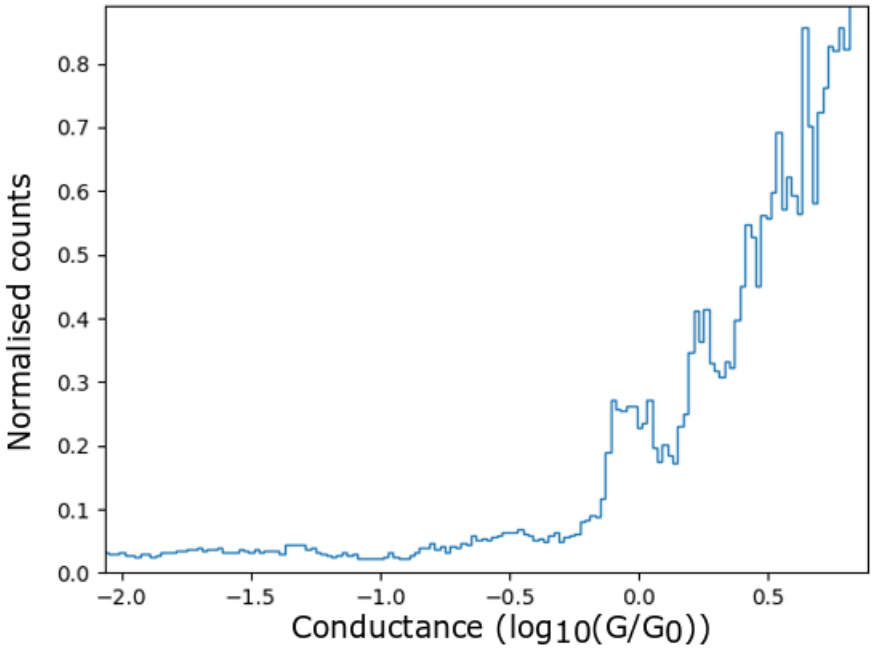

(a)

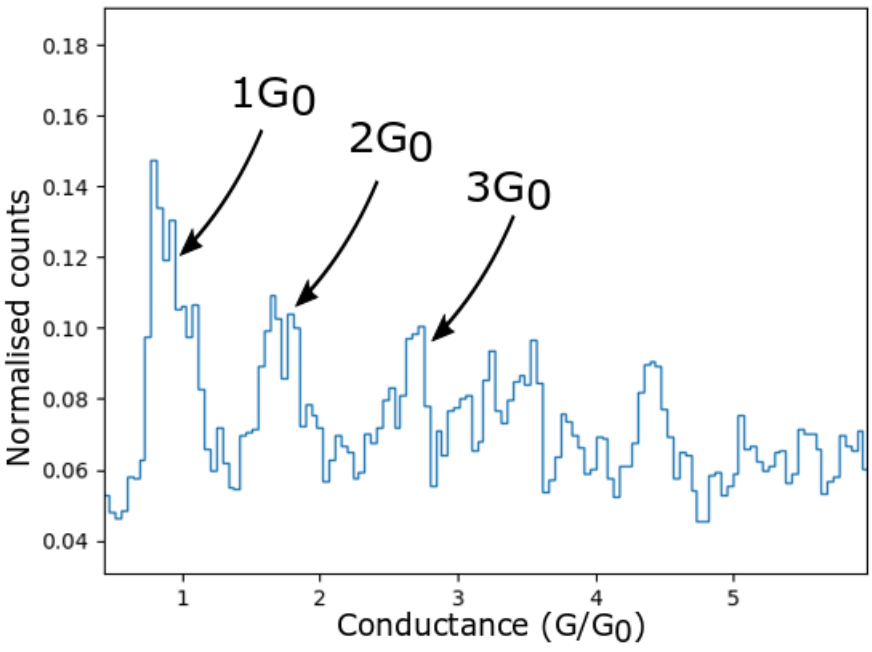

(b)

FIGURE 2.11. Au | Au conductance histograms formed from traces such as those in Figure 2.10. Peaks can be seen close to integer values of G_0 (labelled) demonstrating the quantization of conductance in Au | Au junctions.(a) Plotted on a logarithmic scale and (b) plotted on a linear scale.

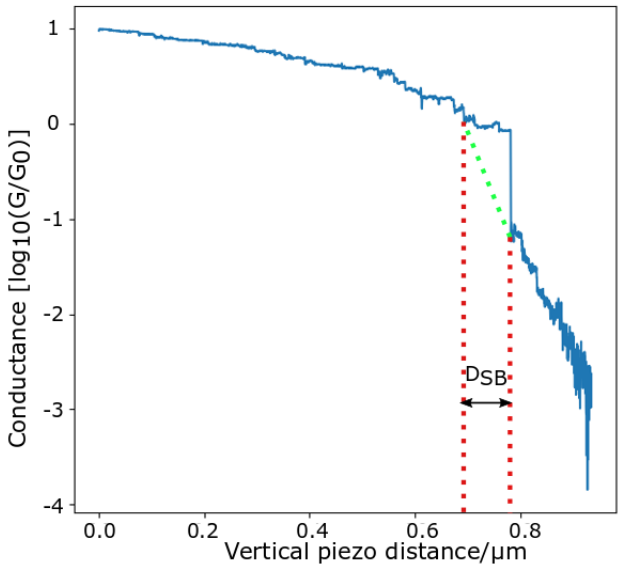

FIGURE 2.12. Measuring the snap-back length of atomic Au contacts from a single conductance trace, where D_{SB} is the snap-back length.

be related to the slow breaking process of the MCBJ, which impacts the micromechanics of the contact area and hence, breaking behaviour [107]. Those traces showing "snap-back" behaviour were analysed and the most probable "snap-back" distance was found to be 0.5 μm vertical motion of the push rod, which translates to approximately 1.5 Å of horizontal electrode separation.

2.4.2 Noise Level

The noise level of the MCBJ determines which molecules it is able to measure. In Figure 2.13, a conductance vs time trace of an Au | Au junction can be seen. It shows the noise level of the MCBJ which was found to be consistent for all gold, cobalt and nickel notched wire samples used for measurements with the MCBJ. A high rate of data acquisition of the Keithley 2400 was used for these measurements. This resulted in increased reading noise and fewer usable digits. Using a lower rate of data acquisition may provide a compromise between speed and noise, however as molecular junctions can have a lifetime of < 100 ms [87], it is important to have a high rate of data acquisition. Specifically, the 'fast' mode of the Keithley 2400 was used. This sets the speed to 0.01 PLC and sets display resolution to 3.5 digits.

2.4.3 I-V Curves

The increased stability of the MCBJ when compared with STM allows further analysis beyond 1D histograms to be carried out. For example, it is possible to pause the opening and closing

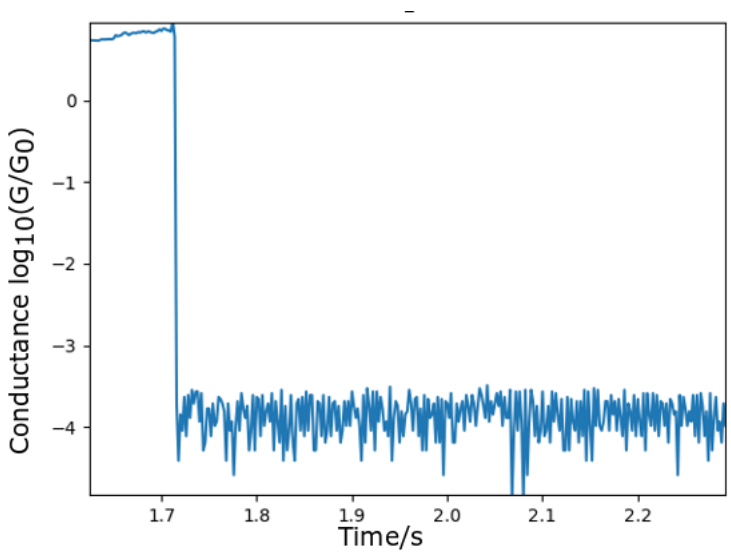

FIGURE 2.13. Conductance vs time trace of an Au | Au junction, demonstrating the noise level of the MCBJ using notched wire samples. Here, the junction was broken and then held open whilst measuring the current to demonstrate the conductance of the noise level.

process of a junction and hold the junction at that point. Previous molecular junctions have been maintained for periods of 30 minutes and more during experiments [194]. A series of I-V curves were measured in order to investigate the nature of transport through Au | Au junctions. These I-V curves were measured using the sweep function of the Keithley 2400. An example of one of these I-V curves can be seen in Figure 2.14 The I-V traces taken of the Au | Au junction are linear and display ohmic characteristics. This is in agreement with I-V measurements taken by Hong and coworkers and Yang and coworkers [63, 194].

2.4.4 Lithographically Patterned MCBJ Samples

Using lithographically patterned samples offers many benefits that notched wire samples can not. For example, they can be highly reproducible and it is possible to achieve a spatial resolution of the order of 10 nm during the patterning process. They are also easily cleaned when compared with notched wire samples as they can be submerged in solvents and they do not contain any components such as epoxy or Kapton® tape that could be damaged by this. Many groups have used samples produced in this way successfully for molecular electronics experiments [52, 107, 113]. Lithographically patterned substrates were fabricated, based on the methods on those of Morikawa and co-workers and Muthusubramanian and co-workers [120, 124]. Muthusbramanian and co-workers fabricated MCBJ samples by spin-coating an insulating layer of polyimide onto polished phosphor bronze substrates [124]. The electrodes were then patterned as a thin wire constricted in the centre using electron-beam lithography. A chromium adhesion

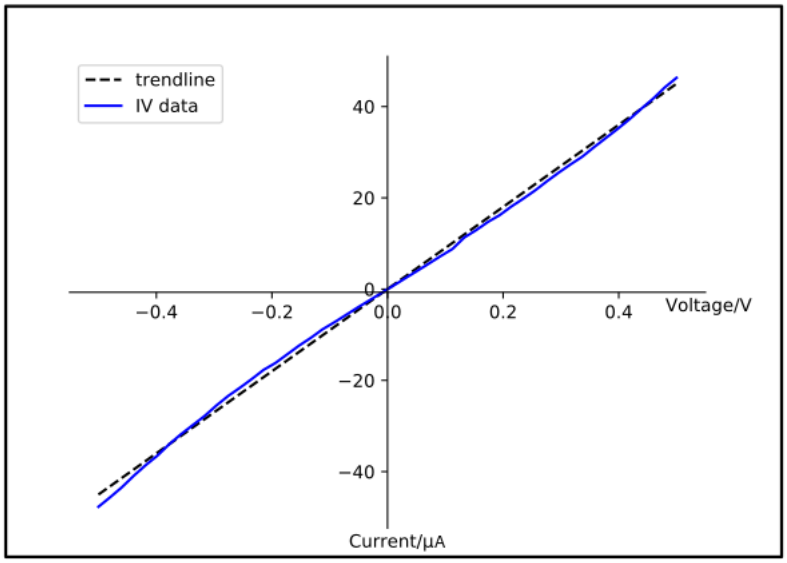

FIGURE 2.14. Typical IV trace of an Au | Au junction plotted with a linear best fit line.

layer was deposited followed by a gold layer with thicknesses of 4 nm and 80 nm, respectively. The gold wires were suspended over a length of 1 μm by etching the underlying polyimide layer using a mixture of O_2/CF_4 plasma. Samples were then covered in Al_2O_3 using chemical vapour deposition. The purpose of this layer was to suppress the leakage current when taking measurements in deionized water. Through this method, they were able to measure the conductance of an amphiphilic oligophenylene ethynylene derivative in deionized water [124].

Herein, the same phosphor bronze foil was used for these samples as for the fabrication of notched wire substrates, described previously. Firstly, the sample was washed with ultrasonic agitation in three solvents: ethanol, acetone and finally isopropanol. It was then rinsed with deionised water and dried using nitrogen. An isolating polyimide layer (HD Microsystems PI 2600 Polyimide) of approximately 8 μm was spin coated in two stages, initially, it was prepared by spinning an adhesive layer (HD Microsystems VM651 polyimide adhesion promoter) at 3000 rpm and baking at 100 °C on a hotplate for 90 s. The polyimide layer was then spin coated at 1500rpm initially for 15 s and then another 30 s as 3000 rpm. To complete the imidization of the polyimide, and harden the layer, it was then baked in a convection oven for three hours at 350 °C. Polyimide was chosen, not only for its insulating effects but for its ability to be reactive ion etched. This is an important step in the sample fabrication as the electrodes need to be free standing to enable them to be separated and brought back together again in the MCBJ process. Another benefit of polyimide is that it can be used in measurements at a large range of temperatures whilst maintaining its mechanical properties.

Photolithography was the process used to pattern the substrate. A double layer of a photo-

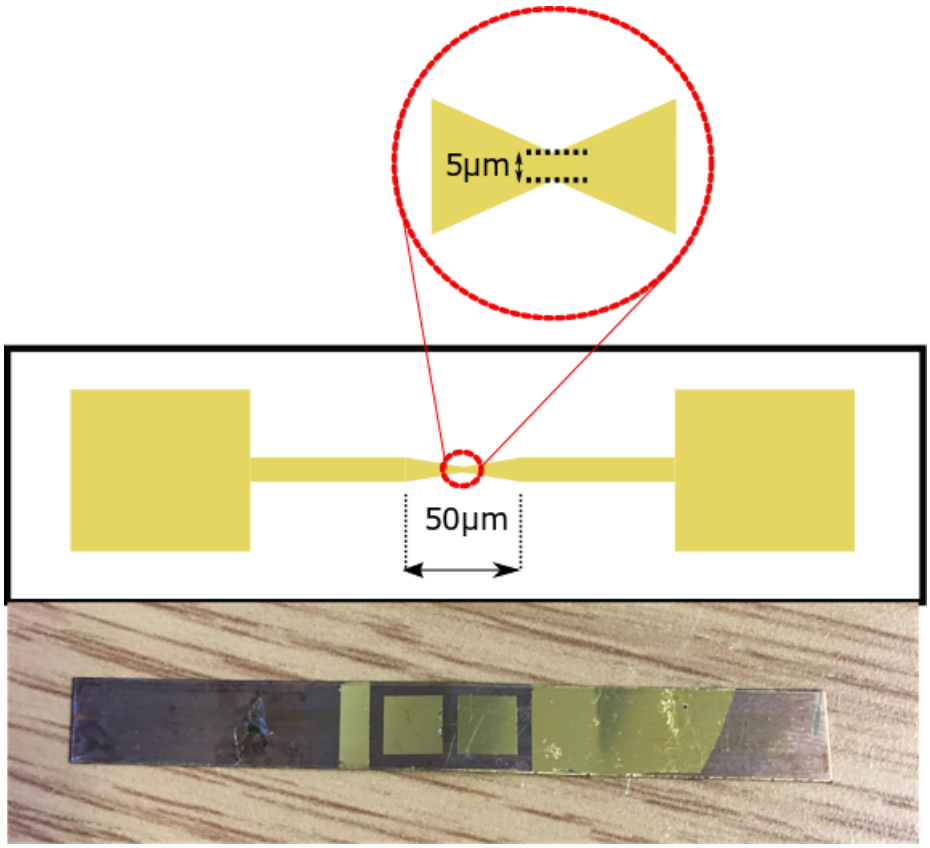

FIGURE 2.15. Schematic diagram showing the gold pattern used to produce the lithographically patterned substrates, with zoomed in diagram showing the size of the constriction that breaks to form the electrodes in red ring. Below shows a photograph of a patterned substrate.

sensitive chemical, photoresist, is applied to the substrate by spin coating. Firstly, resist (S1805) was spin coated at 500 rpm for 60 s then for 60 s increasing in 500 rpm steps up to 3000 rpm. It was then baked at 115°C for 60s on a hotplate to remove excess solvent. Then lift off resist was spin coated firstly at 500 rpm for 60 s, then spun for 60 s increasing in 500 rpm up to 3000 rpm and baked at 190 °C for 60 s. A mask with the desired pattern was used to cover the surface of the substrate, in this case exposing only the areas which will make up the electrodes. The pattern is shown in Figure 2.15. Photoresist that has been exposed to light becomes soluble in a universal developer solution, which is used to remove the exposed areas, providing an area with no photoresist in the shape on the electrodes. Optical microscope images showing the results of this process can be seen in Figure 2.16 A thermal evaporator was then used to coat the substrate in gold. The pattern was revealed by sonicating the sample in acetone. Subsequently, reactive ion etching was used to remove polyimide to leave the thinnest point of the constriction free standing. SEM images were captured of the constriction, shown in Figure 2.17.

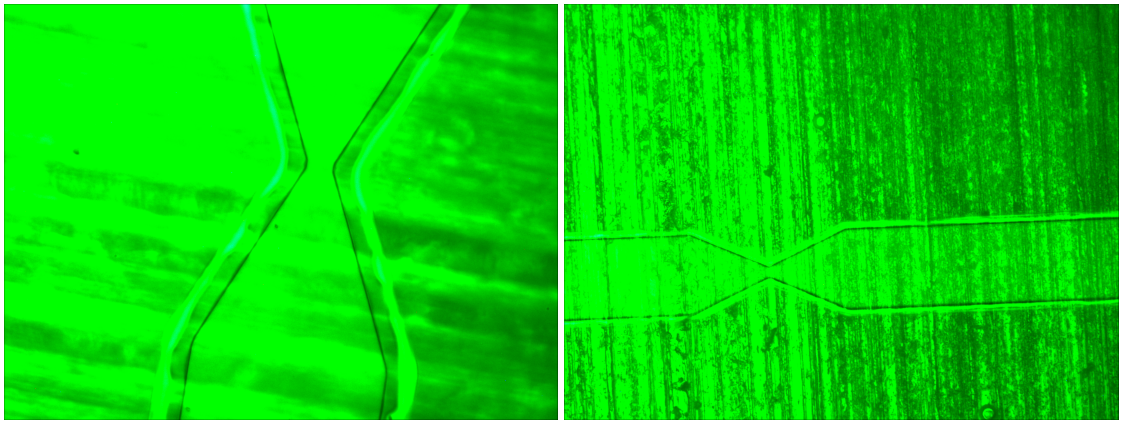

FIGURE 2.16. Optical microscope image of lithographically patterned gold constriction on polyimide coated phosphor bronze which measures approximately $5\mu m$ at the thinnest point.

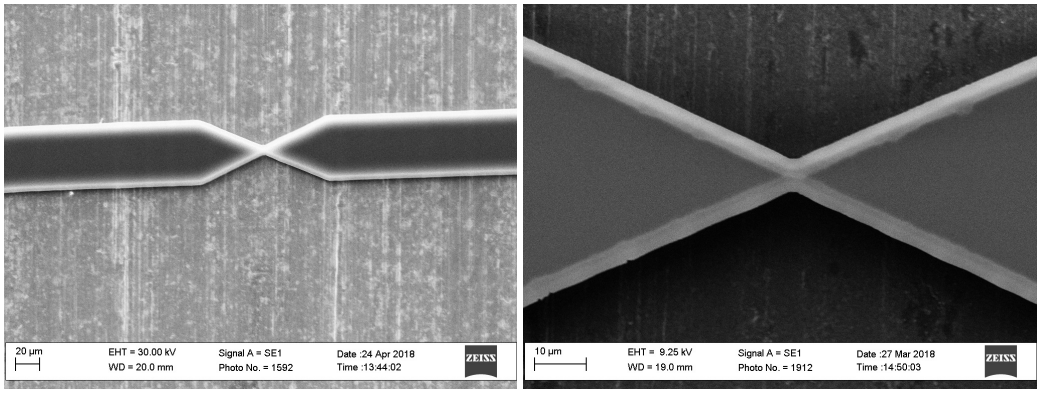

FIGURE 2.17. SEM images of lithographically patterned gold constriction on polyimide coated phosphor bronze MCBJ sample.

2.4.5 Testing Lithographically Patterned Substrates

Firstly, the noise level of the MCBJ using these samples was tested. This is shown in Figure 2.18. It was measured to be between $10^{-4}G_0$ and $10^{-5}G_0$, which would allow for measurement corresponding to a fairly wide range of molecular conductances. When testing the substrates, there was some evidence of conductance quantization, suggesting that the fabrication has been successful. This is shown in Figure 2.19. The figure shows plateaus close to the expected value of 1 G_0 and 2 G_0 (values of quantized conductance, explained in Section 1.1). This signifies (when using Au electrodes) that the electrodes are in contact. For various reasons, plateaus are often found close to, but not exactly on the value of G_0. This could be due to different contact configurations and has also been attributed to back scattering on defects near the contact [202]. The electrodes are initially separate and brought into contact. A G_0 plateau is measured before

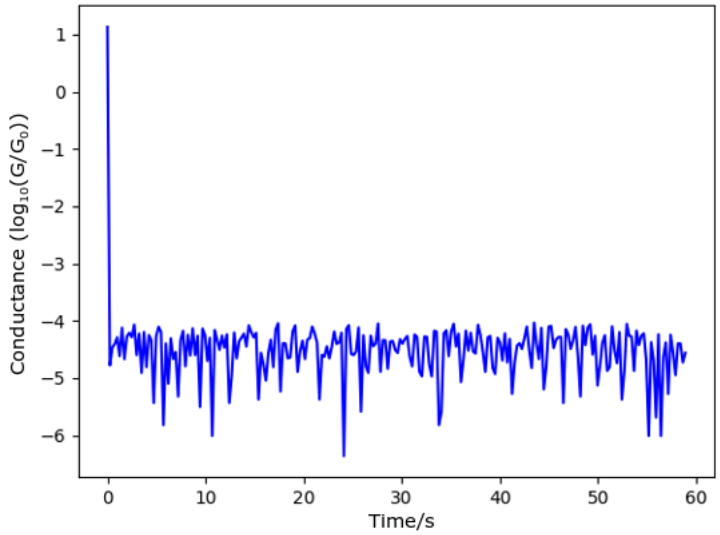

FIGURE 2.18. Graph demonstrating the noise level of the MCBJ with lithographic samples. These measurements were taken by breaking the sample and then holding the electrodes separate whilst measuring the current.

the conductance steps up rapidly to 2 G_0 as the separation of the electrodes is decreased. When the distance between the electrodes is then increased, the conductance returns to G_0. This demonstrates a high level of stability and control within the system.

The tunnelling current between the electrodes of the lithographically patterned samples was also measured. This is shown in Figure 2.20. The figure shows the exponential increase of current with respect to time (which here is directly proportional to the separation of the electrodes). In this case, the electrodes start separated were brought slowly closer together whilst the current was monitored and measured. This is the expected result as tunnelling current across a potential barrier has an exponential relationship with the length of the barrier.

It was not straightforward to find the ideal parameters for fabrication when producing these samples. When breaking the junctions, it was sometimes found that the electrodes, once separated, would not rejoin. One explanation for this is that there may not have been enough gold deposited, as some of it was etched away during the reactive ion etch. This can be seen in Figure 2.21. In Figure 2.21a there is some damage to the gold from the edges of the pattern where the polyimide has etched away. This shows how fragile the samples were, and suggests that the extremely thin layer of remaining gold after the etch may not be robust enough to form a suitable break junction. It also highlights the importance of having the electrodes fully free standing. In Figure 2.21b, it appears that the electrodes are still in contact at the constriction. However, no current was measured through them, suggesting that this connection could be the insulating polyimide layer, which has not been sufficiently etched below the constriction. It is possible that once the gold

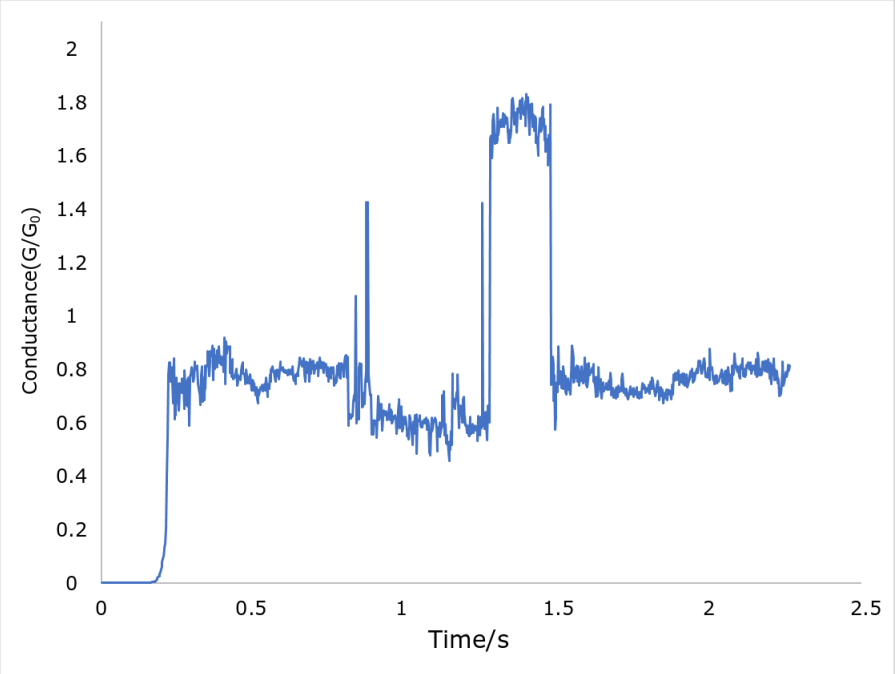

FIGURE 2.19. Evidence of G_0 plateaus measured using lithographically patterned samples. Plateaus close to 1 G_0 and 2 G_0 can be seen.

had broken initially, forming two electrodes, the remaining polyimide acted as a barrier, reducing the mobility and preventing the gold electrodes from meeting again. In addition, the intricacies of the clean room methods involved in fabricating these samples meant that it was not easy to reproduce them consistently. This is because minor changes, which are largely unavoidable, in the patterning or etching processes can result in large differences in the outcome of the sample. Due to the inconsistencies in the lithographically patterned samples, notched wire samples were used for the molecular conductance measurements in this thesis.

2.4.6 Spherical Tips

When the tip of gold wire (diameter 0.25 mm) is heated to melting point using a butane torch, a gold sphere is generally formed with a radius similar to the diameter of the wire. At the nanoscale, using a sphere such as the one described is a good approximation to a flat surface. They have also been shown to have a low surface roughness (less than 1 nm for 500 μm diameter gold spheres formed using the method described) [189]. To form samples, these spherical tips were arranged on a bendable substrate, such as phosphor bronze, with an electrochemically etched STM tip positioned as closely as possible to it. This was done using the set up shown in Figure 2.22. The spherical tip was glued using epoxy to the bendable, phosphor bronze substrate. An electrochemically etched tip was attached to a micropositioner which was used to position the tip as close to the spherical tip as possible on the phosphor bronze substrate by viewing

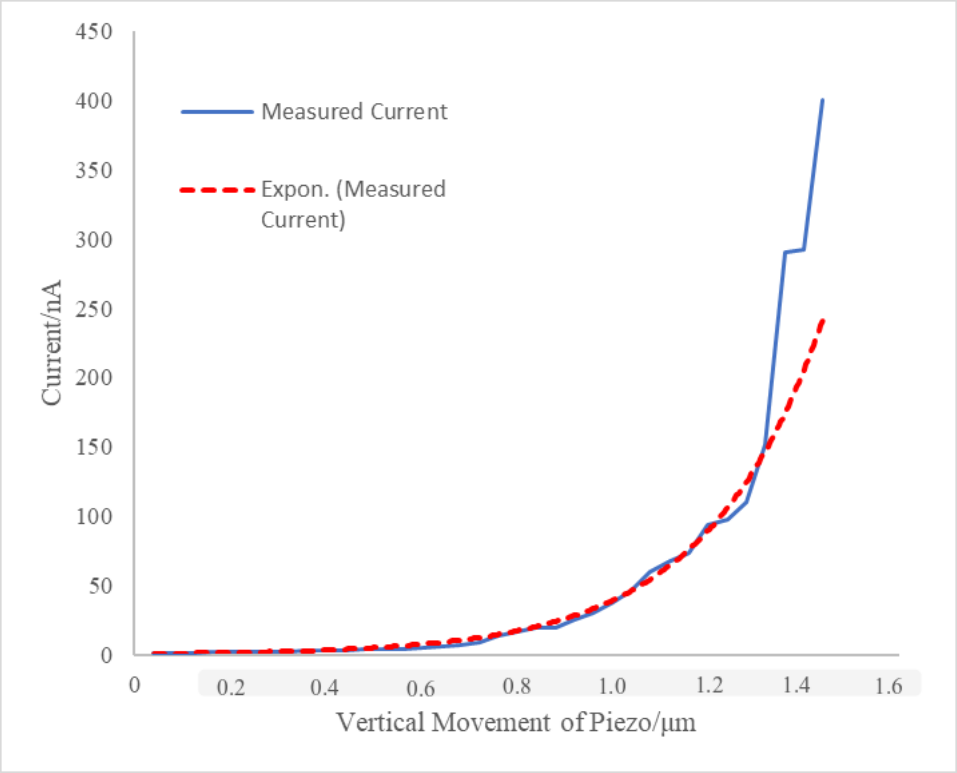

FIGURE 2.20. Tunnelling current between lithographically patterned Au | Au contacts. Red line shows theoretical exponential increase, compared with the blue line which represent the measured current.

(a) 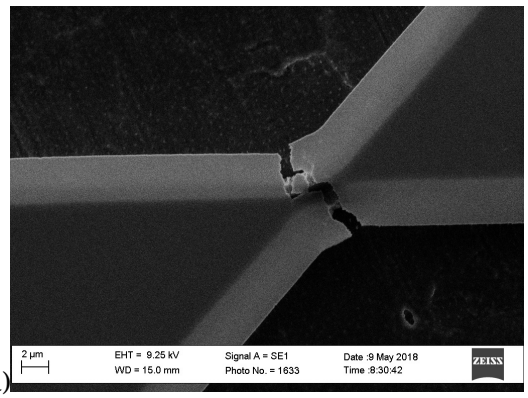

(b) 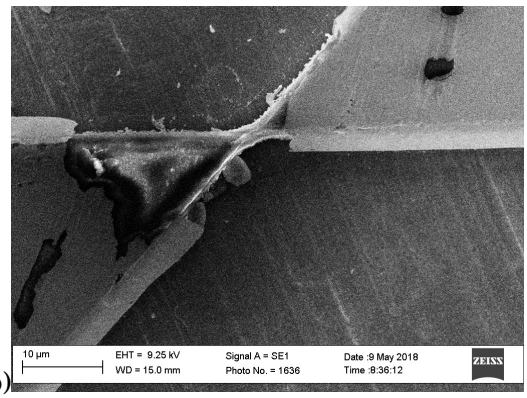

FIGURE 2.21. (a) and (b) SEM images of lithographically patterned constriction, once it has been broken by the MCBJ.

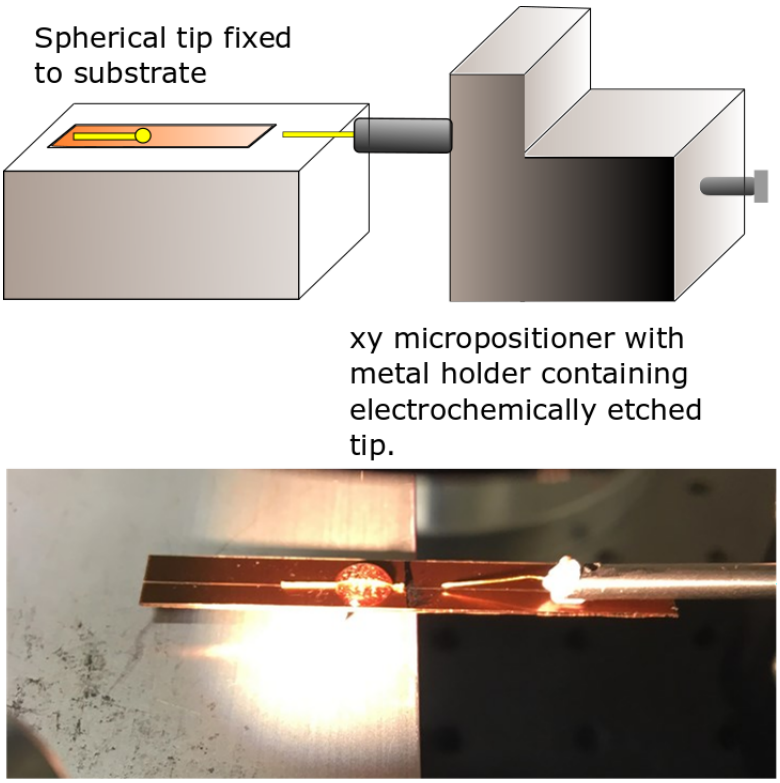

FIGURE 2.22. Schematic image of the set up used to produce spherical tip samples, showing the spherical tip fixed to the substrate and the electrochemically etched tip fixed in the micropositioner. Photograph of the same set up.

the process through an optical microscope. The tip was then glued into place. This set up is a good choice for electrochemical applications as additional metals such as nickel can easily be electrodeposited onto the spherical tip. It also mimics the processes involved in STMBJ experiments, as these tend to involve a flat substrate and a sharp tip. These methods are based on the work by Hong *et al.* [7]. In their work they controlled the electrical conductance and in particular the occurrence of quantum interference in single-molecule junctions through gating effects. They used an electrochemically gated, MCBJ technique to tune the electronic behaviour of thiophene- based molecular junctions that show destructive quantum interference features [7]. The spherical tips were not taken any further than initial Au | Au tests, as these showed that the noise level of the MCBJ when using spherical tips was too high to be of use, as demonstrated by Figure 2.23.

2.5 Calibration

The MCBJ was calibrated with notched wire samples using the methods of Champagne and coworkers [28]. The resistance, R, of a tunnel junction is related to the width, x, of the tunnelling

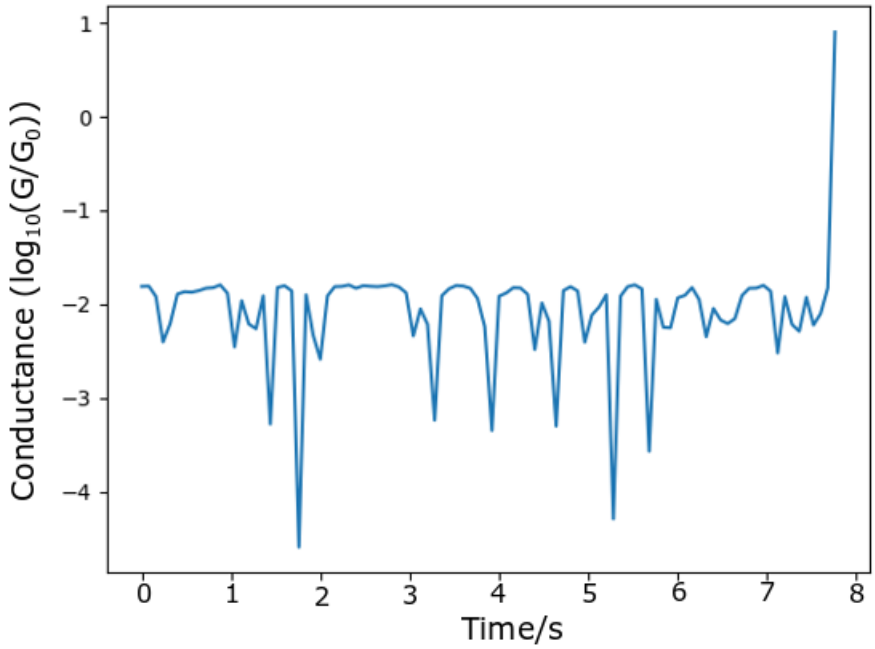

FIGURE 2.23. Noise level of MCBJ when using spherical tips. Electrodes were initially separated to show the noise level and then brought together.

barrier as follows:

$$R \propto e^{2\kappa x}, \qquad \kappa = \frac{\sqrt{2m_e\phi}}{\hbar}, \tag{2.1}$$

where $\phi = 5.1eV$ is the Au work function [2] and m_e is the effective electron mass. Using this equation, it is determined that for a change in electrode separation (δx) of 1Å, the resistance will change by a factor of approximately 10. Using the graph in Figure 2.24, this information can be used to determine that this change in resistance corresponds to a 90 nm change in vertical height of the push rod (δy). This results in a reduction ratio of 1×10^{-3}. Using equation 1.8, the predicted reduction ratio was calculated from the theory to be approximately 3×10^{-6}. The measured value is two orders of magnitude greater than the theoretical prediction. The difference is explained by the fact that equation 1.8, despite being widely used, does not account for any plastic deformation that may occur. The presence of plastic deformation can be confirmed by observing the samples after use. They often appear deformed when compared with how they were shaped initially [202].

[2] This is the work function of Au when measured in a vacuum. Under ambient conditions this value may differ. However, by reducing the work function used in the calculation to 4 eV rather than 5.1 eV, the distance over which the resistance increases by an order of magnitude would increase by just over 10%, which is a fairly small error.

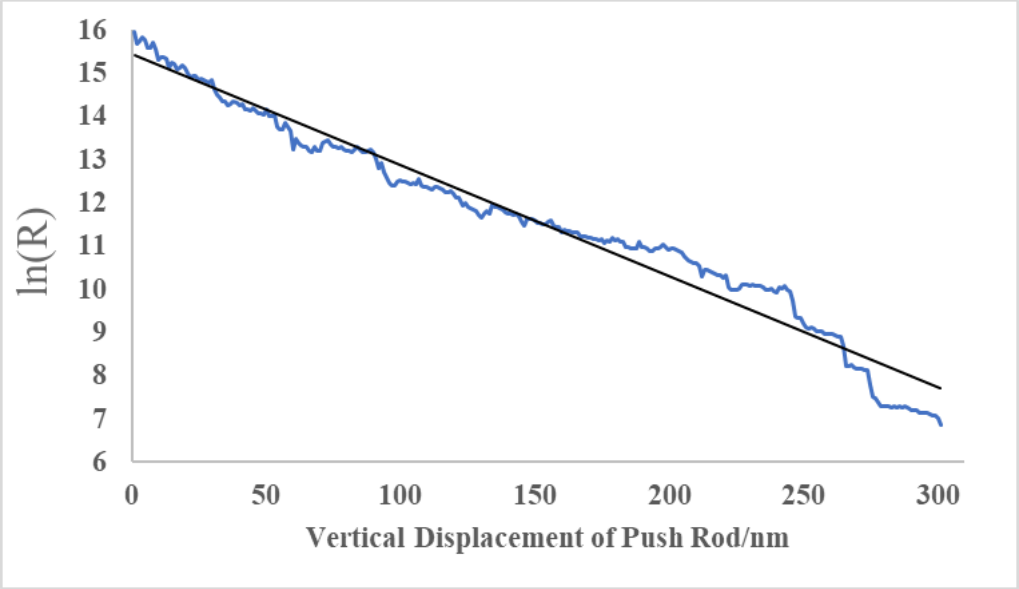

FIGURE 2.24. ln resistance (plotted with best fit line) of a bare Au junction, used to calculate the effective reduction ratio of the samples.

2.6 Chapter Summary

An MCBJ was designed and constructed, along with the software required to operate it and analyse the data acquired. Different varieties of samples were tested (lithographically patterned, notched wire and spherical tip). From these tests it was concluded that experiments would be most successful if carried out using notched wire samples.

CHAPTER 3

MOLECULAR CONDUCTANCE MEASUREMENTS WITH GOLD ELECTRODES

Single-molecule conductance measurements have predominately been carried out with gold electrodes. This is because gold is chemically inert so it is easy to take measurements in ambient conditions without the surface of the substrate becoming contaminated by oxide. It also links easily with molecules including thiols, which allows self assembled monolayers to be formed and increases the likelihood of measuring molecular conductance. The high affinity between gold and the thiol group, in combination with the increased stability of the MCBJ when compared with the STM-BJ method, make it possible to take more sensitive measurements such as I-V curves. The breadth of literature available concerning gold electrodes makes gold a good material with which to test the MCBJ. These measurements have explored the impacts of changing the molecular anchoring group, molecular backbone and contact metals. In addition, more recently, steps towards single molecule devices have been made. This chapter describes the measurements made using MCBJ and STM-BJ techniques with gold electrodes to determine the conductance of a range of different molecules. Using STM-BJ methods provides a good comparison for measurements taken using the home-built MCBJ system.

3.1 STM

3.1.1 STM Measurement Techniques

The STM experiments were carried out using an Agilent 5100 STM and a N9503A scanner. The scanner's built in current amplification electronics were replaced with a home built multichannel current to voltage converter. This provided an increased range over which currents could be measured. The modifications described were developed by Dr Doug S. Szumski [156]. The Pico

view software was used to control the STM during STM-BJ measurements. A bias voltage of 100 mV was applied between the tip and the substrate. The tip was then brought into contact with the substrate until a conductance of approximately 50 G_0 was measured. Current feedback was used to stabilise the tip in this position for 0.1 s before the tip was retracted by 6 nm at a rate of 20 nm/s. The current is measured as the tip is withdrawn from the substrate and this is used to calculate the conductance of structures formed between the tip and the substrate. Each of the currents measured by the pre-amplifier channels of the STM is received by a National Instruments USB-9215A 16-bit analogue to digital converter (ADC). Software written in LabVIEW was then used to plot histograms of the measured data in real time, allowing the user to observe how successful the experiment was at the time of measurement, and make any necessary alterations to improve it. The raw current data was also recorded and saved for further analysis. The current data are collected at a rate of 10 kHz and the tip maintains a constant speed of 20 nm/s as it is withdrawn. The 10 kHz clock and constant tip withdrawal speed are used to determine the distance that the tip has been withdrawn from the substrate.

3.1.1.1 Custom STM Electronics

During STM-BJ measurements, it is important to be able to measure a large range of currents over a short period of time, including the currents through individual molecular junctions which can last for less than a few hundred milliseconds. A quad channel STM preamplifier was designed by Dr Doug S. Szumski, based on the design of Meszaros *et al.* to overcome these issues [113, 156]. The circuit diagram for the pre-amplifier is shown in Figure 3.1. It consists of two operational amplifiers, OPA1 (a low sensitivity amplifier for measuring the currents in the "high" range, with output voltage V_{LS}) and OPA2 (a high sensitivity amplifier for measuring currents in the "low" range, with output voltage V_{HS}) . They both have an individual feedback network of resistors R_1 and R_2 (where R_1<R_2) and a transient voltage suppression (TVS) diode. Assuming ideal op-amp behaviour, the output voltage V_{LS} can be described as

$$V_{LS} = -I_{in}R_1, \tag{3.1}$$

where I_{in} is the measured input current. The feedback network for OPA2 includes resistors, R_1 and R_2, and the TVS diode which is connected in parallel with R_2. If the input current is small, the TVS diode is highly resistive and the current flowing through it will be negligible [18]. The output voltage V_{HS} in this case can be described as

$$V_{HS} = -I_{in}(R_1 + R_2). \tag{3.2}$$

When the threshold voltage, $\pm V_T$, is exceeded, avalanche breakdown occurs in the TVS diode. Its behaviour then switches to allow a current to flow, resulting in resistor R2 being bypassed. This causes output voltage V_{HS} to have a similar value to output voltage V_{LS}. A schematic explaining this behaviour is shown in Figure 3.2. In addition to this preamplifier, the channels experience

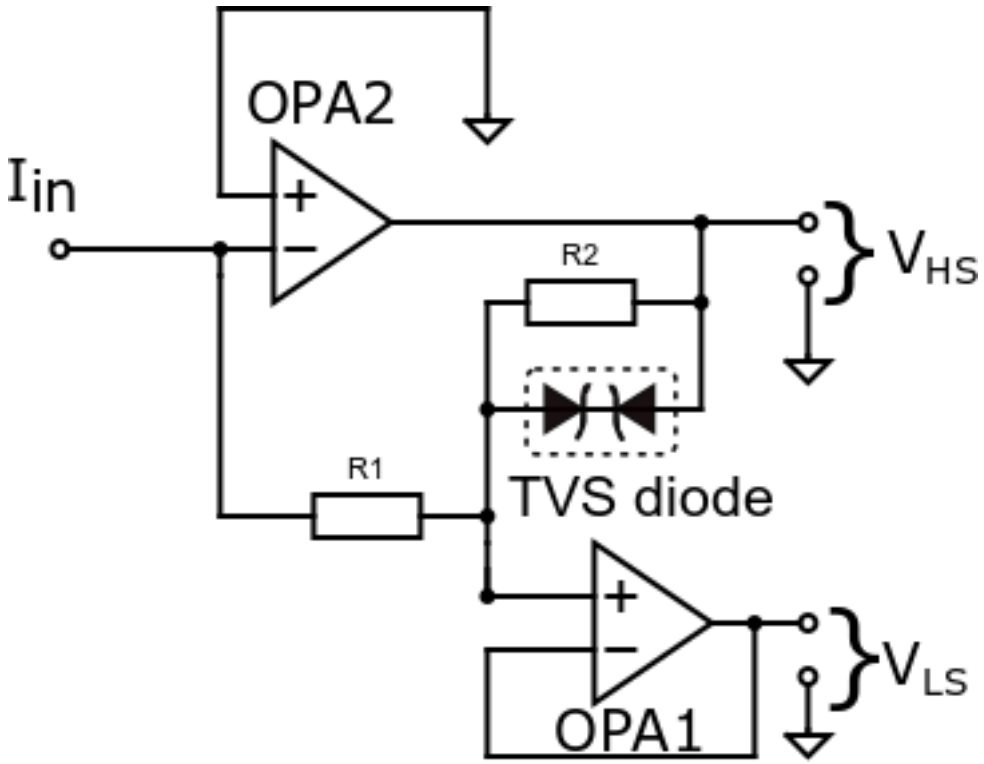

FIGURE 3.1. Circuit diagram showing the quad channel pre-amplifier used to increase the range of currents measured during STM measurements.

another amplification stage. Both output channels undergo ×1 and ×10 amplification, resulting in four separate output channels being recorded. This significantly increases the range over which the input current, I_{in} can be measured. The four measured channels are combined using home-written software written by Dr Doug Szumski with additions from Dr Richard Brooke to form conductance vs distance traces [18, 156]. They are then analysed to produce conductance histograms. Due to the nature of this process, an artefact appears in STM histograms at $10^{-1}G_0$.

3.1.2 STM Data Analysis

During STM-BJ measurements, junctions are repeatedly formed and broken allowing the measurement of the conductance of many different junctions. Although individual traces tend to differ, as the contacts are structurally rearranged every time the junction is opened or closed and molecular configurations may differ, they generally exhibit some common features. As an example of this, conductance vs distance traces for Au | Au junction may show plateaus close to integer multiples of G_0 as explained in Section 1.1.1. These plateaus will correspond to peaks in the histogram in Figure 3.3 labelled. The peaks are not always at an exact integer multiple of G_0, which could be due to back scattering on defects near the contact [202].

The most useful results are collected when opening the junction. In closing curves, initially

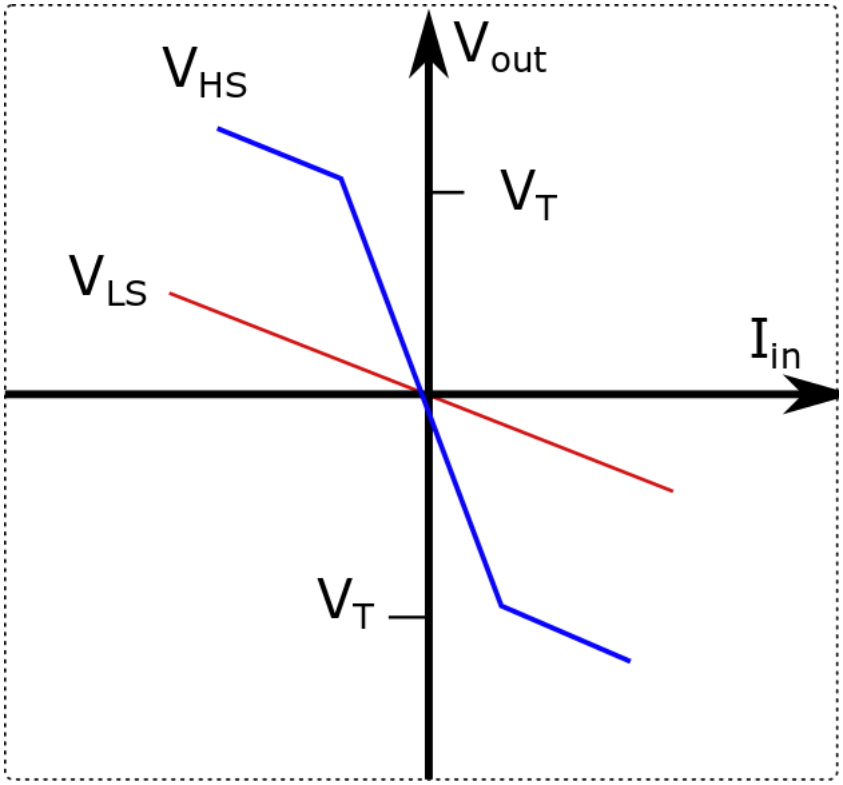

FIGURE 3.2. Schematic graph showing pre-amplifier output voltage as a function of input current where V_{HS} is the output voltage of the high sensitivity channel, V_{LS} is the output voltage of the low sensitivity channel and V_T is the threshold voltage.

the junction is open and transmission occurs via tunnelling. When the junction is closed, a "jump-to-contact" occurs. In this case, the first contact is usually of the order of several G_0 rather than 1 G_0. This is due to a phenomenon known as "adhesive avalanche" which occurs when two surfaces are brought close to each other. The system becomes unstable at a critical distance and so to stabilise the system, the surfaces suddenly jump into contact [202].

When investigating molecular conductance, is useful to use logarithmic binning of the conductance (x) axis as it makes any molecular features much clearer and they can be more easily distinguished from the background level of the histogram. A Gaussian distribution can be fitted to the peaks in the histogram in order to determine more accurately the most probably value of conductance.

In some cases, molecules have a low probability of forming junctions. This can mean it is impossible to distinguish a peak from the background counts of the histogram. The background counts are a result of tip-sample tunnelling in junctions with no molecule, and noisy traces. To overcome this problem, it is sometimes necessary to filter out conductance traces that do not contain a molecular plateau or are particularly noisy. There are a number of ways to do this. Firstly, data selection by visual inspection can be used to select scans that show molecular

plateaus. These scans are then included in the final histogram whereas the scans not showing any molecular features are discarded. This technique is highly susceptible to bias as it relies entirely on human judgement. It is also time consuming and inefficient when compared with other methods.

Within the literature, there are a number of methods that have been developed for automating the selection process. Quek and coworkers used a method that identified plateaus from a change in the gradient of current vs distance traces [139]. Inkpen *et al.* identified a method for I(s) style STM single molecule conductance measurements where an individual histogram was plotted for each scan. If a peak occurred in this histogram, this would identify a plateau in the trace. More recently, Magyarkuti and coworkers developed a feature recognition tool for single molecule break junctions [103]. This is a useful advance in analysis techniques as it uses machine learning to develop the analysis process. Using this method they were able to identify details in the traces that are not obvious to the human eye, but are highly significant for data analysis. In addition, the lack of human input makes these methods much less susceptible to bias.

In this work, an automated data selection technique developed by Dr Richard Brooke was used [18]. Similarly to Quek *et al.*, this technique used the gradient of the current vs distance traces to identify plateaus [139]. If no molecule is present in the junction, following the "snap-back" region (described in Chapter 2) there is an exponential decay of conductance due to tunnelling current between the STM tip and substrate. This trace will not exhibit any plateaus and hence there will be no sharp changes in the gradient and these traces will be rejected. If a molecular junction is formed, the "snap-back" region will be followed by a plateau or a number or plateaus separated by a sharp fall in conductance as the molecule switches between structures. At the end of the final plateau, there will be a sharp decrease in conductance followed by exponential decay. The sharp decreases in conductance can be easily identified using the gradient of the current trace, allowing one to separate traces containing molecular plateaus and traces without any molecular plateaus.

2D conductance vs distance histograms are also used as part of the analysis. The colour scale shows the relative probability of a data point being located within each of the 2-dimensional bins. For the 2D histograms plotted within, the individual conductance traces have been offset laterally so that the start of each scan is synchronised at the point where the current becomes lower than 0.1 G_0.

3.2 STM Molecular Measurements

In this chapter, the STM-BJ technique was used for conductance measurements as it can provide a useful comparison to results collected using the home-built MCBJ. It has the potential to increase the credibility of conductances measured. In contrast, it allows a discussion as to why one may observe different results when measuring the same junction via different methods.

3.2.1 Au Atomic Contacts

Initially, measurements were made without molecules in order to explore the nature of Au atomic contacts.The STM-BJ technique, as described in Chapter 2, was used to perform these measurements. The results can be seen in Figure 3.3. The linear scale histogram in the figure shows peaks close to integer multiples of G_0. These peaks represent the quantization of conductance in gold point contacts as explained in Chapter 1. The quantization is also demonstrated by the 2D histogram in Figure 3.4. The individual scans were offset on the x-axis to synchronise them at a conductance value of 12 G_0.

The Au substrates used in the experiments were cleaned prior to use by placing them for 25 minutes in concentrated sulphuric acid. They were then rinsed in Milli-Q water with resistivity greater than 18 MΩcm and dried using nitrogen gas. The tips were cut manually from 0.25 mm Au wire using scissors. A 100 mV bias voltage was applied between the tip and the sample during these measurements. The conductance of Au atomic contacts was also measured in mesitylene (1,3,5-trimethylbenzene), as this is the solvent that was used to make the molecular solutions used in the molecular conductance measurements. These data are shown in Figure 3.5a, where peaks close to integral values of G_0 can be seen. This confirms that for any future measurements taken with a solution of molecules in mesitylene, any conductance peaks visible below G_0 will be due to the presence of a molecule rather than mesitylene. Figure 3.6 shows some typical STM-BJ conductance traces. One can clearly observe the quantization of conductance in these traces as they show plateaus close to integer multiples of G_0. Particularly clear is the plateau at G_0. Figure 3.6b shows a typical conductance vs distance trace for an Au | Au junction plotted on a logarithmic scale. Below the plateau at G_0, a rapid decrease in conductance is observed. This rapid decrease is caused by the apex atoms, which spontaneously undergo structural rearrangement to minimise the surface energy. This results in rapid separation of the tip and substrate and is known as "snap-back". After the "snap-back" region, there is a linear decrease in conductance. This linear decrease represents the exponential decay of the current between the tip and the substrate. An exponential decay in current in this case is representative of quantum tunnelling, during which the current has an exponential relationship with the distance over which the current is tunnelling.

3.2.2 4,4'-bipyridine

Gold electrodes were used to measure the conductance of junctions formed in mesitylene containing a 1 mM concentration of 4,4'-bipyridine (4,4'-BP). Measurements were performed with a tip-substrate bias of 100 mV. The structure of 4,4'-bipyridine is shown in the inset in Figure 3.7. 575 traces were gathered and, without data selection, the histogram shown in Figure 3.7 was constructed. This histogram shows two peaks: a high conductance peak and a low conductance peak. The low conductance peak appears around 10^{-4} G_0 and the high conductance at 10^{-3}

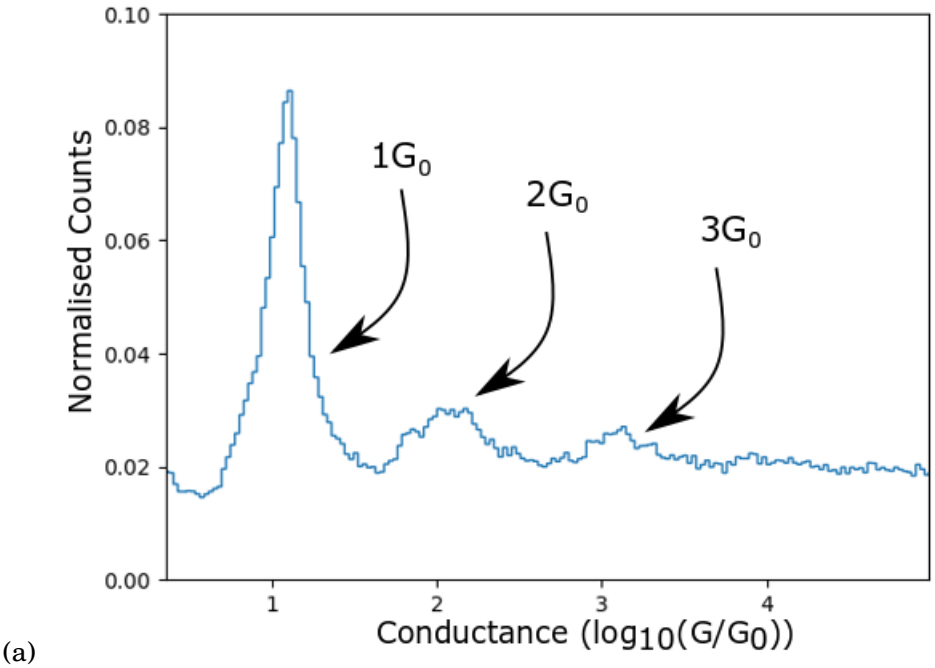

(a)

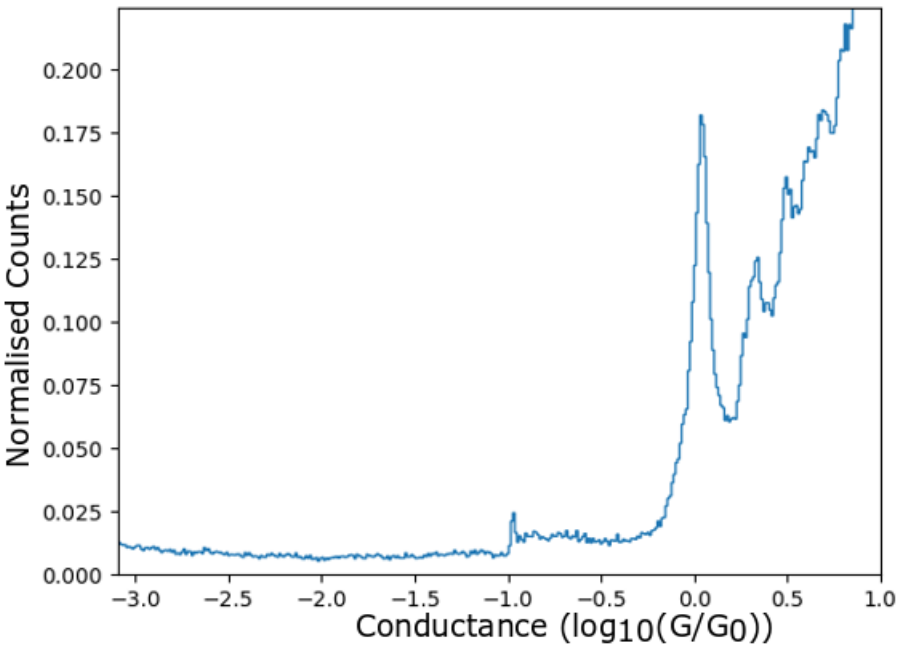

(b)

FIGURE 3.3. STM-BJ conductance measurements of an Au | Au junction in air plotted on (a) linear (peaks from conductance quantization labelled) and (b) logarithmic scales. Formed from 1231 traces.

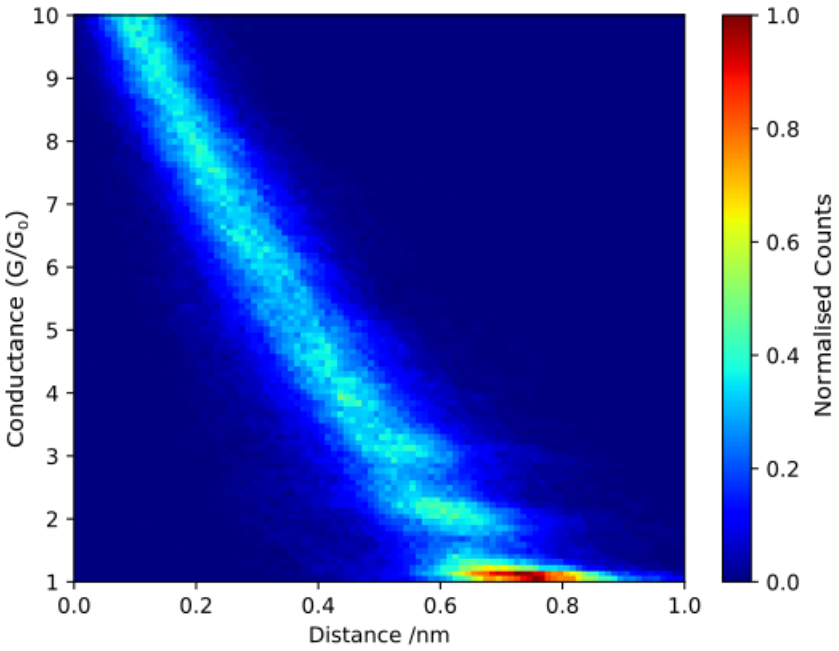

FIGURE 3.4. STM-BJ conductance measurements of an Au | Au junction in air plotted as a 2D histogram. Constructed from 1231 traces.

G_0. The appearance and cause of these two peaks was discussed in detail in Section 1.3.1.2. In addition to these peaks, a shoulder can be seen on the high conductance peak. This may reflect junctions bridged by more than one molecule. A 2D histogram, shown in Figure 3.8 was also produced from the data. This shows that generally, the high conductance configuration is formed directly after the separation of the electrodes, and then as the electrode separation is increased, the low conductance configuration appears and is measured.

Following the methods of Makk *et al.*, a 2D correlation histogram was produced [105]. This is shown in Figure 3.9. Conditional histograms were also plotted, shown in Figure 3.10. 2D correlation histograms are used to determine the nature of the statistical relationship between different junction configurations that correspond to two different conductance values [105]. If those different conductance values are defined as G_i and G_j, the statistical relationship of G_i and G_j is determined from the product $N_i(r)N_j(r)$, where $N_i(r)$ is the number of data points in each trace, r, with conductance G_i [105]. Conditional histograms use a subset of the data to analyse relationships between histogram features such as peaks in greater detail. These subsets generally include traces which provide a major contribution to a particular histogram peak [105]. When there is more than one peak in a histogram, if they are statistically correlated, then selection of traces for one peak will change the second peak. The selection takes place based on the following

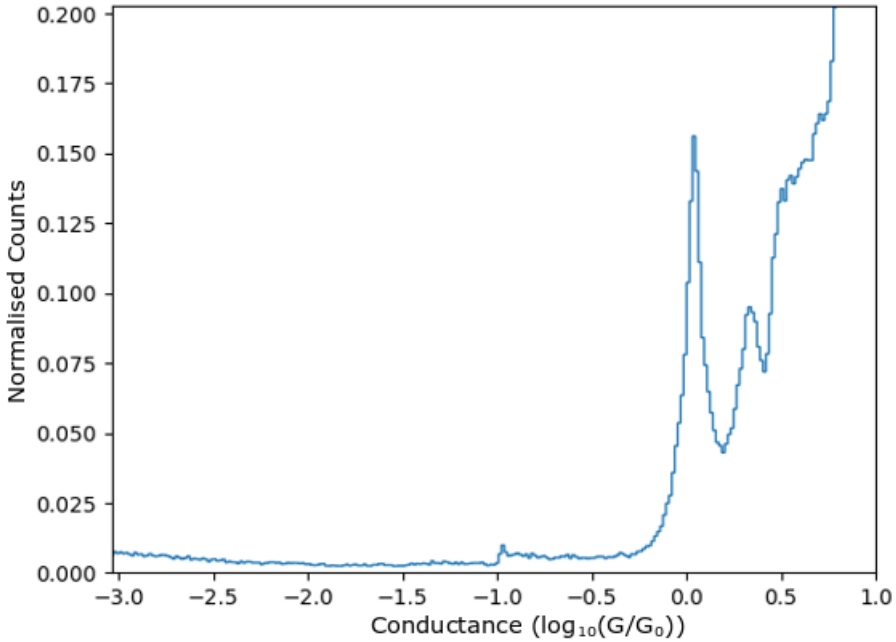

FIGURE 3.5. STM-BJ conductance measurements of an Au | Au junction in mesitylene plotted on a logarithmic scale. Formed from 1143 traces. A conductance quantization peak is visible at G_0.

algorithm: the traces, r', for which the total number of data points in the interval of the reference histogram peak (P) is larger than a threshold value, N_p are selected [105]. Generally N_p is defined as the average number of data points in the chosen conductance region.

Here, correlation analysis was used to investigate the multiple conductance states of the Au | 4,4'-BP | Au junction. To our knowledge, this is the first instance that this type of analysis has been used to analyse this particular junction. The blue regions in Figure 3.9 suggest that there is a negative correlation between the low conductance peak and the high conductance peak. However, it is difficult to interpret the meaning of the 2D correlation histogram without more information. The conditional histograms (Figure 3.10) provide this additional information. For clarity, they have not been normalised. When the histogram is formed from the traces which contribute to the high conductance peak (b), the low conductance peak is reduced and smoothed out. However, when the histogram is formed from the traces which contribute to the low conductance peak (c), the high conductance peak remains clear. This suggests that the high conductance configuration is often measured when the low conductance peak is measured. In contrast, the absence of the low conductance peak in the histogram formed from traces that contribute to the high conductance peak suggests that the high conductance configuration may sometimes be measured as the only configuration in a particular trace. In the histogram formed from traces

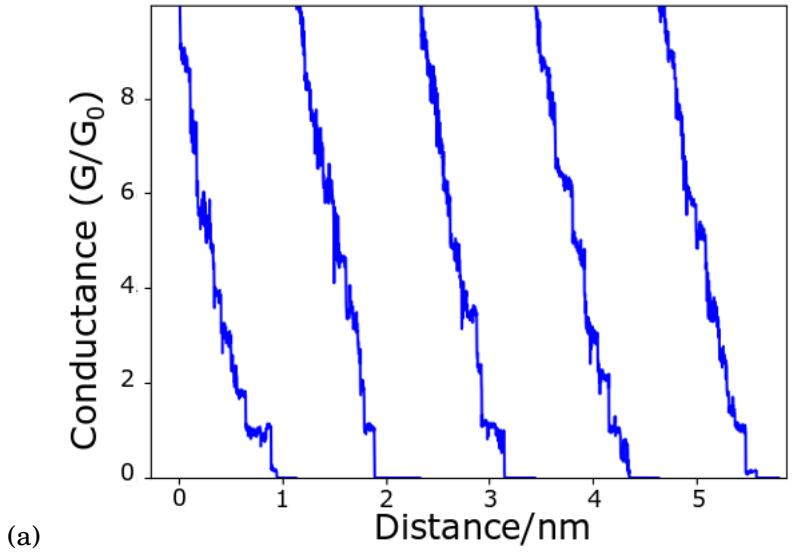

(a)

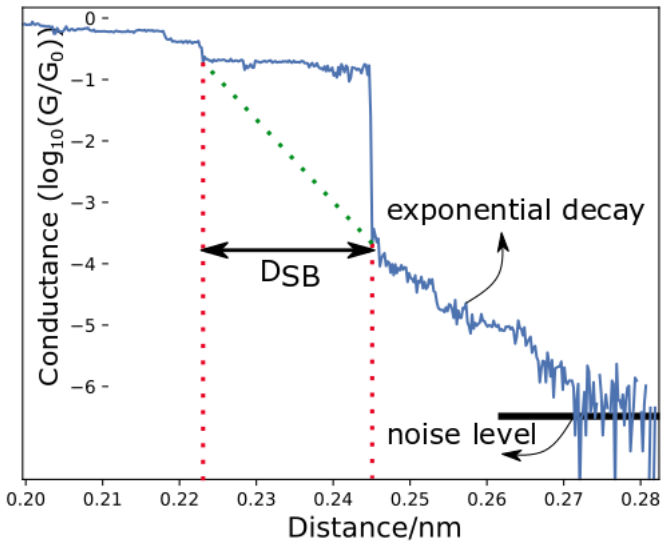

(b)

FIGURE 3.6. (a) Individual traces measured using the STM-BJ technique. (b) A typical Au | Au junction conductance vs distance trace plotted on a logarithmic scale. Horizontal line represents the noise level of the STM.

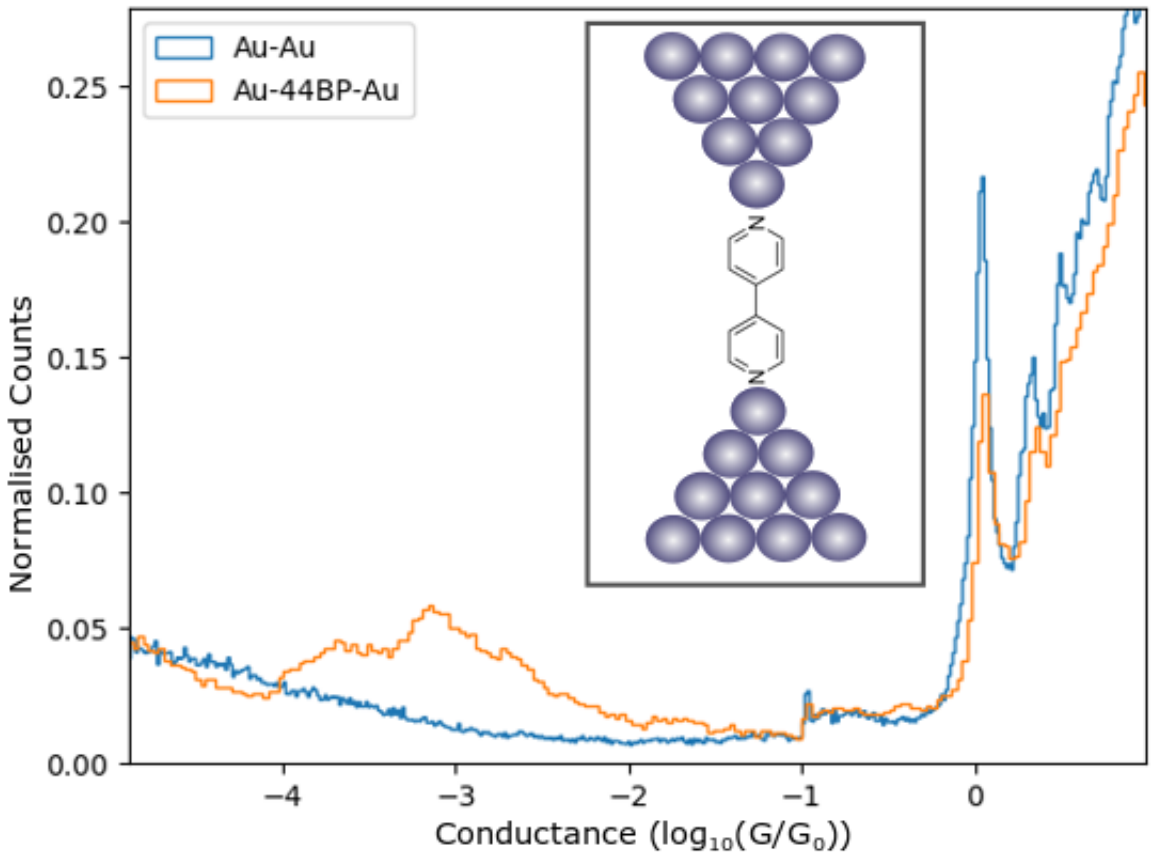

FIGURE 3.7. Molecular conductance histogram of the Au | 4,4'-BP | Au junction, measured using the STM-BJ technique. The histogram is constructed from 575 traces. The inset shows a potential Au-4,4'-BP-Au junction.

that contribute to the shoulder in the high conductance peak, the low conductance peak also appears somewhat reduced. The high conductance peak is still clearly visible. In conclusion, from Figure 3.10 it has been learnt that one is significantly more likely to observe a plateau in the low conductance region in a trace with two plateaus (high conductance and low conductance) present, than a trace containing a single low conductance plateau. However, it is also possible to observe traces containing a single high conductance plateau, with no low conductance plateau present. This means that the shoulder is likely to appear in traces which also contain a plateau corresponding to the high conductance configuration. This suggests that a junction bridged by two molecules initially, may become bridged by just one molecule during the breaking process. Examples of individual traces of these types are shown in Figure 3.11.

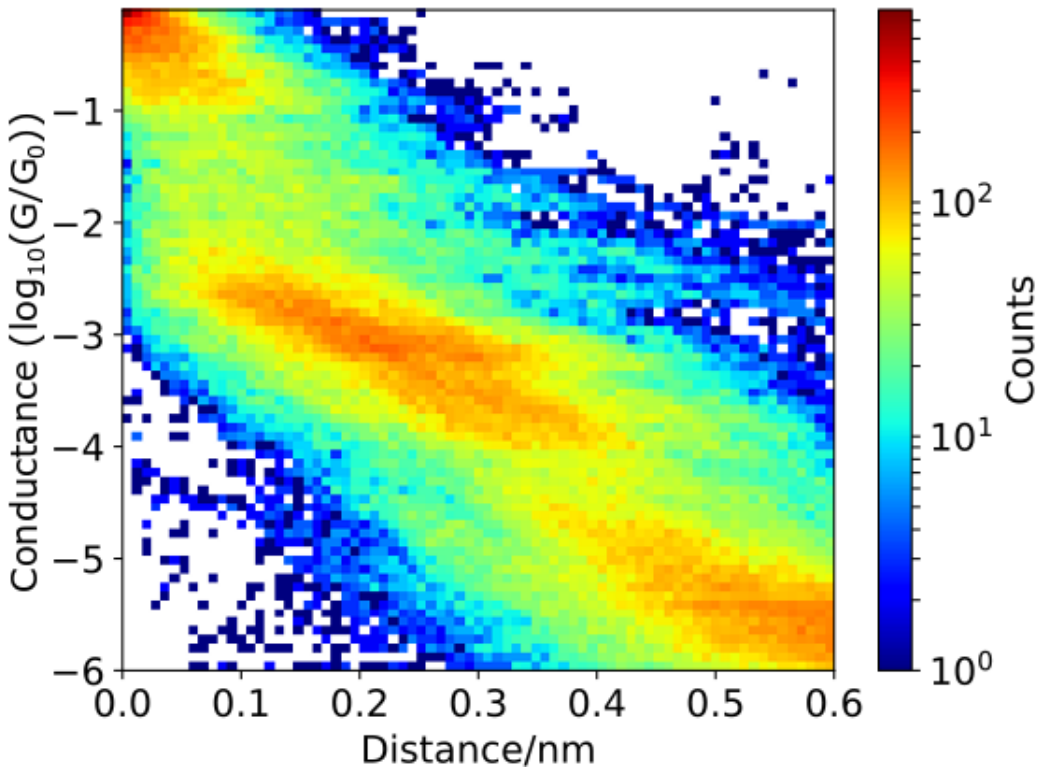

FIGURE 3.8. 2D histogram showing STM-BJ conductance measurements for the Au | 4,4'-BP | Au junction in mesitylene plotted on a logarithmic scale. Formed from 575 traces. Molecular features can be seen between $10^{-}2G_0$ and $10^{-}4G_0$.

3.2.3 4,4'-Vinylenedipyridine

As the chemical structure diagram in the inset of Figure 3.12 shows, 4,4'-vinylenedipyridine (4,4'-VDP) molecules are similar to 4,4'-BP molecules. However, they contain a conjugated ethene moiety which links the two pyridine rings. The measurements were taken using the STM-BJ method and the tip-substrate bias for these measurements was 100 mV. A 0.5 M solution of Na_2SO_4 with a 100 mM concentration of 4,4'-VDP was used. The results of these measurements, shown in Figure 3.12 with individual traces shown in Figure 3.13, were similar to those of 4,4'-BP. Overlapping peaks at approximately 10^{-4} G_0 and 10^{-3} G_0 were observed. The presence of two peaks is again explained by the ability of the pyridine anchor to bind to the Au electrode in two distinct configurations. The peaks observed have lower conductance values than those measured for 4,4'-BP. This may be because the conjugated ethene moiety adds approximately 2.3 Åto the length of the molecule [201]. A difference in length is demonstrated by the 2D histogram in Figure 3.14. When compared with Figure 3.8, it can be seen that the region which represents the

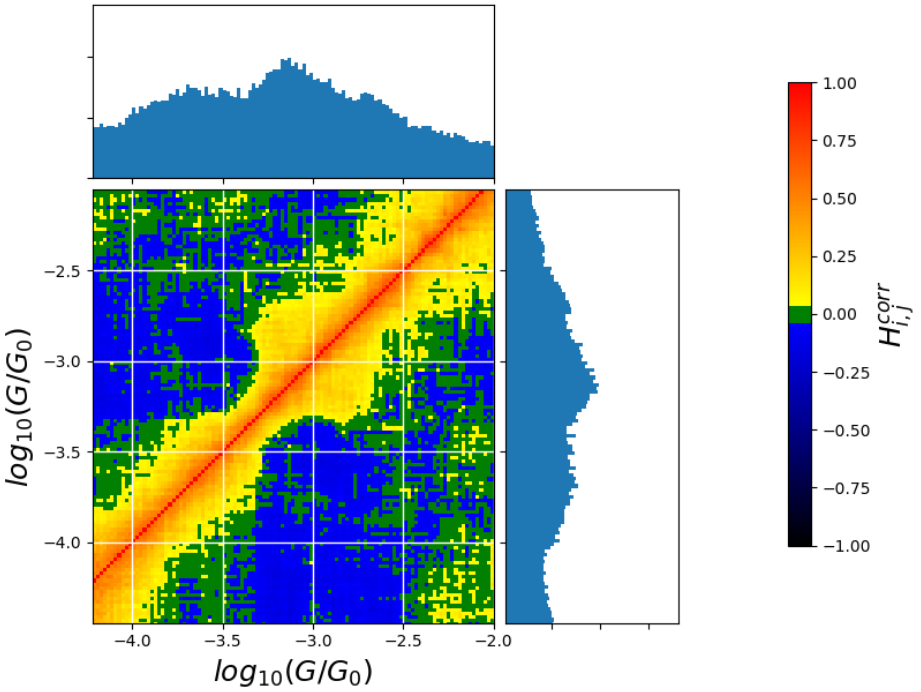

FIGURE 3.9. 2D correlation histogram for the Au | 4,4'-BP | Au junction, focussing on the correlation between the high conductance, low conductance and shoulder on the high conductance peak. The 1D conductance histogram is plotted on the edges of the correlation histogram.

presence of a molecule extends over a greater tip-substrate separation distance. These results are in agreement with those obtained by Quek *et al.* [138].

3.3 MCBJ Molecular Measurements

Due to the slow speed of the MCBJ, long traces in the tunnelling region were observed in a high proportion of measurements. This resulted in an increased number of background counts below 1 G_0 which made any peaks present difficult to analyse as they had been obscured by background counts. To overcome this, in some histograms the data has been cropped at the tunnelling region. This negative effect was also observed by Martin and coworkers [107].

2D histograms were used to analyse the MCBJ data and again, the individual conductance traces have been offset laterally so that the start of each scan is synchronised at the point where the current becomes lower than 0.1 G_0.

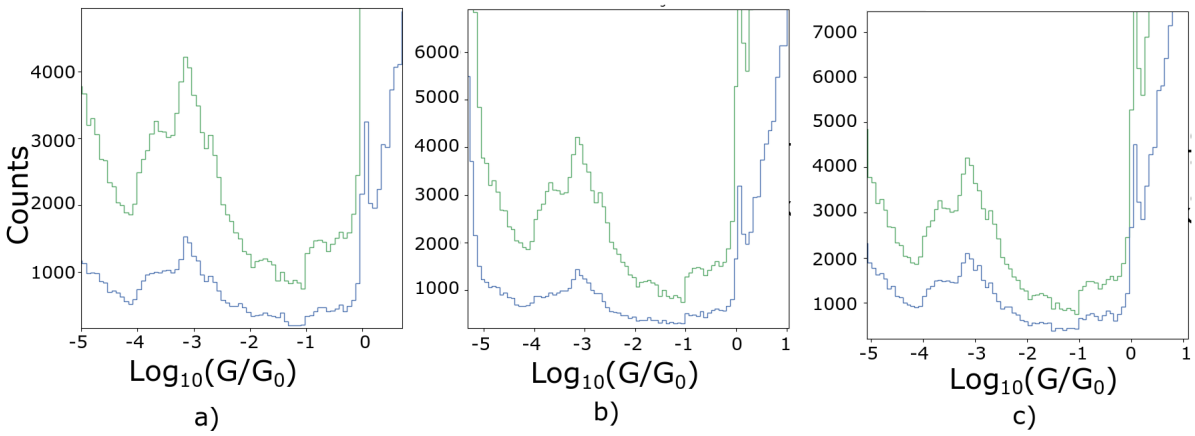

FIGURE 3.10. Conditional histograms where the green line shows the histogram formed from the entire data set and the blue line shows the histogram formed from traces that contribute to (a) the shoulder on the high conductance peak, (b) the high conductance peak and (c) the low conductance peak.

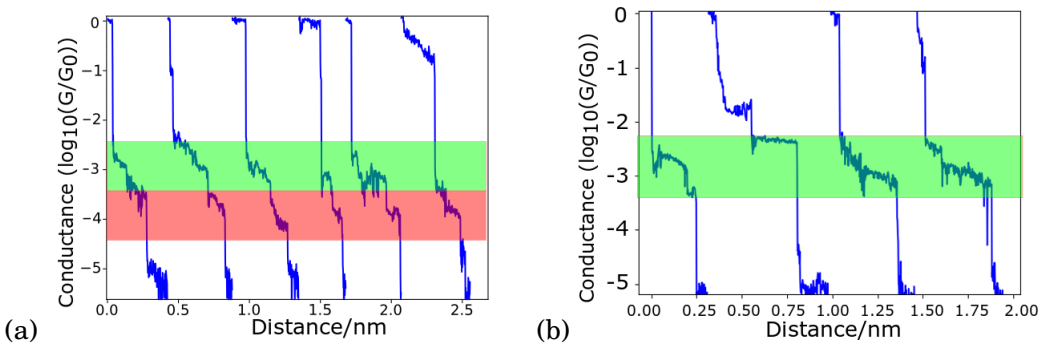

FIGURE 3.11. A selection of individual conductance vs distance traces of the Au | 4,4'-BP | Au junction. (a) shows traces which appear to feature both high conductance and low conductance plateaus. (b) shows traces which only appear to show high conductance plateaus. Green band highlights high conductance plateaus and the red band highlights low conductance plateaus.

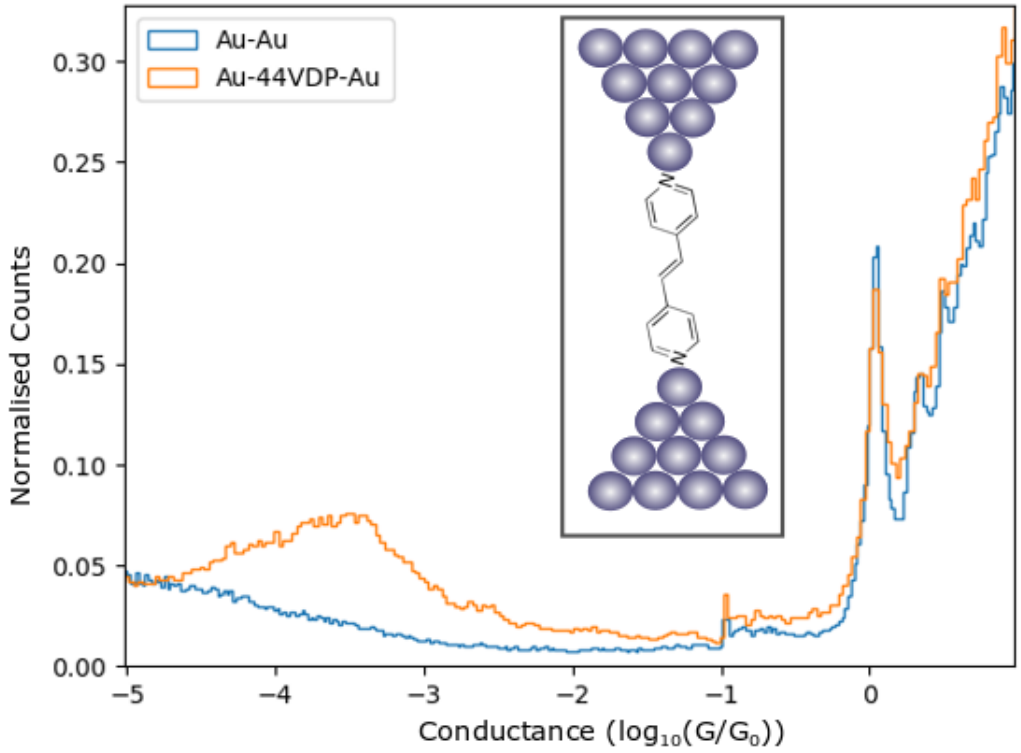

FIGURE 3.12. Conductance histogram for the STM-BJ measurements of the Au | 4,4'-VDP | Au junction, with a diagram showing the chemical structure of 4,4'-VDP. Formed from 784 traces. Molecular feautures are seen as overlapping peaks at approximately 10^{-4} G_0 and 10^{-3} G_0.

3.3.1 Preparation of Samples

Molecules were applied to the substrates via three different methods. The first involved using a 0.05 M aqueous solution of Na_2SO_4 to create a solution with a 1 mM concentration of molecules. A droplet of this was then transferred to the electrodes using a pipette. The second method used an ethanol solution with a 1 mM concentration of molecules. Similarly, this was transferred to the electrodes of the substrate using a pipette. It was left for 5 minutes during which time the ethanol evaporated, leaving molecules on the electrodes [35]. Both of these methods resulted in noisy conductance traces, from which it was not possible to construct a useful histogram. This may have been due to the fact that the notched wire substrates used for MCBJ are difficult to clean. Applying a liquid to them allows contaminants to move around on the substrate and come into contact with the freshly cleaved electrodes. To overcome this issue, a third method was explored. This involved exposing the electrodes of a MCBJ sample to a high concentration of the

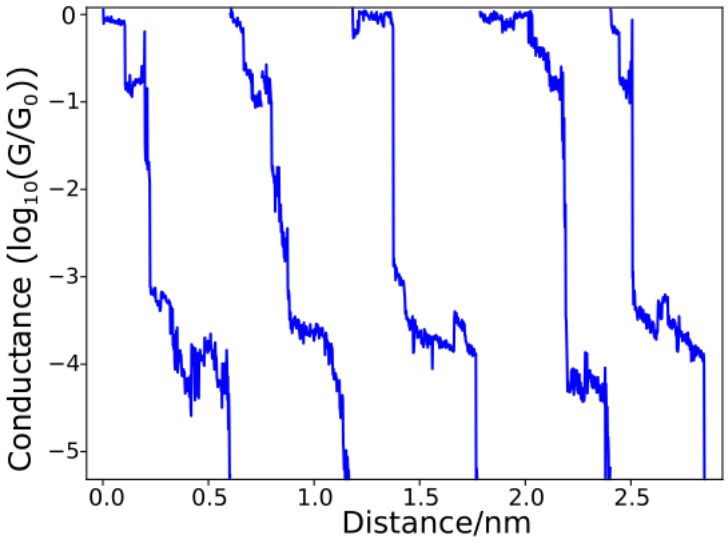

FIGURE 3.13. Typical Au | 4,4'-VDP | Au conductance vs distance STM traces. Start points of the traces have been staggered for clarity.

molecule in ambient air for 48 hours, which was carried out using a saturated aqueous solution of the molecule. The sample was stuck to the wall of a bottle containing this solution, but not in contact with the solution, and the bottle was sealed. The anchoring of thiol groups to metal surfaces has been studied extensively and it is thought that this process will result in a layer of the thiol molecule on the surface of the electrode [107, 111, 164].

3.3.2 Pentanedithiol

The conductance of the Au | pentanedithiol | Au junction was determined using the MCBJ method. Measurements of this junction show a molecular conductance of $(2.0\pm0.1)\times10^{-3}$ G_0 which was determined by fitting a Gaussian to the histogram shown in Figure 3.15. A 2D histogram of the data is displayed in Figure 3.16. In previous work, Li and coworkers measured the conductance of several alkanedithiols [93][141]. For pentanedithiol they found two conductance peaks: A high conductance peak at approximately 8×10^{-4} G_0 and a low conductance peak at approximately 2.5×10^{-5} G_0. They explain the appearance of multiple peaks by suggesting a number of possible arrangements of a single alkanedithiol molecule bridged between Au electrodes. In their work, the high conductance peaks are attributed to an all-*trans* alkyl chain in combination with both sulphurs coordinated to two Au atoms in bridge geometry. The low conductance peaks are attributed to nonequivalent isomers of alkanedithiols with gauche effects [93]. They also obtain theoretical results that are in agreement with their experimental work. More recent investigations have suggested that the presence of multiple conductance peaks may be due to the difference

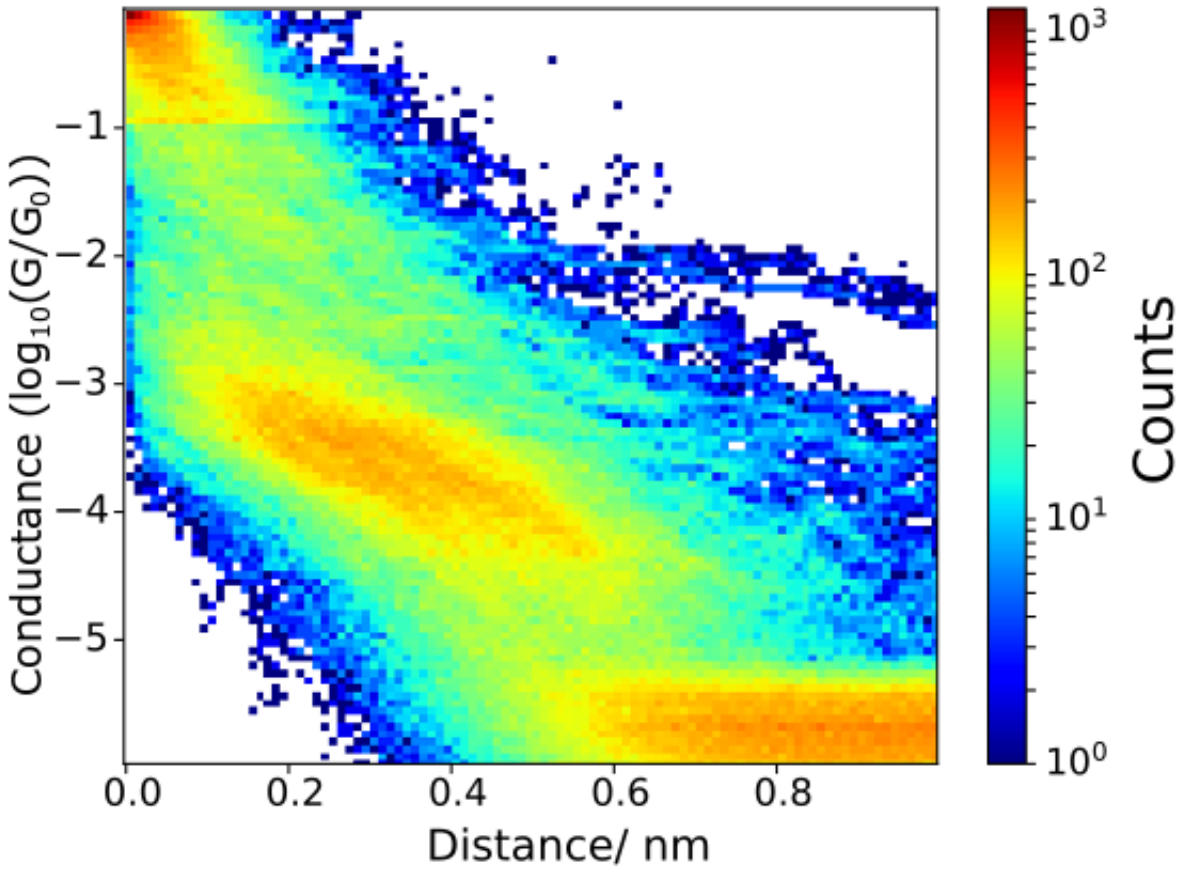

FIGURE 3.14. 2D conductance-distance histogram for the STM-BJ measurements of the Au | 4,4'-VDP | Au junction. Formed from 784 traces. The molecular feature is visible between approximately 10^{-3} G_0 and 10^{-4} G_0.

between measuring a dimer and a monomer [102]. Venkataraman *et al.* used STM-BJ techniques to study pi-stacked dimer junctions. Through this, they demonstrated that the conductance of monomer junctions can differ significantly when compared with junctions containing dimers. The results measured herein using the MCBJ are in agreement with those of Leary *et al.*, who observed a conductance of 1×10^{-3} G_0 [90]. In addition, unpublished STM-BJ measurements of the Au | pentanedithiol | Au junction carried out by a group member, Yang Chaolong support the MCBJ measurements of the same junction as they display a conductance peak in a similar region (approximately 1×10^{-3} G_0) , as is shown in Figure 3.17. These measurements were taken using in a liquid environment using a 0.05 M aqueous solution of Na_2SO_4 to create a solution with a droplet of ethanol saturated with pentanedithiol.

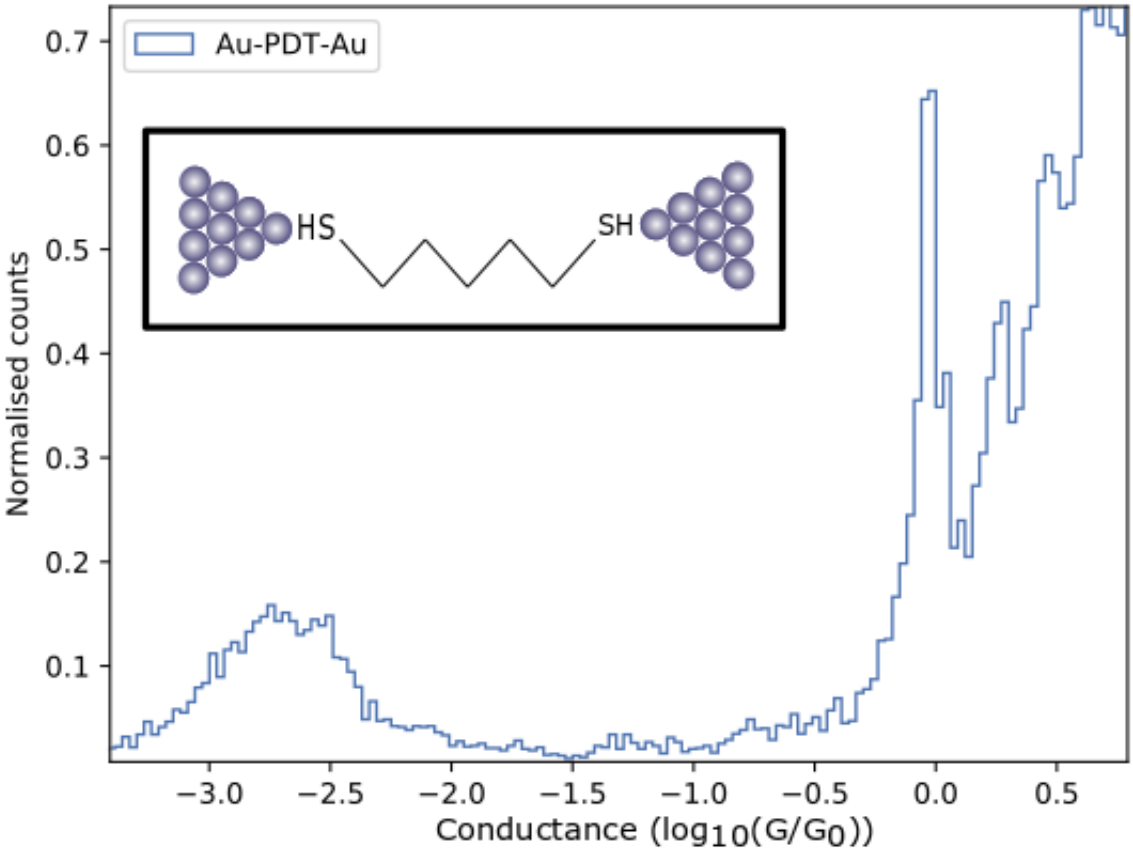

(a)

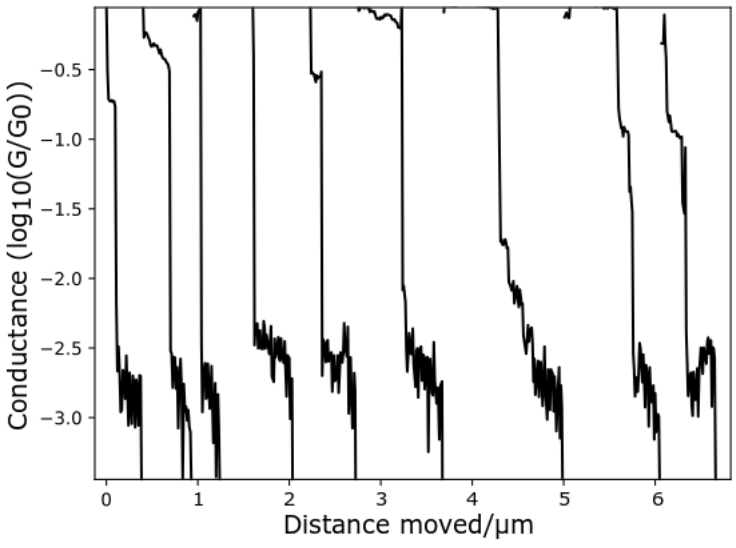

(b)

FIGURE 3.15. (a) MCBJ conductance histogram of an Au | PDT | Au junction. Formed from 135 traces. The inset shows a possible Au | PDT | Au junction. The molecular feature is visible at $(2.0\pm0.1)\times10^{-3}$ G_0. (b) Typical MCBJ conductance vs distance traces shown in bottom figure for an Au | PDT | Au junction. Start points of individual traces have been staggered for clarity.

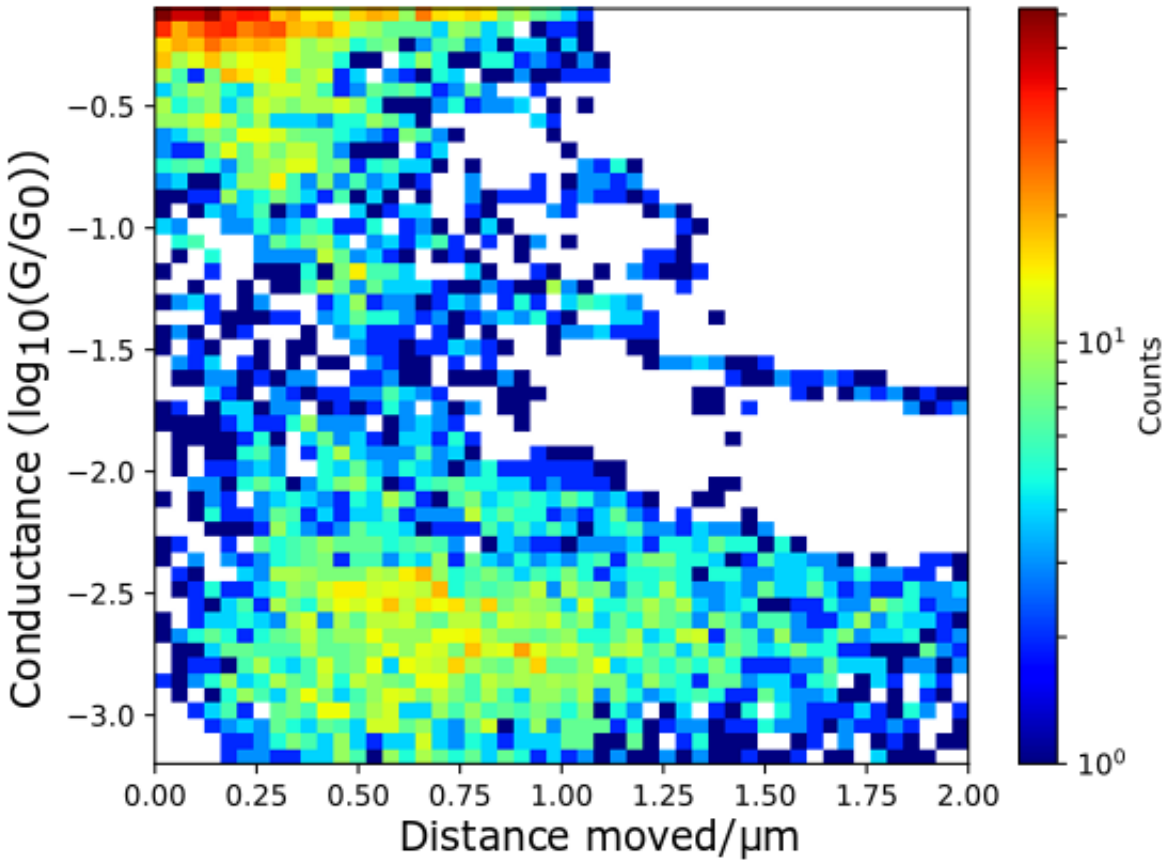

FIGURE 3.16. MCBJ 2D conductance histogram of an Au | PDT | Au junction. Formed from 135 traces. Molecular feature is visible at $(2.0\pm0.1)\times10^{-3}$ G_0.

3.3.2.1 I-V Curves

A series of I-V curves were collected in the same way as those described in Section 2.4.3. Using methods similar to those of Beebe and coworkers, the I-V curve was used to find the conductance of the metal-molecule-metal junction [12]. In this case, the I-V curve shown in Figure 3.18 has an approximately linear and symmetric region between -0.1 V and +0.1 V. This, along with 3 other I-V curves were used to determine an average conductance value of 2×10^{-3} G_0 which is in agreement with the value determined using the histogram in Figure 3.15. A 2D histogram was constructed from the Au | PDT | Au I-V traces, this is shown in Figure 3.19. This shows the preferred path of the I-V data.

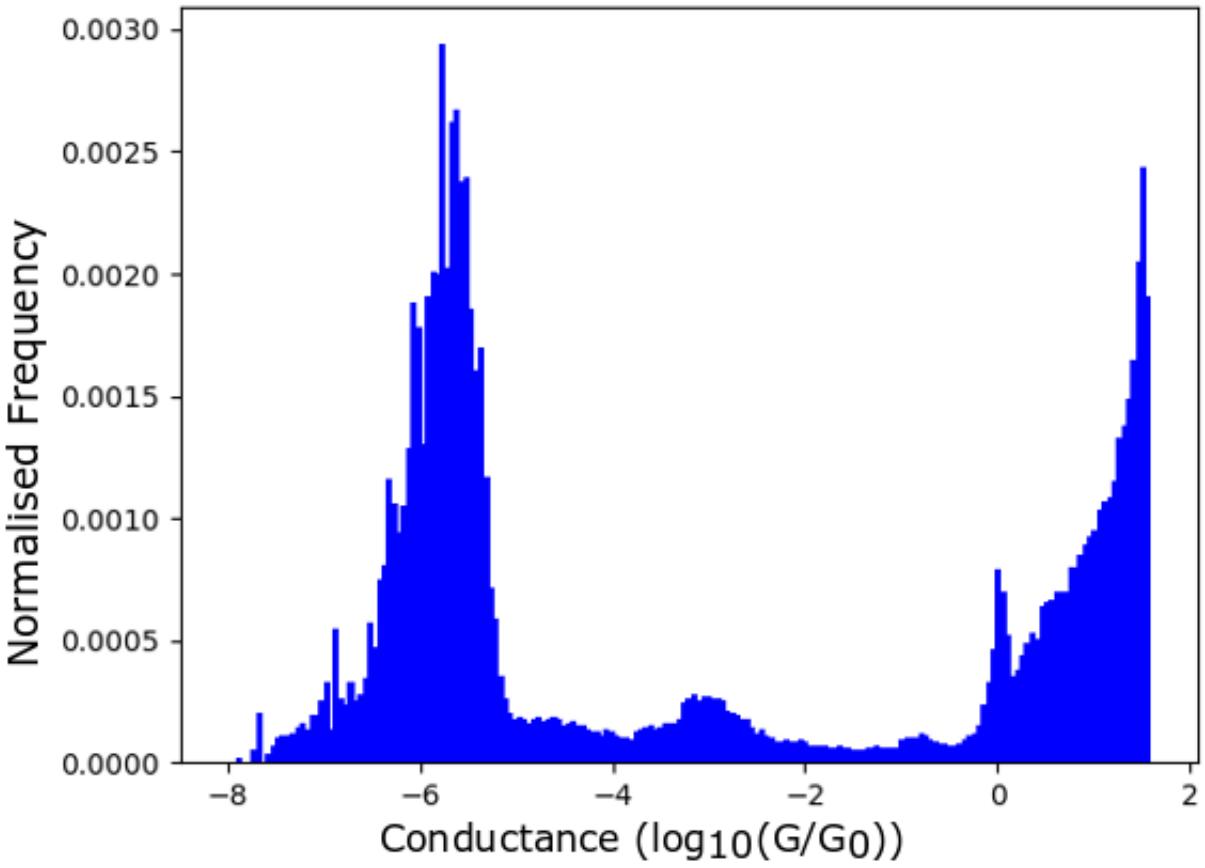

FIGURE 3.17. Conductance histogram for the Au | PDT | Au junction measured with the STM-BJ technique by Yang Chaolong [unpublished]. Large peak at $\log_{10}(G/G_0) = -6$ is caused by the noise level of the STM. Molecular feature is visible around $10^{-3}\ G_0$

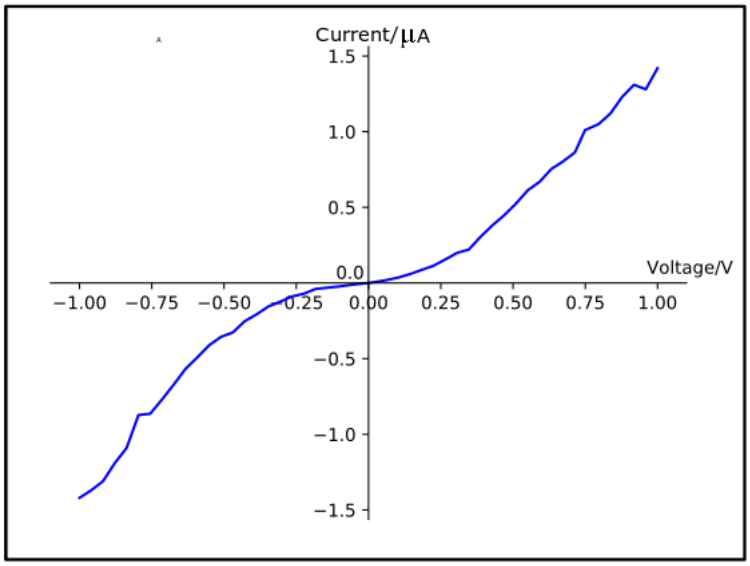

(a)

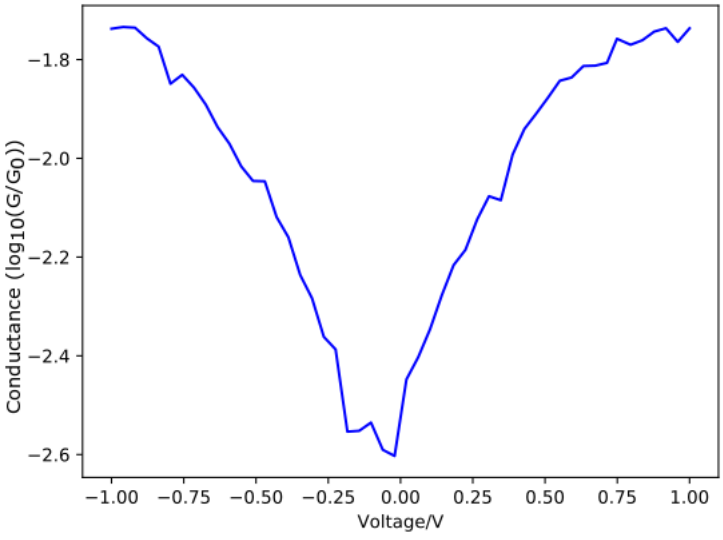

(b)

FIGURE 3.18. (a) A typical I-V trace of an Au|PDT|Au junction. (b) Differential conductance measured during a voltage sweep.

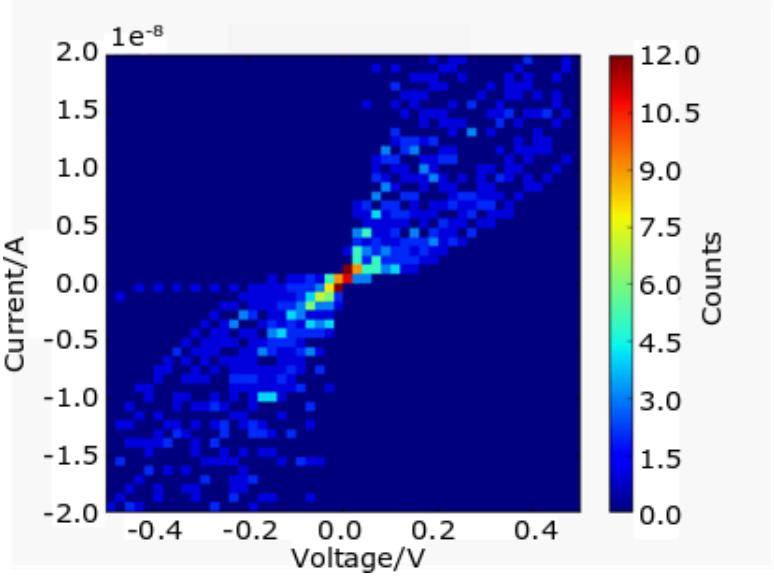

FIGURE 3.19. 2D histogram constructed from 30 Au | PDT | Au I-V traces.

3.3.3 1,4-benzenedithiol

The MCBJ was used to measure the conductance of the Au | 1,4-benzenedithiol | Au junction. As discussed in Section 1.3.1.1, there has been a large variety in the measured conductance of the Au | 1,4-benzenedithiol | Au junction. The values have varied over three orders of magnitude, ranging from 10^{-4} G_0 to close to G_0 [60, 84, 90, 167, 169, 185], whereas some measurements fail to show any peak at all [106, 169]. The measurements reported in this thesis show two conductance peaks at $(8.5 \pm 0.3) \times 10^{-2}$ G_0 and $(1.4 \pm 0.1) \times 10^{-2}$ G_0. These values were found by fitting a Gaussian to the peaks of the histograms shown in Figure 3.20. They are in agreement with several previous reports including Tao *et al.* who observed a peak with a conductance of 1.1×10^{-2} G_0. They also measured junctions with a conductance equal to multiples of this value as a result of two or three molecule junctions [185]. Most similarly, Tsutsui *et al.* found peaks close to 0.01 G_0 and 0.1 G_0 [167]. These were attributed to different binding configurations as explained in Section 1.3.1.1. In addition, Kim *et al.* also found conductance values close to 0.1 G_0 and 0.01 G_0. In Figure 3.20, it is clear from the individual traces that there are a number of different "types" of plateaus. Martin and coworkers have suggested that this is due to a large spread in geometrical variations in the metal-molecule junctions. They conclude that the possible interactions between the benzene core and gold electrodes may contribute to variations in the conductance values measured [107]. Similar to the work reported here, the measurements of Martin and coworkers were performed using self assembled monolayers on a gold surface [107]. It is thought that without the use of a stabilizing solvent, it could be possible to measure junctions that consist of a molecule lying flat on the electrode surface. Figure 3.21 shows some examples of possible linking configurations. The interaction of π-orbitals with the gold electrodes could

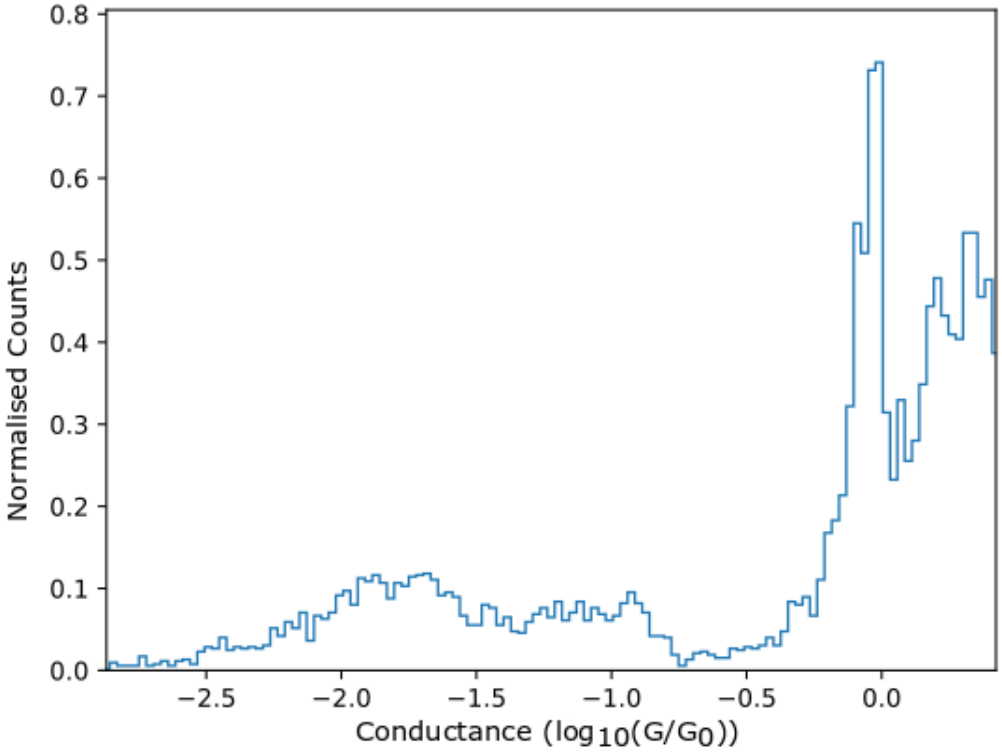

(a)

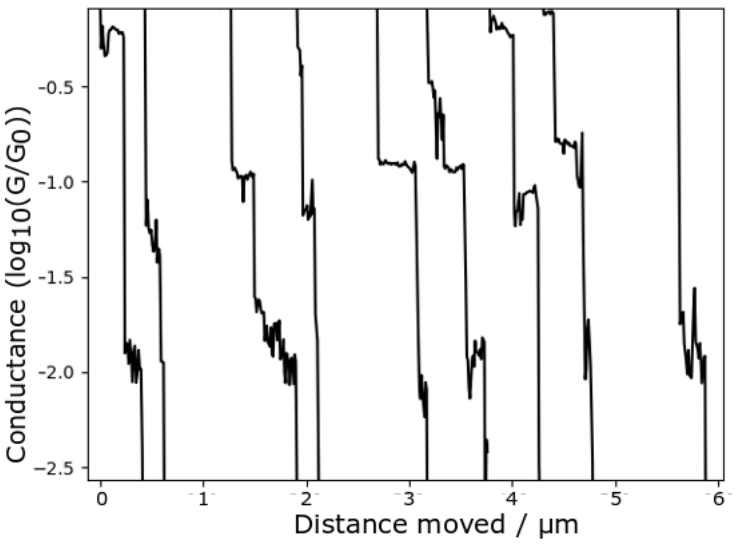

(b)

FIGURE 3.20. (a) Histogram showing conductance of the Au | 1,4-benzenedithiol | Au junction measured using the MCBJ technique. Histogram is constructed from 200 traces. Molecular features are visible at $(8.5 \pm 0.3) \times 10^{-2}$ G_0 and $(1.4 \pm 0.1) \times 10^{-2}$ G_0. (b) Typical traces used to construct the histogram. The starting point of each trace is staggered for clarity.

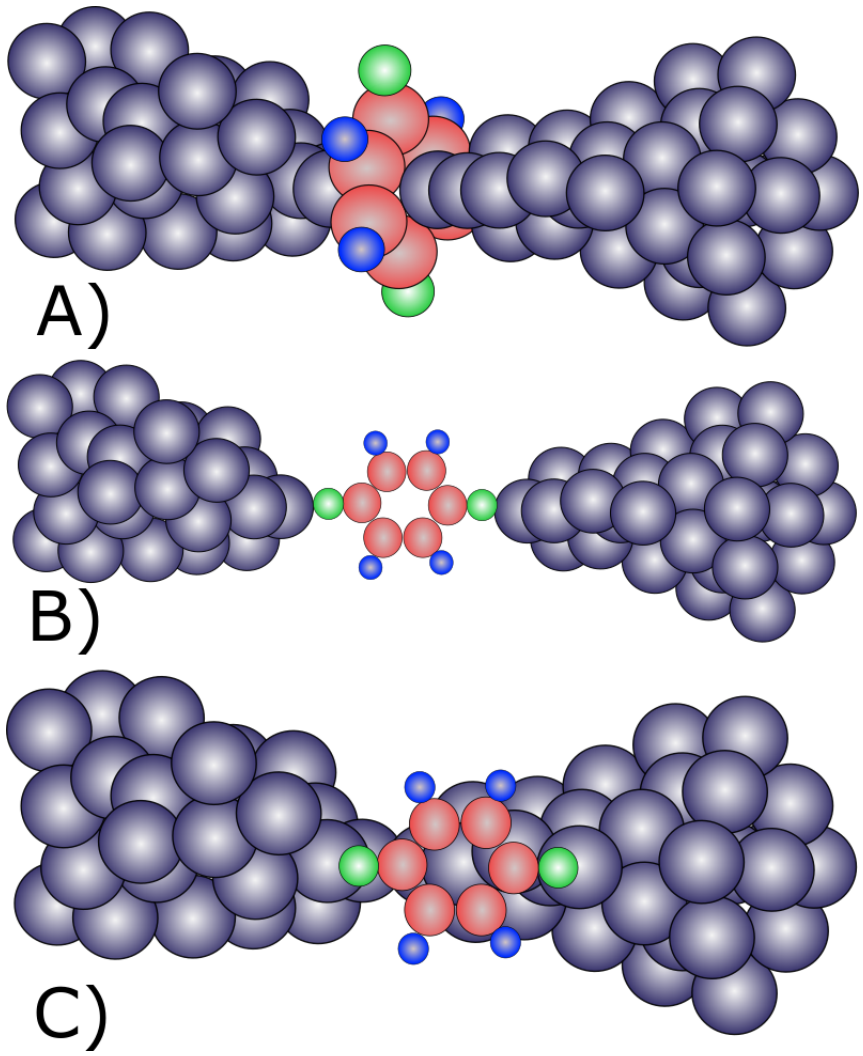

FIGURE 3.21. Some possible configurations of the Au | 1,4-benzenedithiol | Au junction. Red atoms represent carbon, blue atoms represent hydrogen and green atoms represent the thiol group (physisorbed bond) or a single thiol atom (chemisorbed bond).

lead to significantly different measured conductance values than those measured with upright molecules [107].

3.4 Chapter Summary

The conductances of several different molecules have been measured in a junction with Au electrodes, using both the STM-BJ technique and the MCBJ technique. These results are summarised in Table 3.1. This work focused on dithiol linked molecules. I-V measurements were used to demonstrate the stability of the MCBJ. Through I-V measurements it was also possible

Junction	Measurement Technique	Molecular Conductance G_0	
Au | 4,4'-bipyridine | Au	STM-BJ	10^{-4}	10^{-3}
Au | 4,4'-vinyledipyridine | Au	STM-BJ	10^{-4}	10^{-3}
Au | pentanedithiol | Au	MCBJ	$(2.0\pm0.1)\times10^{-3}$	
Au | 1,4-benzenedithiol | Au	MCBJ	$(8.5\pm0.3)\times10^{-2}$	$(1.4\pm0.1)\times10^{-2}$

Table 3.1: A summary of the results obtained within Chapter 3.

to corroborate the conductance values of the Au | PDT | Au junction determined using MCBJ techniques. This value was also found to be in agreement with measurements made using STM-BJ in unpublished work by group memeber Yang Chaolong. Although the literature presents a range of values measured for this junction, the value obtained within is the same order of magnitude as that of Leary *et al.*, who observed a conductance of 1×10^{-3} G_0 [90].

In addition, the conductance of the Au | 1,4-benzenedithiol | Au junction was measured. Similarly, a wide range of conductance values have been obtained for this junction. However, the conductances measured within were in agreement with several previous reports. These include Tao *et al.*, who observed a peak with a conductance of 1.1×10^{-2} G_0; Tsutsui *et al.*, who found peaks close to 0.01 G_0 and 0.1 G_0 [167] and Kim *et al.*, who also found conductance values close to 0.1 G_0 and 0.01 G_0.

The multiple conductance states of the Au | 4,4'-BP | Au junction measured using the STM-BJ technique were investigated in more depth using correlation analysis, this is the first instance of this analysis being used on this particular junction. It was noted during this analysis that it was possible to measure a trace containing a single high conductance plateau. However, one was more likely to observe a low conductance plateau in a trace which also contained a high conductance plateau. It was significantly less likely that one would see a trace containing a single low conductance plateau.

CHAPTER 4

MOLECULAR CONDUCTANCE MEASUREMENTS WITH FERROMAGNETIC ELECTRODES

Increasingly, researchers are choosing to study the impact of changing the contact metal in a metal-molecule-metal junction. A large focus of this work is exploring the effects of using ferromagnetic contacts as they are expected to exhibit interesting and useful spintronic characteristics such as magnetoresistance [61, 191, 199]. Measuring characteristics of ferromagnetic metal-molecule-ferromagnetic metal junctions presents difficulties which must be overcome. This is largely due to the speed at which iron group metals oxidise, which is important as oxide contamination can alter the properties of the junctions and any results measured. Hence, most previous work has been carried out with gold electrodes as it does not oxidise quickly [19]. In addition, the low symmetry in dominant d-orbital conductance channels such as those present in nickel, result in large variation in measured conductances as they are sensitive to small variations in the experimental environment [57].

This chapter explores single molecule conductance measurements using cobalt and nickel electrodes, and ways to overcome the obstacles encountered when measuring using metals that experience rapid oxidation. These measurements were performed using both the STM-BJ technique and MCBJ technique and the two methods are compared. The results obtained using ferromagnetic electrodes will also be compared with those collected using gold electrodes.

4.1 STM Measurements

4.1.1 Electrochemical Control

Electrochemistry can be used during molecular conductance measurements to prevent oxidation of the electrode surfaces [19]. It also allows for investigation into the impact of electrochemical

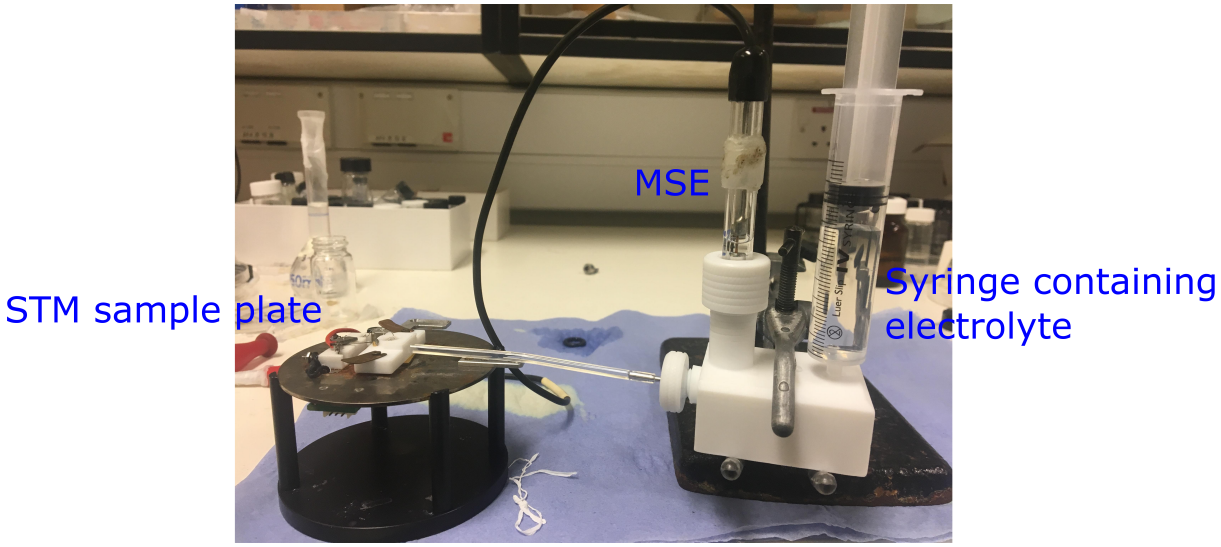

FIGURE 4.1. Photograph showing the set up of electrochemically controlled STM-BJ experiments showing the STM sample plate, where the Pt counterelectrode is situated, and the mercury sulfate reference electrode.

gating on the conductance of single-molecule junctions.

A typical electrochemical set up consists of a three electrode arrangement within a liquid electrolyte environment. A potentiostat is used to control the voltage between the working electrode (WE) and the electrolyte. In STM-BJ experiments, both the tip and substrate are used as two separate working electrodes. Hence, a four-electrode cell configuration is required. A bipotentiostat is used to independently control the potential of each working electrode with respect to the electrolyte, but the potential difference between the tip and the substrate is kept constant during the experiments. The potential of the substrate with respect to the reference electrode was varied.

A photograph detailing this four-electrode set up can be seen in Figure 4.1. A hollow Teflon box is used to secure a syringe containing electrolyte and a typical reference electrode such as mercury sulphate. A tube leaves the box and enters a teflon STM cell which was produced to facilitate the experiments. Teflon was chosen due to its chemical resistance. Before experiments, the cell was immersed into concentrated H_2SO_4 for 20 minutes and then sonicated in an ultrasonic bath in deionised water with resistivity greater than 18 MΩcm. It was then dried in a heated cabinet at 70 °C. The tube carries the electrolyte through to the STM cell. This is shown in Figure 4.2. It contains the substrate (working electrode) and a 0.25 mm diameter Pt wire ring (Goodfellow, 99.99%) (counter electrode). The ring shape allows for a more homogeneous electric field at the working electrodes, but also allows movement of the tip (working electrode) without obstruction.

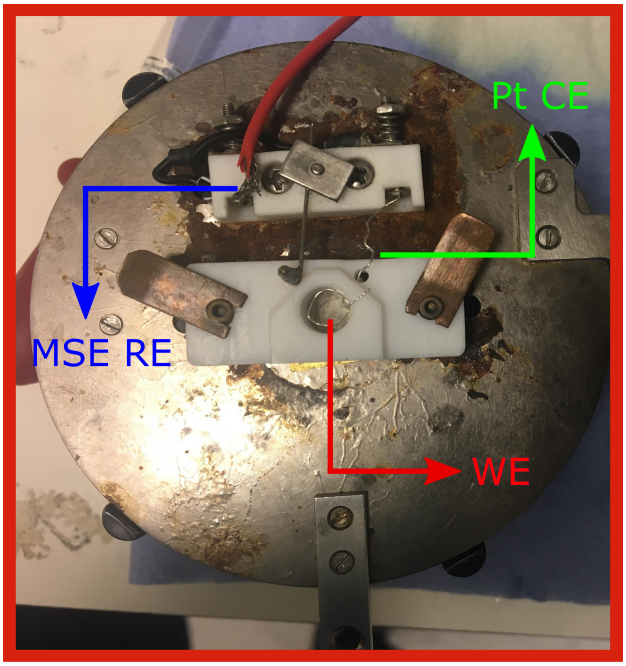

FIGURE 4.2. View of the STM cell on the STM plate from above with connections for reference electrode (RE), counter electrode (CE) and substrate (WE) labelled.

4.1.1.1 Nickel

STM measurements using Ni were taken using a Pt wire reference electrode. Initially, a 0.25 mm diameter Pt wire coated with a partially oxidised film of polypyrrole was used instead as a reference electrode. These types of electrodes are useful as they can be miniaturised easily which allows them to be integrated into compact set ups. The electrodes were produced by following the methods of Ghilane *et al.*, who demonstrated that such electrodes can provide a stable reference in a number of different solutions [51]. However, it was found that these films were highly fragile and when in contact with the electrolyte solution within the STM cell, the films were often stripped from the Pt wire. Hence, a Pt wire was used as the reference electrode. Although these have been known to have potentials which are not well defined and may shift over time, in this case, the potential proved to be well defined for the duration of the experiments. The potential of the Pt electrodes have been shown to have an open circuit potential of +0.55 V with respect to a standard hydrogen electrode [18]. Cyclic voltammetry (CV) was used to determine which potentials would provide an oxygen free surface for the STM-BJ measurements. CV was performed in a pH 3, 0.05 M Na_2SO_4 solution. It has been demonstrated that measurements performed at pH 3 provide a good balance between minimising the current due to hydrogen evolution and maintaining protection against oxide formation whilst preventing anodic dissolution of the nickel [18]. Figure 4.3 shows the CV taken in situ. During the measurements, the substrate was maintained at a potential between -0.75 V vs Pt and -1.05 V vs Pt. More negative than this, the CV shows that

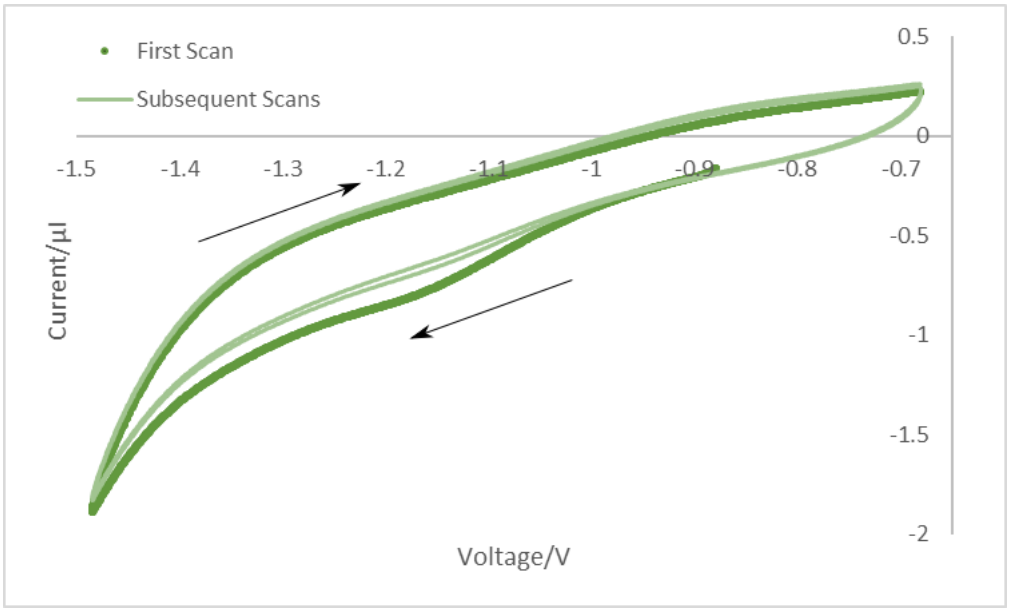

FIGURE 4.3. Example cyclic voltammogram performed on Ni electrodes in-situ in STM cell. Voltage vs Pt. Arrows represent the direction of the voltage scan. From this it was deduced that STM measurements could be carried out with gating potentials between -0.75 V vs Pt and -1.05 V vs Pt

hydrogen reduction begins, demonstrated by the peak in the first scan, centred around -1.15 V vs Pt. Hydrogen reduction can interfere with junction formation.

4.1.1.2 Cobalt

Cobalt measurements were performed using a mercury sulphate reference electrode (MSE). In-situ CVs were carried out to determine which potential would provide an oxygen free surface for the STM-BJ measurements. Again, this was measured in a pH 3, 0.05 M Na_2SO_4 solution. These CVs are shown in Figure 4.4. It was determined that STM-BJ measurements under electrochemical control could be carried out whilst the substrate was maintained at a potential between -0.95 V vs MSE and -1.2 V vs MSE. The peak seen centering around approximately -1.2 V vs MSE signifies the beginning of hydrogen reduction, below which it is undesirable to take measurements. This is the reduction of H_3O^+ rather than electrolysis of water as demonstrated by the finite nature of the peak.

4.1.2 STM Sample Preparation

4.1.2.1 Tips

STM tips were made using electrochemical etching based on the methods of Chen and coworkers and Albonetti and coworkers [2, 3, 27, 31]. A 0.25 mm diameter platinum wire, shaped into a

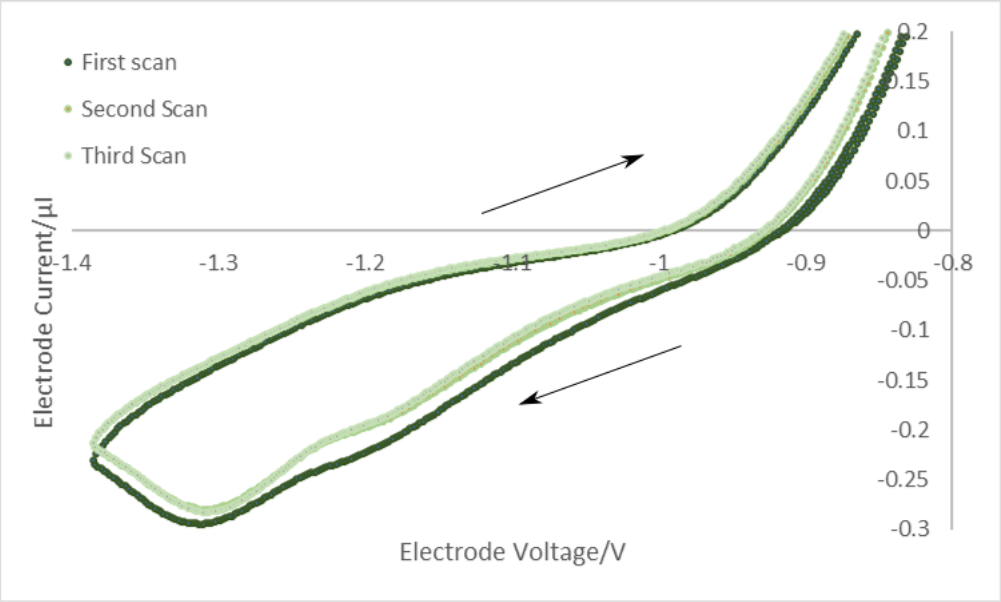

FIGURE 4.4. Example cyclic voltammogram performed on Co electrodes in-situ during STM-BJ measurements. Voltage vs MSE. Arrows represent the direction of the voltage scan. From this graph, it was deduced that STM measurements could be carried out with gating potentials between -0.5 V vs MSE and -1.2 V vs MSE.

ring of approximately 10 mm diameter was used as the counter electrode. It is possible to form a meniscus of aqueous KCl solution in the Pt ring due to surface tension, through which 0.25 mm diameter Ni or Co wire (which acts as the anode and is etched during the process) can be threaded without the meniscus breaking. A small ball of Blu Tack ®was fixed to the end of the wire meaning that when etching was complete, two tips could be gathered: a top tip and a bottom tip. Without the Blu Tack ®, the bottom tip remained suspended from the meniscus due to surface tension resulting in tips with reduced quality, as they over-etched and became blunt. For Ni wire, a Keithley 2400 source meter was used to supply a constant potential difference of 2.4 V between the Ni wire and the Pt electrode. The etching of Ni wire results in $NiCl_2$ forming at the anode and water splitting occuring at the cathode. Initially, this method was also used to produce Co tips, but the quality of these tips was relatively poor. They were often blunt and dull in colour rather than sharp and shiny like the corresponding Ni tips. It has been noted previously by Xu *et al.* that the etching current indicates the amount of charge carriers supplied to the anode per second and hence determines the etching rate. Therefore, varying the current will not provide a stable etching process [190]. As a result, to overcome the issue in etching Co tips, they were etched in constant current mode. A current of 9 mA was maintained throughout etching, whilst the compliance voltage was set at 8 V. In the case of cobalt tips, $CoCl_2$ was produced at the anode and again, water splitting took place at the Pt cathode. Deionised water was then used to remove organic contaminants from the tips before use. The following equations describe the reactions

occuring at the anode and cathode during the etching process (for Co replace Ni with Co):

$$Anode: Ni + 2Cl^- \rightarrow 2e^- + NiCl_2 \tag{4.1}$$

$$Cathode: 2H_2O + 2e^- \rightarrow H_2 + 2OH^- \tag{4.2}$$

For use in electrochemical STM, the etched tips were insulated using chemically inert Apiezon wax. It was necessary to insulate the tips to prevent ionic currents within the electrolyte from dominating the current through the tip during STM measurements. A soldering iron was used to melt the Apiezon wax and STM tips were then passed through the molten wax allowing them to be coated. Surface tension ensured that the sharp apex of the tip remained exposed when the wax had hardened. Optical microscope images of the tips are shown in Figure 4.5.

4.1.2.2 Substrates

Substrates for STM-BJ measurements were produced by electrodeposition of Ni and Co films onto gold coated glass slides. An acidic solution composed of 0.5 M boric acid and 0.2 M nickel (cobalt) sulphate hexahydrate in Milli-Q water was used for the deposition. Boric acid is commonly used in electrodeposition as it can led to higher quality films. This is because of its action as a pH buffer. The H_3BO_3 inhibits local changes in pH taking place close to the working electrode (in this case the gold coated glass slide), which is where the depletion of protons by the hydrogen evolution reaction takes place. As a result of this, a local rise in pH is minimised, preventing the precipitation of $Ni(OH)_2$ ($Co(OH)_2$), which would negatively impact the film quality [109, 196]. Prior to deposition, the gold substrates were cleaned by immersion in concentrated sulphuric acid on a hot plate heated to 90 °C for approximately 20 minutes and then rinsed thoroughly in ultra pure water. During the rinsing, if the surface was hydrophilic, this indicated a clean surface [151]. If the surface was hydrophobic, this indicated that the substrate required more cleaning. The cleaning process was observed to be highly important as dirty Au surfaces lead to low quality Ni (Co) films. A crocodile clip wrapped in Teflon tape was attached to the corner of the substrate ensuring that the plating solution would only contact the gold substrate. The substrate was immersed in the plating solution and then a potentiostat was used to perform the deposition. A potential was applied between the gold coated glass substrate and a platinum foil counter electrode using a mercury sulphate electrode (MSE) as a reference. The potential of the working electrode was chosen to be -1.3 V vs MSE. This decision was based on previous work performed by Dr Doug Szumski who demonstrated that this potential produced mirror-like films with little evidence of pitting when compared with more positive potentials, which resulted in uneven deposition, and more negative potentials which resulted in large amounts of pitting in the film due to hydrogen evolution [156]. The thickness of the film can be calculated using Faraday's law of electrolysis, shown in Equation 4.3

$$m = \left(\frac{Q}{F}\right)\left(\frac{M}{z}\right), \tag{4.3}$$

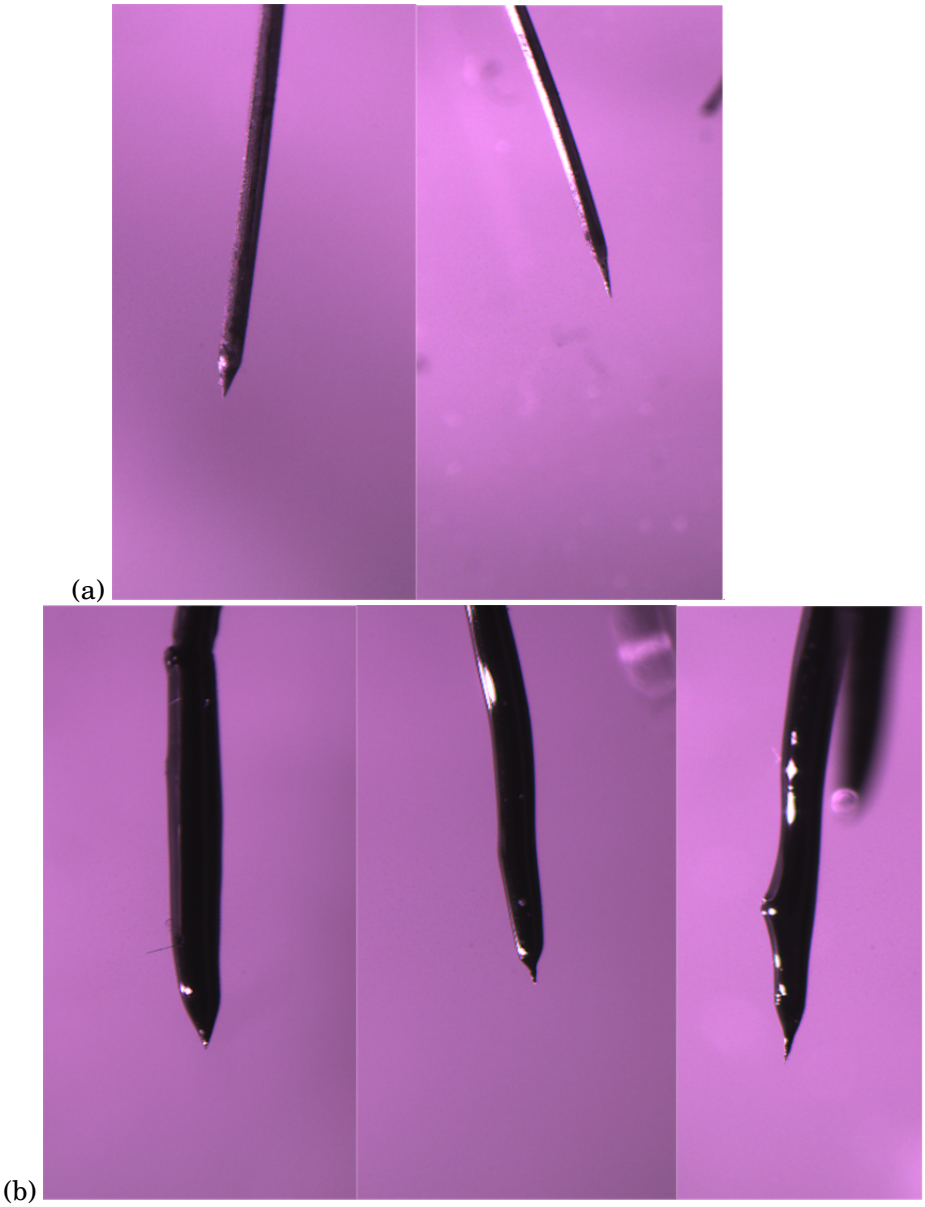

FIGURE 4.5. Optical microscope images of electrochemically etched tips taken at 20 × zoom. (a) Before coating and (b) after coating with Apiezon wax.

where F is the Faraday constant, M is the molar mass, z is the number of electrons which must be transferred to each ion (for Ni this is 2), Q is the total charge accumulated at the working electrode and m is the total mass of deposited film. By observing the charge, Q, during deposition, assuming a current efficiency of 100% and a uniform deposit on the surface, the thickness of the film can be calculated assuming the density of Ni and knowing the surface area of the electrode. A 100 nm thick film on an electrode with a surface area of 1 cm^2 requires approximately 300 mC charge [18]. The charge was monitored by the software, Nova, that was used to control the potentiostat and when the desired level of charge was reached, the current was switched off. The substrate was then removed, rinsed with ultra pure water and blown dry using nitrogen gas.

4.1.3 Atomic Contacts

Before investigating the conductance of metal-molecule-metal junctions, the characteristics of atomic contacts of nickel and cobalt were explored. As discussed in Section 1.4, ferromagnetic contacts behave differently to gold contacts and there have been a large number of contrasting reports on the topic [33, 42, 70, 79, 88, 101, 119]. In particular, measurements with cobalt electrodes are rare and a lot remains to be learnt about their characteristics.

4.1.3.1 Nickel

The STM-BJ method was used to measure the conductance of nickel atomic contacts. These measurements took place in an electrochemically controlled pH 3, 0.05 M Na_2SO_4 environment with a bias of 100 mV applied between the tip and the sample. The measurements were obtained with a gating potential of -0.9 V vs Pt. The results of these measurements are shown in Figure 4.6 which shows 1D conductance histograms on both linear and logarithmic conductance scales. Figure 4.7 shows the same data presented as a 2D histogram. It can be seen from the typical STM-BJ conductance vs distance traces for the Ni atomic contacts shown in Figure 4.6, that conductance plateaus occur within the traces. In contrast to gold, these plateaus do not occur at integer multiples of G_0, or any other regular interval. The histogram shows a broad peak at approximately 1 G_0, in agreement with previous electrochemically controlled measurements using Ni electrodes which exhibit a similar peak [79, 88]. A 2D histogram is shown in Figure 4.7, this shows the region after the Ni | Ni junction has been broken in the case where there is no molecule present.

4.1.3.2 Cobalt

The STM-BJ method was used to measure the conductance of cobalt atomic contacts. These measurements took place in an electrochemically controlled pH 3, 0.05 M Na_2SO_4 environment with a bias of 100 mV applied between the tip and the sample. The gating potential applied to the substrate was -1 V vs MSE. The results of these measurements are shown in Figure 4.8,

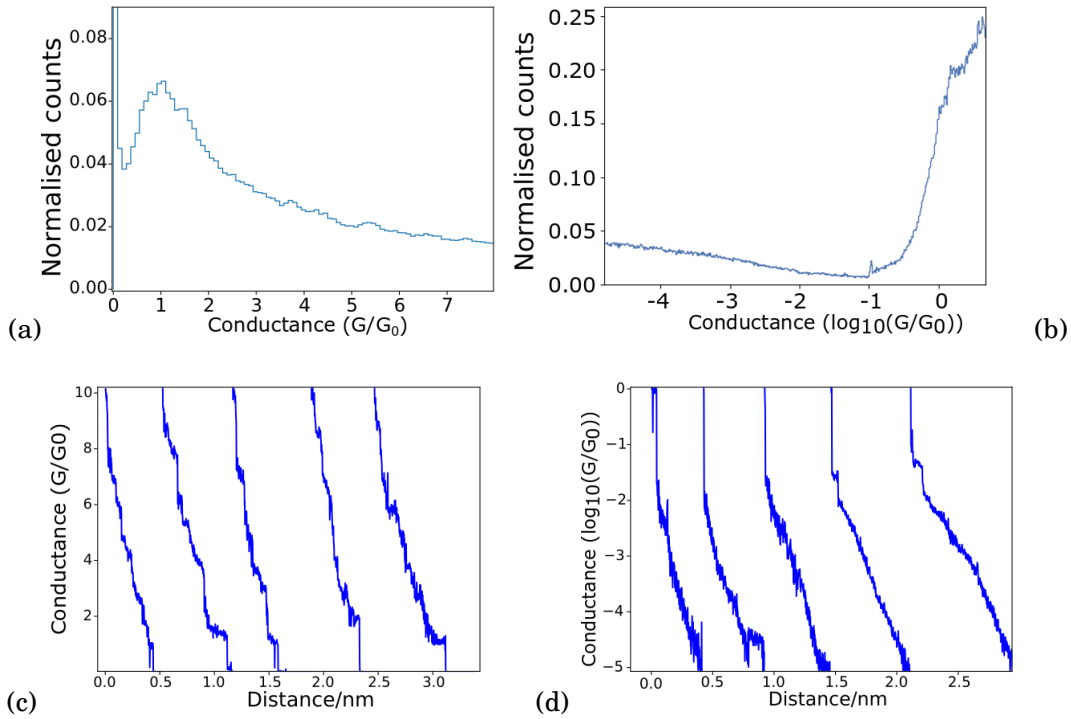

FIGURE 4.6. Conductance histograms and typical conductance vs distance traces of the Ni | Ni junction measured using STM, plotted on an (a),(c) linear conductance scale (b),(d) logarithmic conductance scale, constructed from 1171 traces. In the histograms a feature can be seen near to G_0 as described in the text. Start points of typical conductance traces have been staggered for clarity.

a 1D conductance histogram plotted on a logarithmic conductance scale, and Figure 4.9, a 1D conductance histogram plotted on a linear scale. The cobalt individual conductance vs distance traces seen in Figure 4.9 share some similarities with those of nickel. They exhibit plateaus but the plateaus do not occur at integer values of G_0, or any other regular interval. Previous measurements of cobalt atomic contacts taken at room temperature under electrochemical control and low temperature under UHV have observed a broad peak around 1.3 G_0 [18, 88, 115, 170]. This is in agreement with the histogram seen in Figure 4.8.

4.1.4 4,4'-bipyridine

The conductance of the nickel | 4,4'-bipyridine | nickel junction was explored using the STM-BJ technique under electrochemical control with a Pt counterelectrode and a Pt reference electrode in a pH 3, 0.05 M Na_2SO_4 electrolyte to which a 1 mM solution of the molecule was added. A gating potential of -0.9 V vs Pt was applied to the substrate. These measurements were made as a test in order to validate future results as there is literature available assessing the Ni | 4,4'-bipyridine | Ni junction. Figure 4.10 shows the results of these measurements, including

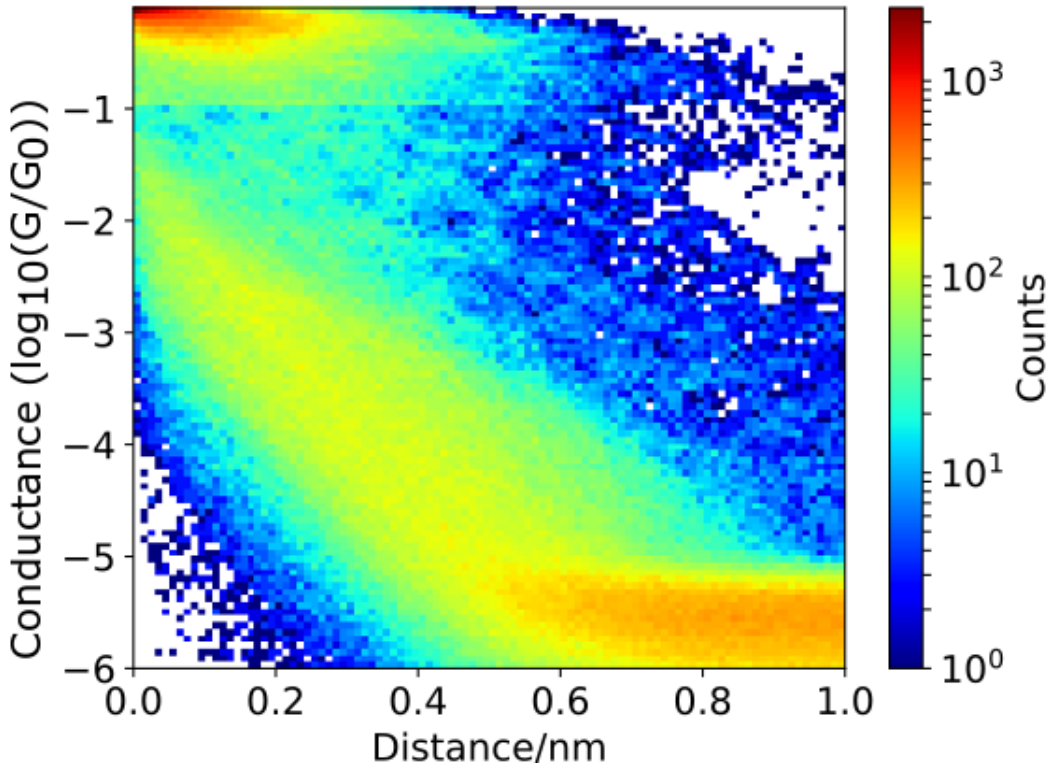

FIGURE 4.7. 2D conductance vs distance histogram of the Ni | Ni junction measured using STM. As expected, no molecular features are visible in this histogram. Formed from 1171 traces.

a conductance histogram and some typical individual conductance vs distance traces. The traces show molecular plateaus between 10^{-2} G_0 and 10^{-3} G_0. The histogram shows a single peak in this region corresponding to these plateaus. Plotted on the same axes is a graph of the conductance of the Ni | Ni junction. As the peak is only observed in the histogram where the molecule was present, it is attributed to the formation of Ni | 4,4'-BP | Ni junctions. This single peak is in contrast to when gold electrodes are used to measure the conductance of 4,4'-BP, shown in Figure 3.7 where two peaks are visible. As discussed, 4,4'-BP can link to gold in two different ways, so two peaks (a high conductance and a low conductance peak) are seen in the conductance histogram. Although the conductance of both configurations of the molecule can also be measured when using Ni electrodes, only a single peak is visible. This may be because the conductance is insensitive to the contact angle, an idea which is supported by DFT-based calculations [19]. In addition, the conductance of a Ni | 4,4'-BP | Ni junction is higher than that of an Au | 4,4'-BP | Au junction. This has also been explained using DFT-based theory calculations which suggest that

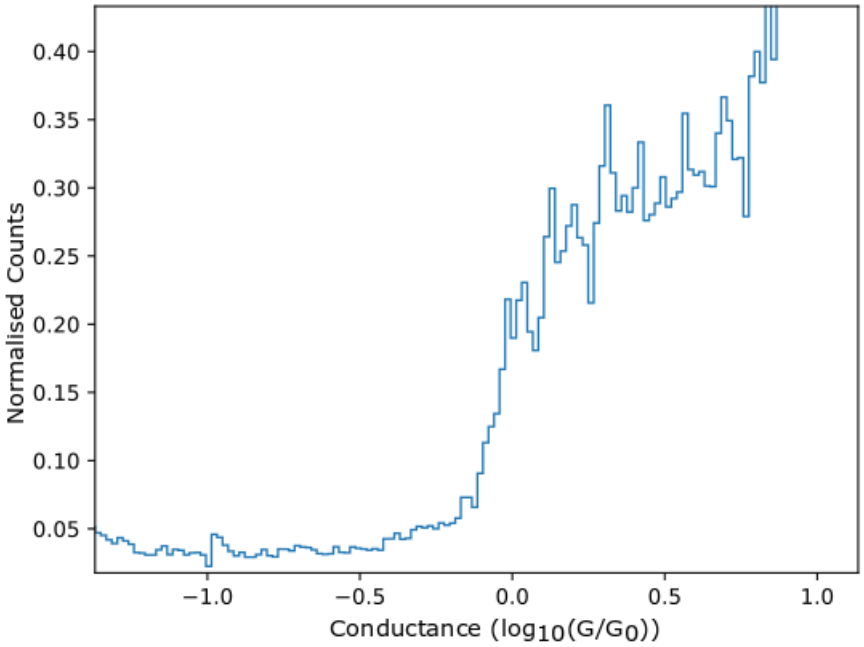

FIGURE 4.8. Conductance histogram for the Co | Co junction measured using STM plotted on a logarithmic conductance scale. Conductance peaks are visible at and above G_0. This histogram is formed from 794 traces.

the Ni *d*-electrons hybridise strongly with the LUMO of the molecule [19]. As a result, they can offer a large transmission at the Fermi energy. The conductances measured here match those in the literature [19]. A small shoulder can be seen in the Ni | 4,4'BP | Ni histogram slightly below G_0. This is a feature that has been frequently reported in previous literature. It is thought that this may be due to the adsorption of hydrogen on the electrodes, as discussed in Section 1.4. However, as hydrogen adsorption exhibits a strong dependence on the crystal orientation of Ni surfaces, this peak is not always observed [1]. A 2D conductance vs distance histogram for the junction was also plotted and displayed in Figure 4.11. The conductance feature observed in the 2D histogram is in agreement with that seen in the 1D histogram. When compared with the 2D histogram when Au electrodes were used (shown in Figure 3.8), the conductance features extend out to the same distance of 0.4nm.

4.1.5 1,4-benzenedithiol

4.1.5.1 Cobalt

The conductance of the cobalt | 1,4-benzenedithiol | cobalt junction was explored using the STM-BJ technique under electrochemical control with a Pt counterelectrode and a mercury sulfate

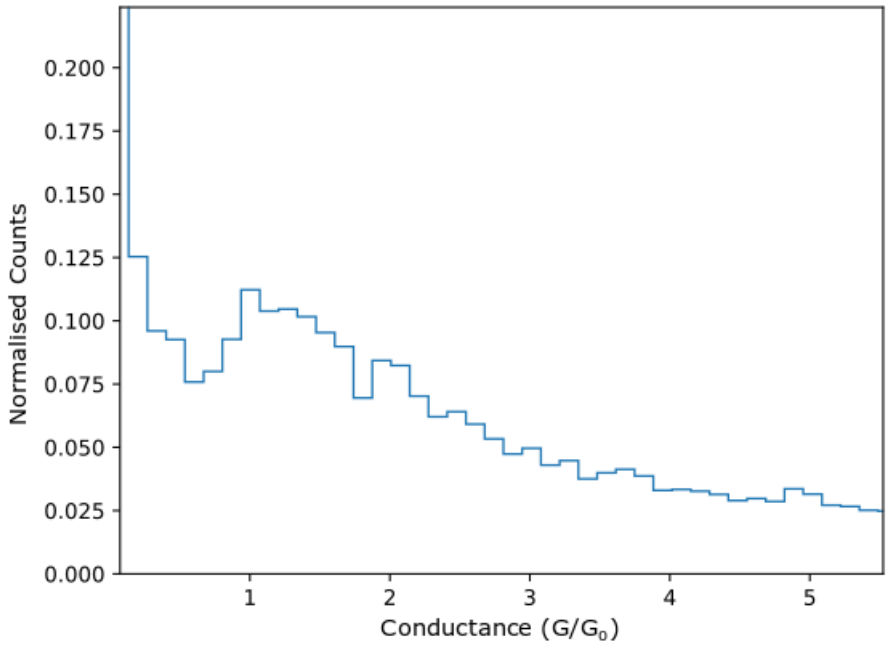

(a)

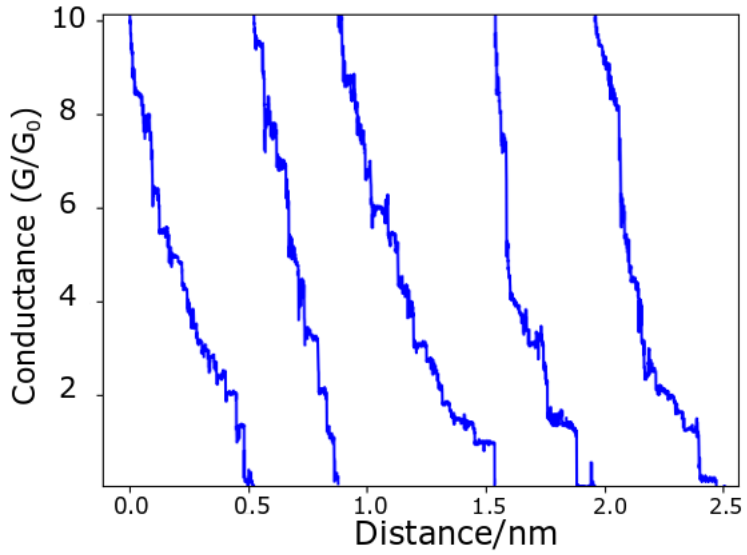

(b)

FIGURE 4.9. (a) Conductance histogram showing the conductance of the Co | Co junction measured using STM plotted on a linear scale, constructed from 794 traces.(b) Typical conductance vs distance traces measured for the Co | Co junction. The start points of these individual traces have been staggered for clarity.

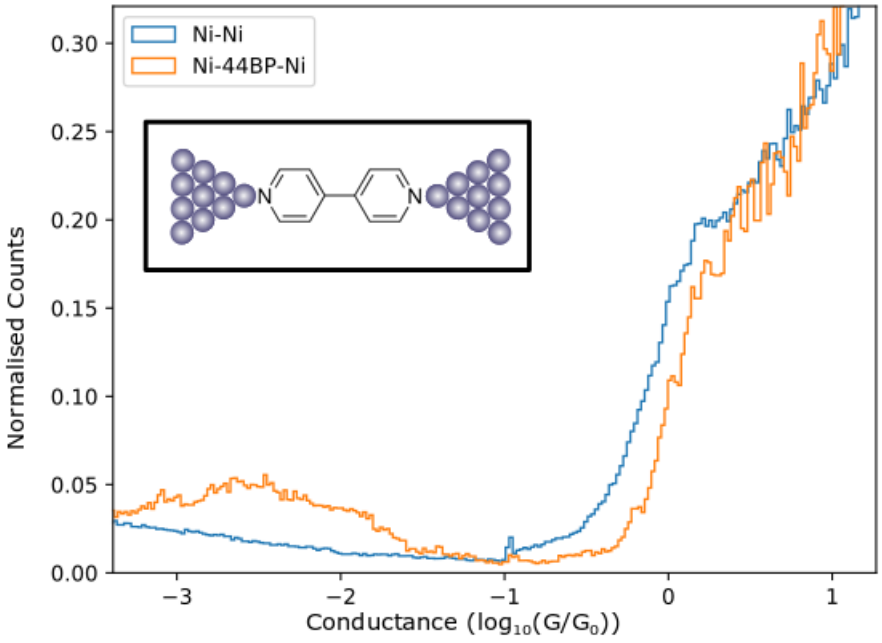

(a)

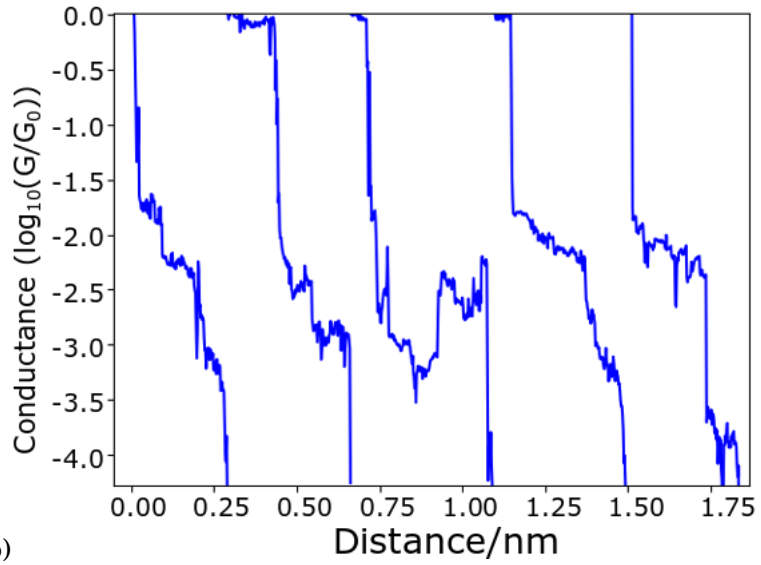

(b)

FIGURE 4.10. (a) Conductance histogram of the Ni|4,4'-BP|Ni junction measured using STM. Formed from 286 traces. A molecular feature is visible between 10^{-2} G_0 and 10^{-3} G_0. (b) Typical conductance vs distance traces for the Ni|4,4'-BP|Ni junction with start points staggered for clarity.

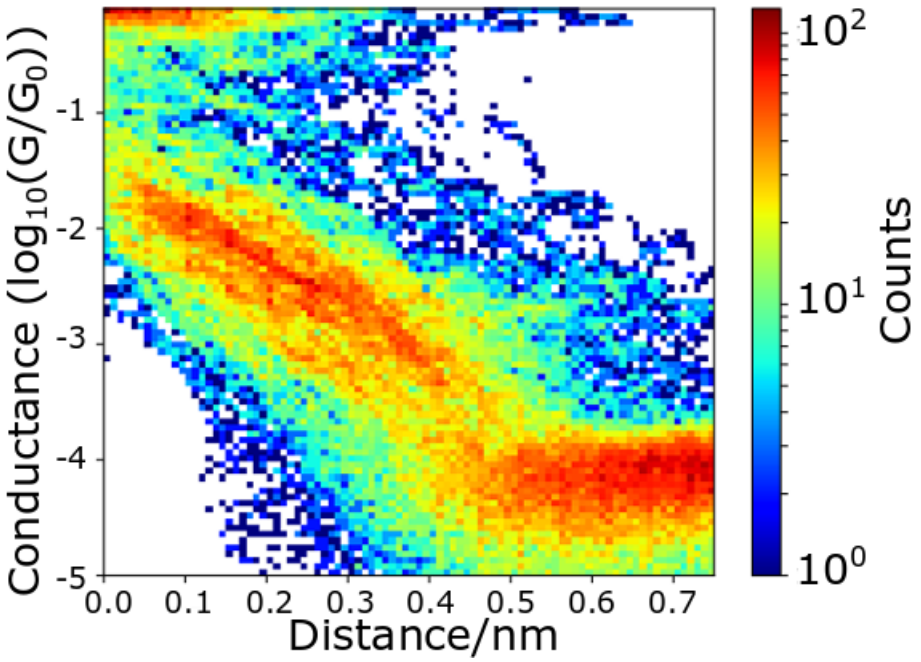

FIGURE 4.11. 2D conductance vs distance histogram of the Ni | 4,4'-B | Ni junction measured using STM. Molecular feature is visible between 10^{-2} G_0 and 10^{-3} G_0. This histogram is formed from 286 traces.

reference electrode in a pH 3, 0.05 M Na_2SO_4 solution. 1,4-benzenedithiol is not soluble in water. Therefore, to prepare the molecular solution, a saturated solution of 1,4-benzenedithiol in ethanol was made. A drop of the ethanol solution was then added to the electrolyte solution and this was used for the measurements. There have been very few investigations into molecular junctions using cobalt electrodes. STM based measurements were used by Catarelli and coworkers to measure the conductance of a cobalt | 1,8-octanedithiol | cobalt junction [26]. They used a self assembled monolayer to passivate the substrate, which helped protect it from surface oxidation and measured the junction in an electrochemically controlled ionic liquid environment [26]. They observed that the conductances measured during experiments with Co electrodes were very similar to those measured using Au electrodes. Here, a histogram shown in Figure 4.12a was constructed using individual conductance vs distance traces which contained plateaus observed between 10^{-1} G_0 and 10^{-2} G_0, such as those in Figure 4.12b. The histogram shows a broad peak at $(3.3 \pm 0.2) \times 10^{-2}$ G_0. Measurements made using 1,4-benzenedithiol often exhibit broad peaks, due to the high number of possible junction configurations 1,4-benzenedithiol can take.

It has previously been shown that changing the gating potential during an STM measurement can impact the measured value of conductance of the metal-molecule-metal junction. Brooke *et al.* demonstrated that making the gating potential applied to both Au and Ni substrates (with respect to the surrounding electrolyte solution) less negative, resulted in a decrease in the conductance of a junction containing 4,4'-BP [19]. The gating effects they observed were larger using Ni electrodes

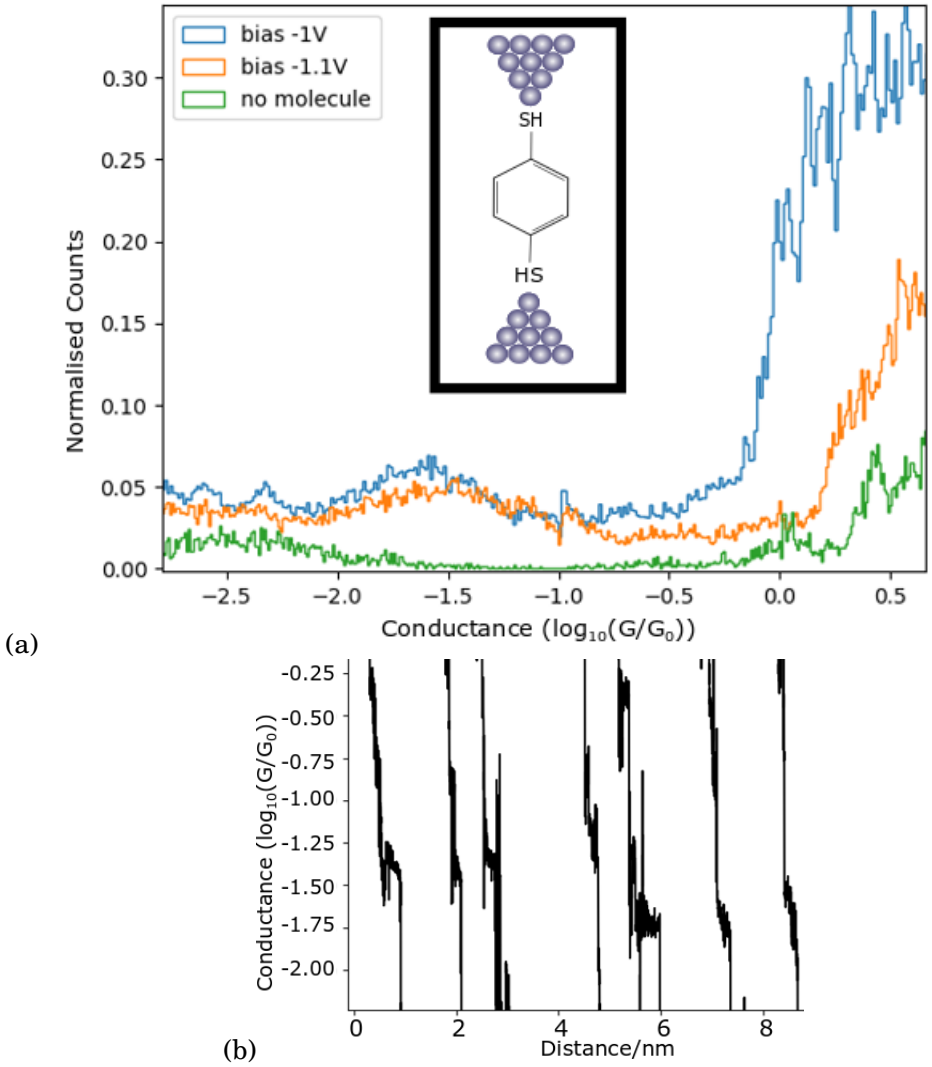

FIGURE 4.12. (a) Conductance histogram for the cobalt | 1,4-benzenedithiol | cobalt junction measured using STM, formed from (blue) bias -1 V vs MSE: 119 traces selected from 297, (orange) bias -1.1 V vs MSE: 168 traces selected from 420. The molecular feature has been identified as a broad peak at $(3.3 \pm 0.2) \times 10^{-2}$ G_0. The inset shows a possible Co | 1,4-benzenedithiol | Co junction. (b) Typical conductance vs distance traces of the Co | 1,4-benzenedithiol | Co junction, where the start points of the individual traces are staggered.

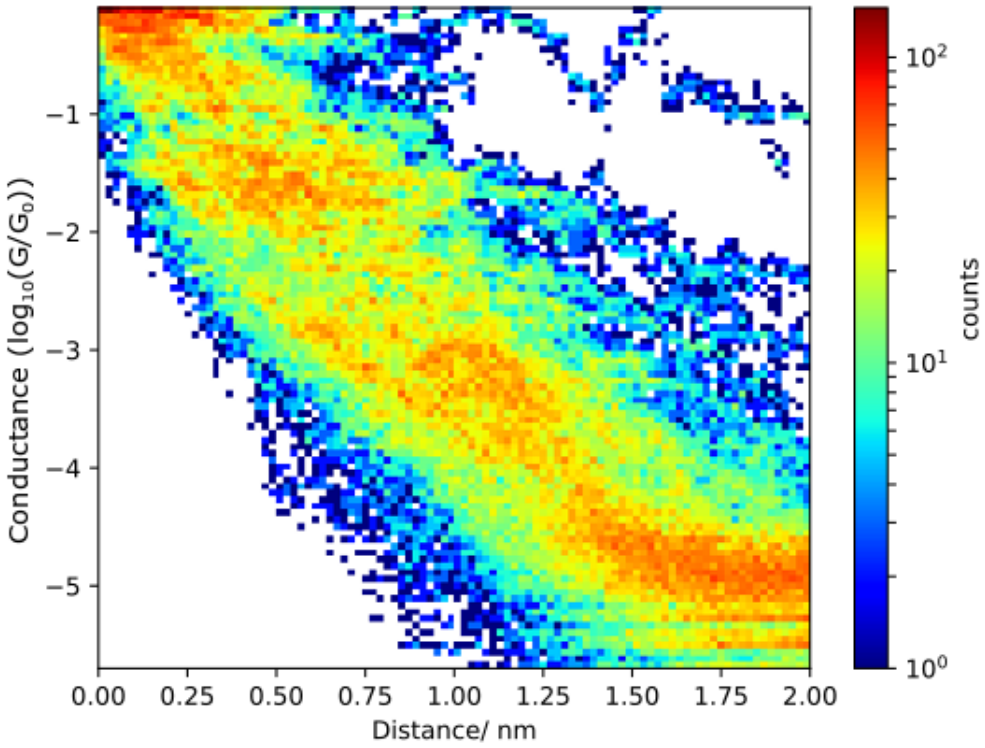

FIGURE 4.13. 2D conductance vs distance histogram for the Co | 1,4-benzenedithiol | Co junction measured at a bias of -1 V vs MSE using STM. Formed from 119 traces. Two molecular features are visible, the low conductance at $(3.2 \pm 0.7) \times 10^{-4}$ G_0 and the high conductance at $(3.3 \pm 0.2) \times 10^{-2}$ G_0.

than using Au. They explain the gating effect as a shift in the Fermi level of the electrodes relative to the Fermi level of the molecule. This shift is due to the potential applied between the electrodes and the electrolyte solution which contains the molecules. The Fermi level of the electrodes is raised when the potential is made more negative and the energy barrier for electron tunnelling between the Fermi level of the electrodes and the lowest unoccupied molecular orbital (LUMO) decreases [141]. For this reason, the conductance of the cobalt | 1,4-benzenedithiol | cobalt junction was measured at two different gating potentials, -1 V vs MSE and -1.1 V vs MSE. These are shown as separate histograms in Figure 4.12. The peaks in the histogram appear in approximately the same position and hence it was concluded that for the cobalt | 1,4-benzenedithiol | cobalt junction, a shift in the gating potential has no impact on the measured value of conductance. This comes in spite of the fact that theories have predicted the conductance of 1,4-benzenedithiol may exhibit an interesting dependence on the gating potential [17, 41]. However, in their experiments measuring

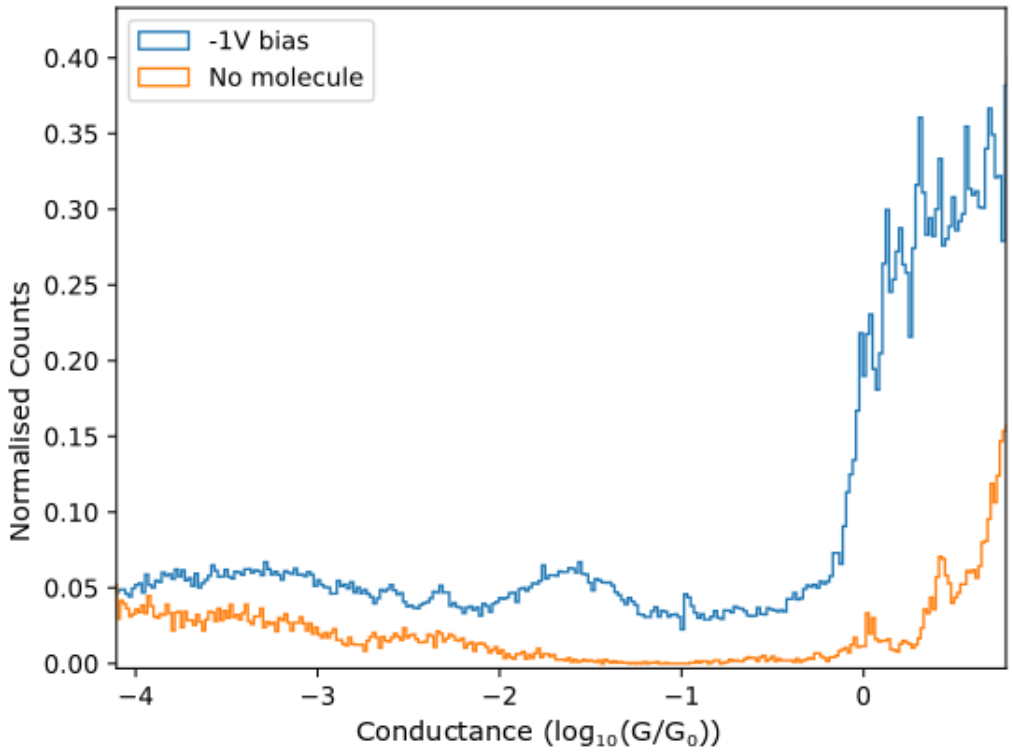

FIGURE 4.14. Histogram displaying the conductance of the Co | BZDT | Co (119 traces) junction, as displayed in Figure 4.12 a, but over an extended conductance range to show the region where the background counts obscure the low conductance peak which was observed in the 2D histogram.

the conductance of the Au | 1,4-benzenedithiol | Au junction, Xiao and coworkers also found that the conductance of the junction did not depend on the gating potential over a range of -1 V - 0.5 V [185].

A 2D histogram was plotted using the data collected at -1 V vs MSE bias, which is shown in Figure 4.13. For this particular metal-molecule-metal junction, the 2D histogram presents evidence for a high conductance configuration and a low conductance configuration. The low conductance region was not clear from the 1D histogram alone due to a high number of background counts. In the data collected with a gating potential of -1.1 V vs MSE, it did not appear present at all due to a higher leakage current that covers the region of the plateaus during these measurements. The low conductance region is measured between 10^{-3} G_0 and 10^{-4} G_0. A Gaussian was used to determine that the peak appears at $(3.3 \pm 0.7) \times 10^{-4}$ G_0. A conductance histogram showing just the data collected with a gating potential of -1 V vs MSE and the data

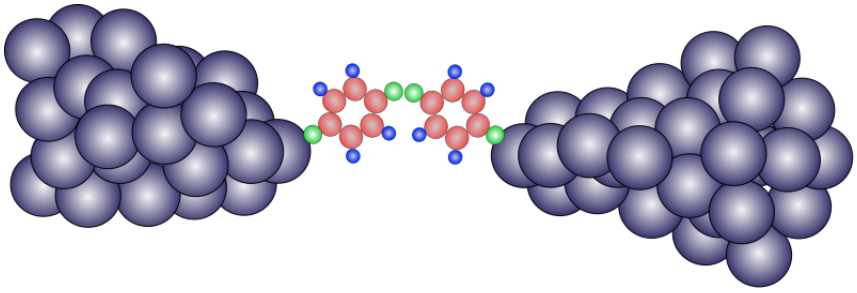

FIGURE 4.15. Possible configuration of dimeric 1,4-benzenedithiol in cobalt contacts where the length of the electrode gap would be approximately 2 nm.

with no molecule is shown in Figure 4.14. From this figure it can be noted that there are more counts in the region where the low conductance is measured compared with the histogram that contains no molecule. However, the histogram does not exhibit a clear peak in this region.

In this experiment, the measurement of dimers is highly likely, as the electrode separation when the low conductance is measured is longer than the length of a 1,4-benzenedithiol molecule which is approximately 0.99 nm [90]. In addition, it has been demonstrated that, under ambient conditions, 1,4-benzenedithiol can convert to dimeric-1,4-benzenedithiol spontaneously as a result of oxidative dimerization [200]. A possible low conductance configuration is shown in Figure 4.15.

4.1.6 Pentanedithiol

The conductance of the cobalt | pentanedithiol | cobalt junction was explored using the STM-BJ technique under electrochemical control with a Pt counterelectrode and a mercury sulfate reference electrode in a pH 3, 0.05 M Na_2SO_4 solution. Like 1,4-benzenedithiol, pentanedithiol is not water soluble. Therefore to prepare the molecular solution, a saturated solution of pentanedithiol in ethanol was made. A drop of the ethanol solution was then added to the electrolyte solution and this was used for the measurements. Due to a high number of background counts, no peak was observed in the initial histogram shown in Figure 4.16. After analysis using the automatic data selection process described in Section 3.1.2, a new histogram was formed from 188 selected traces. The automatic selection process only retains data points that are from within a plateau, so the background is removed and a peak can be resolved. This histogram is also plotted in 4.16, and reveals a peak at $(2.6 \pm 0.2) \times 10^{-3}$ G_0. A 2D histogram of the data is shown in Figure 4.17. This shows a feature at the same conductance as the 1D histogram which extends over a range from 0.25 nm to 1.1 nm. As the length of a pentanedithiol molecule is approximately 1.1 nm [145], it can be assumed that the thiol groups become attached to the electrodes at an angle and then as the electrodes continue to separate, the molecule becomes stretched to its full extent before the junction is broken.

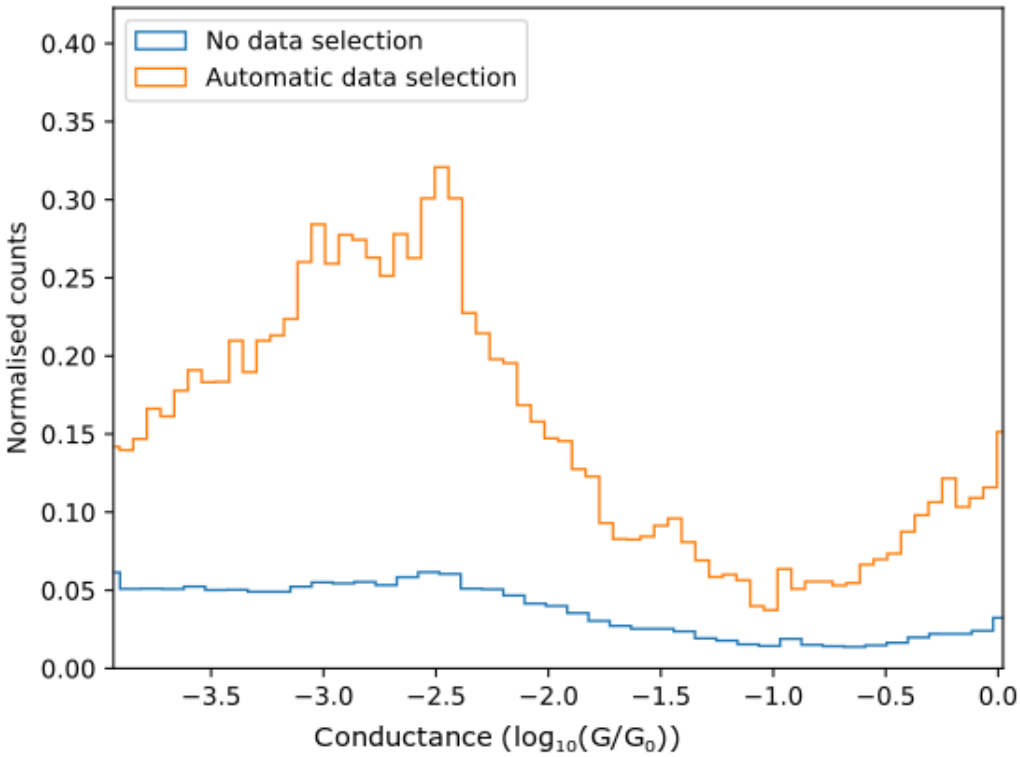

FIGURE 4.16. Conductance histogram of the Co | PDT | Co junction shown before (538 traces) and after (188 traces) automatic data selection. The trace plotted after data selection only contains the counts which contributed to a plateau in a trace. A molecular peak is observed after data selection at at $(2.6 \pm 0.2) \times 10^{-3}$ G_0.

4.2 MCBJ Measurements

4.2.1 Pentanedithiol

The MCBJ method was used to measure the conductance of Co | pentanedithiol | Co junctions. The samples were prepared as described in Section 3.3.1. Measurements were carried out under ambient conditions and the results are shown in the form of a histogram in Figure 4.18 and a 2D histogram in Figure 4.19. A peak was observed between 10^{-1} G_0 and 10^{-2} G_0 and typical traces are also shown which exhibit plateaus in this region. A Gaussian was fitted to the peak to determine a value of $(1.7 \pm 0.2) \times 10^{-2}$ G_0 as the most probable conductance. This is an order of magnitude higher than the value measured using the STM-BJ technique. This result is not in agreement with previous measurements carried out to compare MCBJ and STM-BJ, which show that the measured conductance of molecules is independent of the measurement technique.

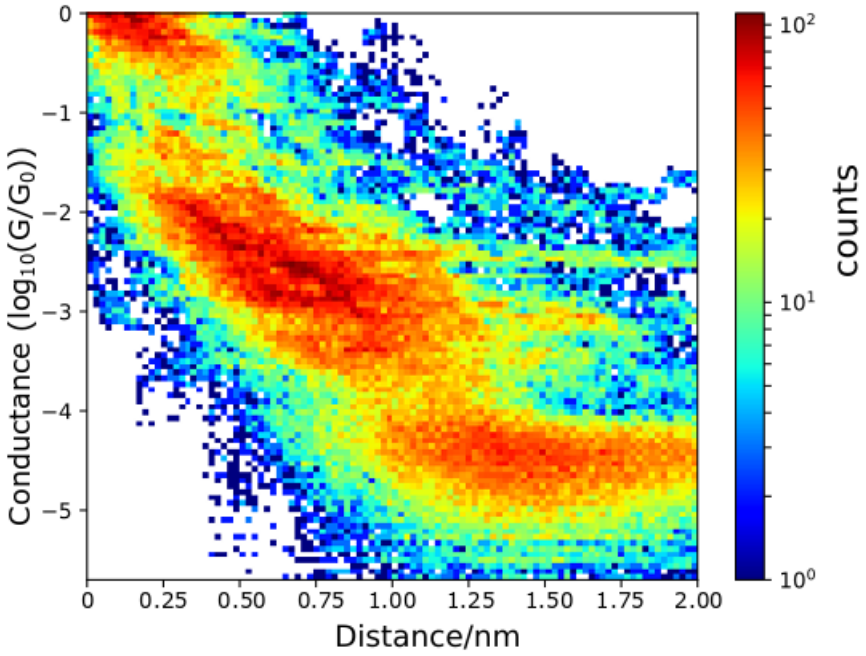

FIGURE 4.17. 2D conductance vs distance histogram for the Co | PDT | Co junction measured using STM-BJ techniques. Formed from 538 traces. Molecular feature is visible between 10^{-2} G_0 and 10^{-4} G_0.

There are differences between measurements taken using STM-BJ and MCBJ methods. The MCBJ method operates at a lower speed than the STM-BJ method. MCBJ junctions are generally not broken at more than 1nm/s, whereas STM measurements can have maximum breaking speeds of more than 100 nm/s [100, 161]. It is thought that this can impact the measured conductance of molecules [66, 165]. Experimental results have indicated that fast stretching of MMMJs (for example, during STM measurements) leads to force dominated breaking of the MMMJ. In contrast, low speed stretching results in spontaneous breakdown [107]. This difference in breaking mechanism in combination with the different electrode shapes used could explain why the measurements of conductance of the Co | PDT | Co junction, collected using the STM-BJ method, shown in Figures 4.16 and 4.17 is an order of magnitude larger than the conductance measured using MCBJ techniques (Figure 4.18).

Another factor that can impact the outcome of single-molecule conductance measurements is the preparation technique of the substrates. Inkpen and coworkers have observed that SAM measurements of dithiol terminated molecular junctions have a considerably lower conductance than measurements of the same molecule in solution [68]. They have shown that the gold-sulfur bond of the SAMs does not have chemisorbed character, where the gold-sulfur bond formed during measurements with the molecule in solution is likely to have chemisorbed character. This

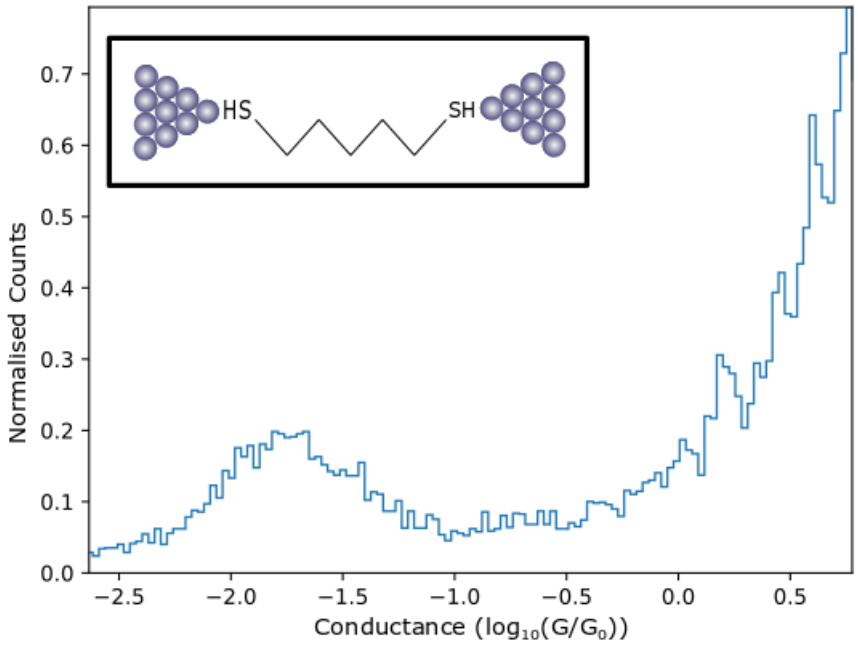

(a)

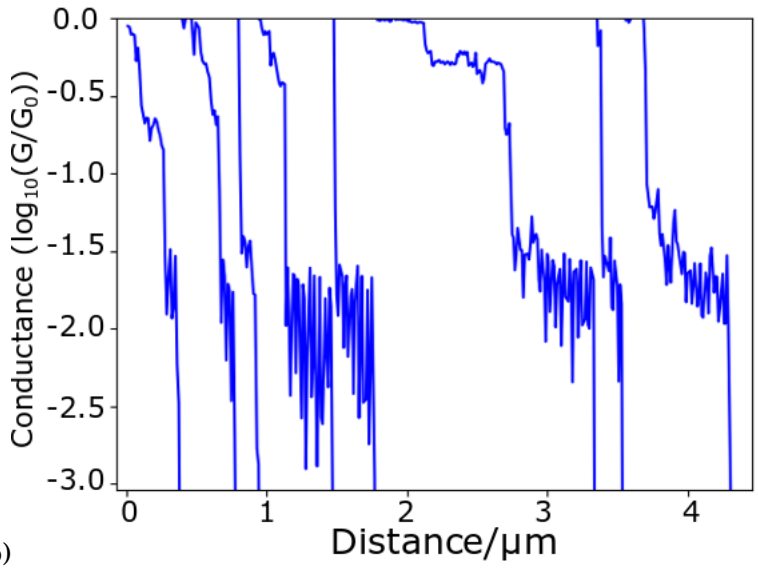

(b)

FIGURE 4.18. (a) 1D conductance histogram showing the conductance of the Co | PDT | Co junction, formed of 136 traces. A molecular peak can be seen at $(1.7 \pm 0.2) \times 10^{-2}$ G_0. (b) Typical MCBJ conductance vs distance traces for the Co | PDT | Co junction.

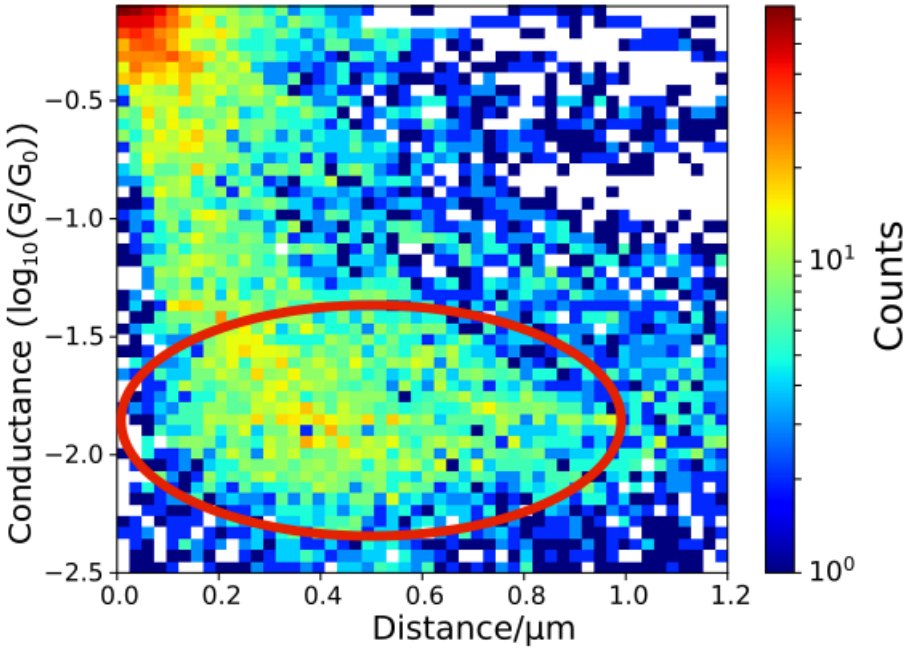

FIGURE 4.19. 2D conductance vs distance histogram of the Co | PDT | Co junction measured using MCBJ, formed of 136 traces. A red ellipse has been used to highlight the molecular conductance region.

can lead to differences between the conductances measured, although these effects were most noticeable in longer chain alkanedithiols. A discrepancy between SAM measurements (MCBJ) and solution measurements (STMBJ) was observed when measuring the conductance of the Co-PDT-Co junction. However, in contrast with the Inkpen work, the SAM measurements in this case have a higher conductance than the solution measurements and as their measurements were carried out using gold electrodes, this is unlikely to be the explanation here.

It was also observed that the conductance of pentanedithiol when measured with cobalt electrodes using the MCBJ method (Figure 4.18) is an order of magnitude higher than when it was measured with MCBJ using gold electrodes (Figure 3.15). There are very few previous measurements using cobalt electrodes available for comparison. However, it has previously been observed that conductance measurements of the Co | 4,4'-BP | Co junction collected with STM-BJ methods produced a conductance value of 0.02 G_0 [18]. This value was significantly larger than values obtained using both Au and Ni electrodes. The high conductance was attributed to the hybridisation of the Co d-band with the molecular orbitals, which may be more pronounced in Co than Ni [18]. This is a similar observation to this work with pentanedithiol. In all likelihood, it is a combination of the above factors that lead to a difference in the measured conductance of the Co-PDT-Co junction. The discrepancies between measured conductance values here reinforces the

fact that measured conductance is highly sensitive to microscopic details of the molecule-electrode contact. As such, when the geometry of the junction changes, a large variation in conductance can occur [185]. In general, the measured conductance of thiol based molecular junctions has varied significantly [93, 95, 169]. Furthermore, there are factors which have been known to cause discrepancies between MCBJ and STM-BJ measurements. Specifically, preparation methods of the samples used and breaking speed. However, it is worth reiterating that in the case of the measurements included herein, observing a difference between the MCBJ and STM-BJ conductance measurements of the cobalt | pentanedithiol | cobalt junction is an anomaly as the conductances measured remain consistent independent of measurement technique.

4.2.2 1,4-benzenedithiol

The measurements presented in Figure 4.20 were carried out using 1,4-benzenedithiol contacted by cobalt electrodes with no data selection. They show a conductance of $(4.0 \pm 0.1) \times 10^{-2}$ G_0 for the Co | 1,4-benzenedithiol | Co junction. The single peak we see in the Co | 1,4-benzenedithiol | Co measurement, as opposed to distinct high and low conductance peaks when the Au | 1,4-benzenedithiol | Au was measured (results seen in Figure 3.20), suggests a strong preference in binding site when dithiols bond with cobalt. A potential explanation of this is that the molecular conductance of this junction may not be impacted by contact angle, a similar result to the measurements of 4,4'-BP taken with nickel. A high number of background counts were observed and in addition, several small peaks between G_0 and 0.1 G_0 were measured.

In Figure 4.12, the STM-BJ technique was used to measure Co | 1,4-benzenedithiol | Co junctions. The lack of additional background counts and peaks in the data collected using STM could be due to the difference in preparation technique of the samples. As these MCBJ measurements of the Co | 1,4-benzenedithiol | Co junction were taken without a stabilizing solvent, it is thought that there could be potential for an increased number of junction configurations, such as a molecule lying flat on the surface. This could lead to different conductance values due to the interaction of π-orbitals with the electrodes [107]. This is explained in Section 3.3.3 and some examples of potential configurations are shown in Figure 3.21. A particularly prominent example of an additional peak is seen in Figure 4.20 at (0.41 ± 0.01) G_0. Figure 4.18 contains the conductance data for a Co | pentanedithiol | Co junction and does not show a similar peak in this region and so the peak is likely to be a consequence of the benzene ring. To add weight to this conjecture, conductance measurements were taken of the Co | biphenyl-4-carboxylic acid | Co junction. The structure of biphenyl-4-carboxlyic acid (BC4PA) is shown in Figure 4.22a. A selection of individual conductance vs distance traces are shown in Figure 4.22b. The plateaus highlighted appear to agree with the peaks seen between 1 G_0 and 0.1 G_0 in Figure 4.20. As the traces exhibited multiple plateaus at various conductance values, the features could not initially be distinguished clearly in the 1D histogram, though an increase in counts between 1 G_0 and 0.5 G_0 could clearly be observed. Manual data selection was carried out where traces with plateaus observed between

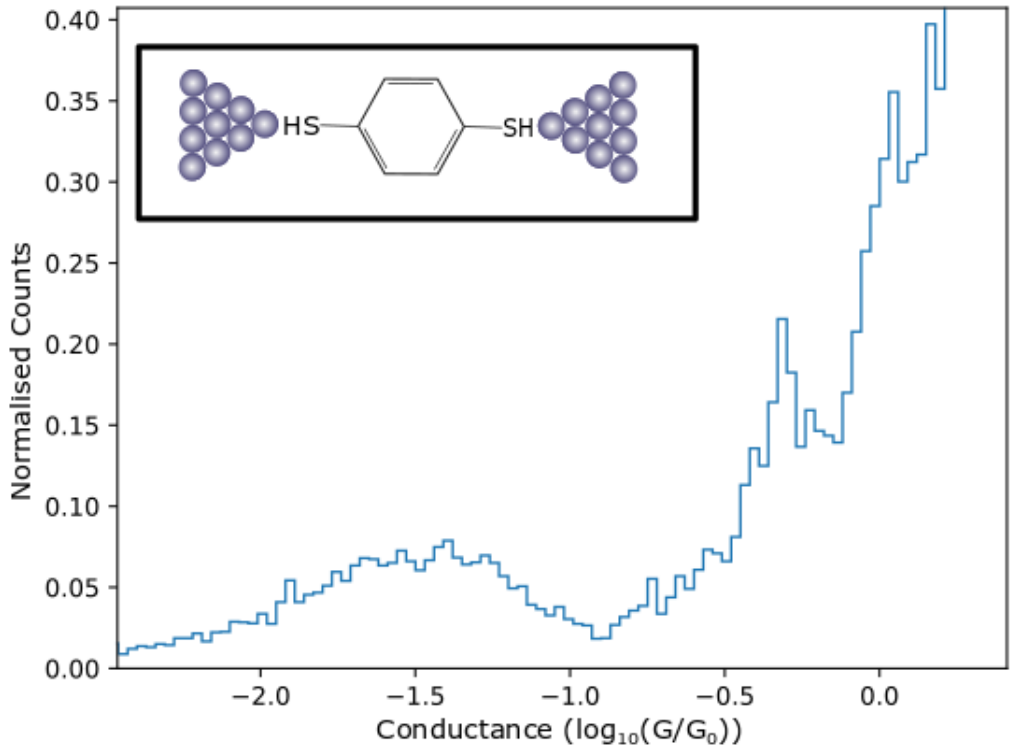

(a)

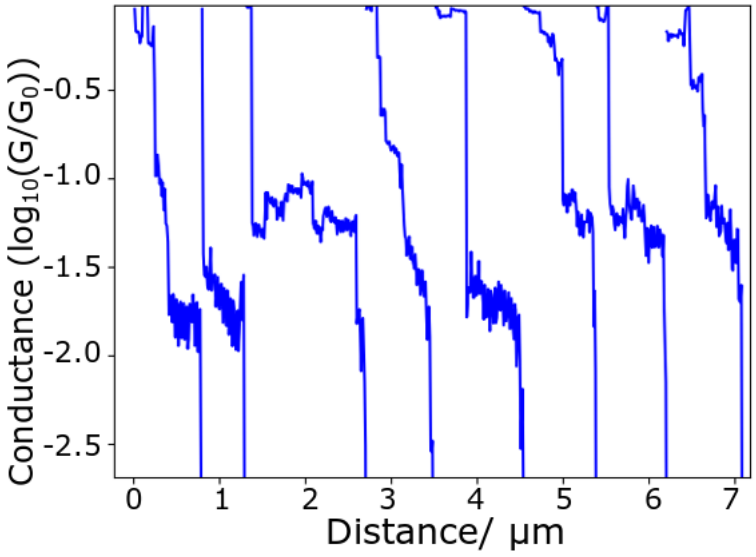

(b)

FIGURE 4.20. (a) Conductance histogram for the Co | 1,4-benzenedithiol | Co junction measured using MCBJ. Formed from 200 traces. Molecular feature can be seen at $(4.0 \pm 0.1) \times 10^{-2}$ G_0. (b) Typical conductance vs distance traces for Co | 1,4-benzenedithiol | Co junctions. Start points of individual traces have been offset for clarity.

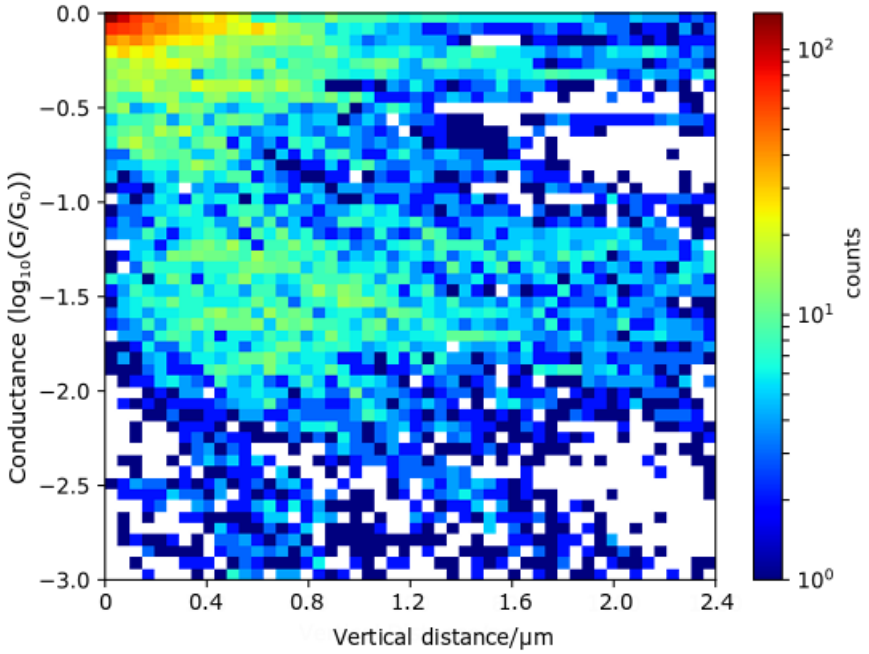

FIGURE 4.21. 2D conductance vs distance histogram for the Co | 1,4-benzenedithiol | Co junction measured using MCBJ. Formed from 200 traces. Molecular feature is visible between 10^{-1} G_0 and 10^{-2} G_0.

1 G_0 and 0.1 G_0 were kept, traces without plateaus in that region were discarded and a peak was resolved at (0.30±0.02) G_0. The original and selected data is shown in histograms in Figure 4.23. The fact that the BC4PA molecule consists of just 2 phenyl rings and a carboxyl group means that the most likely scenarios for junction formation involve current flowing between at least one of the Co contacts and a phenyl ring, without passing through any intermediate contact group.

Manual selection was used to assess the region between 1 G_0 and 0.1 G_0 for cobalt | cobalt, cobalt | pentanedithiol | cobalt, cobalt | 1,4-benzenedithiol | cobalt and cobalt | biphenyl-4-carboxylic acid | cobalt junctions. If traces exhibited a feature resembling a plateau in this region, they were kept, if there was no plateau in the region, they were discarded. For the cobalt | cobalt junction, 4% of traces exhibited features resembling a plateau in the specified region. For the cobalt | pentanedithiol | cobalt junction, 5% of traces exhibited features resembling a plateau in the specified region. For the cobalt | 1,4-benzenedithiol | cobalt junction, 19% of traces exhibited features resembling a plateau in the specified region. Finally, for the cobalt | biphenyl-4-carboxylic acid | cobalt junction, 33% of traces exhibited features resembling a plateau in the specified region. This suggests that the peak is caused by the presence of the benzene ring and its ability to link to electrodes in a number of different configurations.

Kiguchi and coworkers have researched molecular junctions based on direct binding of ben-

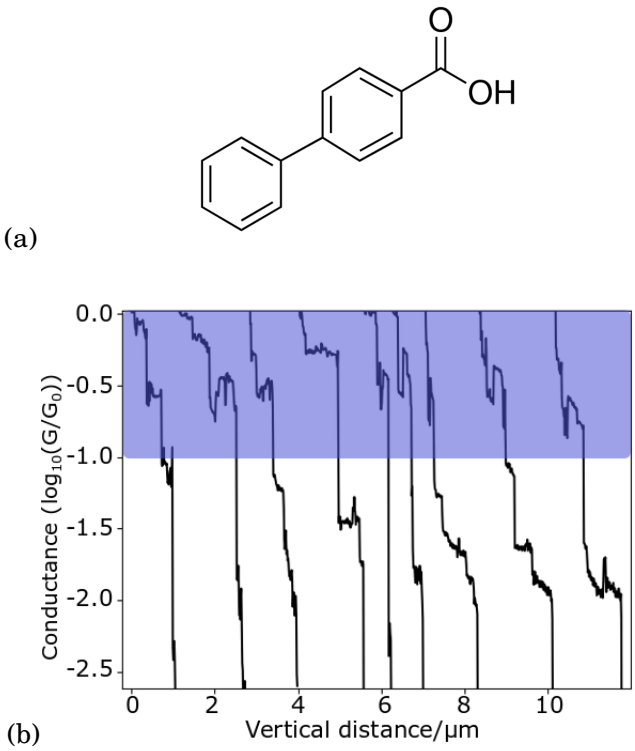

FIGURE 4.22. (a) Schematic image showing the structure of the molecule. (b) Typical conductance vs distance traces for Co | biphenyl-4-carboxylic acid | Co junctions. Blue highlight region shows the plateaus believed to be formed from direct interactions of the benzene ring with the electrodes.

zene (and other π-conjugated molecules) to Pt and Au electrodes [80, 82]. This work is relevant because the molecules used do not have anchoring groups, which are normally relied on in single molecule conductance measurements as they generally provide the link to the electrode. These experiments were carried out in ultra high vacuum. They found that the junction has a similar conductance value to that of metallic atomic junctions, in the region of 0.1-1 G_0, depending on the atomic configuration. In addition, they noted that for a Pt | benzene | Pt junction, when the plane of the benzene molecule was perpendicular to the Pt junction axis, a conductance of approximately 1 G_0 was measured. The conductance then decreased continuously as the molecule was tilted. This demonstrates a precedent for the observation of direct interactions between a metal contact and the π-orbitals of a phenyl ring.

4.2.2.1 Additional Calibration

The 2D histograms constructed for the Co | 1,4-benzenedithiol | Co junction using STM and MCBJ can be used to check the calibration of the MCBJ calculated in Section 2.5. In Figure 4.13 which was measured using the STM-BJ method, the high conductance molecular feature appears at

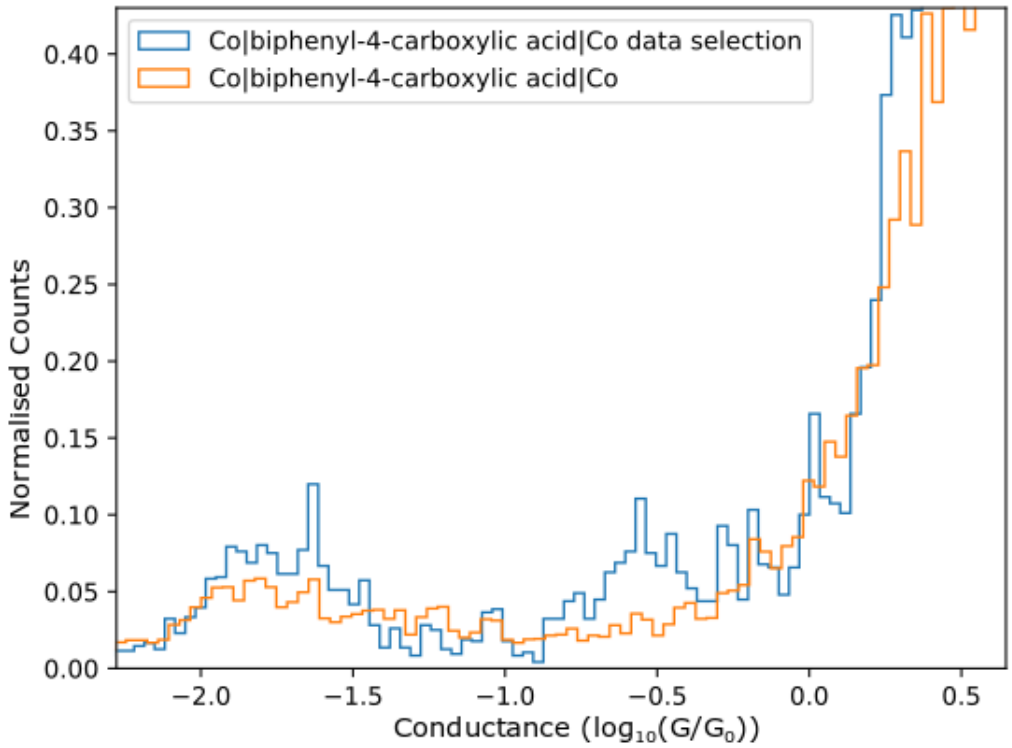

FIGURE 4.23. 1D conductance histogram for the Co | Biphenyl-4-carboxylic acid | Co junction measured using MCBJ, before manual data selection formed from 407 traces and after manual data selection formed from 135 traces. High conductance peak is visible at (0.30±0.02) G_0, low conductance peak is visible at (1.6±0.3) $\times 10^{-3}$ G_0.

an electrode separation between approximately 0.1 nm and 0.9 nm. In Figure 4.21 which was measured using the MCBJ method, the molecular feature occurs at a distance when the piezo has been moved between approximately 0.2 μm and 1.2 μm vertically. This corresponds to a reduction ratio, r≈(6.3±0.1)×10^{-4}, which provides support for the ratio calculated in Section 2.5 (3×10^{-4}), as it has the same order of magnitude.

4.2.3 Why is it Interesting?

As mentioned previously, when working with ferromagnetic electrodes oxidation takes place extremely quickly, and so generally ferromagnetic transition metals measurements are carried out under electrochemical control to prevent oxidation of the electrode surface [19]. Oxide contamination on the electrode surface could alter the electronic properties of the junction and

consequently change any conductances measured. In the work reported here, it was possible to measure the conductance of single thiol-ended molecules without taking any measures to reduce the oxide on the electrode surface. One explanation for this is that a thiol interaction may occur more quickly than cobalt can oxidise in ambient conditions.

The third method described in Section 3.3.1 was used to prepare these MCBJ samples. This method was based on studies by Mekhalif *et al.* who have shown that alkane-thiols can form SAMs on nickel substrates [107, 111, 164]. Critically, they showed that the quality of the SAM is significantly impacted by the length of time for which the nickel surface is exposed to the alkane-thiol. Though in contrast to the methods used herein, they formed monolayers by the immersion of samples into neat alkanethiol liquids or solutions of alkanethiols in different solvents. They compared SAMs formed when the exposure time is 15 minutes with the SAMs formed when the exposure time is 18 hours. From a series of XPS spectra, they observed that after a longer exposure time, the amount of surface oxide is decreased for electrochemically reduced nickel. Interestingly, it was noted that this is also true of oxidised nickel surfaces. During experiments, a substantial decrease in oxygen on the oxidised nickel surface was detected. They claim that this effect is likely due to the reduction of the surface oxide by the alkane-thiol molecules, an effect which has also been observed in copper [111, 112, 164]. The concept of "chemical cleaning" was discussed by Catarelli and coworkers, who used a similar method as the one used herein to prepare SAMs of alkanethiol molecules on cobalt substrates for STM measurements [26]. "Chemical cleaning" is a mechanism first suggested by Pirlot and coworkers [134]. They suggest that oxide free or reduced-oxide coverage metal may occur even if no treatment of the surface has taken place to reduce the oxide initially as the alkanethiol may be oxidised into several products. As these products are more weakly adsorbed than the alkanethiol, they become displaced by fresh alkanethiol, which has the potential to result in an oxide-free alkanethiol covered surface [26, 134]. Hence, this is another potential explanation of why we were able to measure electrical conductance using electrodes in ambient conditions without taking measures to reduce the surface oxide beforehand. The prospect of single molecule conductance measurements with ferromagnetic electrodes taken under ambient conditions without electrochemical control is an exciting one, as it increases the possibility of integrating cobalt into single molecule devices.

4.3 Chapter Summary

The conductance of ferromagnetic atomic contacts and metal-molecule-metal junctions formed using ferrromagnetic electrodes was explored.

The conductance of the Ni | 4,4'-bipyridine | Ni junction was measured and the value obtained was in agreement with the relevant literature [19]. There are very few examples of conductance measurements using cobalt electrodes in the literature, therefore the results obtained using cobalt electrodes within can not be compared with any past works. Significantly, the molecular

Junction	Measurement Technique	Molecular Conductance G_0	
Ni | 4,4'-bipyridine | Ni	STM-BJ	between 10^{-2} and 10^{-3}	
Co | 1,4-benzenedithiol | Co	STM-BJ	$(3.2 \pm 0.7) \times 10^{-4}$	$(3.3 \pm 0.2) \times 10^{-2}$
Co | 1,4-benzenedithiol | Co	MCBJ	$(4.0 \pm 0.1) \times 10^{-2}$	$(4.0 \pm 0.1) \times 10^{-1}$
Co | pentanedithiol | Co	STM-BJ	$(2.5 \pm 0.2) \times 10^{-3}$	
Co | pentanedithiol | Co	MCBJ	$(1.7 \pm 0.2) \times 10^{-2}$	
Co | biphenyl-4-carboxylic acid | Co	MCBJ	$(1.6 \pm 0.3) \times 10^{-2}$	$(3.0 \pm 0.2) \times 10^{-1}$

Table 4.1: A summary of the results obtained in Chapter 4.

conductance of dithiol linked molecules was measured successfully using MCBJ techniques with cobalt electrodes without the use of electrochemical control to ensure the electrode surface is oxide free. This is a novel result and an important finding as it suggests it could be possible to integrate cobalt into single molecule devices without electrochemical control.

Some comparisons were drawn between STM-BJ and MCBJ measurements of the same molecule. In general, it was found that molecular conductance was consistent independent of measurement technique. However, measurements of the Co | pentanedithiol | Co junction taken using the STM-BJ method show a conductance an order of magnitude higher than that for the same junction using MCBJ methods. Although there may be an explanation for this, when compared with other measurements it provides an anomalous result.

MCBJ measurements of the Co | 1,4-benzenedithiol | Co junction exhibited additional peaks in the region between G_0 and 0.1 G_0. This was attributed to coupling between the π-orbitals of the 1,4-benzenedithiol phenyl ring and Co. A similar peak was observed for BP4CA but not for PDT, consistent with our hypothesis. We also observe that conductances of pentanedithiol, 4,4'-bipyridine and 1,4-benzenedithiol are dependent on the contact metal and that for pentanedithiol, using cobalt electrodes results in a higher conductance (approximately an order of magnitude) than gold electrodes. This could be attributed to the hybridisation of the Co d-band with the molecular orbitals.

A table containing a summary of the data collected in this chapter is shown in 4.1.

CHAPTER 5

MAGNETIC EFFECTS IN SINGLE MOLECULE JUNCTIONS

In recent years, many researchers have dedicated a great amount of time to understanding the electron spin and its effect on transport in a material. This area of research is called spintronics and encompasses fundamental effects such as giant magnetoresistance, tunnelling magnetoresistance and anisotropic magnetoresistance. This follows the advances that stemmed from employing the spin degree of freedom of the electron in conventional, charge-based electronics [142, 183].

Several early magnetoresistance measurements were presented showing extremely large values of MR, for example by Garcia and coworkers, who measured the magnetoresistance for few-atom Ni contacts [50]. They found that the values of MR reached up to 280% at room temperature for applied magnetic fields of 100 Oe [50]. In addition, Hua and coworkers observed MR up to 100000% in stable, electrodeposited Ni nanocontacts at room temperature and in fields of only a few hundred oersteds [65]. These large values were attributed to the "ballistic magnetoresistance" (BMR) effect, so called because the electron transport taking place in these instances is ballistic rather than diffusive. In BMR, one expects that the conductance of a ferromagnetic ballistic conductor would change abruptly with the magnetisation direction, rather than exhibiting a $\cos^2$ variation like in AMR. In addition, the BMR relative magnitude would be much larger than bulk AMR (of the order of e^2/h) [45]. However, this interpretation was questioned as the effects were not observed in well-controlled mechanical break junctions [49]. It was deduced in later work that the large values of MR were most likely to be a result of mechanical artefacts including magnetostriction and magnetostatic attraction between the contacts [45, 47, 49]. Egelhoff and coworkers explained that these effects can result in alteration of the electrode shape, causing the junction to open or close [45, 47]. Since then, measures were taken during experiments to prevent magnetostrictive effects impacting the measured magnetoresistance. Ralph *et. al* suggested that

at least three conditions should be met to avoid interference from magnetostriction and magnetostatic forces [15]. Firstly, the electrodes of the sample should be attached rigidly to the substrate. Having no suspended elements reduces the effects of magnetostriction. Secondly, they suggest that the measurements should be performed at cryogenic temperatures to ensure that the contact region is thermally stable. Finally, the design of the geometry of the electrodes should be such that the magnetic moments of the electrodes can be controlled between antiparallel and parallel configurations [15]. They noted that in previous experiments which were carried out at room temperature or which used devices with geometries that were more sensitive to magnetostrictive effects and magnetostatic forces, extremely large values of magnetoresistance were measured, as previously described [49, 50, 175]. Ralph *et. al* measured a low temperature magnetoresistance of <3% for permalloy contacts and up to 85% in the tunnelling regime. Measurements taken by Von Bieren *et al.* presented a magnetoresistance of up to 50 % using similar precautions [176]. These results match the predictions of theorists more closely [71].

In the early 2000s, theoretical predictions suggested that metal-molecule-metal junctions consisting of a nonmagnetic, organic molecule linked by two ferromagnetic electrodes should exhibit magnetoresistance when the two ferromagnetic layers switch between parallel and antiparallel configurations relative to each other [37, 94, 132]. This is known as giant magnetoresistance and is discussed in detail in Section 1.4.1. GMR can be defined as

$$GMR = \frac{R(AP) - R(P)}{R(P)} \times 100\%, \tag{5.1}$$

where $R(AP)$ is the resistance with an antiparallel orientation for the magnetisations of the electrodes and $R(P)$ is the resistance with parallel magnetisations. Schmaus *et al.* measured the giant magnetoresistance in UHV across a single hydrogen phthalocyanine molecule contacted by a cobalt coated, tungsten tip [146]. They measured a GMR of 60% in ultra high vacuum at 4 K.

Yamada and coworkers used a mechanically controllable break junction to determine the anisotropic magnetoresistance of a nickel | 1,4-benzenedithiol | nickel junction by changing the orientation of the external field with respect to the current flow [191]. A negative magnetoresistance up to 30% for the molecular junction and up to 30% for the anisotropic magnetoresistance of Ni atomic contacts and tunnel junctions were observed. Similarly, Sakai *et al.* measured electron transport through the Ni | 1,4-benzenedithiol | Ni single molecule junction in the presence of a magnetic field [64]. They observed magnetoresistance up to 90% when varying the magnetic field strength from 0 T to 250 mT. More recently, in 2015, Li and coworkers formed terephthalic acid single-molecule junctions with Fe electrodes using the STM-BJ approach in combination with an external magnetic field which was either parallel or perpendicular to the direction of current flow [94]. These measurements were performed at room temperature. Using this method, they reported a giant single-molecule tunnelling anisotropic magnetoresistance of up to 53 %.

A small number of reports demonstrate magnetoresistance through single C_{60} molecules contacted with magnetic electrodes. Kawahara and coworkers investigated magnetoresistance in C_{60} molecules deposited on an antiferromagnetic Cr(001) surface [77]. The measurements

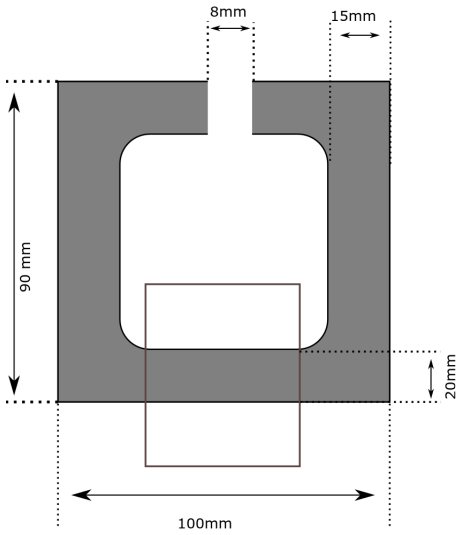

FIGURE 5.1. Schematic diagram of the electromagnet used in STM-BJ experiments. It consists of 700 windings of copper around an iron core and has two pole pieces that fit on either side of the STM sample plate.

were carried out under UHV at 5K and relied on the use of different atomic terraces of the Cr(001) surface, which exhibit opposite magnetisation directions due to the antiferromagnetic ordering of the Cr. Magnetoresistance up to 100% was observed at zero bias. In addition, negative tunnelling magnetoresistance (TMR) was noted, something which was also measured by Yoshida and coworkers who observed TMR values up to -80% in a junction formed from two Ni electrodes contacting a C_{60} molecule [77, 195]. Beyond these examples, experimental evidence of magnetoresistance in molecular junctions is limited. This is most likely a result of the difficulties involved with constructing magnetic junctions with good reproducibility [94]. This difficulty stems partly from the previously mentioned magnetostriction effects. In addition, both MCBJ and STM-BJ techniques work using a "crash-to-contact" principle which means that a new junction is formed with every measurement. As a result, the structure of the junction is not consistent or reproducible and so it is not uncommon to observe significant variability within a single set of measurements [94]. Another obstacle is the speed at which ferromagnetic metal electrodes oxidise as this makes it difficult to conduct investigations under ambient conditions.

This chapter will focus on the effects a magnetic field has on ferromagnetic atomic contacts and single-molecule junctions formed using ferromagnetic electrodes. The investigations were carried out using both MCBJ and STM-BJ methods.

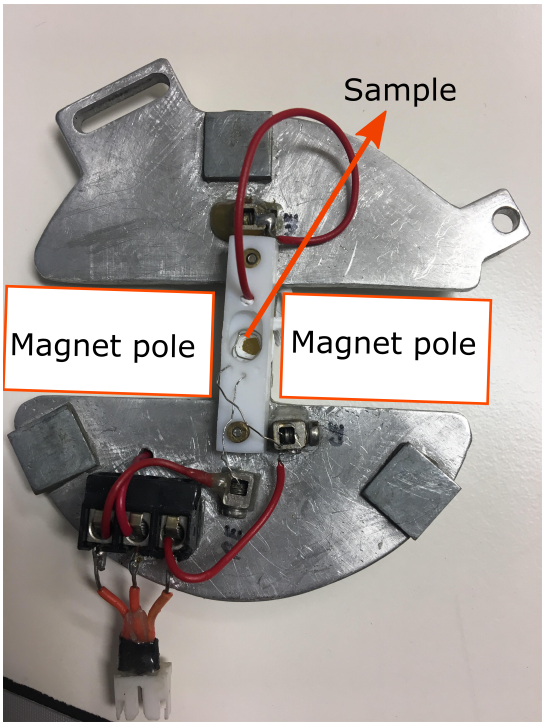

FIGURE 5.2. Photograph of STM sample plate that is used in conjunction with the electromagnet, with the places where the magnet's pole pieces fit and the sample labelled.

5.1 Magnetic STM set up

5.1.1 Electromagnet

For the STM-BJ experiments using cobalt and nickel electrodes in the presence of a magnetic field, an electromagnet was used. The magnet used in conjunction with the STM was designed by Dr Richard Brooke and constructed by the University of Bristol workshop [18]. It was designed to fit within the components of the STM. It consists of 700 windings of copper wire wound around an iron core, shaped so that the opposite poles face each other across an air gap, as shown in Figure 5.1. Initially, the electromagnet was powered by a Kepco BOP36-12D bipolar power supply but this resulted in highly noisy current-distance traces. Hence, a Keithley 2400 was used to power the electromagnet. However, this caused other limitations as the maximum current that can be provided by this power supply is 1 A, which reduced the maximum magnetic field available. The electromagnet was calibrated by Dr Richard Brooke using a Hall probe gaussmeter, the results of which are shown in Figure 5.3. This electromagnet does not have an inbuilt cooling system and it has previously been observed that electrical heating of the coil at higher current values can result in a higher electrical resistance. This causes the voltage required to maintain a constant current to become non-linear and it increases more quickly as a function of current [18]. In

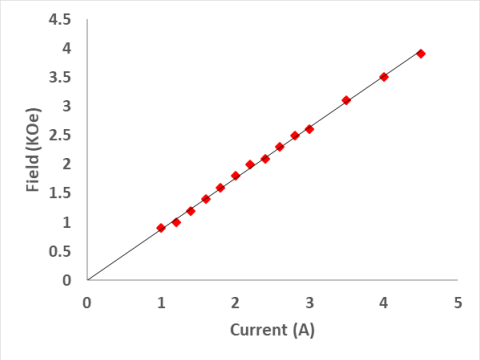

FIGURE 5.3. Calibration curve of the electromagnet showing the magnetic field strength measured as a function of the current as measured by Dr Richard Brooke.

addition, heating of the sample during STM measurements can result in the molecular solution evaporating. However, as these experiments were typically carried out using a current of 1 A, which produced a magnetic field of approximately 1 kOe, the heating was generally insignificant.

Due to the restricted amount of space when doing electrochemically controlled STM-BJ experiments using the electromagnet, a teflon cell small enough to fit in the air gap between the poles of the magnet is used. In addition, the glass casing of reference electrodes such as mercury sulphate is too bulky. Therefore, a Pt wire was used as a reference electrode for these experiments. Although the potential of a Pt electrode is not usually well defined and may shift over time due to the formation of surface oxide [51], here it proved capable of providing a stable reference.

5.2 STM Measurements in a Magnetic Field

5.2.1 Atomic Contacts

5.2.1.1 Nickel

The STM-BJ technique was used to investigate nickel atomic contacts in the presence of a magnetic field with a substrate potential of -0.9 V vs Pt. Figures 5.4 and 5.5 show a comparison of the measured conductance of these contacts with and without the application of a 1 kOe magnetic field applied in the plane of the substrate surface. The individual scans have been offset on the x-axis to synchronise them at a conductance value of 12 G0. Figure 5.4 demonstrates that without an applied magnetic field, the atomic contacts are maintained over larger tip-sample separations than when there is an applied magnetic field. It has been suggested that this may be due to the magnetostatic interaction between the tip and the sample. When a magnetic field is applied, it causes the electrodes to become magnetically aligned. As it is energetically unfavourable for the electrodes to be magnetised in the same direction in the substrate surface plane, this could result in the electrodes being forced to separate more quickly [18]. This result is similar to that of

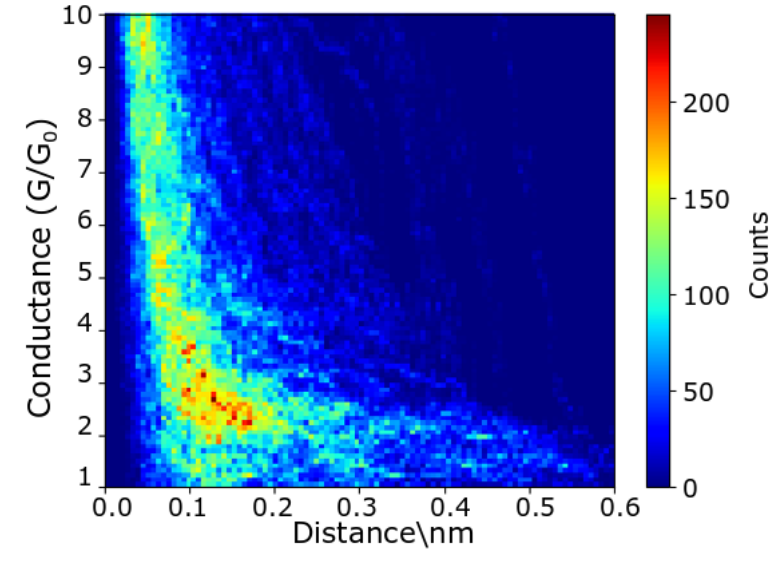

(a)

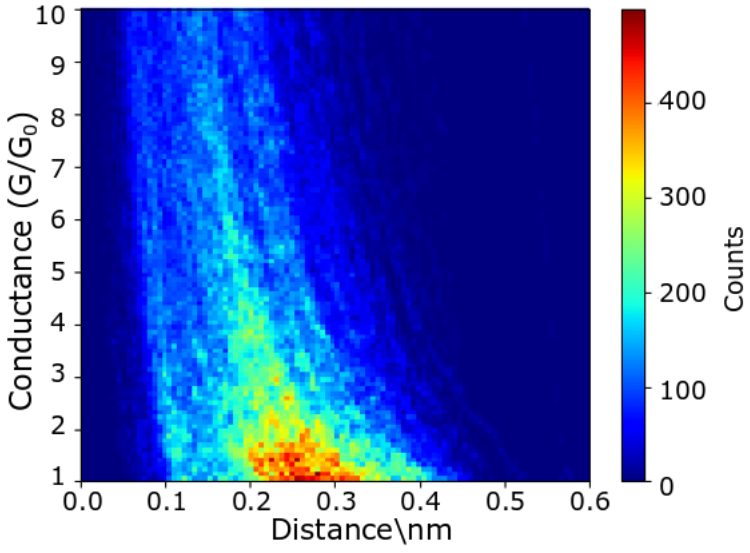

(b)

FIGURE 5.4. 2D conductance vs distance histogram showing the conductance of the Ni | Ni atomic junction measured using STM, (a) without (constructed from 1171 traces) and (b) with a 1 kOe magnetic field (constructed from 254 traces).

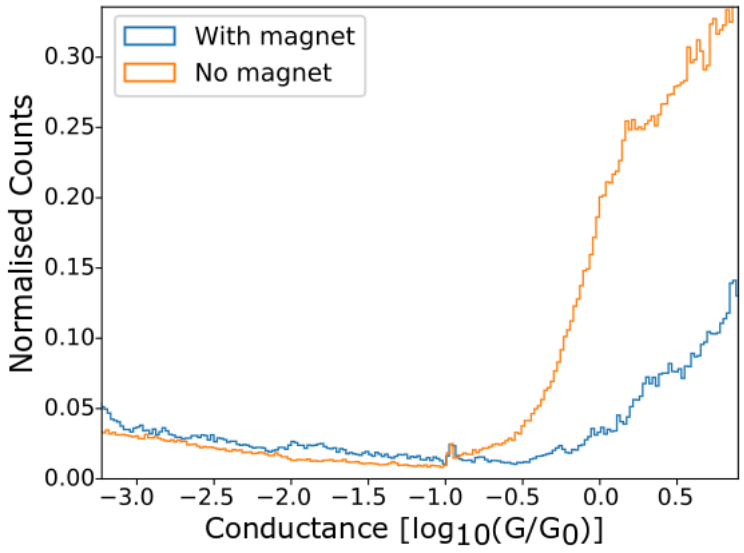

(a)

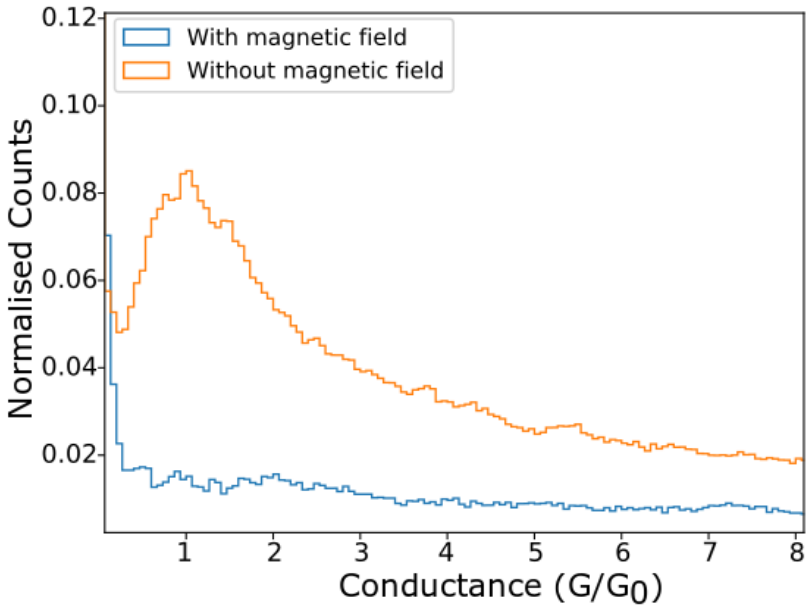

(b)

FIGURE 5.5. 1D conductance histogram showing the conductance of the Ni | Ni atomic junction measured using STM with (254 traces) and without (1171 traces) a 1 kOe magnetic field applied in the plane of the substrate. (a) Logarithmic conductance scale (b) Linear conductance scale.

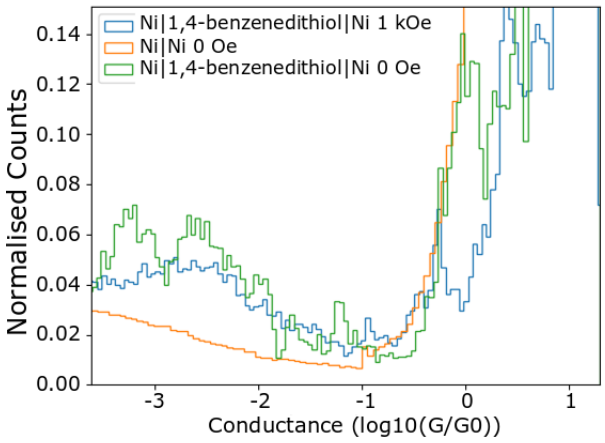

FIGURE 5.6. 1D histogram showing a comparison between the conductance of Ni | 1,4-benzenedithiol | Ni junction in the presence and absence of a 1 kOe magnetic field and the Ni | Ni junction in the absence of field. These measurements were taken using the STM-BJ technique. The histogram for the Ni | 1,4-benzenedithiol | Ni junction in the presence of magnetic field is formed from 86 traces selected using automatic data selection from 557 traces.The histogram for the Ni | 1,4-benzenedithiol | Ni junction in the absence of magnetic field is formed from 56 traces selected using automatic data selection from 403 traces.

Miyano *et al.* who also observed that the separation of Ni wires in an applied magnetic field at room temperature was much faster than with no magnetic field [131]. As the tip and the substrate are magnetised in the same direction, this provides a well defined magnetic configuration, hence there is a larger variation in the conductance vs distance traces collected without a magnetic field. From Figure 5.5, one can see that the peak close to 1 G_0 visible in the histogram produced from data with no magnetic field was not visible when a magnetic field was present. This observation is in agreement with the results of Miyano *et al.* and Serena *et al.* who both observed that in a magnetic field, curves with a conductance step close to 1 G_0 do not appear [42, 131]. As previously mentioned, in a magnetic field, the electrodes separate more quickly than in the absence of field. Hence, the lack of a peak close to 1 G_0 could be attributed to shorter plateaus during the opening process. However, referring back to Figure 5.4b, it is clear that there are a high number of counts around 1 G_0 and so the presence of a 1 G_0 peak in Figure 5.5 may have been obscured by background counts due to the noise introduced by the addition of the electromagnet in the set-up.

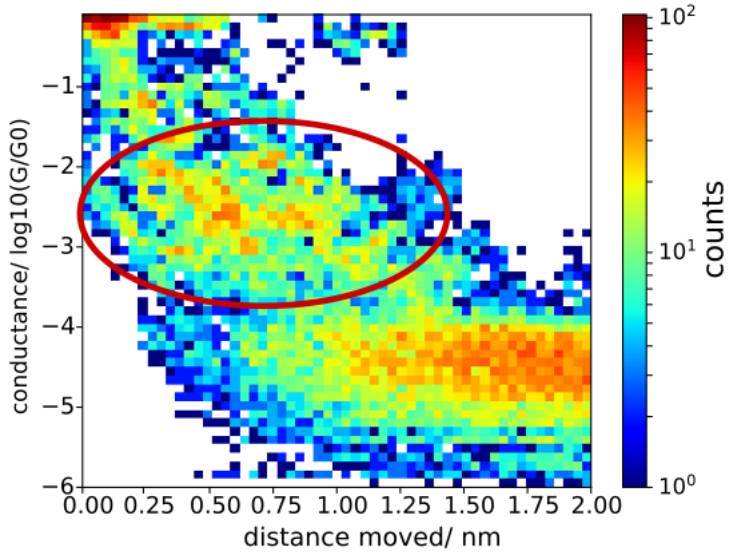

(a)

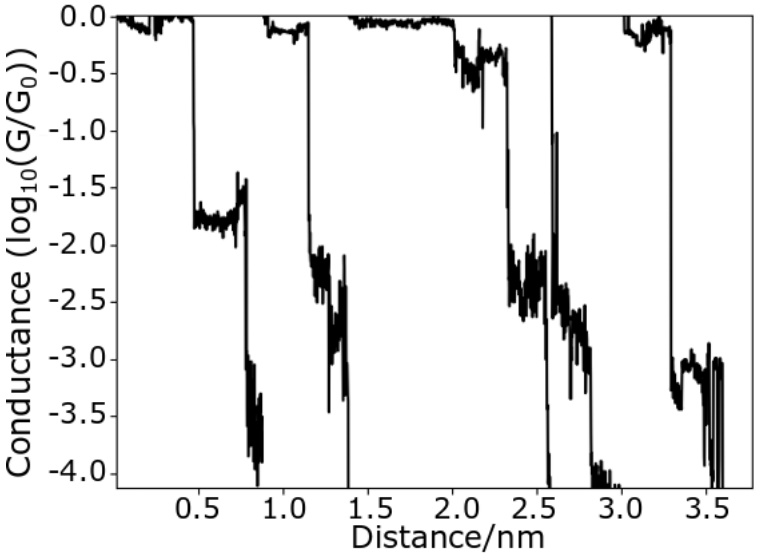

(b)

FIGURE 5.7. (a) 2D conductance vs distance histogram for the Ni | 1,4-benzenedithiol | Ni junction in the absence of magnetic field constructed from 56 traces. The red ellipse highlights the molecular feature in the histogram. (b) Individual conductance vs distance traces for the Ni | 1,4-benzenedithiol | Ni junction in the absence of magnetic field. The start points of the individual traces have been offset for clarity.

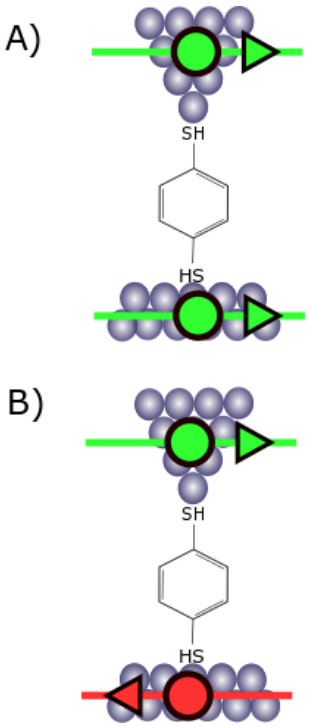

FIGURE 5.8. Diagrams showing some possible magnetic configuration of the electrodes (A) in the presence of a magnetic field large enough to align the electrodes parallel to each other and (B) without the presence of a magnetic field.

5.2.2 Molecular Measurements

5.2.2.1 STM Measurements

The Ni | 1,4-benzenedithiol | Ni junction was measured in the absence of a magnetic field. A saturated solution of 1,4-benzenedithiol in ethanol was produced and a droplet of this was then added to a pH 3, 50 mM Na_2SO_4 aqueous solution. The histograms constructed are fairly low quality as they are only made up of 56 traces. However, the 1D histogram shown in Figure 5.6 shows two peaks. The first peak is at $(6.4\pm0.4)\times10^{-4}$ G_0 and the second peak is at $(2.5\pm0.3)\times10^{-3}$ G_0. In the 2D histogram shown in Figure 5.7a, a molecular feature can be identified in the region between 10^{-2} G_0 and 10^{-3} G_0. In addition, this is supported by the individual conductance vs distance traces in Figure 5.7b, which exhibit plateaus in the same conductance region, though many of these traces exhibited noisy decay. These values are not in agreement with those measured by Yamada *et al.* (0.6×10^{-2} G_0 and 2.4×10^{-2} G_0) and Sakai *et al.* (2×10^{-2} G_0). [64, 191]

The Ni | 1,4-benzenedithiol | Ni junction was measured in the same way but in the presence of a 1 kOe magnetic field applied in the plane of the substrate (perpendicular to the current flow). Possible magnetic configurations of the electrodes are shown in Figure 5.8. 557 traces were used

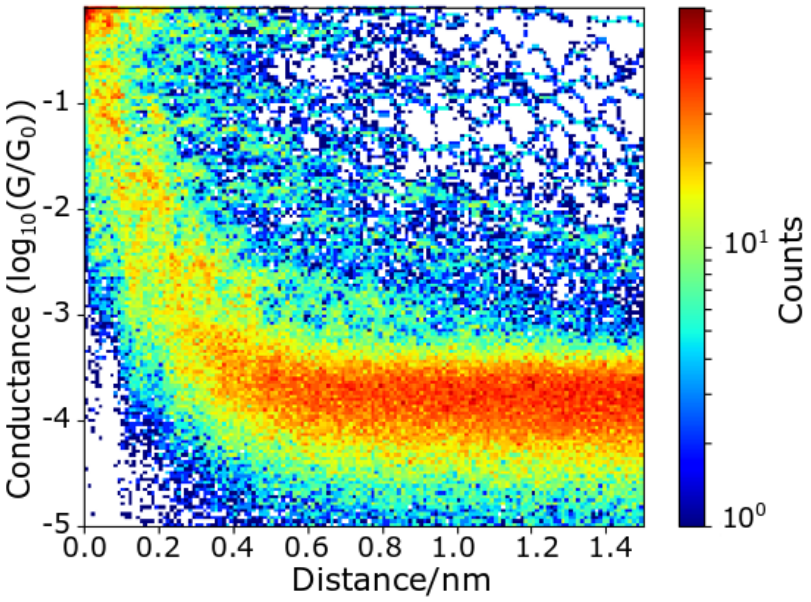

(a)

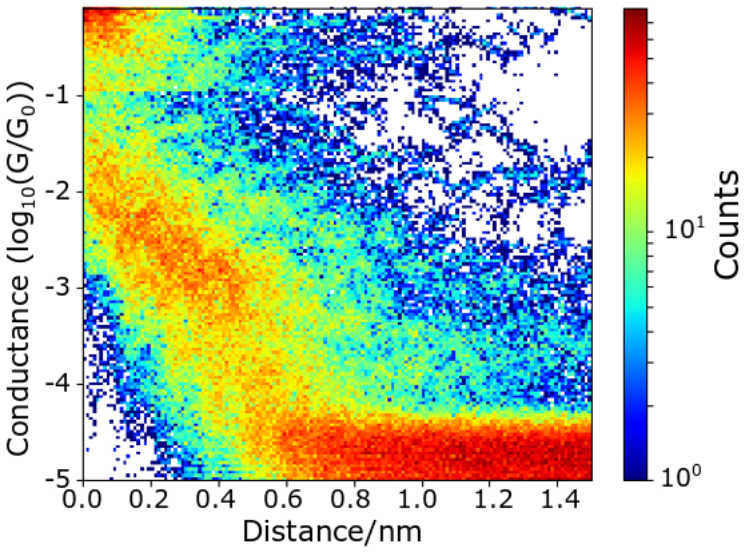

(b)

FIGURE 5.9. 2D histogram showing the conductance of the (a) Ni | Ni junction (b) Ni | 1,4-benzenedithiol | Ni junction in the presence of a 1 kOe magnetic field perpendicular to the current flow with a molecular conductance feature visible between $10^{-}2$ G_0 and $10^{-}3$ G_0. These measurements were carried out using the STM-BJ technique.

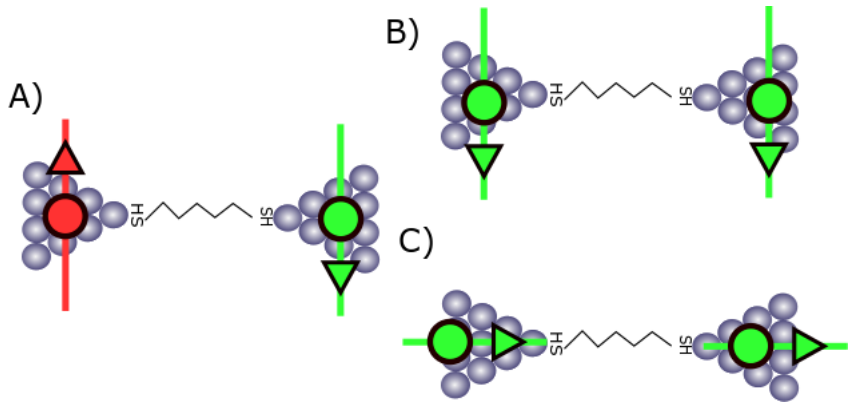

FIGURE 5.10. Diagrams showing some possible magnetic configuration of the electrodes (A) without the presence of a magnetic field and with the magnetic field applied parallel and perpendicular to the junction (B) and (C).

to construct a 1D conductance histogram which appeared featureless. This was due to additional noise introduced by the presence of the magnet which obscured peaks created by plateaus. Automatic data selection was used to identify traces which contained plateaus in the conductance region below G_0. From this, 86 traces were selected and used to form the 1D histogram shown in Figure 5.6. Figure 5.9a shows a 2D conductance vs distance histogram of the Ni | Ni junction for comparison. A 2D histogram is shown in Figure 5.9b, constructed from all 557 traces. This histogram exhibits a molecular feature at $(1.7 \pm 0.2) \times 10^{-3}$ G_0, which corresponds to a negative magnetoresistance of 47%. The molecular feature in Figure 5.7b extends out approximately twice as far as the molecular feature in Figure 5.5b and also appears flatter. Previous measurements have identified MR in the Ni | 1,4-benzenedithiol | Ni junction [64, 191].

5.2.2.2 MCBJ Measurements

An MCBJ was used to measure Co | pentanedithiol | Co junctions in the presence of a 1 kOe magnetic field provided by the quadrupole magnet described in Chapter 2. Possible magnetic configurations of the MCBJ electrodes are shown in Figure 5.10. The sample was prepared with the molecule by exposing it to a pentanedithiol rich environment for 48 hours, as described in section 3.3.1. The results are shown in Figure 5.11. The conductance of the Co | pentanedithiol | Co junction with no magnet was $(1.7 \pm 0.2) \times 10^{-2}$ G_0 as presented in Chapter 4. When the magnetic field was applied parallel to the direction of the current flow, this resulted in the conductance of the junction dropping to $(3.5 \pm 0.2) \times 10^{-3}$ G_0, a negative MR of 567%. This is an order of magnitude larger than accepted values for similar systems and the values predicted by theory [94]. However, the conductance value agrees relatively well with the conductance measured for the Co | PDT | Co junction measured using the STM-BJ technique in Chapter 4. When the 1 kOe magnetic field was applied perpendicularly, the conductance was $(1.3 \pm 0.1) \times 10^{-2}$ G_0 which represents a negative

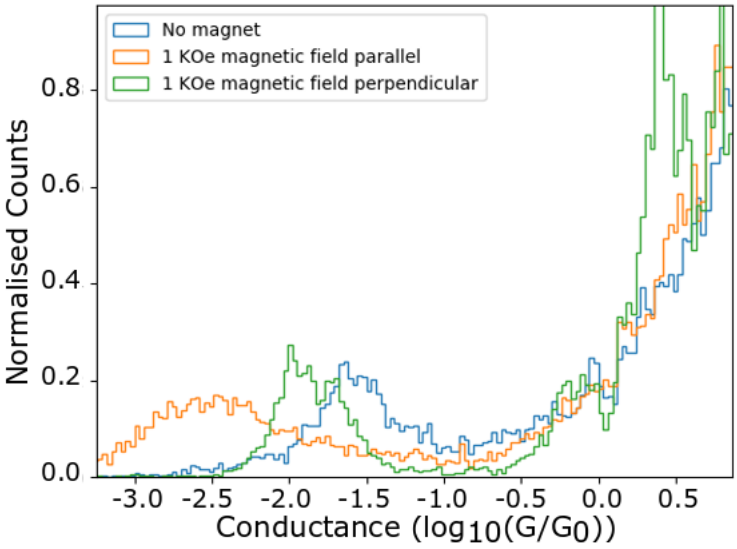

FIGURE 5.11. 1D histogram showing the conductance of the Co | pentanedithiol | Co junction measured using the MCBJ without a magnetic field ($(1.7 \pm 0.2) \times 10^{-2}$ G_0) and in the presence of a magnetic field with various orientations. The histogram for the Co | PDT | Co junction with parallel magnetic field ($(3.5 \pm 0.2) \times 10^{-3}$ G_0) was constructed from 165 traces manually selected from 635 traces. The histogram for the Co | PDT | Co junction with perpendicular magnetic field ($(1.3 \pm 0.1) \times 10^{-2}$ G_0) was constructed from 201 traces manually selected from 1458 traces.

MR of 54%. This MR value is the same order of magnitude as those previously measured by Horiguchi *et al.* and Yamada *et al.*. However, the measurements of Horiguchi and Yamada involve the use of a conjugated molecule and it has been both predicted by theorists and observed during experiments that the MR for π-conjugated molecules is higher than for non-conjugated molecules [142]. Values of this magnitude are much more credible than previous measurements of up to 100000% MR which have been discredited due to the influence of magnetostriction on the results [65]. In addition, the three histograms in Figure 5.11 were formed from data collected during a minimum of three repeats of the experiment, using different samples each time. When adding data from the repeat experiments to the original histograms, the positions of the peaks appeared unchanged. The conductance shown in Figure 5.11 varies with the orientation of the magnetic field, which is a characteristic of tunnelling anisotropic magnetoresistance. The measured AMR in this case is 77%. This is the same order of magnitude as the AMR observed in Li's work on Fe | terephthalic acid | Fe single-molecule junctions (53%) which was also carried out at room temperature [94].

The 2D histogram shown for the Co | PDT | Co junction with no magnet in Figure 4.19 shows that the conductance feature is relatively flat. This suggests that the impact of magnetostriction

on the conductance measurements taken with an applied magnetic field may not be significant. Additionally, to reduce the impact of magnetostrictive effects, the magnetic field was applied when the junction was open. A static field was then maintained as the measurements were carried out. This is important because one is more likely to observe magnetostrictive effects if the separation of the electrodes is kept constant and the conductance measurements are made in different fields. Despite these measures, previous magnetoresistance investigations have required much stricter experimental procedures to eliminate the influence of magnetostriction and magnetostatic effects on the measurements. These included performing the experiments at cryogenic temperature and using a particular electrode geometry as discussed in the introduction to this chapter [15]. The MCBJ samples used for the experiments within consisted of Co wires, used as electrodes, fixed to a substrate using epoxy. Samples constructed in this way have been proven to be highly susceptible to the consequences of magnetostriction as epoxy has a modulus of elasticity a factor of 100 smaller than Co [47]. This means the epoxy will deform with the Co electrodes, allowing them to reshape easily. In fact, it is thought that artefacts resembling magnetoresistance are highly likely to be observed in any data recorded using the sample geometry used for these measurements [15].

Figure 5.12 shows conductance of the Co | Co junctions in the presence of a 1 kOe magnetic field perpendicular to the direction of current flow. The individual traces used to construct this histogram mostly showed noisy decay, likely due to the electrodes being oxidised. However, even after manually selecting for plateaus, there are no clear peaks visible. In particular, there is no peak around $\log_{10}(G/G_0) \approx -2$, the region where a peak is seen in the conductance histogram for the Co | pentanedithiol | Co junction. This strongly suggests that the peak in Figure 5.11 is a result of the presence of a molecule in the junction and not an artefact due to the magnetic field.

To validate these results further, future work should include taking conductance measurements of the Au | pentanedithiol | Au junction in the presence of a magnetic field. As gold is not ferromagnetic, it would be surprising if any change in conductance on the application of a magnetic field were to occur. Therefore if the conductance of the Au | pentanedithiol | Au junction did shift under these conditions, it would suggest that the supposed magnetoresistance effect seen in the Co | pentanedithiol | Co junction was actually a result of another factor. In addition, the data collected were not sufficient to form useful 2D histograms so more data should be collected to improve this. Good quality 2D histograms would allow the electrode separation at which the molecular feature occurs in the three histograms in Figure 5.11 to be compared. If the feature appears at the same electrode separation in each histogram, this would suggest that the peaks observed result from the same junction configuration and may be the result of magnetoresistive effects.

Producing lithographically patterned substrates would allow electrodes to be formed in geometries which reduce the likelihood of significant magnetostriction impacting the results. For example, von Bieren *et al.* suggest the use of electrodes shaped like those in Figure 5.13 [176].

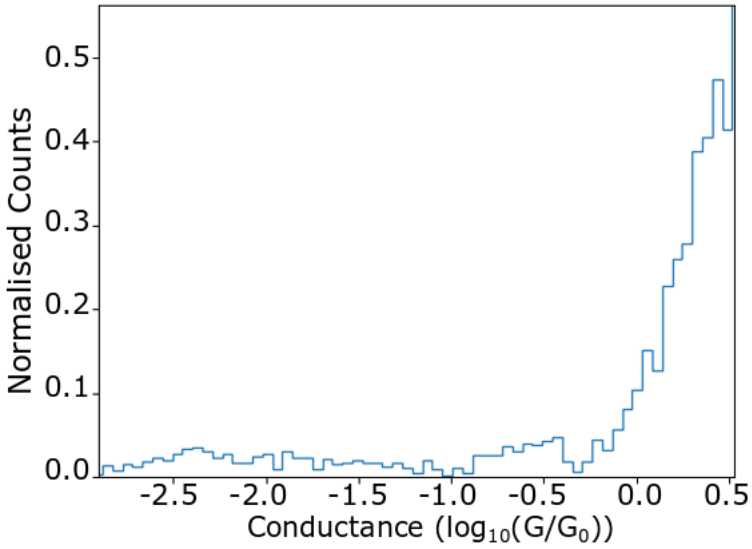

FIGURE 5.12. 1D histogram showing the conductance for the Co | Co atomic junction with a 1 kOe magnetic field applied measured using the MCBJ. The histogram is constructed from 362 traces.

In this case, domain walls can be positioned precisely. Hence if a saturating field is applied in the direction $\theta = 0°$, when the field is removed the magnetization of the electrodes will be antiparallel as shown in Figure 5.13B. In contrast, Figure 5.13C shows the parallel magnetization of the electrodes after a saturating field is applied in the direction $\theta = 90°$. These states are remanant, and so remain magnetized in the described configurations when H=0. This means artefacts caused by magnetostriction can be avoided during GMR style measurements, as it is not necessary to apply a magnetic field while the measurements are taking place.

5.3 Chapter Summary

The conductances of two metal-molecule-metal junctions have been measured in the presence of magnetic fields. Specifically, the Ni | 1,4-benzenedithiol | Ni junction was investigated using the STM-BJ technique in combination with a custom-made electromagnet. A negative magnetoresistance of 47% was measured. This value is the same order of magnitude as measurements of MR in the same system taken by Horiguchi *et al.* (90%) and Yamada *et al.* (30%).

The Co | pentanedithiol | Co junction was also investigated using the MCBJ technique and a quadrupole magnet. These measurements showed evidence of magnetoresistance. The measured AMR was 77%. No previous attempts have been made to measure the AMR of this system but the value obtained was the same order of magnitude as the AMR observed in Li's work on

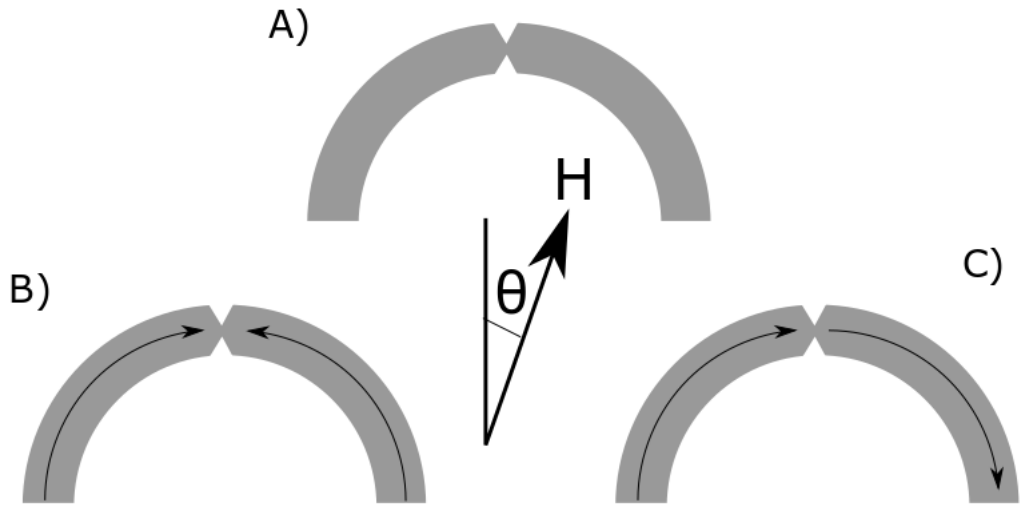

FIGURE 5.13. Schematic view of curved electrode geometry that can be used to eliminate magnetostriction during magnetoresistance measurements and the corresponding magnetic configurations at H= 0 after applying a magnetic field, H, parallel to (b) θ = 0° and (c) θ= 90 °.

Fe | terephthalic acid | Fe single-molecule junctions (53%) which was also carried out at room temperature [94]. The MR in this case was -567%. Again, this is the first attempt to measure MR in this system. However, values of MR measured for similar systems display MR an order of magnitude smaller than this value and theory also predicts values of MR an order of magnitude smaller than -567% [94]. Despite the fact that precautions were taken to reduce the impact of magnetostriction on the results, it is likely that the shift in conductance of the junction in the presence of a magnetic field is due to this and other magnetostatic effects rather than an observation of magnetoresistance. Future work is suggested which would help to determine the cause of the conductance shift. Improvements to the experimental set up, in particular development of the current samples into lithographically patterned samples with a particular geometry, which may prevent false results due to magnetostriction are also suggested.

A table containing the results obtained in this chapter is shown in Table 5.1.

Junction	Measurement Technique	Molecular Conductance G_0	Magnetic Field/ kOe
Co | pentanedithiol | Co	MCBJ	$(3.5 \pm 0.2) \times 10^{-3}$	1 (parallel to current)
Co | pentanedithiol | Co	MCBJ	$(1.3 \pm 0.1) \times 10^{-2}$	1 (perpendicular to current)
Ni | 1,4-benzenedithiol | Ni	STM-BJ	$(1.7 \pm 0.2) \times 10^{-3}$	1 (perpendicular to current)

Table 5.1: A summary of the results obtained in Chapter 5.

CHAPTER 6

CONCLUSIONS AND FUTURE PATHS

The main aim of this work was to investigate the electronic and spintronic transport properties of metal-molecule-metal junctions. This was achieved via two methods: STM-BJ and MCBJ.

The design and construction of a mechanically controllable break junction was discussed in Chapter 2. The device was then tested using Au electrodes in order to determine its suitability for molecular conductance measurements. Au electrodes were chosen at this stage due to the breadth of relevant literature available, which enabled the legitimacy of results obtained with this device to be validated.

After ascertaining the capabilities of the device, single molecule conductance measurements carried out with Au electrodes were explored and discussed in Chapter 3. The conductance of dithiol linked and bipyridyl linked molecules were investigated using MCBJ and STM-BJ methods and the values measured were generally in agreement with previously measured literature values. For example, high conductance and low conductance peaks were observed in bipyridyl linked molecules due to the different linking capabilities that the molecule have with gold.

A number of additional analysis techniques were used to support the information gathered from 1D conductance histograms. These include I-V curves, 2D histograms, conditional histograms and 2D correlation histograms. 2D correlation histograms and conditional histograms were used to determine the relationship between high conductance and low conductance peaks in the histogram showing the conductance of the Au | 4,4'-bipyridine | Au junction. From this analysis, it was determined that in this case, it was possible to observe both high and low conductance plateaus within one conductance vs distance trace. There were also some cases where traces exhibited solely a high conductance plateau were detected. However, one was far less likely to observe traces where only low conductance plateaus where measured.

Single molecule conductance measurements were carried out with both STM-BJ and MCBJ methods using Co electrodes in Chapter 4. The conductance values obtained were compared with those collected using Au electrodes. It has been reported within that the conductance of metal-molecule-metal junctions may rely on the choice of metal contact. MCBJ measurements have shown that the conductance of a Co | PDT | Co junction is close to an order of magnitude larger than that of an Au | PDT | Au junction. In addition, STM-BJ measurements were used to demonstrate that where Au | 4,4'-bipyridine | Au junctions exhibit both high conductance and low conductance peaks, Ni | 4,4'-bipyridine | Ni junctions only exhibit a single peak. The differences between measurements taken with ferromagmetic electrodes and gold electrodes is thought to be due to the increased role of the d-band electrons in electronic transport experienced in ferromagnetic metals.

The differences between measurements taken using the MCBJ method and the STM method were also discussed in Chapter 4. Previous literature has suggested that the significantly slower breaking speed of the MCBJ when compared with the STM could result in different conductance values for the same metal-molecule-metal junctions [107]. However, It has been observed that the conductance of a metal-molecule-metal junction measured with using the MCBJ, is often in agreement with that measured using the STM.

During the discussions in Chapter 4, it was determined that single-molecule conductance MCBJ measurements could be taken using cobalt electrodes without taking any measures, such as electrochemically reducing the oxide, to prevent oxidation of the surface. This is a significant result as it increases the likelihood that metal-molecule-metal junctions with ferromagnetic electrodes will be incorporated into electronic devices. It is suggested that the thiol, which linked to the electrodes, can help clean the substrate surface and hence prevent the formation of surface oxide. In addition, it is possible that on separating the electrodes, a thiol-cobalt bond forms between the molecule and the exposed cobalt before the cobalt has oxidised.

Finally, the impacts of a magnetic field on atomic contacts and metal-molecule-metal junctions were explored in Chapter 5 using both STM-BJ and MCBJ methods. An attempt was made to measure magnetoresistance in a Co | PDT | Co junction using an MCBJ. An MR of up to 567% was measured however it is likely that this is due to artefacts rather than magnetoresistance. An AMR of 77% was also measured. This is the same order of magnitude as previous measurements of similar systems [94]

Important improvements for future work involve the development of a reproducible lithographically patterned substrate for use with the MCBJ. This would allow electrodes to be produced on a much finer scale and in a reproducible way, which could lead to a more predictable breaking mechanism. It would also allow samples to be produced with a geometry more suitable for magnetoresistance measurements. Using a curved geometry, for example, may help to reduce the effects of magnetostriction when measuring the conductance of the junction.

Secondly, development of a pre-amplifier to use in conjunction with the MCBJ. It is possible

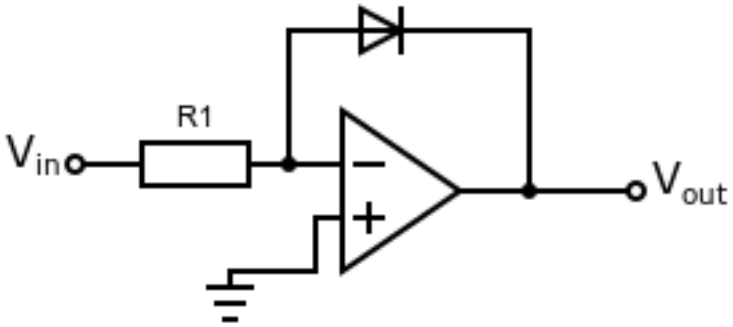

FIGURE 6.1. logarithmic amplifier chip circuit diagram.

to purchase commercial logarithmic amplifier chips, for example LOG101 and LOG112 manufactured by Texas Instruments. A log amplifier is an amplifier for which the output voltage, V_{out} is described by the following equation

$$V_{out} = Kln(\frac{V_{in}}{V_{ref}}), \tag{6.1}$$

where V_{ref} is the normalisation constant, V_{in} is the input voltage and K is the scale factor. Logarithmic amplifier chips can be used to extend the dynamic range of circuits. This could be particularly useful for measuring the conductance of single molecules as a high number of measurements need to be taken over a wide range of currents. It would also allow for the measurement of molecules with lower conductance values which would provide a more extensive analysis of molecular conductance.

In Chapter 5, improvements to the experimental method and potential future experiments have been suggested as a way to more convincingly prove or disprove whether what we have observed is a magnetoresistive effect. This includes control experiments using Au electrodes. As they are not ferromagnetic, one would not expect to see any changes in conductance of molecular junctions linked with Au due to the influence of a magnetic field. In addition, the quantity of data collected should be increased so that high quality 2D histograms can be constructed with conductance data for junctions in a magnetic field. The resulting 2D histograms could then be compared to the 2D histograms constructed using data collected in the absence of a magnetic field which would provide further insight into what may be causing the shift in conductance of the junctions under magnetic field.

Table 6.1 contains a summary of all the results obtained in this thesis.

Junction	Measurement Technique	Primary Conductance Peaks G_0	Junction Formation Probability	Magnetic Field/ kOe
Au | pentanedithiol | Au	MCBJ	$(2.0 \pm 0.1) \times 10^{-3}$	29%	0
Co | pentanedithiol | Co	MCBJ	$(1.7 \pm 0.2) \times 10^{-2}$	27%	0
Co | pentanedithiol | Co	MCBJ	$(3.5 \pm 0.2) \times 10^{-3}$	26%	1 (parallel to current)
Co | pentanedithiol | Co	MCBJ	$(1.3 \pm 0.1) \times 10^{-2}$	14%	1 (perpendicular to current)
Co | pentanedithiol | Co	STM-BJ	$(2.5 \pm 0.2) \times 10^{-3}$	35%	0
Au | 1,4-benzenedithiol | Au	MCBJ	$(1.3 \pm 0.1) \times 10^{-2}$	$(8.5 \pm 0.3) \times 10^{-2}$	28%	0
Co | 1,4-benzenedithiol | Co	MCBJ	$(4.0 \pm 0.1) \times 10^{-2}$	$(4.0 \pm 0.1) \times 10^{-1}$	22%	0
Co | 1,4-benzenedithiol | Co	STM-BJ	$(3.2 \pm 0.7) \times 10^{-4}$	$(3.3 \pm 0.2) \times 10^{-2}$	40%	0
Ni | 1,4-benzenedithiol | Ni	STM-BJ	$(6.4 \pm 0.4) \times 10^{-4}$	$(2.5 \pm 0.3) \times 10^{-3}$	14%	0
Ni | 1,4-benzenedithiol | Ni	STM-BJ	$(1.7 \pm 0.2) \times 10^{-3}$		15%	1 (perpendicular to current)
Co | biphenyl-4-carboxylic acid | Co	MCBJ	$(1.6 \pm 0.3) \times 10^{-2}$	$(3.0 \pm 0.2) \times 10^{-1}$	33%	0

Table 6.1: A summary of the results obtained within this thesis.

6.1 2D histograms

The 2D conductance vs distance histograms for the data collected in this thesis and corresponding to the results shown in Table 6.1 are shown below. The 2D conductance histograms for junctions containing pentanedithiol are shown first. The Au | PDT | Au junction histogram is shown in Figure 6.2. The Co | PDT | Co histogram measured using the MCBJ technique is shown in Figure 6.3 and the histogram measured of the same junction using the STM-BJ technique is shown in Figure 6.4. The 2D histograms formed when the Co | PDT | Co junction was measured in the presence of a magnetic field are shown in Figures 6.5 and 6.6. These histograms do not show clear molecular features due to poor quality traces because of the noise introduced by adding a magnet to the system. Next, the 2D histograms for junctions containing 1,4-benzenedithiol are shown. Firstly, Au | 1,4-benzenedithiol | Au in Figure 6.7 and secondly Co | 1,4-benzenedithiol | Co in Figure 6.8. STM-BJ measurements of the Co | 1,4-benzenedithiol | Co junction are shown in Figure 6.9. Measurements of the Ni | 1,4-benzenedithiol | Ni junction were taken in the absence (Figure 6.10) and presence (Figure 6.11) of a 1 kOe magnetic field. Finally, the 2D conductance vs distance histogram for the Co | BP4CA | Co junction is shown in Figure 6.12. In this histogram there is no clear molecular feature due to a large number of molecular plateaus occuring at different values of conductance in the individual conductance vs distance traces.

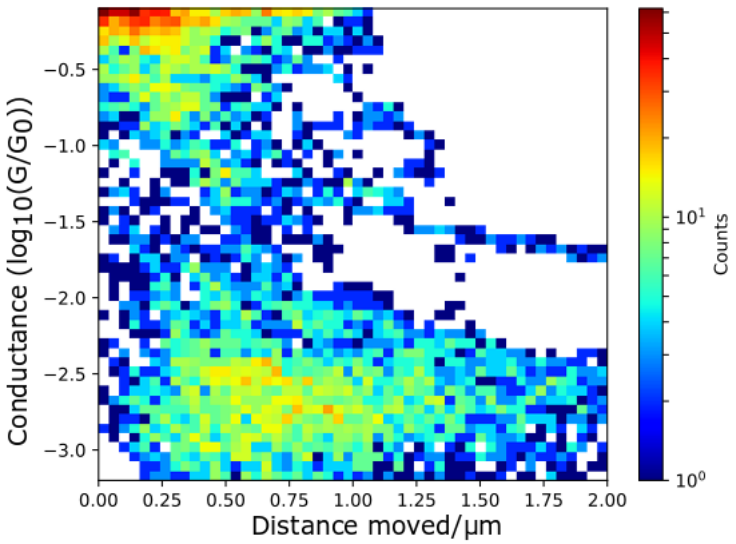

FIGURE 6.2. MCBJ 2D conductance histogram of an Au | PDT | Au junction. Formed from 135 traces. Molecular feature is visible at (2.0±0.1)×10^{-3} G_0.

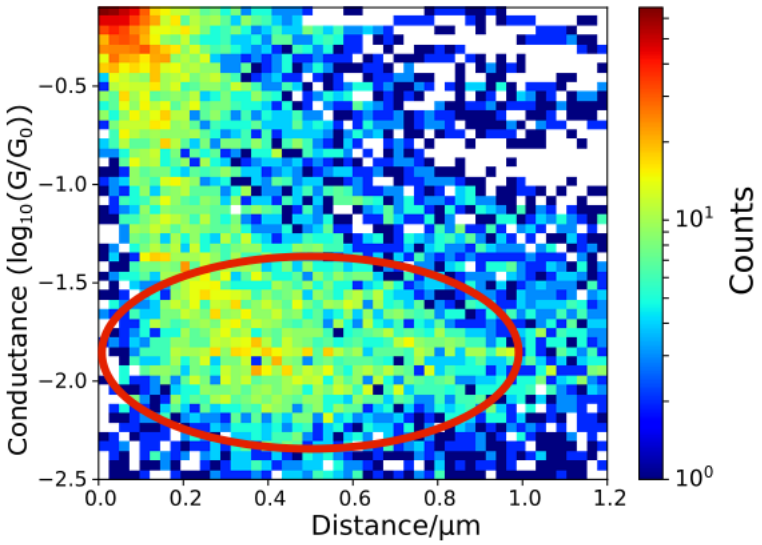

FIGURE 6.3. 2D conductance vs distance histogram of the Co | PDT | Co junction measured using MCBJ, formed of 136 traces. A red ellipse has been used to highlight the molecular conductance region.

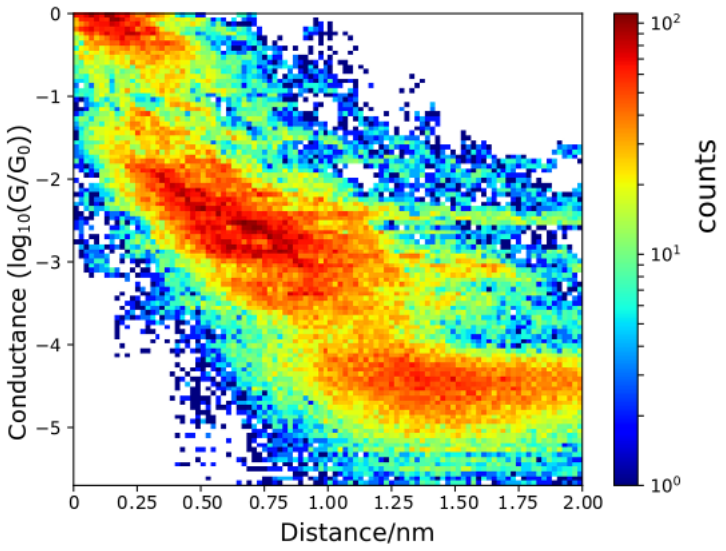

FIGURE 6.4. 2D conductance vs distance histogram for the Co | PDT | Co junction measured using STM-BJ techniques. Formed from 538 traces. Molecular feature is visible between 10^{-2} G_0 and 10^{-4} G_0.

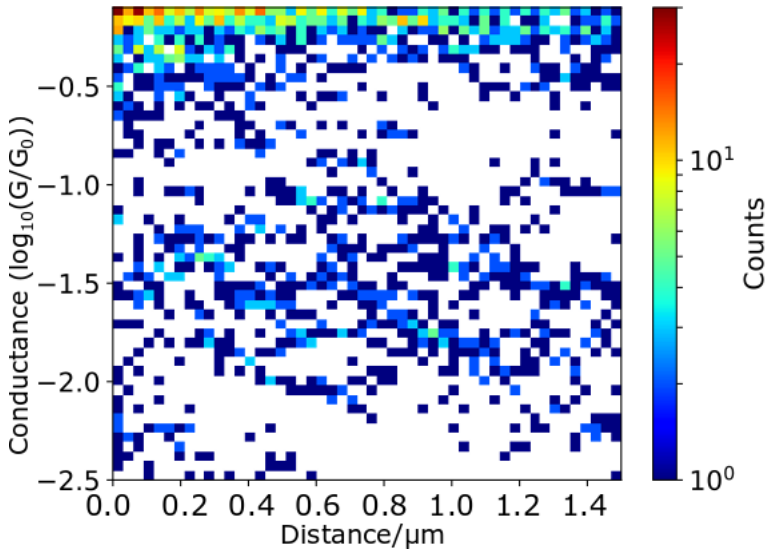

FIGURE 6.5. MCBJ 2D conductance histogram of an Co | PDT | Co junction in the presence of a 1 kOe magnetic field perpendicular to the current flow. Formed from 201 traces. No molecular feature is visible due to the poor quality of the data.

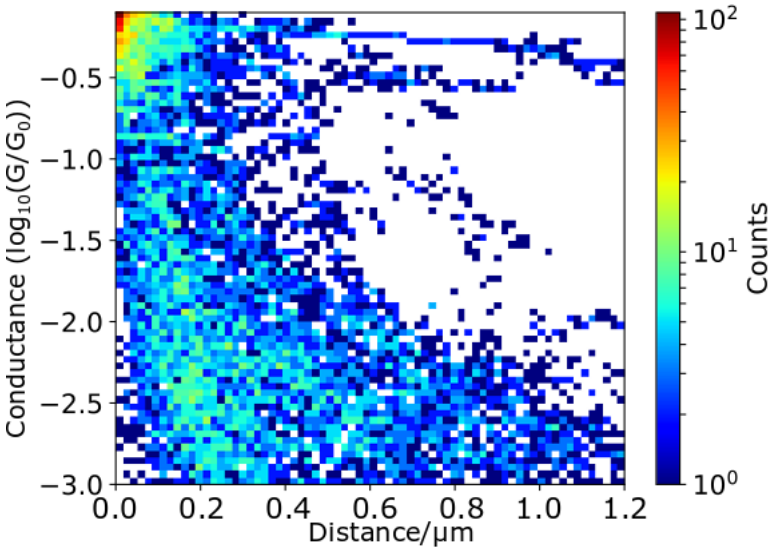

FIGURE 6.6. MCBJ 2D conductance histogram of an Co | PDT | Co junction in the presence of a 1 kOe magnetic field parallel to the current flow. Formed from 165 traces. No clear molecular feature is visible due to noisy traces.

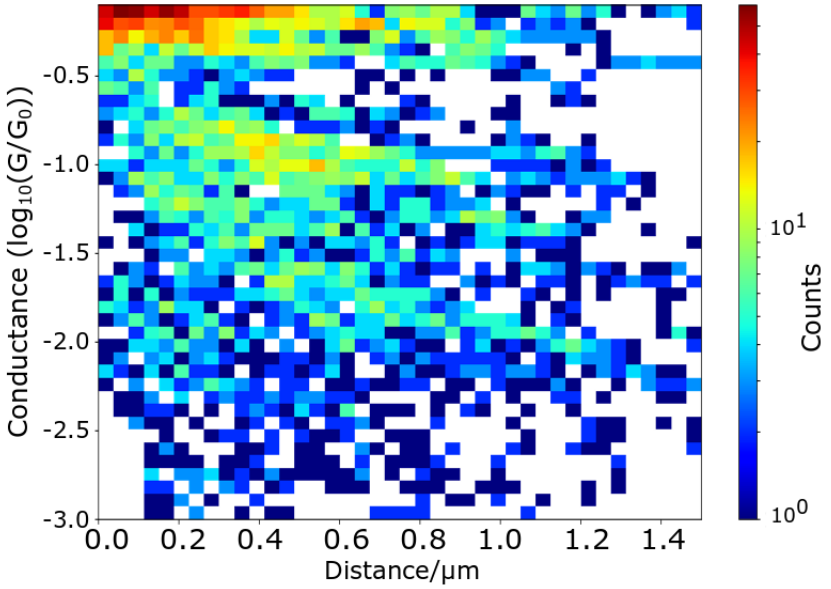

FIGURE 6.7. MCBJ 2D conductance histogram of an Au | 1,4-benzenedithiol | Au junction. Formed from 200 traces. Molecular features are visible around 10^{-1} G_0 and another can be seen between $10^{-1.5}$ G_0 and 10^{-2} G_0.

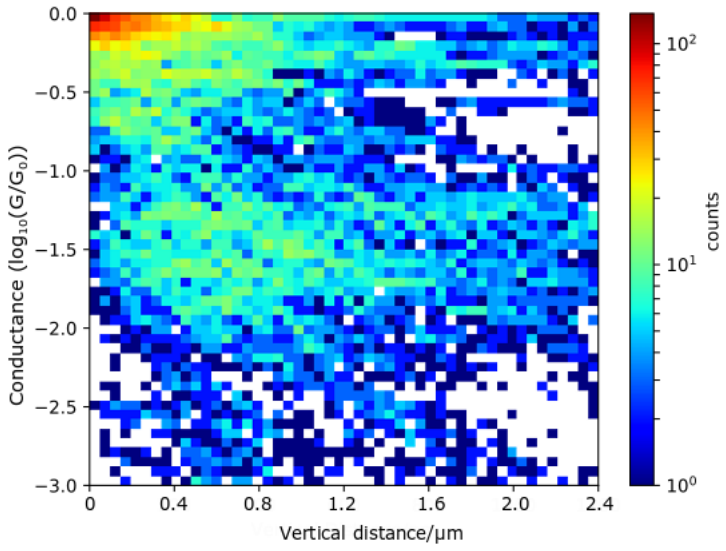

FIGURE 6.8. 2D conductance vs distance histogram for the Co | 1,4-benzenedithiol | Co junction measured using MCBJ. Formed from 200 traces. Molecular feature is visible between 10^{-1} G_0 and 10^{-2} G_0.

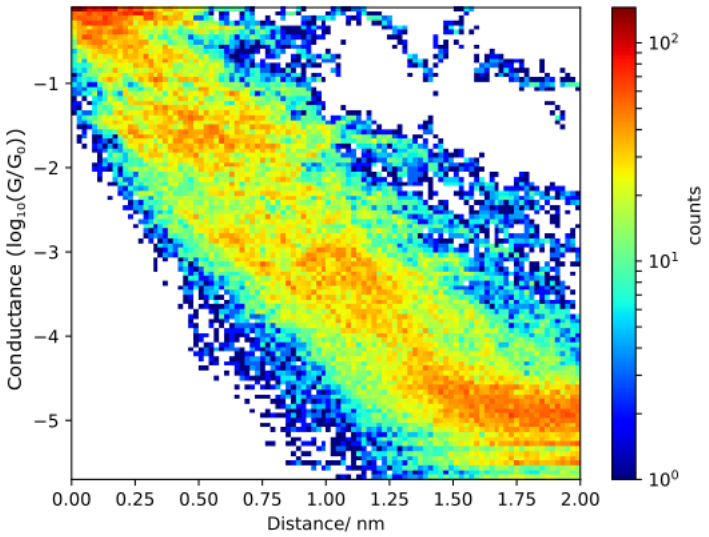

FIGURE 6.9. 2D conductance vs distance histogram for the Co | 1,4-benzenedithiol | Co junction measured at a bias of -1 V vs MSE using STM. Formed from 119 traces. Two molecular features are visible, the low conductance at $(3.2 \pm 0.7) \times 10^{-4}$ G_0 and the high conductance at $(3.3 \pm 0.2) \times 10^{-2}$ G_0.

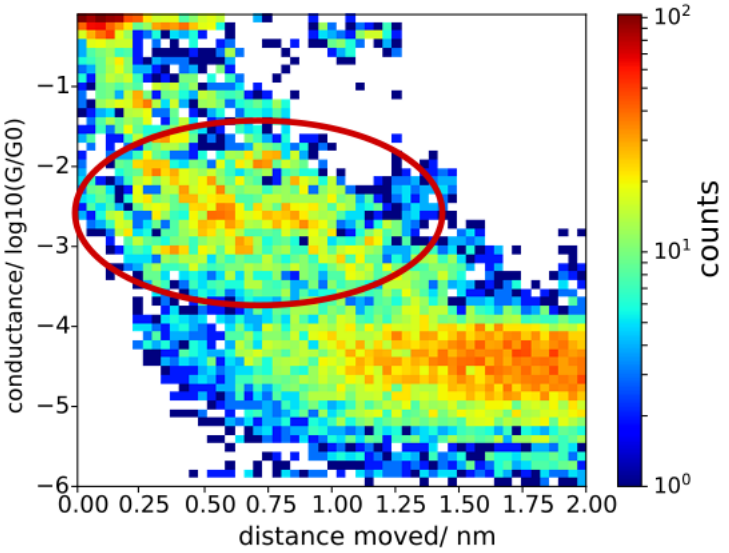

FIGURE 6.10. (a) 2D conductance vs distance histogram for the Ni | 1,4-benzenedithiol | Ni junction in the absence of magnetic field constructed from 56 traces. The red ellipse highlights the molecular feature in the histogram.

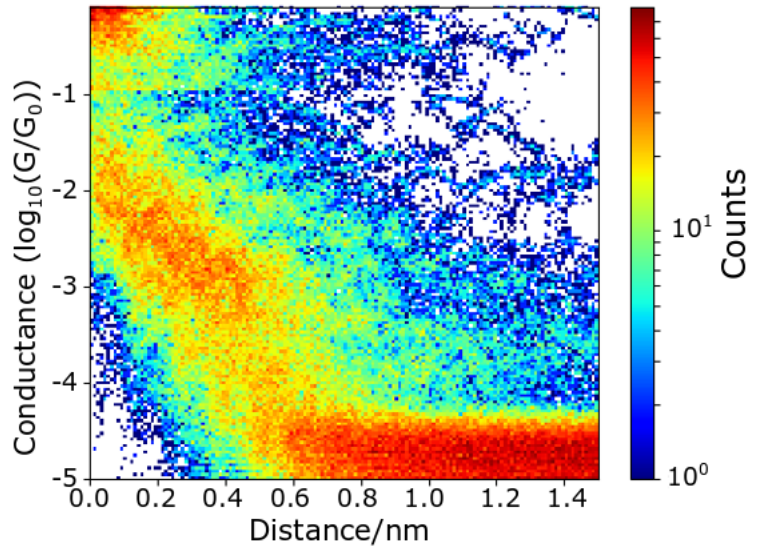

FIGURE 6.11. 2D histogram showing the conductance of the Ni | 1,4-benzenedithiol | Ni junction in the presence of a 1 kOe magnetic field perpendicular to the current flow with a molecular conductance feature visible between $10^{-}2$ G_0 and $10^{-}3$ G_0. These measurements were carried out using the STM-BJ technique.

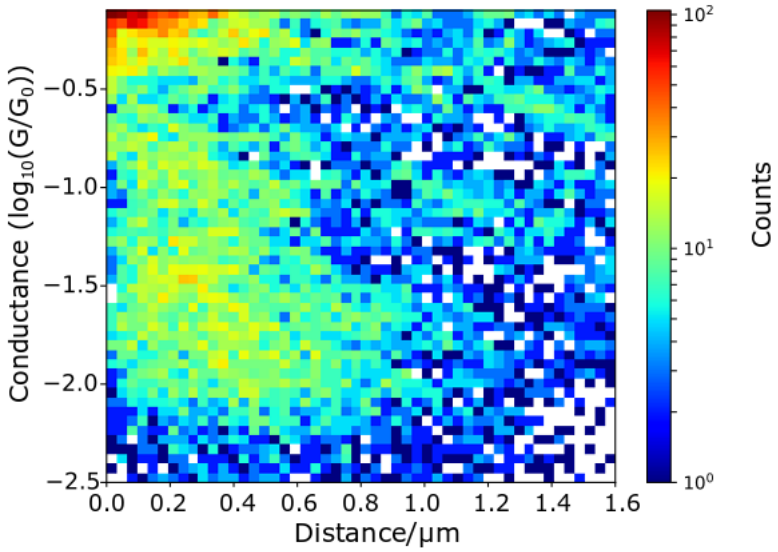

FIGURE 6.12. 2D histogram showing the conductance of the Co | BP4CA | Co junction. There is no molecular feature due to the small amount of data collected during this experiment. These measurements were carried out using the MCBJ technique.

BIBLIOGRAPHY

[1] S. H. AHN, S. J. HWANG, S. J. YOO, I. CHOI, H. J. KIM, J. H. JANG, S. W. NAM, T. H. LIM, T. LIM, S. K. KIM, AND J. J. KIM, *Electrodeposited Ni dendrites with high activity and durability for hydrogen evolution reaction in alkaline water electrolysis*, Journal of Materials Chemistry, 22 (2012), pp. 15153–15159.

[2] C. ALBONETTI, I. BERGENTI, M. CAVALLINI, V. DEDIU, M. MASSI, J. F. MOULIN, AND F. BISCARINI, *Electrochemical preparation of cobalt tips for scanning tunneling microscopy*, Review of Scientific Instruments, 73 (2002), pp. 4254–4256.

[3] C. ALBONETTI, M. CAVALLINI, M. MASSI, J. F. MOULIN, AND F. BISCARINI, *Electrochemical fabrication of cobalt and nickel tips for scanning tunneling microscopy*, Journal of Vacuum Science and Technology B: Microelectronics and Nanometer Structures, 23 (2005), pp. 2564–2566.

[4] S. V. ARADHYA, M. FREI, M. S. HYBERTSEN, AND L. VENKATARAMAN, *Van der Waals interactions at metal/organic interfaces at the single-molecule level*, Nature Materials, 11 (2012), pp. 872–876.

[5] A. C. ARAGONÈS, D. ARAVENA, F. J. VALVERDE-MUÑOZ, J. A. REAL, F. SANZ, I. DÍEZ-PÉREZ, AND E. RUIZ, *Metal-Controlled Magnetoresistance at Room Temperature in Single-Molecule Devices*, Journal of the American Chemical Society, 139 (2017), pp. 5768–5778.

[6] A. AVIRAM AND M. A. RATNER, *Molecular rectifiers*, Chemical Physics Letters, 29 (1974), pp. 277–283.

[7] J. BAI, A. DAAOUB, S. SANGTARASH, X. LI, Y. TANG, Q. ZOU, H. SADEGHI, S. LIU, X. HUANG, Z. TAN, J. LIU, Y. YANG, J. SHI, G. MÉSZÁROS, W. CHEN, C. LAMBERT, AND W. HONG, *Anti-resonance features of destructive quantum interference in single-molecule thiophene junctions achieved by electrochemical gating*, Nature Materials, 18 (2019), pp. 364–369.

[8] M. N. BAIBICH, J. M. BROTO, A. FERT, F. N. VAN DAU, F. PETROFF, P. EITENNE, G. CREUZET, A. FRIEDERICH, AND J. CHAZELAS, *Giant magnetoresistance of*

(001)Fe/(001)Cr magnetic superlattices, Physical Review Letters, 61 (1988), pp. 2472–2475.

[9] C. BARRAUD, P. SENEOR, R. MATTANA, S. FUSIL, K. BOUZEHOUANE, C. DERANLOT, P. GRAZIOSI, L. HUESO, I. BERGENTI, V. DEDIU, F. PETROFF, AND A. FERT, *Unravelling the role of the interface for spin injection into organic semiconductors*, Nature Physics, 6 (2010), pp. 615–620.

[10] H. BASCH, R. COHEN, AND M. A. RATNER, *Interface geometry and molecular junction conductance: Geometric fluctuation and stochastic switching*, Nano Letters, 5 (2005), pp. 1668–1675.

[11] A. BATRA, P. DARANCET, Q. CHEN, J. S. MEISNER, J. R. WIDAWSKY, J. B. NEATON, C. NUCKOLLS, AND L. VENKATARAMAN, *Tuning rectification in single-molecular diodes*, Nano Letters, 13 (2013), pp. 6233–6237.

[12] J. M. BEEBE, V. B. ENGELKES, L. L. MILLER, AND C. D. FRISBIE, *Contact resistance in metal-molecule-metal junctions based on aliphatic SAMs: Effects of surface linker and metal work function*, Journal of the American Chemical Society, 124 (2002), pp. 11268–11269.

[13] G. BINASCH, P. GRÜNBERG, F. SAURENBACH, AND W. ZINN, *Enhanced magnetoresistance in layered magnetic structures with antiferromagnetic interlayer exchange*, Physical Review B, 39 (1989), pp. 4828–4830.

[14] L. BOGANI AND W. WERNSDORFER, *Molecular spintronics using single-molecule magnets*, Nature Materials, 7 (2008), pp. 179–186.

[15] K. I. BOLOTIN, F. KUEMMETH, A. N. PASUPATHY, AND D. C. RALPH, *From ballistic transport to tunneling in electromigrated ferromagnetic breakjunctions*, Nano Letters, 6 (2006), pp. 123–127.

[16] A. BORGES, E. D. FUNG, F. NG, L. VENKATARAMAN, AND G. C. SOLOMON, *Probing the Conductance of the σ-System of Bipyridine Using Destructive Interference*, Journal of Physical Chemistry Letters, 7 (2016), pp. 4825–4829.

[17] A. M. BRATKOVSKY AND P. E. KORNILOVITCH, *Effects of gating and contact geometry on current through conjugated molecules covalently bonded to electrodes*, Phys. Rev. B, 67 (2003), p. 115307.

[18] R. J. BROOKE, *Ferromagnetic Contacts for Single-Molecule Devices*, PhD thesis, 2015.

[19] R. J. BROOKE, C. JIN, D. S. SZUMSKI, R. J. NICHOLS, B. W. MAO, K. S. THYGESEN, AND W. SCHWARZACHER, *Single-molecule electrochemical transistor utilizing a nickel-pyridyl spinterface*, Nano Letters, 15 (2015), pp. 275–280.

[20] R. J. BROOKE, D. S. SZUMSKI, A. VEZZOLI, S. J. HIGGINS, R. J. NICHOLS, AND W. SCHWARZACHER, *Dual Control of Molecular Conductance through pH and Potential in Single-Molecule Devices*, Nano Letters, 18 (2018), pp. 1317–1322.

[21] C. BRUOT, J. HIHATH, AND N. TAO, *Mechanically controlled molecular orbital alignment in single molecule junctions*, Nature Nanotechnology, 7 (2012), pp. 35–40.

[22] L. A. BUMM, J. J. ARNOLD, M. T. CYGAN, T. D. DUNBAR, T. P. BURGIN, L. JONES, D. L. ALLARA, J. M. TOUR, AND P. S. WEISS, *Are single molecular wires conducting?*, Science, 271 (1996), pp. 1705–1707.

[23] J. D. BURTON, R. F. SABIRIANOV, J. P. VELEV, O. N. MRYASOV, AND E. Y. TSYMBAL, *The Origin of Tunneling Anisotropic Magnetoresistance in Break Junctions*, Physical Review B, 76 (2007), pp. 12–15.

[24] N. M. CAFFREY, S. SCHRÖDER, P. FERRIANI, AND S. HEINZE, *Tunneling anisotropic magnetoresistance effect of single adatoms on a noncollinear magnetic surface*, Journal of Physics Condensed Matter, 26 (2014), p. 394010 (9pp).

[25] C. CARTER, M. BRUMBACH, C. DONLEY, R. D. HREHA, S. R. MARDER, B. DOMERCQ, S. YOO, B. KIPPELEN, AND N. R. ARMSTRONG, *Small molecule chemisorption on indium - Tin oxide surfaces: Enhancing probe molecule electron-transfer rates and the performance of organic light-emitting diodes*, Journal of Physical Chemistry B, 110 (2006), pp. 25191–25202.

[26] S. R. CATARELLI, S. J. HIGGINS, W. SCHWARZACHER, B. W. MAO, J. W. YAN, AND R. J. NICHOLS, *Ionic liquid based approach for single-molecule electronics with cobalt contacts*, Langmuir, 30 (2014), pp. 14329–14336.

[27] M. CAVALLINI AND F. BISCARINI, *Electrochemically etched nickel tips for spin polarized scanning tunneling microscopy*, Review of Scientific Instruments, 71 (2000), pp. 4457–4460.

[28] A. R. CHAMPAGNE, A. N. PASUPATHY, AND D. C. RALPH, *Mechanically adjustable and electrically gated single-molecule transistors*, Nano Letters, 5 (2005), pp. 305–308.

[29] F. CHEN, Z. HUANG, AND N. TAO, *Forming single molecular junctions between indium tin oxide electrodes*, Applied Physics Letters, 91 (2007), p. 162106.

[30] F. CHEN, X. LI, J. HIHATH, Z. HUANG, AND N. TAO, *Effect of Anchoring Groups on Single-Molecule Conductance: Comparative Study of Thiol-, Amine-, and Carboxylic-Acid-Terminated Molecules*, Journal of the American Chemical Society, 128 (2006), pp. 15874–15881.

[31] H. CHEN, W. XIAO, X. WU, K. YANG, AND H.-J. GAO, *Electrochemically etched Ni tips in a constant-current mode for spin-polarized scanning tunneling microscopy*, Journal of Vacuum Science & Technology B, Nanotechnology and Microelectronics: Materials, Processing, Measurement, and Phenomena, 32 (2014), p. 061801.

[32] X. Z. CHEN, J. F. FENG, Z. C. WANG, J. ZHANG, X. Y. ZHONG, C. SONG, L. JIN, B. ZHANG, F. LI, M. JIANG, Y. Z. TAN, X. J. ZHOU, G. Y. SHI, X. F. ZHOU, X. D. HAN, S. C. MAO, Y. H. CHEN, X. F. HAN, AND F. PAN, *Tunneling anisotropic magnetoresistance driven by magnetic phase transition*, Nature Communications, 8 (2017), p. 449.

[33] J. COSTA-KRÄMER, *Conductance quantization at room temperature in magnetic and nonmagnetic metallic nanowires*, Physical Review B, 55 (1997), pp. R4875–R4878.

[34] J. L. COSTA-KRÄMER, M. DÍAZ, AND P. A. SERENA, *Magnetic field effects on total and partial conductance histograms in Cu and Ni nanowires*, Applied Physics A: Materials Science and Processing, 81 (2005), pp. 1539–1543.

[35] J. C. CUEVAS AND E. SCHEER, *Molecular Electronics: An Introduction to Theory and Experiment*, World Scientific Publishing Co. Pte. Ltd., Singapore, 2010.

[36] X. D. CUI, A. PRIMAK, X. ZARATE, J. TOMFOHR, O. F. SANKEY, A. L. MOORE, T. A. MOORE, D. GUST, G. HARRIS, AND S. M. LINDSAY, *Reproducible measurement of single-molecule conductivity*, Tech. Rep. 5542, 2001.

[37] H. DALGLEISH AND G. KIRCZENOW, *Theoretical study of spin-dependent electron transport in atomic Fe nanocontacts*, Physical Review B, 72 (2005), p. 155429.

[38] S. DATTA, *Electronic Transport in Mesoscopic Systems*, Cambridge University Press, Cambridge, 1995.

[39] V. DEDIU, M. MURGIA, F. MATACOTTA, C. TALIANI, AND S. BARVANERA, *Room temperature spin polarized injection in organic semiconductor*, Solid State Communications, 122 (2002), pp. 181–184.

[40] V. A. DEDIU, L. E. HUESO, I. BERGENTI, AND C. TALIANI, *Spin routes in organic semiconductors*, Nature Materials, 8 (2009), pp. 707–716.

[41] M. DI VENTRA, S. T. PANTELIDES, AND N. D. LANG, *First-Principles Calculation of Transport Properties of a Molecular Device*, Phys. Rev. Lett., 84 (2000), pp. 979–982.

[42] M. DÍAZ, J. L. COSTA-KRÄMER, AND P. A. SERENA, *Partial versus total conductance histograms: A tool to identify magnetic effects in nanocontacts*, Journal of Magnetism and Magnetic Materials, 305 (2006), pp. 497–503.

[43] I. DÍEZ-PÉREZ, J. HIHATH, Y. LEE, L. YU, L. ADAMSKA, M. A. KOZHUSHNER, I. I. OLEYNIK, AND N. TAO, *Rectification and stability of a single molecular diode with controlled orientation*, Nature Chemistry, 1 (2009), pp. 635–641.

[44] M. DOROGI, J. GOMEZ, R. OSIFCHIN, R. P. ANDRES, AND R. REIFENBERGER, *Room-temperature Coulomb blockade from a self-assembled molecular nanostructure*, Physical Review B, 52 (1995), pp. 9071–9077.

[45] B. DOUDIN AND M. VIRET, *Ballistic magnetoresistance?*, Journal of Physics Condensed Matter, 20 (2008), p. 083201.

[46] D. DULIČ, F. PUMP, S. CAMPIDELLI, P. LAVIE, G. CUNIBERTI, AND A. FILORAMO, *Controlled stability of molecular junctions*, Angewandte Chemie - International Edition, 48 (2009), pp. 8273–8276.

[47] W. F. EGELHOFF, L. GAN, H. ETTEDGUI, Y. KADMON, C. J. POWELL, P. J. CHEN, A. J. SHAPIRO, R. D. MCMICHAEL, J. J. MALLETT, T. P. MOFFAT, M. D. STILES, AND E. B. SVEDBERG, *Artifacts that mimic ballistic magnetoresistance*, Journal of Magnetism and Magnetic Materials, 287 (2005), pp. 496–500.

[48] R. FUKUZUMI, S. KANEKO, S. FUJII, T. NISHINO, AND M. KIGUCHI, *Formation of a Chain-like Water Single Molecule Junction with Pd Electrodes*, Journal of Physical Chemistry C, 122 (2018), pp. 4698–4703.

[49] M. GABUREAC, M. VIRET, F. OTT, AND C. FERMON, *Magnetoresistance in nanocontacts induced by magnetostrictive effects*, Physical Review B, 69 (2004), p. 100401.

[50] N. GARCÍA, M. MUÑOZ, AND Y. W. ZHAO, *Magnetoresistance in excess of 200% in ballistic Ni nanocontacts at room temperature and 100 Oe*, Physical Review Letters, 82 (1999), pp. 2923–2926.

[51] J. GHILENE, P. HAPLOT, AND A. J. BARD, *Metal/polypyrrole quasi-reference electrode for voltammetry in nonaqueous and aqueous solutions*, Analytical Chemistry, 78 (2006), pp. 6868–6872.

[52] S. GHOSH, H. HALIMUN, A. K. MAHAPATRO, J. CHOI, S. LODHA, AND D. JANES, *Device structure for electronic transport through individual molecules using nanoelectrodes*, Applied Physics Letters, 87 (2005), p. 233509.

[53] C. GOULD, C. RUESTER, G. SCHMIDT, AND L. MOLENKAMP, *Tunnelling Anisotropic MagnetoResistance (TAMR)*, INTERMAG 2006 - IEEE International Magnetics Conference, (2006), p. 116.

[54] C. GOULD, G. SCHMIDT, AND L. W. MOLENKAMP, *Tunneling anisotropic magnetoresistance-based devices*, IEEE Transactions on Electron Devices, 54 (2007), pp. 977–983.

[55] G. GUEVARA-CARRION, H. HANS, AND V. JADRAN, *Thermodynamic Properties for Applications in Chemical Industry via Classical Force Fields*, Multistage Molecular Methods in Applied chemistry, (2011), pp. 201–249.

[56] C. GUO, K. WANG, E. ZERAH-HARUSH, J. HAMILL, B. WANG, Y. DUBI, AND B. XU, *Molecular rectifier composed of DNA with high rectification ratio enabled by intercalation*, Nature Chemistry, 8 (2016), pp. 484–490.

[57] M. HÄFNER, J. K. VILJAS, D. FRUSTAGLIA, F. PAULY, M. DREHER, P. NIELABA, AND J. C. CUEVAS, *Theoretical study of the conductance of ferromagnetic atomic-sized contacts*, Physical Review B, 77 (2008), p. 104409.

[58] W. HAISS, S. MARTÍN, E. LEARY, H. VAN ZALINGE, S. J. HIGGINS, L. BOUFFIER, AND R. J. NICHOLS, *Impact of junction formation method and surface roughness on single molecule conductance*, Journal of Physical Chemistry C, 113 (2009), pp. 5823–5833.

[59] W. HAISS, H. VAN ZALINGE, S. J. HIGGINS, D. BETHELL, H. HÖBENREICH, D. J. SCHIFFRIN, AND R. J. NICHOLS, *Redox State Dependence of Single Molecule Conductivity*, Journal of the American Chemical Society, 125 (2003), pp. 15294–15295.

[60] W. HAISS, C. WANG, R. JITCHATI, I. GRACE, S. MARTÍN, A. S. BATSANOV, S. J. HIGGINS, M. R. BRYCE, C. J. LAMBERT, P. S. JENSEN, AND R. J. NICHOLS, *Variable contact gap single-molecule conductance determination for a series of conjugated molecular bridges*, Journal of Physics Condensed Matter, 20 (2008).

[61] R. HAYAKAWA, M. A. KARIMI, J. WOLF, T. HUHN, M. S. ZÖLLNER, C. HERRMANN, AND E. SCHEER, *Large Magnetoresistance in Single-Radical Molecular Junctions*, Nano Letters, 16 (2016), pp. 4960–4967.

[62] C. HE, Q. ZHANG, Y. FAN, C. ZHAO, C. ZHAO, J. YE, Y. J. DAPPE, R. J. NICHOLS, AND L. YANG, *Effect of Asymmetric Anchoring Groups on Electronic Transport in Hybrid Metal/Molecule/Graphene Single Molecule Junctions*, ChemPhysChem, 20 (2019), pp. 1830–1836.

[63] W. HONG, H. VALKENIER, G. MÉSZÁROS, D. Z. MANRIQUE, A. MISHCHENKO, A. PUTZ, P. M. GARCÍA, C. J. LAMBERT, J. C. HUMMELEN, AND T. WANDLOWSKI, *An MCBJ case study: The influence of π-conjugation on the single-molecule conductance at a solid/liquid interface*, Beilstein Journal of Nanotechnology, 2 (2011), pp. 699–713.

[64] K. HORIGUCHI, T. SAGISAKA, S. KUROKAWA, AND A. SAKAI, *Electron transport through Ni/1,4-benzenedithiol/Ni single-molecule junctions under magnetic field*, Journal of Applied Physics, 113 (2013), p. 144313.

[65] S. Z. HUA AND H. D. CHOPRA, *100,000 % ballistic magnetoresistance in stable Ni nanocontacts at room temperature*, Physical Review B - Condensed Matter and Materials Physics, 67 (2003), p. 060401.

[66] Z. HUANG, F. CHEN, P. A. BENNETT, AND N. TAO, *Single molecule junctions formed via Au-thiol contact: Stability and breakdown mechanism*, Journal of the American Chemical Society, 129 (2007), pp. 13225–13231.

[67] M. S. HYBERTSEN, L. VENKATARAMAN, J. E. KLARE, A. C. WHALLEY, M. L. STEIGERWALD, AND C. NUCKOLLS, *Amine-linked single-molecule circuits: Systematic trends across molecular families*, Journal of Physics Condensed Matter, 20 (2008), p. 374115.

[68] M. S. INKPEN, Z. [U+FFFD]IU, H. LI, L. M. CAMPOS, J. B. NEATON, AND L. VENKATARAMAN, *Non-chemisorbed gold–sulfur binding prevails in self-assembled monolayers*, Nature Chemistry, 11 (2019), pp. 351–358.

[69] Y. ISSHIKI, S. FUJII, T. NISHINO, AND M. KIGUCHI, *Impact of junction formation processes on single molecular conductance*, Physical Chemistry Chemical Physics, 20 (2018), pp. 7947–7952.

[70] D. JACOB, M. CATURLA, R. CALVO, C. UNTIEDT, AND J. PALACIOS, *Mechanical and electrical properties of Ni*, Journal of thermal analysis, 37 (1991), pp. 2465–2471.

[71] D. JACOB, J. FERNÁNDEZ-ROSSIER, AND J. J. PALACIOS, *Magnetic and orbital blocking in Ni nanocontacts*, Physical Review B, 71 (2018).

[72] Y. JANSSEN, H. FUJII, AND T. EKINO, *Giant magnetoresistance*, Physical Review B - Condensed Matter and Materials Physics, 56 (1997), pp. 13716–13719.

[73] M. JULLIERE, *Tunneling between ferromagnetic films*, Physics Letters A, 54 (1975), pp. 225–226.

[74] M. KAMENETSKA, S. Y. QUEK, A. C. WHALLEY, M. L. STEIGERWALD, H. J. CHOI, S. G. LOUIE, C. NUCKOLLS, M. S. HYBERTSEN, J. B. NEATON, AND L. VENKATARAMAN, *Conductance and geometry of pyridine-linked single-molecule junctions*, Journal of the American Chemical Society, 132 (2010), pp. 6817–6821.

[75] S. KANEKO, D. MURAI, S. MARQUÉS-GONZÁLEZ, H. NAKAMURA, Y. KOMOTO, S. FUJII, T. NISHINO, K. IKEDA, K. TSUKAGOSHI, AND M. KIGUCHI, *Site-Selection in*

Single-Molecule Junction for Highly Reproducible Molecular Electronics, Journal of the American Chemical Society, 138 (2016), pp. 1294–1300.

[76] M. A. KARIMI, S. G. BAHOOSH, M. HERZ, R. HAYAKAWA, F. PAULY, AND E. SCHEER, *Shot Noise of 1,4-Benzenedithiol Single-Molecule Junctions*, Nano Letters, 16 (2016), pp. 1803–1807.

[77] S. L. KAWAHARA, J. LAGOUTE, V. REPAIN, C. CHACON, Y. GIRARD, S. ROUSSET, A. SMOGUNOV, AND C. BARRETEAU, *Large magnetoresistance through a single molecule due to a spin-split hybridized orbital*, Nano Letters, 12 (2012), pp. 4558–4563.

[78] M. KIGUCHI, *Single-Molecule Electronics*, Springer Nature, Singapore, 2016.

[79] M. KIGUCHI, T. KONISHI, AND K. MURAKOSHI, *Hydrogen-assisted stabilization of Ni nanowires in solution*, Applied Physics Letters, 87 (2005), pp. 1–4.

[80] M. KIGUCHI AND K. MURAKOSHI, *Highly conductive single molecular junctions by direct binding of π-conjugated molecule to metal electrodes*, Thin Solid Films, 518 (2009), pp. 466–469.

[81] M. KIGUCHI, S. NAKASHIMA, T. TADA, S. WATANABE, S. TSUDA, Y. TSUJI, AND J. TERAO, *Single-molecule conductance of μ-conjugated rotaxane: New method for measuring stipulated electric conductance of μ-Conjugated molecular wire using STM break junction*, Small, 8 (2012), pp. 726–730.

[82] M. KIGUCHI, O. TAL, S. WOHLTHAT, F. PAULY, M. KRIEGER, D. DJUKIC, J. C. CUEVAS, AND J. M. VAN RUITENBEEK, *Highly conductive molecular junctions based on direct binding of benzene to platinum electrodes*, Physical Review Letters, 101 (2008), p. 046801.

[83] T. KIM, P. DARANCET, J. R. WIDAWSKY, M. KOTIUGA, S. Y. QUEK, J. B. NEATON, AND L. VENKATARAMAN, *Determination of energy level alignment and coupling strength in 4,4′-bipyridine single-molecule junctions*, Nano Letters, 14 (2014), pp. 794–798.

[84] Y. KIM, T. PIETSCH, A. ERBE, W. BELZIG, AND E. SCHEER, *Benzenedithiol: A broad-range single-channel molecular conductor*, Nano Letters, 11 (2011), pp. 3734–3738.

[85] C. H. KO, M. J. HUANG, M. D. FU, AND C. H. CHEN, *Superior contact for single-molecule conductance: Electronic coupling of thiolate and isothiocyanate on Pt, Pd, and Au*, Journal of the American Chemical Society, 132 (2010), pp. 756–764.

[86] M. KOEPF, C. KOENIGSMANN, W. DING, A. BATRA, C. F. NEGRE, L. VENKATARAMAN, G. W. BRUDVIG, V. S. BATISTA, C. A. SCHMUTTENMAER, AND R. H. CRABTREE,

Controlling the rectification properties of molecular junctions through molecule-electrode coupling, Nanoscale, 8 (2016), pp. 16357–16362.

[87] Y. KOMOTO, S. FUJII, H. NAKAMURA, T. TADA, T. NISHINO, AND M. KIGUCHI, *Resolving metal-molecule interfaces at single-molecule junctions*, Scientific Reports, 6 (2016), pp. 1–9.

[88] T. KONISHI, M. KIGUCHI, AND K. MURAKOSHI, *Stable iron-group metal nano contact showing quantized conductance in solution*, Surface Science, 602 (2008), pp. 2333–2336.

[89] E. KOWALSKA, A. FUKUSHIMA, V. SLUKA, C. FOWLEY, A. KÁKAY, Y. ALEKSANDROV, J. LINDNER, J. FASSBENDER, S. YUASA, AND A. M. DEAC, *Tunnel magnetoresistance angular and bias dependence enabling tuneable wireless communication*, Scientific Reports, 9 (2019), p. 9541.

[90] E. LEARY, L. A. ZOTTI, D. MIGUEL, I. R. MÁRQUEZ, L. PALOMINO-RUIZ, J. M. CUERVA, G. RUBIO-BOLLINGER, M. T. GONZÁLEZ, AND N. AGRAIT, *The Role of Oligomeric Gold-Thiolate Units in Single-Molecule Junctions of Thiol-Anchored Molecules*, Journal of Physical Chemistry C, 122 (2018), pp. 3211–3218.

[91] T. LEE, W. WANG, AND M. A. REED, *Mechanism of Electron Conduction in Self-Assembled Alkanethiol Monolayer Devices*, Annals of the New York Academy of Sciences, 1006 (2003), pp. 21–35.

[92] D. V. LEFF, L. BRANDT, AND J. R. HEATH, *Synthesis and characterization of hydrophobic, organically-soluble gold nanocrystals functionalized with primary amines*, Langmuir, 12 (1996), pp. 4723–4730.

[93] C. LI, I. POBELOV, T. WANDLOWSKI, A. BAGRETS, A. ARNOLD, AND F. EVERS, *Charge transport in single Au | alkanedithiol | Au junctions: Coordination geometries and conformational degrees of freedom*, Journal of the American Chemical Society, 130 (2008), pp. 318–326.

[94] J. J. LI, M. L. BAI, Z. B. CHEN, X. S. ZHOU, Z. SHI, M. ZHANG, S. Y. DING, S. M. HOU, W. SCHWARZACHER, R. J. NICHOLS, AND B. W. MAO, *Giant Single-Molecule Anisotropic Magnetoresistance at Room Temperature*, Journal of the American Chemical Society, 137 (2015), pp. 5923–5929.

[95] X. LI, J. HE, J. HIHATH, B. XU, S. M. LINDSAY, AND N. TAO, *Conductance of Single Alkanedithiols: Conduction Mechanism and Effect of Molecule−Electrode Contacts*, Journal of the American Chemical Society, 128 (2006), pp. 2135–2141.

[96] Y. Li, J. M. Artés, J. Qi, I. A. Morelan, P. Feldstein, M. P. Anantram, and J. Hihath, *Comparing Charge Transport in Oligonucleotides: RNA:DNA Hybrids and DNA Duplexes*, Journal of Physical Chemistry Letters, 7 (2016), pp. 1888–1894.

[97] W. Liang, M. P. Shores, M. Bockrath, J. R. Long, and H. Park, *Kondo resonance in a single-molecule transistor*, Nature, 417 (2002), pp. 725–729.

[98] J. Liao, J. S. Agustsson, S. Wu, C. Schönenberger, M. Calame, Y. Leroux, M. Mayor, O. Jeannin, Y. F. Ran, S. X. Liu, and S. Decurtins, *Cyclic conductance switching in networks of redox-active molecular junctions*, Nano Letters, 10 (2010), pp. 759–764.

[99] L. Liu, Q. Zhang, S. Tao, C. Zhao, E. Almutib, Q. Al-Galiby, S. W. Bailey, I. Grace, C. J. Lambert, J. Du, and L. Yang, *Charge transport through dicarboxylic-acid-terminated alkanes bound to graphene-gold nanogap electrodes*, Nanoscale, 8 (2016), pp. 14507–14513.

[100] E. Lörtscher, H. B. Weber, and H. Riel, *Statistical approach to investigating transport through single molecules*, Physical Review Letters, 98 (2007), p. 176807.

[101] B. Ludoph and J. M. van Ruitenbeek, *Conductance fluctuations as a tool for investigating the quantum modes in atomic-size metallic contacts*, Physical Review B, 61 (2000), pp. 2273–2285.

[102] A. Magyarkuti, O. Adak, A. Halbritter, and L. Venkataraman, *Electronic and mechanical characteristics of stacked dimer molecular junctions*, Nanoscale, 10 (2018), pp. 3362–3368.

[103] A. Magyarkuti, N. Balogh, Z. Balogh, L. Venkataraman, and A. Halbritter, *Unsupervised feature recognition in single-molecule break junction data*, Nanoscale, 12 (2020), pp. 8355–8363.

[104] S. Majumdar, H. S. Majumdar, R. Laiho, and R. Österbacka, *Comparing small molecules and polymer for future organic spin-valves*, Journal of Alloys and Compounds, 423 (2006), pp. 169–171.

[105] P. Makk, D. Tomaszewski, J. Martinek, Z. Balogh, S. Csonka, M. Wawrzyniak, M. Frei, L. Venkataraman, and A. Halbritter, *Correlation analysis of atomic and single-molecule junction conductance*, ACS Nano, 6 (2012), pp. 3411–3423.

[106] C. A. Martin, D. Ding, J. K. Sørensen, T. Bjørnholm, J. M. Van Ruitenbeek, and H. S. Van Der Zant, *Fullerene-based anchoring groups for molecular electronics*, Journal of the American Chemical Society, 130 (2008), pp. 13198–13199.

[107] C. A. MARTIN, D. DING, H. S. VAN DER ZANT, AND J. M. VAN RUITENBEEK, *Lithographic mechanical break junctions for single-molecule measurements in vacuum: Possibilities and limitations*, New Journal of Physics, 10 (2008), p. 065008.

[108] S. MARTÍN, D. Z. MANRIQUE, V. M. GARCÍA-SUREZ, W. HAISS, S. J. HIGGINS, C. J. LAMBERT, AND R. J. NICHOLS, *Adverse effects of asymmetric contacts on single molecule conductances of HS(CH2)n COOH in nanoelectrical junctions*, Nanotechnology, 20 (2009), p. 125203.

[109] J. MATULIS AND R. SLIŽYS, *On some characteristics of cathodic processes in nickel electrodeposition*, Electrochimica Acta, 9 (1964), pp. 1177–1188.

[110] R. L. MCCREERY, *Molecular Electronic Junctions*, Chemistry of Materials, 16 (2004), pp. 4477–4496.

[111] Z. MEKHALIF, F. LAFFINEUR, N. COUTURIER, AND J. DELHALLE, *Elaboration of self-assembled monolayers of n-alkanethiols on nickel polycrystalline substrates: Time, concentration, and solvent effects*, Langmuir, 19 (2003), pp. 637–645.

[112] Z. MEKHALIF, J. RIGA, J. J. PIREAUX, AND J. DELHALLE, *Self-assembled monolayers of n-dodecanethiol on electrochemically modified polycrystalline nickel surfaces*, Langmuir, 13 (1997), pp. 2285–2290.

[113] G. MÉSZÁROS, S. KRONHOLZ, S. KARTHÄUSER, D. MAYER, AND T. WANDLOWSKI, *Electrochemical fabrication and characterization of nanocontacts and nm-sized gaps*, Applied Physics A: Materials Science and Processing, 87 (2007), pp. 569–575.

[114] R. M. METZGER, B. CHEN, U. HÖPFNER, M. V. LAKSHMIKANTHAM, D. VUILLAUME, T. KAWAI, X. WU, H. TACHIBANA, T. V. HUGHES, H. SAKURAI, J. W. BALDWIN, C. HOSCH, M. P. CAVA, L. BREHMER, AND G. J. ASHWELL, *Unimolecular electrical rectification in hexadecylquinolinium tricyanoquinodimethanide*, Journal of the American Chemical Society, 119 (1997), pp. 10455–10466.

[115] S. MIURA, M. KIGUCHI, AND K. MURAKOSHI, *Formation of stable nanowires from ferromagnetic metals using 2-butyne-1,4-diol*, Surface Science, 601 (2007), pp. 287–291.

[116] T. MIYAZAKI AND N. TEZUKA, *Giant magnetic tunneling effect in Fe/Al2O3/Fe junction*, 1 1995.

[117] G. E. MOORE, *Cramming more components onto integrated circuits*, Electronics, 38 (1965), p. pp. 114–117.

[118] J. MORELAND AND J. W. EKIN, *Electron tunneling experiments using Nb-Sn break junctions*, Journal of Applied Physics, 58 (1985), p. 3888.

[119] Y. MORIGUCHI, K. YAMAUCHI, S. KUROKAWA, AND A. SAKAI, *Conductance of atom-sized contacts of transition metals at room temperature*, Surface Science, 606 (2012), pp. 928–932.

[120] T. MORIKAWA, K. YOKOTA, M. TSUTSUI, AND M. TANIGUCHI, *Fast and low-noise tunnelling current measurements for single-molecule detection in an electrolyte solution using insulator-protected nanoelectrodes*, Nanoscale, 9 (2017), pp. 4076–4081.

[121] N. A. MORLEY, A. RAO, D. DHANDAPANI, M. R. GIBBS, M. GRELL, AND T. RICHARDSON, *Room temperature organic spintronics*, Journal of Applied Physics, 103 (2008), pp. 5–8.

[122] N. F. MOTT, *The Electrical Conductivity of Transition Metals*, Proceedings of the Royal Society of London. Series A. Mathematical and Physical Sciences, 167 (1935), pp. 580–593.

[123] C. J. MULLER, J. M. VAN RUITENBEEK, C. W. BEENAKKER, AND R. DE BRUYN OUBOTER, *Conductance and supercurrent discontinuities in atomic size point contacts*, Physica B: Physics of Condensed Matter, 189 (1993), pp. 225–234.

[124] N. MUTHUSUBRAMANIAN, E. GALAN, C. MAITY, R. EELKEMA, F. C. GROZEMA, AND H. S. VAN DER ZANT, *Insulator-protected mechanically controlled break junctions for measuring single-molecule conductance in aqueous environments*, Applied Physics Letters, 109 (2016), p. 013102.

[125] R. J. NICHOLS, W. HAISS, S. J. HIGGINS, E. LEARY, S. MARTIN, AND D. BETHELL, *The experimental determination of the conductance of single molecules*, Physical Chemistry Chemical Physics, 12 (2010), pp. 2801–2815.

[126] R. J. NICHOLS AND S. J. HIGGINS, *Single-Molecule Electronics: Chemical and Analytical Perspectives*, Annual Review of Analytical Chemistry, 8 (2015), pp. 389–417.

[127] N.J.TAO, *Electron transport in molecular junctions*, Nature Nanotechnology, 1 (2006), pp. 173–181.

[128] R. G. NUZZO AND D. L. ALLARA, *Adsorption of Bifunctional Organic Disulfides on Gold Surfaces*, Journal of the American Chemical Society, 105 (1983), pp. 4481–4483.

[129] T. ONO, Y. OOKA, H. MIYAJIMA, AND Y. OTANI, *2E2/H To E2/H Switching of Quantum Conductance Associated With a Change in Nanoscale Ferromagnetic Domain Structure*, Applied Physics Letters, 75 (1999), pp. 1622–1624.

[130] Y. OOKA, T. ONO, AND H. MIYAJIMA, *Conductance quantization in ferromagnetic Ni nanowire*, Journal of Magnetism and Magnetic Materials, 226-230 (2001), pp. 1848–1849.

[131] H. OSHIMA AND K. MIYANO, *Spin-dependent conductance quantization in nickel point contacts*, Applied Physics Letters, 73 (1998), pp. 2203–2205.

[132] R. PATI, L. SENAPATI, P. AJAYAN, AND S. NAYAK, *First-principles calculations of spin-polarized electron transport in a molecular wire: Molecular spin valve*, Physical Review B, 68 (2003), p. 100407.

[133] M. L. PERRIN, E. BURZURÍ, AND H. S. VAN DER ZANT, *Single-molecule transistors*, Chemical Society Reviews, 44 (2015), pp. 902–919.

[134] C. PIRLOT, J. DELHALLE, J. J. PIREAUX, AND Z. MEKHALIF, *Surface modification of polycrystalline iron surfaces by n-dodecanethiol: An XPS investigation*, Surface and Coatings Technology, 138 (2001), pp. 166–172.

[135] E. PODSTAWKA, Y. OZAKI, AND L. M. PRONIEWICZ, *Part III: Surface-Enhanced Raman Scattering of Amino Acids and Their Homodipeptide Monolayers Deposited onto Colloidal Gold Surface*, Appl. Spectrosc., 59 (2005), pp. 1516–1526.

[136] S. PRAMANIK, C.-G. STEFANITA, S. PATIBANDLA, S. BANDYOPADHYAY, K. GARRE, N. HARTH, AND M. CAHAY, *Observation of extremely long spin relaxation times in an organic nanowire spin valve*, Nature Nanotechnology, 2 (2007), pp. 216–219.

[137] J. PUEBLA, J. KIM, K. KONDOU, AND Y. OTANI, *Spintronic devices for energy-efficient data storage and energy harvesting*, Communications Materials, 1 (2020), pp. 1–9.

[138] S. Y. QUEK, M. KAMENETSKA, M. L. STEIGERWALD, H. J. CHOI, S. G. LOUIE, M. S. HYBERTSEN, J. B. NEATON, AND L. VENKATARAMAN, *Mechanically controlled binary conductance switching of a single-molecule junction*, Nature Nanotechnology, 4 (2009), pp. 230–234.

[139] S. Y. QUEK, L. VENKATARAMAN, H. J. CHOI, S. G. LOUIE, M. S. HYBERTSEN, AND J. B. NEATON, *Amine - Gold linked single-molecule circuits: Experiment and theory*, Nano Letters, 7 (2007), pp. 3477–3482.

[140] M. A. REED, C. ZHOU, C. J. MULLER, T. P. BURGIN, AND J. M. TOUR, *Conductance of a molecular junction*, Science, 278 (1997), pp. 252–254.

[141] ROBERT M. METZGER, *Unimolecular and Supramolecular Electronics II: Chemistry and Physics Meet at Metal-Molecule Interfaces*, Springer-Verlag Berlin Heidelberg, Heidelberg, 2012.

[142] A. R. ROCHA, V. M. GARCÍA-SUÁREZ, S. W. BAILEY, C. J. LAMBERT, J. FERRER, AND S. SANVITO, *Towards molecular spintronics*, Nature Materials, 4 (2005), pp. 335–339.

[143] S. SANVITO, *Injecting and controlling spins in organic materials*, Journal of Materials Chemistry, 17 (2007), pp. 4455–4459.

[144] S. SANVITO AND A. R. ROCHA, *Molecular-spintronics: The art of driving spin through molecules*, Journal of Computational and Theoretical Nanoscience, 3 (2006), pp. 624–642.

[145] K. D. SATTLER, ed., *Handbook of Nanophysics: Nanoparticles and Quantum Dots*, CRC Press, Boca Raton, 2011.

[146] S. SCHMAUS, A. BAGRETS, Y. NAHAS, T. K. YAMADA, A. BORK, M. BOWEN, E. BEAUREPAIRE, F. EVERS, AND W. WULFHEKEL, *Giant magnetoresistance through a single molecule*, Nature Nanotechnology, 6 (2011), pp. 185–189.

[147] F. SCHWARZ, G. KASTLUNGER, F. LISSEL, C. EGLER-LUCAS, S. N. SEMENOV, K. VENKATESAN, H. BERKE, R. STADLER, AND E. LÖRTSCHER, *Field-induced conductance switching by charge-state alternation in organometallic single-molecule junctions*, Nature Nanotechnology, 11 (2016), pp. 170–176.

[148] J. M. SEMINARIO, C. E. DE LA CRUZ, AND P. A. DEROSA, *A theoretical analysis of metal-molecule contacts*, Journal of the American Chemical Society, 123 (2001), pp. 5616–5617.

[149] T. I. SHARIPOV AND R. Z. BAKHTIZIN, *The study of electrical conductivity of DNA molecules by scanning tunneling spectroscopy*, IOP Conference Series: Materials Science and Engineering, 256 (2017), p. 012009.

[150] J. H. SHIM, K. V. RAMAN, Y. J. PARK, T. S. SANTOS, G. X. MIAO, B. SATPATI, AND J. S. MOODERA, *Large spin diffusion length in an amorphous organic semiconductor*, Physical Review Letters, 100 (2008), p. 226603.

[151] T. SMITH, *The hydrophilic nature of a clean gold surface*, Journal of Colloid And Interface Science, 75 (1980), pp. 51–55.

[152] H. SONG, Y. KIM, Y. H. JANG, H. JEONG, M. A. REED, AND T. LEE, *Observation of molecular orbital gating*, Nature, 462 (2009), pp. 1039–1043.

[153] T. A. SU, H. LI, M. L. STEIGERWALD, L. VENKATARAMAN, AND C. NUCKOLLS, *Stereoelectronic switching in single-molecule junctions*, Nature Chemistry, 7 (2015), pp. 215–220.

[154] T. A. SU, H. LI, V. ZHANG, M. NEUPANE, A. BATRA, R. S. KLAUSEN, B. KUMAR, M. L. STEIGERWALD, L. VENKATARAMAN, AND C. NUCKOLLS, *Single-Molecule Conductance in Atomically Precise Germanium Wires*, Journal of the American Chemical Society, 137 (2015), pp. 12400–12405.

[155] L. SUN, Y. A. DIAZ-FERNANDEZ, T. A. GSCHNEIDTNER, F. WESTERLUND, S. LARA-AVILA, AND K. MOTH-POULSEN, *Single-molecule electronics: From chemical design to functional devices*, Chemical Society Reviews, 43 (2014), pp. 7378–7411.

[156] D. S. SZUMSKI, *Single Molecule Spintronics*, PhD thesis, University of Bristol, 2010.

[157] C. TANG, J. ZHENG, Y. YE, J. LIU, L. CHEN, Z. YAN, Z. CHEN, L. CHEN, X. HUANG, J. BAI, Z. CHEN, J. SHI, H. XIA, AND W. HONG, *Electric-Field-Induced Connectivity Switching in Single-Molecule Junctions*, iScience, 23 (2020), p. 100770.

[158] M. TANIGUCHI, *Paving the way to single-molecule chemistry through molecular electronics*, Physical Chemistry Chemical Physics, 21 (2019), pp. 9641–9650.

[159] A. TANINAKA, S. YOSHIDA, Y. SUGITA, O. TAKEUCHI, AND H. SHIGEKAWA, *Evolution of local conductance pathways in a single-molecule junction studied using the three-dimensional dynamic probe method*, Nanoscale, 11 (2019), pp. 5951–5959.

[160] K. TERABE, T. HASEGAWA, T. NAKAYAMA, AND M. AONO, *Quantized conductance atomic switch*, Nature, 433 (2005), pp. 47–50.

[161] M. TERESA GONZÁLEZ, S. WU, R. HUBER, S. J. VAN DER MOLEN, C. SCHÖNENBERGER, AND M. CALAME, *Electrical conductance of molecular junctions by a robust statistical analysis*, Nano Letters, 6 (2006), pp. 2238–2242.

[162] W. THOMSON, *On the Electro-Dynamic Qualities of Metals:—Effects of Magnetization on the Electric Conductivity of Nickel and of Iron*, Proc. Royal Soc. Lond, 8 (1857), pp. 546–550.

[163] J. H. TIAN, Y. YANG, B. LIU, B. SCHÖLLHORN, D. Y. WU, E. MAISONHAUTE, A. S. MUNS, Y. CHEN, C. AMATORE, N. J. TAO, AND Z. Q. TIAN, *The fabrication and characterization of adjustable nanogaps between gold electrodes on chip for electrical measurement of single molecules*, Nanotechnology, 21 (2010), p. 274012.

[164] L. TORTECH, Z. MEKHALIF, J. DELHALLE, F. GUITTARD, AND S. GÉRIBALDI, *Self-assembled monolayers of semifluorinated thiols on electrochemically modified polycrystalline nickel surfaces*, Thin Solid Films, 491 (2005), pp. 253–259.

[165] M. TSUTSUI, K. SHOJI, M. TANIGUCHI, AND T. KAWAI, *Formation and self-breaking mechanism of stable atom-sized junctions*, Nano Letters, 8 (2008), pp. 345–349.

[166] M. TSUTSUI AND M. TANIGUCHI, *Single molecule electronics and devices*, Sensors (Switzerland), 12 (2012), pp. 7259–7298.

[167] M. TSUTSUI, Y. TERAMAE, S. KUROKAWA, AND A. SAKAI, *High-conductance states of single benzenedithiol molecules*, Applied Physics Letters, 89 (2006), p. 163111.

[168] A. ULMAN, *Formation and structure of self-assembled monolayers*, Chemical Reviews, 96 (1996), pp. 1533–1554.

[169] J. ULRICH, D. ESRAIL, W. PONTIUS, L. VENKATARAMAN, D. MILLAR, AND L. H. DOERRER, *Variability of conductance in molecular junctions*, Journal of Physical Chemistry B, 110 (2006), pp. 2462–2466.

[170] C. UNTIEDT, D. M. DEKKER, D. DJUKIC, AND J. M. VAN RUITENBEEK, *Absence of magnetically induced fractional quantization in atomic contacts*, Physical Review B - Condensed Matter and Materials Physics, 69 (2004), p. 081401.

[171] S. J. VAN DER MOLEN, J. LIAO, T. KUDERNAC, J. S. AGUSTSSON, L. BERNARD, M. CALAME, B. J. VAN WEES, B. L. FERINGA, AND C. SCHÖNENBERGER, *Light-controlled conductance switching of ordered metal-molecule-metal devices*, Nano Letters, 9 (2009), pp. 76–80.

[172] L. VENKATARAMAN, J. E. KLARE, I. W. TAM, C. NUCKOLLS, M. S. HYBERTSEN, AND M. L. STEIGERWALD, *Single-Molecule Circuits with Well-Defined Molecular Conductance*, Nano Letters, 6 (2006), pp. 458–462.

[173] A. VEZZOLI, R. J. BROOKE, N. FERRI, S. J. HIGGINS, W. SCHWARZACHER, AND R. J. NICHOLS, *Single-Molecule Transport at a Rectifying GaAs Contact*, Nano Letters, 17 (2017), pp. 1109–1115.

[174] A. VILAN, *Analyzing Molecular Current-Voltage Characteristics with the Simmons Tunneling Model: Scaling and Linearization*, The Journal of Physical Chemistry C, 111 (2007), pp. 4431–4444.

[175] M. VIRET, S. BERGER, M. GABUREAC, F. OTT, D. OLLIGS, I. PETEJ, J. F. GREGG, C. FERMON, G. FRANCINET, AND G. LE GOFF, *Magnetoresistance through a single nickel atom*, Physical Review B, 66 (2002), p. 220401(R).

[176] A. VON BIEREN, A. K. PATRA, S. KRZYK, J. RHENSIUS, R. M. REEVE, L. J. HEYDERMAN, R. HOFFMANN-VOGEL, AND M. KLÄUI, *Domain-wall induced large magnetoresistance effects at zero applied field in ballistic nanocontacts*, Physical Review Letters, 110 (2013), p. 067203.

[177] S. A. G. VROUWE, E. VAN DER GIESSEN, S. J. VAN DER MOLEN, D. DULIC, M. L. TROUWBORST, AND B. J. VAN WEES, *Mechanics of lithographically defined break junctions*, Phys. Rev. B, 71 (2005), p. 35313.

[178] F. J. WANG, Z. H. XIONG, D. WU, J. SHI, AND Z. V. VARDENY, *Organic spintronics: The case of Fe/Alq3/Co spin-valve devices*, Synthetic Metals, 155 (2005), pp. 172–175.

[179] H. WANG, C. LU, J. CHEN, Y. LIU, S. L. YUAN, S. W. CHEONG, S. DONG, AND J. M. LIU, *Giant anisotropic magnetoresistance and nonvolatile memory in canted antiferromagnet Sr2IrO4*, Nature Communications, 10 (2019), p. 2280.

[180] K. WANG, J. G. SANDERINK, T. BOLHUIS, W. G. VAN DER WIEL, AND M. P. DE JONG, *Tunnelling anisotropic magnetoresistance due to antiferromagnetic CoO tunnel barriers*, Scientific Reports, 5 (2015), p. 15498.

[181] K. WANG, J. ZHOU, J. M. HAMILL, AND B. XU, *Measurement and understanding of single-molecule break junction rectification caused by asymmetric contacts*, Journal of Chemical Physics, 141 (2014), p. 054712.

[182] P. WIŚNIEWSKI, *Giant anisotropic magnetoresistance and magnetothermopower in cubic 3:4 uranium pnictides*, Applied Physics Letters, 90 (2007), pp. 8–11.

[183] S. A. WOLF, D. D. AWSCHALOM, R. A. BUHRMAN, J. M. DAUGHTON, S. VON MOLNÁR, M. L. ROUKES, A. Y. CHTCHELKANOVA, AND D. M. TREGER, *Spintronics: A spin-based electronics vision for the future*, Science, 294 (2001), pp. 1488–1495.

[184] D. XIANG, H. JEONG, T. LEE, AND D. MAYER, *Mechanically controllable break junctions for molecular electronics*, Advanced Materials, 25 (2013), pp. 4845–4867.

[185] X. XIAO, B. XU, AND N. J. TAO, *Measurement of Single Molecule Conductance: Benzenedithiol and Benzenedimethanethiol*, Nano Letters, 4 (2004), pp. 267–271.

[186] F. Q. XIE, L. NITTLER, C. OBERMAIR, AND T. SCHIMMEL, *Gate-controlled atomic quantum switch*, Physical Review Letters, 93 (2004), pp. 128303–1.

[187] Z. H. XIONG, D. WU, Z. VALY VARDENY, AND J. SHI, *Giant magnetoresistance in organic spin-valves*, Nature, 427 (2004), pp. 821–824.

[188] B. XU AND N. J. TAO, *Measurement of Single-Molecule Resistance by Repeated Formation of Molecular Junctions*, Science, 301 (2003), pp. 1221–1223.

[189] B. XU, P. ZHANG, X. LI, AND N. TAO, *Direct conductance measurement of single DNA molecules in aqueous solution*, Nano Letters, 4 (2004), pp. 1105–1108.

[190] G. XU, Z. LIU, K. XU, Y. ZHANG, H. ZHONG, Y. FAN, AND Z. HUANG, *Constant current etching of gold tips suitable for tip-enhanced Raman spectroscopy*, Review of Scientific Instruments, 83 (2012).

[191] R. YAMADA, M. NOGUCHI, AND H. TADA, *Magnetoresistance of single molecular junctions measured by a mechanically controllable break junction method*, Applied Physics Letters, 98 (2011), pp. 2011–2014.

[192] W. YANG, Q. SHI, T. MIAO, Q. LI, P. CAI, H. LIU, H. LIN, Y. BAI, Y. ZHU, Y. YU, L. DENG, W. WANG, L. YIN, D. SUN, X.-G. ZHANG, AND J. SHEN, *Achieving large and nonvolatile tunable magnetoresistance in organic spin valves using electronic phase separated manganites*, Nature Communications, 10 (2019), pp. 1–10.

[193] Y. YANG, Z. CHEN, J. LIU, M. LU, D. YANG, F. YANG, AND Z. TIAN, *An electrochemically assisted mechanically controllable break junction approach for single molecule junction conductance measurements*, Nano Research, 4 (2011), pp. 1199–1207.

[194] Y. YANG, J. LIU, S. FENG, H. WEN, J. TIAN, J. ZHENG, B. SCHÖLLHORN, C. AMATORE, Z. CHEN, AND Z. TIAN, *Unexpected current–voltage characteristics of mechanically modulated atomic contacts with the presence of molecular junctions in an electrochemically assisted–MCBJ*, Nano Research, 9 (2016), pp. 560–570.

[195] K. YOSHIDA, I. HAMADA, S. SAKATA, A. UMENO, M. TSUKADA, AND K. HIRAKAWA, *Gate-tunable large negative tunnel magnetoresistance in Ni-C 60-Ni single molecule transistors*, Nano Letters, 13 (2013), pp. 481–485.

[196] N. ZECH AND D. LANDOLT, *The influence of boric acid and sulfate ions on the hydrogen formation in Ni-Fe plating electrolytes*, Electrochimica Acta, 45 (2000), pp. 3461–3471.

[197] Q. ZHANG, S. TAO, Y. FAN, C. ZHAO, C. ZHAO, W. SU, Y. J. DAPPE, R. J. NICHOLS, AND L. YANG, *Technical Effects of Molecule-Electrode Contacts in Graphene-Based Molecular Junctions*, Journal of Physical Chemistry C, 122 (2018), pp. 23200–23207.

[198] Q. ZHANG, S. TAO, R. YI, C. HE, C. ZHAO, W. SU, A. SMOGUNOV, Y. J. DAPPE, R. J. NICHOLS, AND L. YANG, *Symmetry Effects on Attenuation Factors in Graphene-Based Molecular Junctions*, Journal of Physical Chemistry Letters, 8 (2017), pp. 5987–5992.

[199] Y. ZHANG, X. H. YAN, Y. D. GUO, AND Y. XIAO, *Negative tunneling magnetoresistance of Fe/MgO/NiO/Fe magnetic tunnel junction: Role of spin mixing and interface state*, Applied Physics Letters, 111 (2017).

[200] J. ZHENG, J. LIU, Y. ZHUO, R. LI, X. JIN, Y. YANG, Z. B. CHEN, J. SHI, Z. XIAO, W. HONG, AND Z. Q. TIAN, *Electrical and SERS detection of disulfide-mediated dimerization in single-molecule benzene-1,4-dithiol junctions*, Chemical Science, 9 (2018), pp. 5033–5038.

[201] X. S. ZHOU, Z. B. CHEN, S. H. LIU, S. JIN, L. LIU, H. M. ZHANG, Z. X. XIE, Y. B. JIANG, AND B. W. MAO, *Single molecule conductance of dipyridines with conjugated ethene and nonconjugated ethane bridging group*, Journal of Physical Chemistry C, 112 (2008), pp. 3935–3940.

[202] O. ZILBERBERG, *Gold-atoms motion on mechanically controllable break junctions contacts*, PhD thesis, University of Basel, 2006.